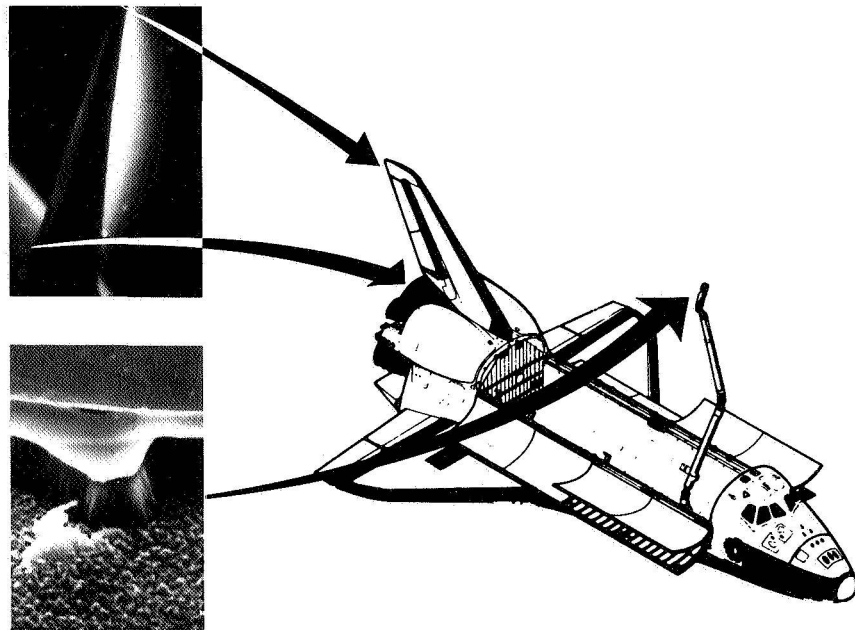


Second Workshop on Spacecraft Glow



*Proceedings of a workshop held at
George C. Marshall Space Flight Center
Huntsville, Alabama
May 6-7, 1985*

NASA

NASA Conference Publication 2391

Second Workshop on Spacecraft Glow

Edited by

J. H. Waite, Jr., and T. W. Moorehead
*NASA George C. Marshall Space Flight Center
Marshall Space Flight Center, Alabama*

Proceedings of a workshop sponsored by
NASA George C. Marshall Space Flight Center,
Huntsville, Alabama, and Universities Space
Research Association, Washington, D.C.,
and held at Space Science Laboratory,
George C. Marshall Space Flight Center
Huntsville, Alabama
May 6-7, 1985

NASA

National Aeronautics
and Space Administration

**Scientific and Technical
Information Branch**

1985

SUMMARY

The glows induced by the interaction of orbiting spacecraft with the atmosphere present a complex problem of interpretation whose solution requires a collaborative multidisciplinary approach embracing research in aeronomy, surface chemistry, plasma physics, fluid dynamics, and atomic and molecular spectroscopy. All these disciplines are represented in this collection of papers delivered at the Second Workshop on Spacecraft Glow. The workshop was held at the Space Science Laboratory of NASA's Marshall Space Flight Center in May 1985, and was partially sponsored by the Universities Space Research Association.

Observations of the space shuttle glows were summarized by Mende and Swenson. The spatial distributions of the ram glows on the vertical stabilizer are consistent with a distance of 20 cm in the case where the emitting species is released from an isotropic scattering surface. The glow spectrum has the appearance of a continuum. It peaks in intensity near 700 nm dropping below the detection limit at wavelengths shorter than 400 nm and longer than 800 nm. The fall-off at longer wavelengths is not firmly established because of possible effects of varying spacecraft window transmission. The $\cos^2 \phi$ dependence on the angle of attack (ϕ) was discussed and some results on the duration of the enhancement of the ram glow following thruster firings were given. The glow intensity varies exponentially with altitude with a scale height approximating that of atomic oxygen. The glow did not change in intensity through the mission duration, suggesting that outgassing is not responsible. Mende concluded by arguing that the continuum is due to NO_2 produced by recombining O and NO.

An attempt to obtain glow spectra at higher resolution by Kendall et al. was described by Llewellyn.

A more detailed examination of the NO_2 hypothesis was presented by Swenson, Mende, and Clifton and further comments on it were made by Green, Marinelli, and Rawlins, by Kofsky and Barrett, and by Kendall et al. Mass spectrometric studies carried out on the Atmosphere Explorer satellites of the odd nitrogen chemistry and the formation of NO and NO_2 were described by Engebretson. He found that increasing the wall temperature greatly reduced the NO_2 formation. The observation of large amounts of NO_2 in the open source instruments was attributed to the entrance of ramming oxygen atoms through the orifice followed by a three-body recombination.

High-resolution spectra obtained from the ISO experiment on Spacelab 1 were presented by M. Torr and preliminary interpretations were offered by D. Torr, Khoyloo, and M. Torr and by Green, Marinelli, and Rawlins. Most of the N_2^+ emission was attributed to the dayglow. A 14 kilorayleigh emission apparently emanating from the wake may arise from charge exchange collisions between the ramming oxygen ions and the enhanced N_2 bulge in front of the spacecraft surfaces producing N_2^+ ions that are swept into the wake by the spacecraft motion through the magnetic field. The N_2 Vegard-Kaplan bands between 160 and 190 nm were seen looking downward at low altitudes and the N_2^+ Meinel bands also appeared strongly in some of the spectra. Anomalous vibrational distributions appear to be necessary to interpret the data. The identification of carbon compounds was discussed. A very bright visible continuum of non-atmospheric origin was found to underly the nightside spectra, and is possibly also present on the dayside. Detailed analysis is necessary to separate the spacecraft-induced glows from the atmospheric emissions.

Chakrabarti and Sasseen described observations of a 1 kilorayleigh glow in Lyman alpha at 600 km with an EUV instrument carried on a polar orbiting satellite. Its origin is as yet uncertain, but it is a potentially serious hazard to ultraviolet observations. Experiments to obtain glow data between 190 and 300 nm were presented by Spear, Ucker, and Tobiska and by Anderson. The latest results of a continuing analysis of Atmosphere Explorer glow data were reported by Dalgarno, Yee, and LeCompte. Their analysis of the data below 160 km indicates a spectrum differing from the high-altitude observations and an intensity apparently varying as the product of any pair of molecules N_2 , O_2 , and NO . In the following discussions, it was pointed out that near 160 km the mean free path in the ram direction may be of the same order as the baffle dimensions.

At high altitudes, the spectra, measured in band passes centered at 732 nm, 656 nm, 428 nm, and 3371 nm, are consistent with emission from vibrationally excited OH, supplemented by an additional source with a spectrum similar to that observed for the shuttle glows. The glow at 280 nm may be due to surface recombination of OH into the electronically excited $A^2\Sigma^+$ state.

The implications of these observations of the spacecraft glows and the Atmosphere Explorer glows for the Space Telescope mission were discussed by Clarke.

Several studies of the recombination, chemical reaction, and impact excitation mechanisms for producing the glow were reported. Papadopoulos surveyed his critical velocity theory and suggested that currents driven by the existence of sheaths in the vicinity of the vehicle can heat the ambient electrons to a degree that can excite a variety of vibrational and rotational emissions in the molecular component of the gas. He emphasized the similarity of the volume glow emission in the shuttle vicinity and the glow produced during thruster firings.

The presence of solid surfaces in orbit may provide the means of producing or enhancing glow in other ways. A spacecraft front surface at 250 km altitude, moving with its surface normal parallel to the direction of motion, is struck by atmospheric species at the rate of $10^{15} \text{ cm}^{-2} \text{ s}^{-1}$. Since the predominant species is atomic oxygen at this altitude, extensive oxidation of the surface may take place. Volatile products leaving the surface in an excited state may emit photons. The surface also acts to concentrate the emitted and ambient gas species by a pile-up effect as the spacecraft moves through the atmosphere at 8 km s^{-1} . Concentration increases of a factor of about 50 above ambient have been calculated by Hueser, Brock, and Melfi and by Rantanen, Swanson, and D. Torr resulting in effective interaction mean free paths between free atmospheric species and surface-emitted species of a few tens of meters.

It is evident that in addition to the plasma processes, at least two other kinds of phenomena exist, one giving rise to the intense but spectrally diffuse red glow extending off surfaces with a characteristic length of $\sim 20 \text{ cm}$, and another probably associated with collisional excitation between the atmosphere and the ambient gas cloud which piles up on the front side of a satellite. This cloud may have an effective radius of tens of meters. The discussions of the first type of process by Kofsky and Barrett, Green et al., Kendall et al., and Swenson et al. emphasized the chemistry of the energized nitrogen-oxygen system. Mechanisms occur involving energetic oxygen and nitrogen which react on surfaces producing and desorbing an excited nitrogen oxide molecule which subsequently decays emitting a photon. Similar mechanisms have included desorbing of excited N_2 , CO , and other species.

Evidence supporting the second source of glows includes the observations of glows following thruster firings and the ISO spectrometer observations of Spacelab 1. The latter included line spectra of such species as O_2 , which may have been produced by reactive excitation of surface-emitted organic molecules with ambient atmospheric species. Such a scenario is supported by the ground-based infrared observations of Witteborn who has previously reported a glow extending beyond the shuttle by tens of meters. In this class of mechanism the surface is the source of the glow precursors. Reactive collisions between O atoms and organic molecules or radicals have a high probability of producing excited products. A paper by Gregory and Peters described the erosion of carbonaceous materials in orbit and provided a basis for estimating the source function of glow precursors. In addition to these two classes of processes, there may be a range of processes with intermediate decay lengths. An interesting extreme was described by Peters. The measurements of the shuttle red glow show maximum intensity at or near the shuttle tail fin surface, consistent with an intense emission from species absorbed on the surface. Peters suggested this may be simply caused by oxygen atoms collisionally excited into 1S and 1D states decaying while still in contact with the surface. Under such conditions, the usual atomic line emission would be broadened into bands of width qualitatively in agreement with the orbital measurements.

The chemical nature of the shuttle environment is a significant parameter. Neutral mass spectrometer data for several flights were presented by Miller and Carignan. Of particular value are measurements of the oxidation rate of different material surfaces in the shuttle environment. Leger and Visentine reported data from STS-5 and STS-8 which showed high reactivities of atomic oxygen with organic films, polymers, and many composites. The dependence of the glow intensity on different materials was reported by Mende and Swenson who also explored the effects of thruster firings.

Laboratory oxygen and nitrogen beam systems were discussed. While velocities of ~ 8 km s^{-1} and fluxes of at least 10^{15} s^{-1} are needed for a thorough study of glow and erosion, much useful work could be done at lower energies and fluxes. No system has yet reliably produced the energies and fluxes desired but active development programs are underway by Gregory, Green, Langer et al., Tolk et al., and Arnold and Peplinski.

Approximately 2 to 3 hours of the workshop were devoted to presentations of future plans for vehicle glow related studies. These plans ranged from concepts still in the proposal phase, to measurement sequences already approved for implementation on forthcoming missions (Mumma and Jennings, Fazio and Koch, and Leger and Visentine). The available data on surface glows are limited in spectral extent and in spectral resolution. Thus, fundamental information on these glows has yet to be acquired in the form of multi-spectral measurements of surfaces directed into the velocity vector. One category of future experiments dealt with this issue and included "improvised" experiments using existing mission hardware to do such things as measuring the glow of the surface of one instrument with another. Another dealt with more elaborate proposed cause-effect studies in which surfaces would not only be spectrally viewed, but would also be subjected to gas or charged particle beams.

The links between surface glows and the corrosion caused by the highly chemically active atomic oxygen environment are poorly understood, and a second category of future experiments focused on this topic, including both on-orbit studies and laboratory beam experiments.

Two points were brought out by these presentations and the related discussions. First, because the subject of vehicle optical environments is not the special concern of any one group and has no champion at NASA, attempts are being made to address the problem with non-optimized hardware and with hopes of only partial results. Second, while some progress could be made with instrumentation already included in future payloads, because shuttle glow is not the primary objective of these missions, it becomes a formidable task to obtain approval to use even nominal amounts of the mission resources for such studies.

Shuttle glow and an induced optical contamination surrounding vehicles in space is of concern to several disciplines, and it is in our interest to understand the nature of this optical environment and the limitations that it places on studies from space and the use of materials in space. In order to gain this understanding, a focused effort is needed, one that addresses the full extent of the problem. This workshop and the subsequent meetings of the steering committee will be used to develop a proposal for a NASA/Marshall Space Flight Center program to conduct such an effort.

A. Dalgarno

Program Committee:

Hunter Waite, Convener

John Clarke
Alex Dalgarno
Alex Dessler
John Gregory
Dennis Papadopoulos
Gary Swenson
Marsha Torr

TABLE OF CONTENTS

	Page
IN SITU OBSERVATIONS	
Vehicle Glow Measurements on the Space Shuttle	
S. B. Mende and G. R. Swenson	1
Space Shuttle Ram Glow: Implication of NO ₂ Recombination Continuum	
G. R. Swenson, S. B. Mende, and S. Clifton	35
AE and DE Mass Spectrometer Observations Relevant to the Shuttle Glow	
M. J. Engebretson	46
The Atmosphere Explorer and the Shuttle Glow	
A. Dalgarno, J-H. Yee, and M. LeCompte	55
Orbiter Glow Observations at High Spectral Resolution	
D.J.W. Kendall, R. L. Gattinger, E. J. Llewellyn, I. C. McDade, and S. B. Mende	63
Neutral Mass Spectrometer Measurements in the Shuttle Bay Environment	
E. Miller and G. Carignan	74
Spectral Identification/Elimination of Molecular Species in Spacecraft Glow	
B. D. Green, W. J. Marinelli, and W. T. Rawlins	82
The UV-VIS Optical Environment of the Shuttle	
M. R. Torr	98
Enhanced N ₂ ⁺ Emissions in the Shuttle Environment (Abstract only)	
D. G. Torr, A. Khoyloo, and M. R. Torr	107
Investigation of Vehicle Glow in the Far Ultraviolet	
S. Chakrabarti and T. Sasseen	108
THEORETICAL CALCULATIONS	
Spacecraft-Induced Plasma Energization and Its Role in Flow Phenomena	
K. Papadopoulos and R. A. Smith	119
Shuttle Vertical Fin Flowfield by the Direct Simulation Monte Carlo Method	
J. E. Hueser, F. J. Brock, and L. T. Melfi	129

TABLE OF CONTENTS (Continued)

	Page
A Mechanism for the Local Concentration Enhancement of the Shuttle Atmosphere	
R. O. Rantanen, R. A. Swanson, and D. G. Torr	139
Surface-Catalyzed Recombination into Excited Electronic, Vibrational, Rotational, and Kinetic Energy States: A Review	
I. L. Kofsky and J. L. Barrett	149
Infrared Emission from Desorbed NO_2^* and NO^*	
I. L. Kofsky and J. L. Barrett	155
The NO- NO_2 System at Laboratory Surfaces	
J. L. Barrett and I. L. Kofsky	165
A Model for Explaining Some Features of Shuttle Glow	
P. N. Peters	169
The Production of Glow Precursors by Oxidative Erosion of Spacecraft Surfaces	
J. C. Gregory and P. N. Peters	174
Activated Recombinative Desorption: A Potential Component in Mechanisms of Spacecraft Glow	
J. B. Cross	180

LABORATORY MEASUREMENTS

Optical Radiation from the Interaction of Energetic Atoms, Ions, Electrons, and Photons with Surfaces	
N. H. Tolk, R. G. Albridge, R. F. Haglund, Jr., and M. H. Mendenhall	191
A Ground-Based Experimental Test Program to Duplicate and Study the Spacecraft Glow Phenomenon	
W. D. Langer, S. A. Cohen, D. M. Manos, D. H. McNeill, R. W. Motley, M. Ono, and S. Paul	202
Application of an Atomic Oxygen Beam Facility to the Investigation of Shuttle Glow Chemistry	
G. S. Arnold and D. R. Peplinski	212

TABLE OF CONTENTS (Concluded)

	Page
FUTURE EXPERIMENTS	
An Assessment of the Impact of Spacecraft Glow on the Hubble Telescope J. T. Clarke	229
Infrared Measurements of Spacecraft Glow Planned for Spacelab 2 G. G. Fazio and D. G. Koch	243
Planned Investigation of Infrared Emissions Associated with the Induced Spacecraft Glow: A Shuttle Infrared Glow Experiment (SIRGE) M. J. Mumma and D. E. Jennings	250
Data Requirements for Verification of Ram Glow Chemistry G. R. Swenson and S. B. Mende	260
A Possible Experiment for the EOM 1-2 Mission (Abstract only) M. R. Torr	269
Space Shuttle Mechanistic Studies to Characterize Atomic Oxygen Interactions with Surfaces L. J. Leger and J. T. Visentine	270
The Shuttle Glow: A Program to Study the Ram-Induced Phenomena H. R. Anderson	274
Survey of Ultraviolet Shuttle Glow K. A. Spear, G. J. Ucker, and K. Tobiska	277
AGENDA	279
LIST OF ATTENDEES	283

IN SITU OBSERVATIONS

VEHICLE GLOW MEASUREMENTS ON THE SPACE SHUTTLE

S. B. Mende and G. R. Swenson

Lockheed Palo Alto Research Laboratory

Abstract. From the combined data set of glow observations on shuttle flight STS-3, STS-4, STS-5, STS-8, STS-9, 41-D, and 41-G some of the properties of the shuttle glow are discussed. Comparison of the STS-3 and STS-5 (240 and 305 km altitude, respectively) photographs shows that the intensity of the glow is about a factor of 3.5 brighter on the low-altitude (STS-3) flight. In an experiment to observe the dependence of the intensity on the ram angle, the angle of incidence between the spacecraft surface normal and the velocity vector, the Orbiter was purposely rotated about the x axis on the STS-5 mission. For a relatively large angle between the velocity vector and the surface normal there is an appreciable glow, provided the surface is not shadowed by some other spacecraft structure. As the angle becomes less the glow intensifies. Material samples were also exposed in the ram direction during nightside orbits and the glow surrounding the samples was photographed. The glow intensity varied depending on the nature of the sample surface. The thruster-induced light was also investigated in an experiment. Thrusters were initiated individually and the resulting luminosities were recorded by photographic and television techniques. These results show that the largest optical disturbance is created by the downward firing tail thrusters (-ve pitch) presumably because these thrusters fire towards the Orbiter wing which then thermalizes the exhaust gases by collisions. On the STS-8 mission when the altitude was 220 km the thruster-induced spacecraft glow was found to decay with a time constant which is 1/5th of the time constant obtained on STS-3. More recent data featured resolved spectrum and imagery of the glow with spectroscopic resolution of 31 Å FWHM between 4000 and 8000 Å. The spectrum of the glow on the shuttle tail pod could be clearly separated from spectrum of the reflected light from the Orbiter. From the measurements it is clear that the spectrum of the glow is a continuum in the passband of the instrument. Analyses have been performed which strongly suggest the emission originates from recombination continuum of NO₂. The spectral shape of NO₂ emission is highly variable with recombination process according to numerous laboratory studies. The spectral shape of the observed continuum may be the result of the recombination process involving surface-bonded NO and fast ram O atoms. If the recombined NO₂ retains 10% of the kinetic energy of the ram OI, the thickness of the glow layer can be explained by the lifetime of NO(2B2) continuum. Previous satellite mass spectrometer measurements show that adequate NO₂

is generated on spacecraft surfaces and that the recombining NO is produced by the reaction of atmospheric atomic N and O.

Introduction

The apparent vehicle glow of the space shuttle was detected during the flight of STS-3 [Banks et al., 1983]. Although the shuttle glow was not specifically predicted it has now been associated with other spacecraft glow which was shown to surround free flier satellites such as the Atmospheric Explorer [Torr et al., 1977; Torr, 1983; Yee and Abreu, 1983]. Specific investigation of the shuttle glow was started on STS-4 when a transmission grating was mounted in front of a photographic camera and several exposures were taken on-orbit to make preliminary spectral measurements of the spacecraft glow [Mende et al., 1983]. The space shuttle observations have also reported glows associated with thruster firings.

The physical process leading to the glow phenomenon is relatively poorly understood at present. Programs such as Space Telescope, IRT and other optical facilities can be planned and optimized around ram glow phenomena given an understanding of the physical process. These planning considerations can include operational restraints with respect to telescope ram during observations, orbit altitude, instrument baffle materials and coatings, and surface conditioning of the Orbiter (for shuttle payloads).

The AE-E satellite was equipped with a Visual Airglow Experiment (VAE) which observed atomic and molecular features in the Earth's airglow layer. Backgrounds in the photometer filter channels were found to have a variability with ram angle. These data were reported by Yee and Abreu [1982, 1983] and displayed a detectable level of luminosity in the near UV channels of the instrument (3371 Å) with increasing luminosity towards the red wavelengths (7320 Å). The background in all filter channels, when plotted, described a bright ram source, increasing in brightness toward the red wavelengths. The analysis presented suggested the glow extended well away from the spacecraft alluding to the probability the emitter is metastable. OH Meinel bands were reported as being a likely candidate species for emission since the general red character and emission lifetime seemed to fit the evidence. The Yee and Abreu [1982] analysis had found a strong correlation between the ram emission intensity and altitude. The emission intensity closely followed the atomic oxygen scale height above 160 km altitude. Atomic oxygen then is the probable aeronomical constituent to be a chemical catalyst for whatever process is occurring. Slinger [1983] was among the first to report the OH hypothesis.

The DE-B spacecraft was equipped with a high resolution Fabry-Perot Interferometer (FPI) [Hays et al., 1973]. In this instrument, a 7320 Å filter was utilized in series with the Fabry-Perot etalon. Abreu et al. [1983] reported on the background with ram effect associated with this channel. A ram glow was reported and the deduced etalon spectrum showed similarity with the OH spectrum observed in nightglow from the atmospheric limb. The available evidence from these two spacecraft seems to favor the OH hypothesis for the observed glows.

High resolution spectral measurements of the ISO spectrometer on Spacelab 1 show the presence of N₂ 1PG bands [Torr and Torr, 1985]. There are also a number of other observed emission features which may be

part of the natural aurora airglow background environment and therefore may not be part of the shuttle glow. There are no associated imaging data with the ISO measurements and therefore the precise determination of the source of the emission could be difficult.

Green [1984] recently reviewed the ram glow data and theory for the shuttle environment. The review described the two classes of mechanisms, one being molecular emission from surface collisions and another due to the plasma critical velocity effect. In his discussions vibrationally excited CO, OH, or electronically excited N₂ were postulated as most likely candidates and were chemically plausible² with the evidence at hand.

There is a proposed plasma process for glow production [Papadopoulos, 1983] which involves a two-stream instability between incoming ram and reflected ions. The ion instability sets up an electrostatic wave which in turn heats the ambient electrons. The energetic electrons can in turn excite in situ and ramming constituents. Pumping the electrons to 20+ eV will allow e + X reactions. The energy is sufficient to excite N₂ to 2nd positive, and possibly ionize to 1st negative. A lot of UV emissions could arise with this process whereas the chemical processes postulated are energetically limited to be red and infrared emitters. N₂ 1st negative (1,0) at 3914 Å and N₂ 2nd positive band at 3371 Å are spectral features expected for this physical process.

In this paper we shall review the measurements of the spacecraft glow which were carried out on the shuttle. Having discussed all the known measured properties of the glow we shall discuss a glow mechanism which at present seems to be the most plausible explanation of the observations.

The Dependence of the Glow Intensity on the Ram Angle

Examination of the early glow photographs from STS-3 showed that only those surfaces exhibited the glow phenomena which were in the direction of the velocity vector. In an experiment on the STS-5 mission it was verified that the glow intensity strongly depends on the attitude of the surface with respect to the velocity vector.

In the experiment during the first half of a night pass a full >360 degree roll was executed about the shuttle x axis while the orbital velocity vector was approximately in the shuttle y-z plane. The reader should note that the conventional shuttle coordinate system puts the x axis forward of the nose, the y axis out of the starboard wing, and the z axis straight down through the floor of the payload bay (e.g., see Figure 13). During the experiment photographs were taken of the tail section at 2-minute intervals to record the intensity of the glow on the shuttle tail surfaces. The resultant images are presented in Figure 1.

The roll experiment started just prior to the taking of the first picture at 16 hours and 33 minutes Mission Elapse Time (MET). The velocity vector at this time is out of the port and upward directions as shown by the arrow on Figure 1. Two minutes later at 16:35 the shuttle has rolled and the velocity vector is now essentially at about 35 degrees above the -y axis (port wing). This can be verified because one can see the shadowing caused by the engine pod on the port side. At

16:37 the velocity vector dipped below the horizontal (x-y plane) at about 50 degrees and there is only a faint glow remaining on the port side of the stabilizer. The pictures taken at 16:39 and 16:40 show no glow at all because the velocity vector is from the bottom up and all the surfaces to be photographed were shadowed.

On each photograph the approximate direction of the velocity vector is indicated. The direction of the velocity vector was first calculated from Orbiter data provided by the Johnson Space Center. The time code on each picture is only accurate within a minute and therefore the accurate value of the velocity vector for each photograph had to be interpolated from the position of the stars. By using a frame taken at 16:35 (Figure 1) we can establish the direction of the velocity vector fairly accurately from the shadowing of the engine pod. By comparison with a star atlas we could establish the rotation angle with respect to the rotation angle for each exposure in the star coordinata system. Since the velocity vector was essentially in the y-z plane the rotation of the stars gave a fairly accurate value for the angle of the velocity vector. Note that correction had to be made for the change of the direction of the velocity vector due to the orbital motion which amounts to approximately 4 degrees per minute.

The relative magnitude of the glow intensity could be obtained by microdensitometry of the original negative films. Tracings were made to measure the density of the glow luminosity on the tail section. This density was turned into equivalent exposure and the result are presented on Table 1.

TABLE 1. THE RELATIVE INTENSITY OF THE STS-5 STABILIZER GLOW

Time Code	Net relative exposure	Side	Angle of Velocity to surface normal	Cosine of angle
13:16:33	38	Port	80 deg.	0.17
13:16:35	89	Port	28 deg.	0.88
13:16:37	tail in shadow		-50 deg.	
13:16:37	tail in shadow		-97 deg.	
13:16:41	113	STBD	29 deg.	0.87

Unfortunately there are too few data points to draw very solid conclusions. However the numbers support the type of qualitative conclusions one was able to draw from the pictures. The intensity of the glow is not strictly proportional to the cosine of the angle and therefore not proportional to the flux of incoming atmospheric constituents. It appears that very large angles between the surface normal and the velocity vector provide substantial glow, for example, in frame 13:16:33 the angle is 80 degrees to the port side of the tail. When the angle decreases to 28 degrees the increase in glow is just a little over a factor of two. It would seem that the glow detected in the last frame (13:16:41) is anomalously too bright when compared to frame taken at 13:16:35. However the explanation is clear when we examine the actual photographs of Figure 1. The glow on the starboard side is viewed tangentially presenting a much narrower and therefore brighter profile than on the portside where the glow is visible over a larger region of the tail surface. If we were to integrate the glow over the larger region no doubt the overall intensity would be of the same order as the

more tangential view of the starboard side for the same angle. The comparison between the two sides is clearly dependent on the detailed geometry of the problem and we have not pursued this in greater detail.

The conclusion that the glow intensity is not proportional to the cosine of the ram angle signifies that the glow is not directly proportional to the incoming flux of atmospheric particles showing that incoming particles at large ram angles are more likely to produce glow than particles at normal incidence.

The Dependence of Glow Intensity on Shuttle Altitude - Comparison of the STS-3 and STS-5 Glow Intensities

It has been rather difficult to use shuttle data to obtain a significant measurement of the altitude dependence of the glow intensity. Using a spacecraft which has an eccentric orbit such as the AE-C provides a much better data base [Yee and Abreu, 1983]. From the AE measurement Yee and Abreu [1983] found that in the altitude regime of the shuttle, the intensity of the spacecraft glow varied in the same manner as the atomic oxygen density. Since most shuttle flights were essentially in a circular orbit the measurements were restricted to comparisons between one flight to the next. The altitude of STS-3 was 240 km. On STS-5 (altitude of 305 km) the Hasselblad camera sequence was repeated in order to generate pictures for comparison with STS-3.

A relatively good comparison is provided in Figure 2 where we present an STS-3 and STS-5 photograph side by side. In these pictures the direction of the velocity vectors is similar. Both photographs were taken by the same type of camera and the same type of lens (F/3.5). Both negative originals were processed similarly, and a control exposure wedge was used to obtain the exposure density curve of each flight film. From comparison of the two photographs of Figure 2, one can see that the glow generated density is roughly the same. This was confirmed by taking a microdensitometer trace of both images using the original negatives. However the exposure duration for the STS-3 and STS-5 photographs were 10 and 100 seconds, respectively. This would suggest a brightness ratio of the order of 10. In reality however the films exhibit reciprocity failure, and the equivalent exposure is not directly proportional to the exposure time. Using data supplied by the Johnson Space Center we could correct for the film reciprocity failure and obtain the real ratio of the glow intensities. In summary, the best estimate of the intensity ratio between the STS-3 and STS-5 glow is about 3.5. This ratio for glow intensities for altitudes of 240 and 300 km is fairly well in agreement with the trend shown by Yee and Abreu [1983] and therefore in fairly good agreement with the scale height variation of an atomic constituent such as O or N.

The Intensity of the Glow as a Function of the Distance from the Surface of the Spacecraft

From the early pictures depicting the space shuttle Orbiter it was evident that the glow appears to be standing off from the ram surfaces. The analysis of one of these early pictures [Yee and Dalgarno, 1983] shows that the standoff distance is of the order of a few centimeters from the surface. There is generally a consensus that the excited molecule is formed on the spacecraft surface and it leaves the surface

with some exit velocity. Thus the standoff distance is a characteristic parameter of the lifetime of the emitting species which is leaving the surface and emitting the glow photons.

In November/December 1983 during the Spacelab 1 mission the standoff distance of the glow was investigated. Mission Specialist Dr. O. K. Garriott took several image-intensified photographs of the tail section. Some of these images were digitized and analyzed in detail. The view of the tail from the Spacelab 1 module provides a suitable observing geometry for a close-up view of the tail. The images from this observation point give a much more detailed view of the tail and the glow on the tail. The appearance of the width of the glow layer appears to be somewhat irregular from this view. However appropriate modeling calculations were carried out using the geometry shown in Figure 3. In this calculation the shadowing of other Orbiter parts and the appropriate perspective effects were both included to show that the basic law or exponential decay with distance holds. The resulting observed curve is shown on Figure 4. An appropriate exponential curve with an exponential characteristic standoff distance of 20 cm was superimposed on the curve. Thus the characteristic standoff distance associated with the tail, which can be assumed to be a flat plate, is about 20 cm. If the exit velocity of the emitting species were known, then it would be possible to calculate the lifetime of the emission.

On the STS-5 mission a glow experiment was carried out to monitor the intensity of the glow in front of a number of material samples. The intensity of the glow as a function of the material samples will be discussed later. At this point we shall discuss the question of the possible dependence of the standoff distance on the nature of the material surface. For this experiment material samples were used to cover the remote manipulating system (RMS) arm (see Figure 11). The samples were in the form of tapes which were bonded to the arm. Image intensifier photography of the arm enabled our studying the dependence of the standoff distance with the sample of the materials.

The RMS arm is a cylindrical object with a diameter of 15 inches. In the view on the photographs the ram glow appears directly above the arm since the ram vector is from straight up (-Z) direction. Microdensitometer tracings were obtained to show the decay of the glow with distance from the arm. On Figure 5 two curves are shown. The top curve is the microdensitometer tracing associated with the glow in front of the chemglaze sample. The bottom curve represents the glow in front of the Kapton sample. The baseline brightness is the intensity representing the night sky and on the tracing left corresponds to the top of the image and right to the bottom. The RMS region is indicated being 15 inches in diameter. Note that the region of the chemglaze sample is closer to the observer and therefore the dimensions are slightly larger. The curves represent the uncorrected film density of the image. The linear distance from the arm where the intensity falls to one-half of its value is measured in each case and is indicated on the figure.

Although there is a large difference in the intensity between the two material samples the distance associated with the decay of the glow remains the same. The true intensity ratio between the glow in front of the two samples is about 3. As we have discussed previously the standoff distance is a characteristic of the lifetime of the emitting species. From our measurement it appears quite clear that the standoff distance in front of the two different material samples is the same; thus, the lifetime of the emitting species is presumably also the same.

The Spectra of the Glow

During the STS-4 mission the spectrum of the glow was recorded by an unaided Hasselblad camera using the objective grating [Mende et al., 1983]. Based on a single photograph it was derived that the spectrum of the glow consisted of a relatively diffuse spectrum primarily at the red-infrared end of the visible spectrum. Although it was hard to obtain quantitative information from this glow spectrum it seemed to be most intense in the region between 6300 Å and the window cutoff at 8000 Å. Because of the lack of sensitivity of the unaided F/3.5 camera and the unfavorable direction of the velocity vector, long exposure duration (400 seconds) was required.

On STS-5 the intensified camera permitted the taking of short exposure grating spectra. Unfortunately the STS-5 spectral results are not spectacular because the direction of the velocity vector was unfavorable during the time the grating exposures were taken. An additional problem was the presence of the Earth near the field-of-view producing a strong unwanted background.

The first truly successful objective grating glow spectrum was obtained on STS-8 in September 1983. One of the objectives of this experiment was to obtain a good signal-to-noise ratio objective spectrum of the tail glow. The velocity vector was aligned with the Orbiter y axis (this direction is in the direction of the starboard wing). Five exposures were taken with the grating in position and the lens set at F/2.8. The durations of the five exposures were 8, 4, 1, 1/4, and 1/15 second, respectively. The 1-second duration exposure is reproduced in Figure 6. The glow illuminated the starboard side of the tail and the starboard engine pod. These can be observed most clearly in the right side of the picture where the zero order image is located. The horizontal streaks on the photographs are the first-order images or spectra of stars. Some stars have both their zero-order point images and their first-order spectral streak images in the picture. The large diffuse image a little left of the center is the first-order or spectral image of the glow. Approximate wavelength scale was superimposed on the frame.

From Figure 6 it is qualitatively evident that the shuttle glow is spectrally diffuse. It is also clear that there is very little glow in the wavelength range of 4300 to about 5000 Å. In the range above 5000 Å the glow becomes more intense falling off towards the higher end presumably due to the falling response of the image intensifier photocathode [Mende, 1983].

In the spectral image of Figure 6 there is an apparent line emission. This is evident because of the presence of a well-defined image of the tail in first order. Since it is a well-defined image its wavelength can be derived fairly accurately. Within the accuracy of the measurements the wavelength of this feature was found to be 7600 ± 50 Å. This suggests that the observed emission is scattered airglow in the O_2 atmospheric airglow band at 7619. There is other evidence that this feature is not part of the spacecraft glow. Close examination of the figure will reveal that the first-order image is equally bright on both sides of the tail while the glow in the zero-order image is very much brighter on the starboard side. Only extended scattered light sources could provide equal luminosity on both sides of the tail. Our previous

results [Mende, 1983] already shows that the 7619 \AA component of the airglow is the most intense airglow component reaching several hundred kilorayleighs in the limb view.

In view of the state of knowledge it was essential to obtain spectral data with improved resolution and with simultaneous documentation of the spatial extent of the glow source region. For mission 41-D a special glow spectrometer was constructed. The instrument has three operating modes. The three modes are schematically illustrated in Figure 7. The top illustration shows the instrument with the grating and slit out of the optical path. In this mode the intensifier camera works in a straight through imaging mode with a real image formed at the plane of the slit by the objective lens. A permanent targeting slit is superimposed on the image to provide a fiducial for aiming the system. The image is then collimated by the collimating lens and refocused on the image intensifier photocathode by the camera objective lens. The image intensifier has a light amplification gain of 50,000. The output phosphor of the image intensifier tube is re-imaged on the film or in the viewfinder of the 35-mm single lens reflex camera attached to the system. The observer looking through the viewfinder will see the targeting slit superimposed on the image. In this mode the astronaut is able to point the instrument and accurately document the position of the spectral slit on the image. The second mode shows the spectrometer with the grating in the optical path. In this mode the grating produces an objective spectrum. In addition to the image which was produced in the previous mode another image, the first-order image, also appears. The distance between the two images is proportional to the wavelength of the light forming the image. This type of slitless objective grating was used for previous glow investigations by Mende et al. [1983], Mende [1983], Mende et al. [1984].

The third mode represents the high resolution spectrographic mode. In this mode the slit covers are also placed into the optical train. They cover up the image except the narrow slit formed by two parallel bars of the targeting slit. In this mode the system is equivalent to a transmission grating spectrometer with grating rulings of 300 lines per mm. Three identical lenses were used all three were F/1.4 f=50 mm. The slit width was 0.0508 mm.

The theoretical resolution $d\lambda$ of the spectrometer with a 300 line per mm grating can be estimated as:

$$d\lambda = 1/3000 * \sin (0.0508/50) \text{ (cm)}$$
$$d\lambda = 34 \text{ \AA}$$

The reference photographic image of the shuttle tail and engine pods is shown on Figure 8 taken on September 4, 1984, at 17 34 50. In this image the targeting slit was superimposed on the tail section, the engine pod, and a bulkhead in the payload bay. The slit crosses some other areas on the Orbiter skin which are also somewhat luminous. The sources of the light on the Orbiter are the glow, reflected airglow, or starlight.

The corresponding spectrum taken with the grating and slit in the optical train is shown on Figure 7 (17:36:01). From the comparison of Figures 6 and 7 spectrum of the glow and the Orbiter surfaces may be identified. Starting from the top of the photograph, the top region is the spectrum of the bulkhead. This shows two distinct lines. From the

preflight calibration of the wavelength dispersion these lines are clearly identified as atomic O at 5577 Å and the O₂(0,0) band at 7620 Å. It may be seen that while 5577 is a narrow spectral line showing up as a thin line, the O₂(0,0) band is quite wide representing the larger wavelength extent of the O₂(0,0) band. This demonstrates that the observed luminosity on the Orbiter is mainly due to scattering of the Earth's airglow.

Microdensitometer tracings of this glow were obtained and the calibrated intensity response of the film was applied to the measured film density and plotted in Figure 10 (bottom curve). The curve was corrected for device responsivity by using the preflight calibration data obtained from a light source of known emissivity as a function of wavelength and is also shown in Figure 10 (top curve). The corrected curve represents a normalized intensity of the source emission.

The measured spectral responsivity of the spacecraft glow on STS 41-D shown in Figure 10 is very similar to the result found on STS-8 [Mende et al., 1984b], both of which show a peak near 7000 Å. Our approach of using the spectral slit in this instrument eliminates the contamination of earlier results by the scattered airglow and leaves no doubt about the absence of any distinct spectral features in the spectrum of the spacecraft glow.

The experiment data show quite conclusively that the spacecraft glow has a continuum spectra within the spectral resolution of the instrument. It shows that the glow is not simple atomic or molecular band spectra. Considerations of the thickness of the glow layer around the spacecraft and associated lifetimes of the excited states exclude the possibility of a many-component molecular spectra produced by a wide variety of emitting materials. Thus we need to look for a single component which has a complex continuum spectra. Emission continuum is rare in molecular systems. The most abundant elements in the ramming atmosphere are OI and N₂ and the simplest combination of these constituents producing a continuum is NO₂. Heppner and Meredith [1958] reported seeing an NO₂ continuum in a rocket wake. The suggestion that spacecraft glow could be caused by NO and O recombination was made by Torr et al. [1977] in connection with the emissions observed on the Atmosphere Explorer (AE) satellite. However this suggestion was discarded in favor of other mechanisms because the observed glow spectrum did not totally agree with laboratory spectrum.

The measured spectrum of the spacecraft glow on STS 41-D shown in Figure 10 portrays the same features as those reported on STS-8. A peak is obtained around 7100 Å with a gradual fall off towards both the short and longer wavelengths. The approach of using the spectral slit eliminates the contamination of earlier results from scattered airglow and leaves no doubt about the absence of any distinct spectral features in the spectrum of the spacecraft glow.

In a recent report of Torr and Torr [1985], a high resolution spectrum of the glow taken by the Spacelab 1 ISO instrument was published. The ISO spectrum was taken while the Orbiter and atmosphere were in full sunlight, and the instrument was looking directly into the ram. Since many features of this spectrum were attributable to natural airglow and vehicle glow in front of and within the instrument it might be very fruitful to compare the two spectra. Since the resolution of the ISO instrument is 6 Å it would be desirable perhaps to convolute the ISO spectrum with a 35 Å slit width prior to comparison. Nevertheless even

without such a convolution it seems evident that the two spectra are somewhat dissimilar.

Glow Intensity Dependence on the Spacecraft Surface

The dependence of the glow intensity on the nature of the spacecraft surface was investigated on STS-5 and 41-D missions. In the STS-5 experiment the Orbiter velocity was aligned parallel to the Orbiter-z axis (this direction is vertically up in the Orbiter bay). The material samples were photographed with the intensifier camera without the grating. First samples mounted on the remote manipulator system (RMS) arm were photographed with varied exposure times. The material samples on the RMS arm were mounted in the form of 4-inch-wide tapes. The layout of the tapes was selected to maximize the "limb glow" over the curvature of the cylindrical arm. The layout is illustrated photographically in Figure 11a. This picture was taken prior to flight. The samples are in the following sequence: kapton, aluminum, black chemglaze, aluminum, and kapton. The samples were repeated in order to avoid the possible ambiguity caused by the slightly different geometry of the different view angles of the samples.

Kapton was chosen because of its known high weight loss property in shuttle orbital environment, aluminum was chosen because of its known stability, and black chemglaze (carbon filled, urethane based, matt black light absorbing paint) because of its application in low light level detecting devices [see image intensified photograph (Figure 11b) of the RMS arm with the material samples]. The glow above the chemglaze is stronger than the glow above the other materials. Aluminum glows the least. The kapton samples and their associated glow are indistinguishable from the covering material of the arm. This photograph is the first solid evidence that the spacecraft ram glow depends on the material surface properties of the spacecraft.

This experiment was essentially repeated on the 41-D mission with nine different material samples. Unfortunately mission 41-D flight was combined with another mission and the replanned mission did not fly at the desired altitude of 220 km. Instead the altitude for 41-D was close to 300 km which reduced the signal-to-noise ratio in the experiment to barely detectable levels. The camera was in the spectrometer configuration and was aimed so that the slit was perfectly parallel with the arm. Due to the weakness of the image, the glow within the slit could not be analyzed. To obtain the best data we used the region between the slit and the arm. Since the glow was very faint, the comparison proved to be very difficult.

Microdensitometer tracings parallel with the arm were obtained. The first tracing shown in Figure 12 included the region of the glow which is between the black bar of the targeting slit and the arm. Another densitometer tracing was taken of the night sky just above the slits. This night sky tracing was used as a basis for correction because of a non-uniform response in the system.

Figure 12 shows the uncorrected microdensitometer tracings, the position identification of each material sample, and a horizontal bar representing averaged glow intensity above the sample. The intensity above the sample was corrected for the apparent non-uniformity derived from the night sky trace. The correction resulted in an increase of the glow intensities above the material samples on the left side of the

image. The corrected values were represented by the upper horizontal bars. It is interesting to note our corrections are consistent with visual observations of the flight crew. During the performance of the experiment the crew reported that the samples furthest to the left of the image were glowing the most intensely.

Based on the data obtained from the 41-D experiment (Figure 12) the materials samples were ranked from 1 to 9 in order of their glow producing properties from minimum to maximum, respectively.

One was assigned to polyethylene and nine to the apparently brightest glowing Z302 overcoated with Si. However the marginality of the signal-to-noise ratio makes it difficult to draw strong conclusions.

It has been well established that the spacecraft glow is generated by emission from metastable molecules which had been excited on the surface of the spacecraft. There are several possibilities regarding the source of the metastable molecules. These molecules could be resident on the surface as contaminants. In that case, however, one would expect the glow intensity greatly variable depending on the length of the on orbit exposure or the temperature of the surface. No such evidence has been reported so far. One would also expect adjacent surface samples to be contaminated equally; therefore no surface material specific glow intensity would be expected. Another source of the molecules could be the bulk surface material. This contradicts the evidence discussed by Mende et al. [1984] where it was reported that on STS-8 the intensity of the glow in front of the kapton sample was much less than in front of the chemglaze sample and the depletion rate of kapton was much higher than that of the chemglaze. We can draw similar conclusions from the 41-D experiment. For example the chemically stable MgF2 sample exhibits intense glow characteristics. Polyethylene seems to produce the least glow. All these results point to the fact that in the glow production the surface accommodation property of the sample is important and not the chemical stability of the bulk material. Thus it can be deduced that the surface acts as a catalyst. The source of the metastable molecules producing the glow must be the environment itself.

Thruster Firings and Associated Glow

It was discovered on the early shuttle flights that the firing of a shuttle thruster creates a great deal of observable light [Banks et al., 1983]. This effect was thought to be the result of the unburned fuel combining with the ambient atomic O. It was also observed that in addition to this spontaneous light emission after a thruster firing, there is also a marked enhancement of the spacecraft ram glow. To investigate the effects of the various thrusters an experiment was performed on the STS-8 mission. In this experiment the camera was opened for 2 seconds. During the exposure a selected thruster was fired for a minimum single impulse by manual operation of a crew member. There are six vernier thrusters on the Orbiter (Figure 13); some of them can be operated singly while others are usually operated in pairs. Four different combination of thruster firings were performed and the results photographed. A 2-second duration background exposure was also taken between each thruster firing to assure that all thruster effects disappeared prior to the next firing. The results are shown in Figure 14 in the form of a collage of the photographic images. The top left picture represents the background image with no thruster firings.

Since the camera was in the objective grating configuration and the Orbiter attitude was such that the velocity vector is from the direction of the starboard wing, this picture is identical to Figure 6. Note that the only thruster which has a noticeable effect on the picture background is the downward firing tail thrusters. The following explanation can be provided. The downward tail thruster is directed towards the wing. The gases emitted by the other thrusters leave the vicinity of the Orbiter with their emission velocity, however, the downward tail thrusters throw their output on the wing where the gases thermalize and will take up the velocity of the spacecraft. This luminous cloud will travel with the spacecraft.

The time development of the thruster firings can be best studied by means of the Orbiter closed-circuit TV cameras. A thruster firing event documented by the orbiter TV cameras on video tape are included in Figure 15. To aid in the timing of the event a time counter which ran in seconds and one-hundredth seconds was superimposed on the frames. The status of this time counter provided a unique identification of the TV frame. The first image at time is a background frame at :53:32. The second and third images show the thrusters while in operation. The following frames show the decay of the glow on the engine pods which persists well after the thrusters had been shut off. The TV sequence (Figure 15) was taken on mission STS-8 at an altitude of 220 km.

Figure 16 shows the thruster-induced glow intensity as a function of time. This was obtained by integrating the video signal from all pixels inside of a rectangular area which includes the glow on the port side engine pods. This integrated signal was plotted by a chart recorder. Note that the video signal may include a number of relatively unknown parameters such as the signal non-linearities and the time response characteristics of the television system. Nevertheless the effects of these parameters on our conclusions are believed to be negligible. Two observations were plotted in Figure 16. The top one is from the low-altitude portion of STS-8 at 220 km altitude and the bottom is from STS-3 [Banks et al., 1983] at 240 km altitude. The decay is considerably longer for the low-altitude case.

Discussion

Understanding of the spacecraft glow is important because it may shed light on unanticipated upper atmospheric chemical and physical processes and the spacecraft glow has also its practical significance as a contaminant to light-sensitive instrumentation.

The spectral results of mission 41-D are not altogether new. From previous measurements STS-4, STS-5, and STS-8 we have come to realize that the spacecraft glow had a continuum spectra and was devoid of significant lines. The present results are confirming these findings and have yielded high enough signal-to-noise ratios to permit quantitative interpretation of the emissivity as a function of wavelength. Preliminarily we can say that the spectra of the glow shows relatively little emission intensities below 500 nm and above this the emissions reached a peak between 600 and 700 nm. Without more quantitative densitometry it is hard to interpret the data any further. The basic shape of the spectral content is of course no surprise when we look at the color photos with the orange-red images of the spacecraft glow.

Perhaps it is even more significant to mention that there are no distinct spectral features in the spectrum. From the observation of the reflected airglow light at 557.7 nm and 762.2 nm we can see that the instrumentation is fairly sensitive to distinct line emissions, had they been present.

We have examined many of the properties of the shuttle glow. It is now our task to examine the theoretical ideas which are consistent with the above findings.

From our new observations of the continuum emission from the shuttle and from the realization that the NO_2 recombination spectrum is largely variable depending on the reaction conditions and the catalyst, we strongly suggest that the shuttle glow is produced by NO_2 recombination continuum. It has been suggested by Green [1984] that N_2 molecules having a collisional energy of 9.3 ± 2 eV are capable of dissociating on the surface (dissociation energy is 9.8 eV). In the simplest picture the reaction $\text{N} + \text{O} = \text{NO}(\text{B}_2)$ takes place on the surface where the ambient $\text{OI}(3\text{P})$ originates from the atmosphere. Reeves et al. [1960] found this to occur in laboratory experiments when NI and OI were mixed. They found that the $\text{NO}(\text{B}_2)$ was formed and the associated beta band emission was observed in their wall catalysis experiment with N and O atoms. If a significant portion of the formed NO remains in contact with the wall, then the NO would be exposed to the ramming OI . Reaction of NO with ramming OI would create NO_2 , which would be removed from the surface in the process. It is well known that the 3-body recombination is efficient for NO and OI , i.e., $\text{NO} + \text{OI} + (\text{M}) \rightarrow \text{NO}_2 + (\text{M})$.

The spectrum shown in Figure 10 has many similarities to that published by Fontijn et al. [1964]. In Figure 17, the spectrum is replotted and compared with the Fontijn et al. measurement. The Fontijn et al. measurement of NO_2 continuum was produced when NO was mixed with OI where the OI was produced with a microwave discharge. Their published spectrum was acquired by viewing end-on into a 2-cm-diameter by 20-cm-long vessel. Paulsen et al. [1970] performed an experiment which also measured the NO_2 continuum in recombination as well as that continuum produced with thermal emission with gas temperature between 900 K and 1335 K. In their experiment, they found the peak of the recombination continuum at 6400 Å also but found some discrepancy at red wavelengths between their spectrum and that of Fontijn et al. The Paulsen et al. spectrum is also plotted in Figure 17. It is clear that the laboratory spectrum is not within the error of the measured spectrum produced here.

Recombination spectrum also can be very different in shape dependent on the recombinant species. $\text{NO} + \text{O}_3$ produces a spectral peak near 1.2 microns [Greaves and Garvin, 1959]. With excited O_3 , the recombination shifts to the blue proportionally with the internal vibration state of O_3 [Braun et al., 1974]. Recombination with O_2 [Kenner and Ogryzlo, 1984] produces a recombination continuum which peaks near 8000 Å. The continuum populated thermal distribution peaks > 1 micron [Paulsen et al., 1970]. The recombination of ramming OI atoms with a surface monolayer of NO has not been studied in the laboratory. Golomb and Brown [1975] found laboratory evidence for thermal effects on the spectral shape of the OI recombination spectrum at low temperature (200-350 K range). They found a trend with the blue portion of the continuum to decrease with increasing temperature. They also found the peak of their spectrum at 6800 Å which is the same as that measured on the shuttle. The effect

of the ram velocity may be responsible for considerable alteration of the observed spacecraft spectrum. An equivalent temperature for ramming OI is ~100,000 K.

NO₂ has a complex vibrational structure which has been widely studied in recombination experiments. Upper state mixing of NO₂ can occur, likely between the 2B1 and 2B2 states. The complex upper state population has been described by Neuberger and Duncan [1954], Douglas [1966], Paulsen et al. [1970], and Gangi and Burnelle [1971]. Very short lifetimes in the blue and red have been only reported in thermal production of the continuum [Paulsen et al., 1970]. It has been assumed here that the upper state of NO₂ in recombination with OI(3P) has a representative lifetime as found in fluorescence and the values found by Schwartz and Johnston [1969] are valid.

The NO₂ continuum is a superposition of many states. The resultant average lifetime of NO₂ in fluorescence is ~80 microseconds at 5500 Å and decreases in the blue to ~60 microseconds at 4000 Å according to Schwartz and Johnston [1969]. It was previously reported by Yee and Dalgarno [1983] that the effective e-folding distance in the glow from the surface is ~20 cm. This has been reverified as discussed here for several STS-9 glow images. If the emission is represented by the red-green wavelengths of emission, the average lifetime would be ~70 microseconds. If we assume $x = t \cdot v$ [Yee and Dalgarno, 1983], where $x = 20$ cm, we would infer that the exit velocity from the surface would be ~2.5 km/sec (<1/3 the ram velocity) if NO₂ were the emitter. This corresponds to an effective exit temperature of 10,000 K. This is ~25% the ram energy of OI yet considerably higher than the expected surface temperature of near 300 K. In the process of producing the NO₂ then, total thermal accommodation of the OI does not occur.

Most of our photography took advantage of the oblique viewing of the shuttle surfaces to maximize the intensity. A preliminary estimate of the STS-8 glow intensity would suggest between 10 and 100 kilorayleighs for these oblique views. For viewing the glow in a direction normal to the shuttle surfaces, we estimate the intensity to be in the 1 to 10 kilorayleighs category. Assuming that it is of the order of 5 kilorayleighs, then the total number of radiating particles is 5×10^9 per cm⁻² of the surface area.

The oxygen density was estimated to be 2.3×10^9 cm⁻³ for the STS-8 flight (Hedin, private communication, 1983). The spacecraft velocity of 7.3 km/sec yields a total O flux of 1.7×10^{15} cm⁻². Accordingly if the glow is caused by the O flux incident on the spacecraft, then approximately one in 10^6 O particles causes the emission of a glow photon.

It is interesting to examine the efficiency of the NO₂ production and compare it to the total light output. The atomic N density is of the order of 10^7 per cm³ at shuttle altitude. From the mass spectrometer observations of Engebretson and Mauersberger [1979], a large fraction of this N will combine with the wall and form NO in a surface-absorbed state. There are about 2 orders of magnitude more O atoms available for the NO production. Assuming that the rate of NO production, r_{NO} , is determined by the N flux,

$$r_{NO} = N_N \cdot v \cdot \epsilon_{NO} \sim 8 \times 10^{12} \epsilon_{NO}$$

where N_N is the density of atomic nitrogen, v is the velocity of the Orbiter, and ϵ_{NO} is the efficiency for producing NO per surface impact of N. The portion of the spectrum between 4000 Å and 8000 Å of Orbiter glow from the

stabilizer corresponds to ~5 kilorayleighs of surface normal intensity. In other words, the observed photon yield to atomic nitrogen flux is ~25%.

According to Engebretson and Mauersberger [1979], the efficiencies for producing NO and NO₂ are high. Since each recombinant NO₂ emits in the recombination process, there appears to be adequate NO₂ production to feed the glow process.

TABLE 2. THE MATERIAL SAMPLES AND THE GLOW INTENSITY IN ARBITRARY UNITS

<u>Material</u>	<u>Ranking</u>
Mgf2	8
Z306	6
Z302 Overcoated with Si	9
Z302	7
Polyethylene	1
401-C10	2
Carbon Cloth	4
Chemical Conversion Film	5
Anodized Al	3

Acknowledgments. The authors wish to express their gratitude to personnel of the Marshall and Johnson Space Flight Centers for their support of the experiments. Special mention should be made of Mr. K. S. Clifton and Dr. R. Gause at Marshall Space Flight Center. Encouragement and help is acknowledged from Dr. P. M. Banks of Stanford University and Dr. L. Leger and Dr. O. K. Garriott of the Johnson Space Center. Helpful discussions are acknowledged with Dr. Irving Kofsky of PhotoMetrics, Inc. These series of experiments would not have been possible without the active collaboration and enthusiastic participation of the astronaut flight crews on the various missions. This research was supported by NASA through the Space Telescope program and under the Atmospheric Emissions Photometric Imager Program NAS8-32579 and by a Lockheed Independent Research Program.

References

- Abreu, V. J., W. R. Skinner, P. B. Hays, and J. H. Yee, Optical effects of spacecraft-environment interaction: Spectrometric observations by the DE-B satellite, AIAA-83-2657-CP, Shuttle Environment and Operations Meeting, Washington, D.C., 1983.
- Banks, P. M., P. R. Williamson, and W. J. Raitt, Space Shuttle glow observations, Geophys. Res. Lett., 10, L118, 1983.
- Braun, W., M. J. Kurylo, A. Kaldor, and R. Wayne, Infrared laser enhanced reactions: Spectral distribution of the NO₂ chemiluminescence produced in the reaction of vibrationally excited O₃ with NO, J. Chem. Phys., 61, 461, 1974.
- Douglas, A. E., Radiative lifetimes of molecular states, J. Chem. Phys., 45, 1007, 1966.

- Engbretson, M. J., and K. Mauersberger, The impact of gas-surface interactions on mass spectrometric measurements of atomic nitrogen, J. Geophys. Res., 84, 839, 1979.
- Fontijn, A., C. B. Meyer, and H. I. Schiff, Absolute quantum yield measurements of the NO-O reaction and its use as a standard for chemiluminescent reactions, J. Chem. Phys., 40, 64, 1964.
- Gangi, R. A., and L. Burnelle, Electronic structure and electronic spectrum of nitrogen dioxide. III. Spectral interpretation, J. Chem. Phys., 55, 851, 1971.
- Greaves, J. C., and D. Garvin, Chemically induced molecular excitation: Excitation spectrum of the nitric oxide-ozone system, J. Chem. Phys., 30, 348, 1959.
- Green, B. D., Atomic recombination into excited molecular-A possible mechanism for shuttle glow, Geophys. Res. Lett., 11, 576, 1984.
- Golomb, D., and J. H. Brown, The temperature dependence of the NO-O chemiluminous recombination. The RMC mechanism, J. Chem. Phys., 63, 5246, 1975.
- Hays, P. B., G. Carignan, B. C. Kennedy, G. G. Shephert, and J. C. G. Walker, The Visible Airglow Experiment on Atmosphere Explorer, Radio Sci., 8, 369, 1973.
- Heppner, J. P., and L. H. Meredith, Nightglow emission altitudes from rocket measurements, J. Geophys. Res., 63, 51, 1958.
- Kenner, R. D., and E. A. Ogryzlo, Orange chemiluminescence from NO₂, J. Chem. Phys., 80, 1, 1984.
- Mannella, G., and P. Harteck, Surface-catalyzed excitations in the oxygen system, J. Chem. Phys., 34, 2177, 1961.
- Mende, S. B., Vehicle glow, AIAA-83-2067-CP, Shuttle Environment and Operations Meeting, Washington D.C., 1983.
- Mende, S. B., Experimental measurement of Shuttle Glow, AIAA-84-0550, presented at AIAA 2nd Aerospace Sciences Meeting, Reno, January 1984.
- Mende, S. B., O. K. Garriott, and P. M. Banks, Observations of optical emissions on STS-4, Geophys. Res. Lett., 10, 122, 1983.
- Mende, S. B., P. M. Banks, and D. A. Klingelsmith, III, Observation of orbiting vehicle induced luminosities on the STS-8 mission, Geophys. Res. Lett., 11, 527, 1984.
- Neuberger, D., and A. B. F. Duncan, Fluorescence of nitrogen dioxide, J. Chem. Phys., 22, 1693, 1954.
- Paulsen, D. E., W. F. Sheridan, and R. E. Huffman, Thermal and recombination emission of NO₂, J. Chem. Phys., 53, 647, 1970.
- Schwartz, S. E., and H. S. Johnston, Kinetics of nitrogen dioxide fluorescence, J. Chem. Phys., 51, 1286, 1969.
- Reeves, R. R., G. Mannella, and P. Harteck, Formation of excited NO and N₂ by wall catalysis, J. Chem. Phys., 32, 946, 1960.
- Slanger, T. G., Conjectures on the origin of the surface glow of space vehicles, Geophys. Res. Lett., 10, 130, 1983.
- Torr, M. R., P. B. Hays, B. C. Kennedy, and J. C. G. Walker, Intercalibration of airglow observations with the Atmosphere Explorer satellites, Planet. Space Sci., 25, 173, 1977.
- Torr, M. R., Optical emissions induced by spacecraft-atmospheric interactions, Geophys. Res. Lett., 10, 114, 1983.
- Torr, M. R., and D. G. Torr, A preliminary spectroscopic assessment of the Spacelab 1/Shuttle optical environment, J. Geophys. Res., 90, 1683, 1985.

- Yee, J. H., and V. J. Abreu, Optical contamination on the Atmosphere Explorer-E satellite, Proceedings of the SPIE, 338, 120, 1982.
- Yee, J. H., and V. J. Abreu, Visible glow induced by spacecraft-environment interaction, Geophys. Res. Lett., 10, 126, 1983.
- Yee, J. H., and A. Dalgarno, Radiative lifetime analysis of the Shuttle optical glow, AIAA-83-2660-CP, AIAA Shuttle Environment and Operations Meeting, Washington D.C., 1983.

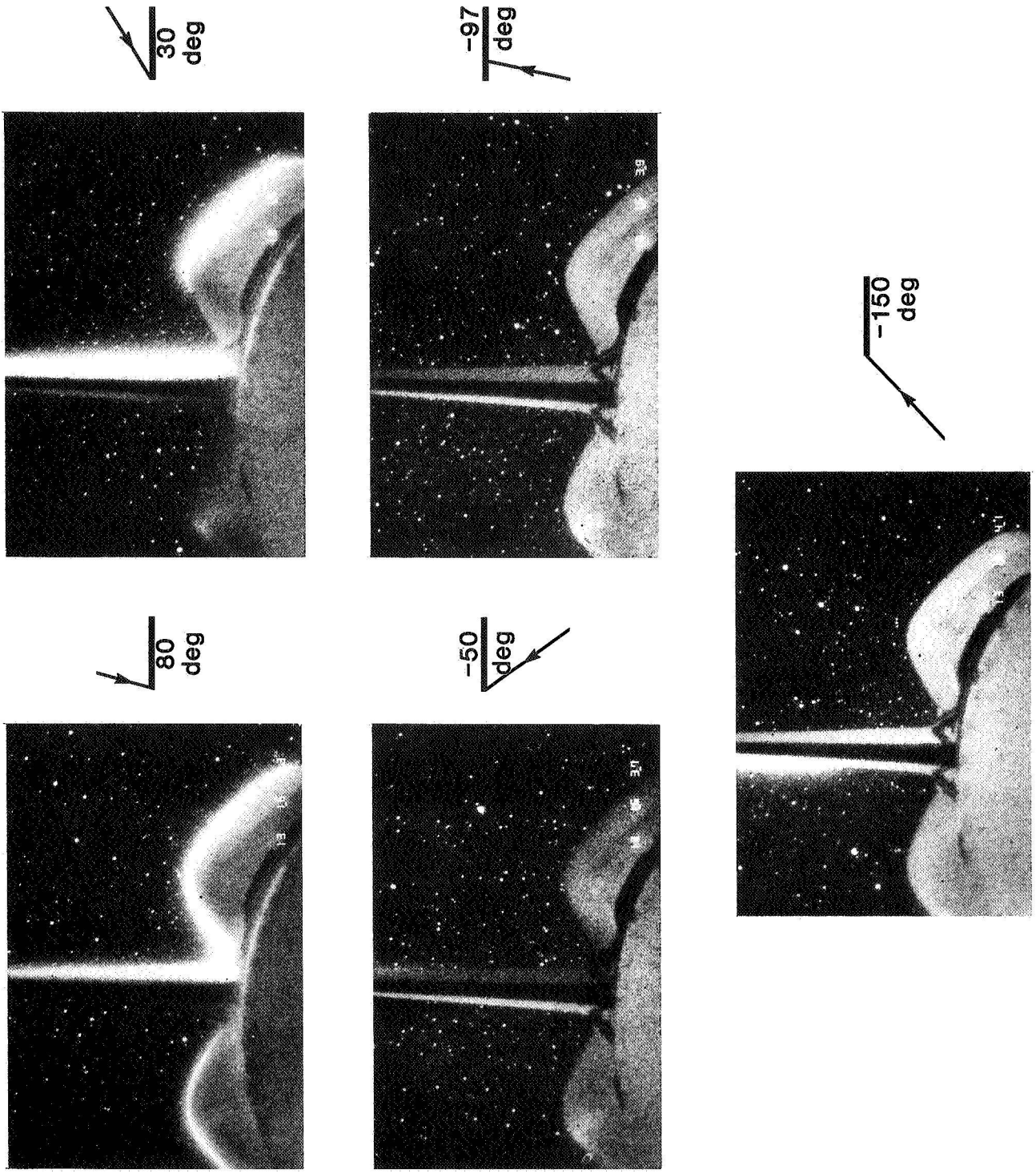


Fig. 1. The glow as appears on different parts of the Orbiter as the Orbiter rotates around the x axis.

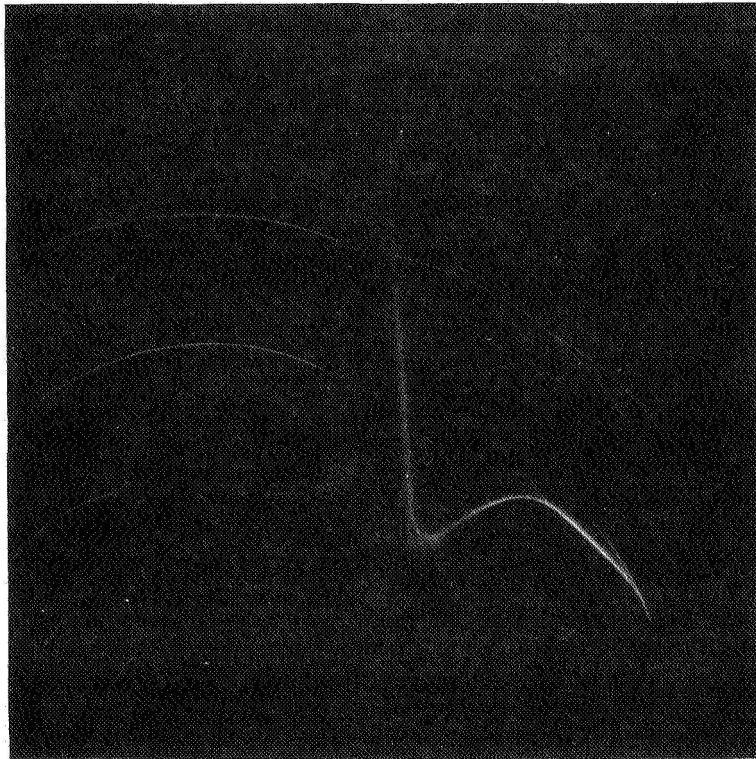
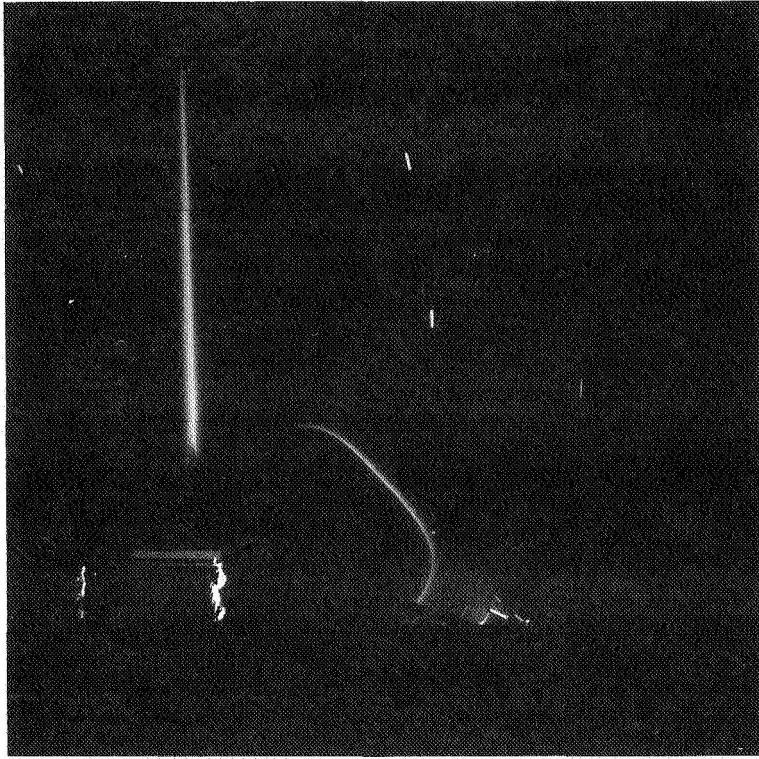


Fig. 2. Unaided Hasselblad photographs on STS-3 and STS-5. The exposure times are 10 and 100 seconds, respectively. The velocity vector is more or less from the same direction for each.

GLOW VIEWING GEOMETRY

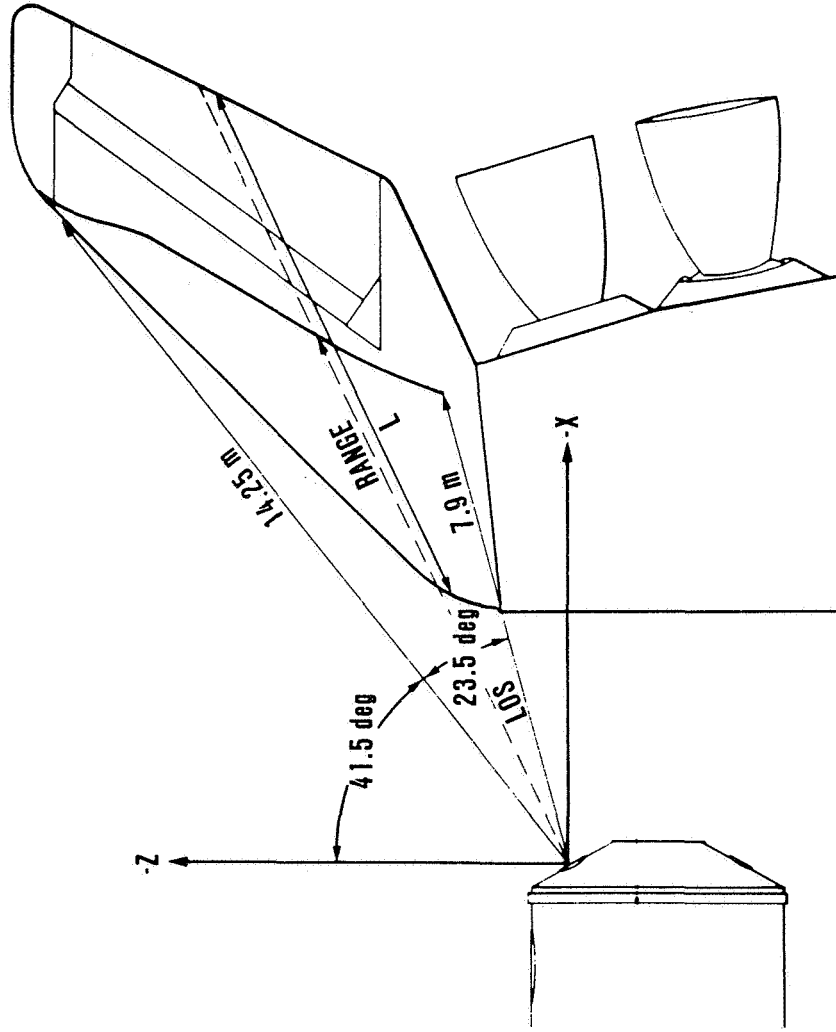


Fig. 3. The viewing geometry of the tail from the Spacelab 1 module on STS-9.

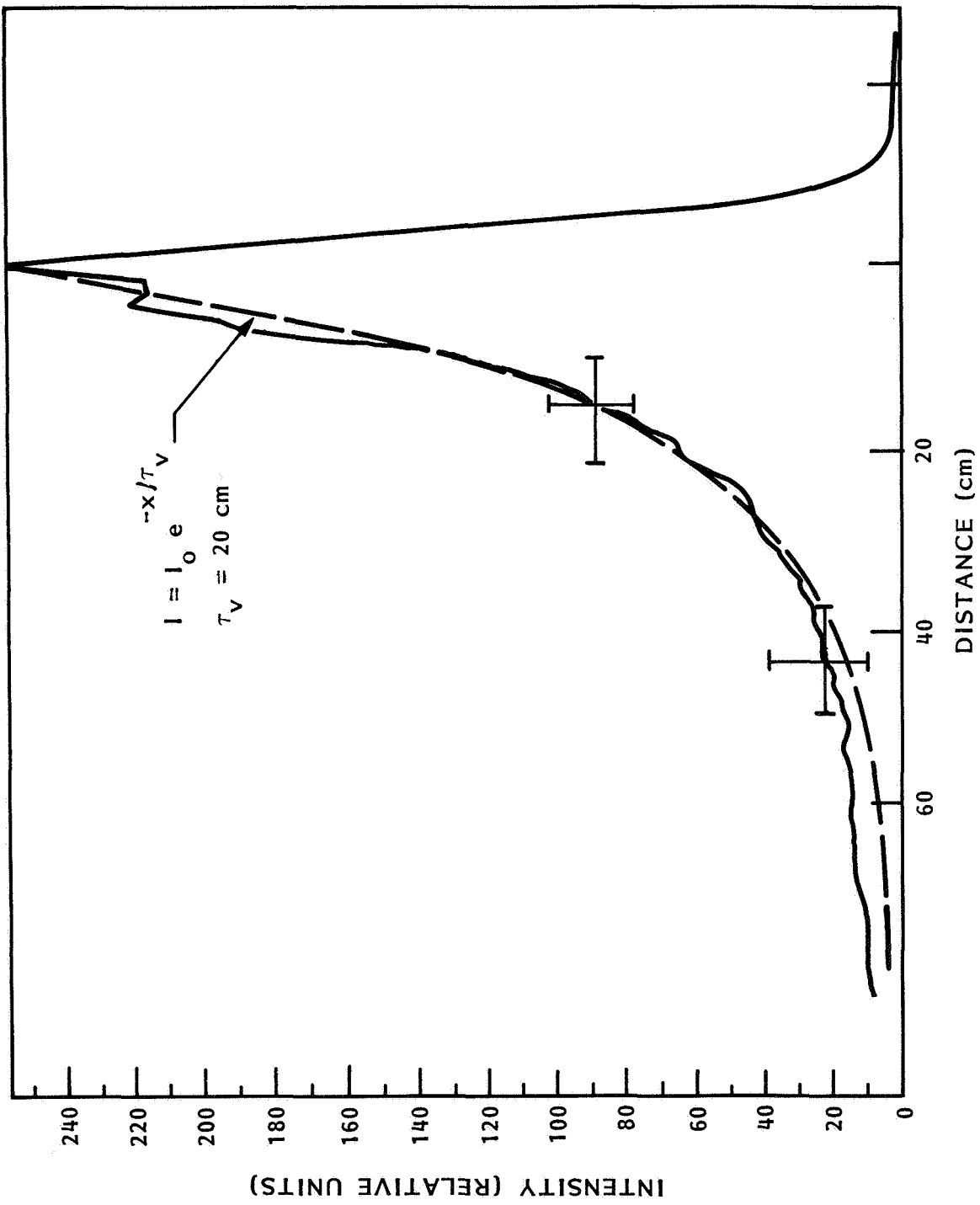


Fig. 4. Glow intensity as a function of the distance from the tail.

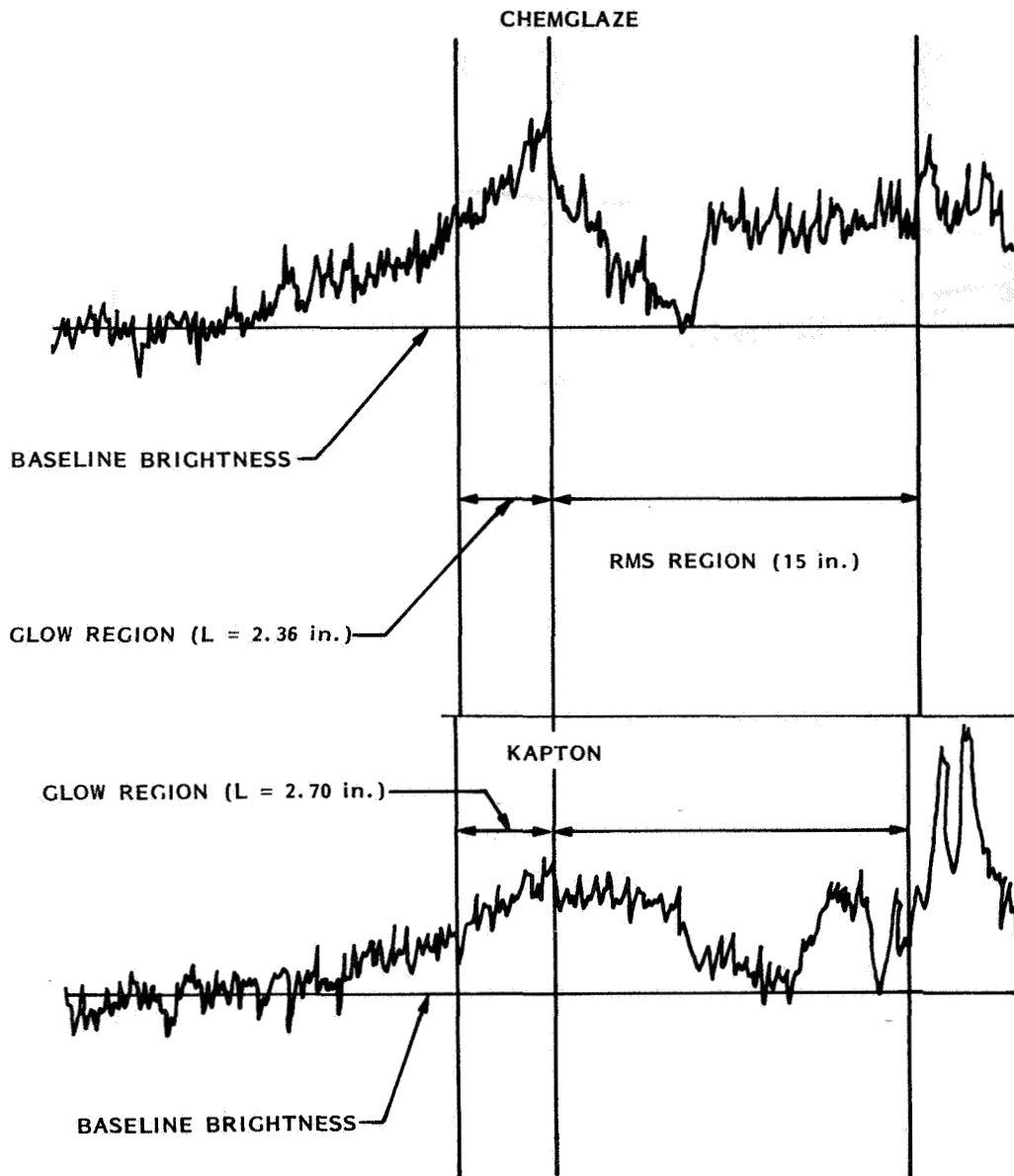


Fig. 5. Glow intensity as a function of distance from the RMS arm for two material samples, chemglaze and kapton.

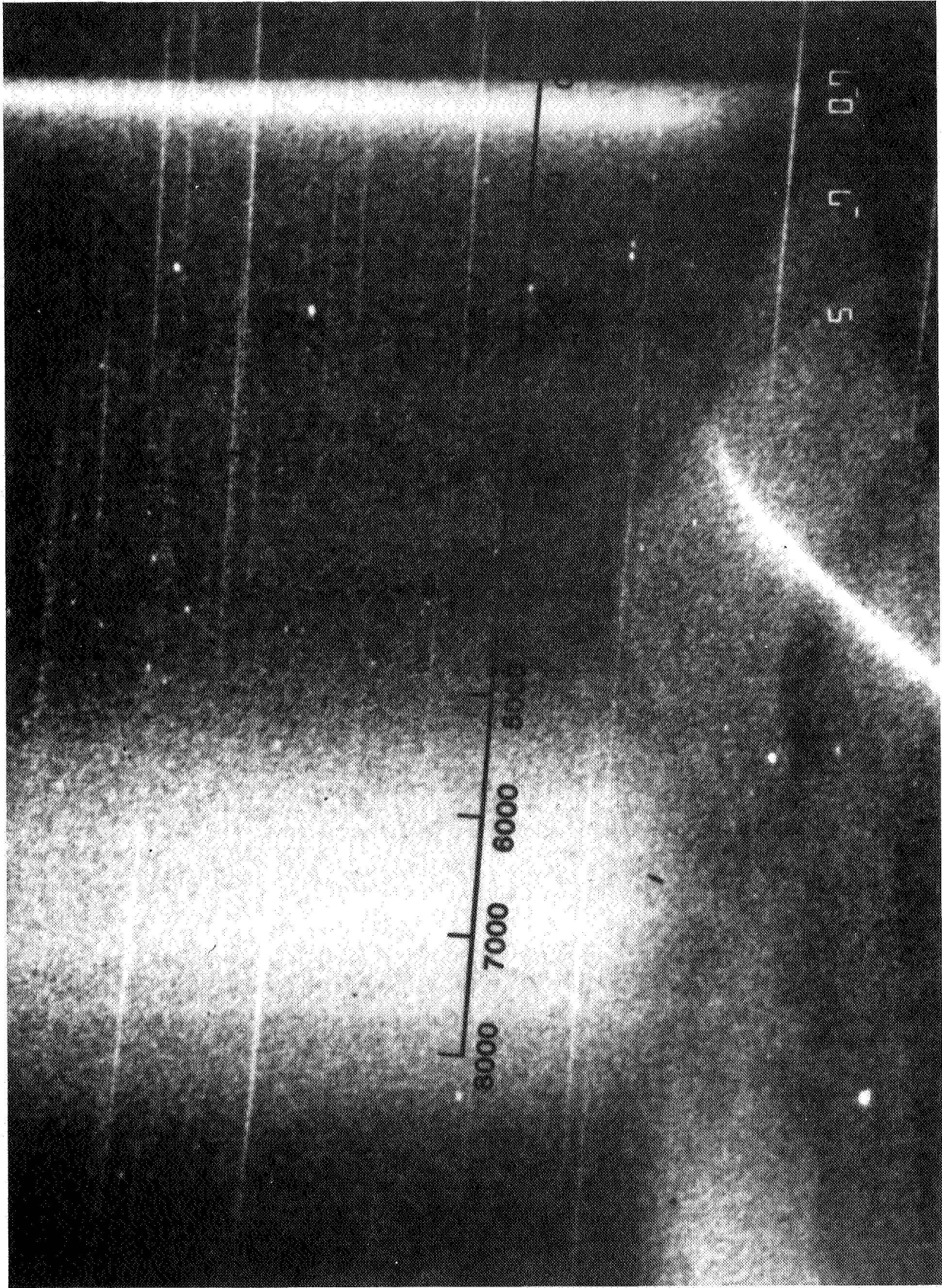


Fig. 6. Objective spectrum of the shuttle glow from STS-8.

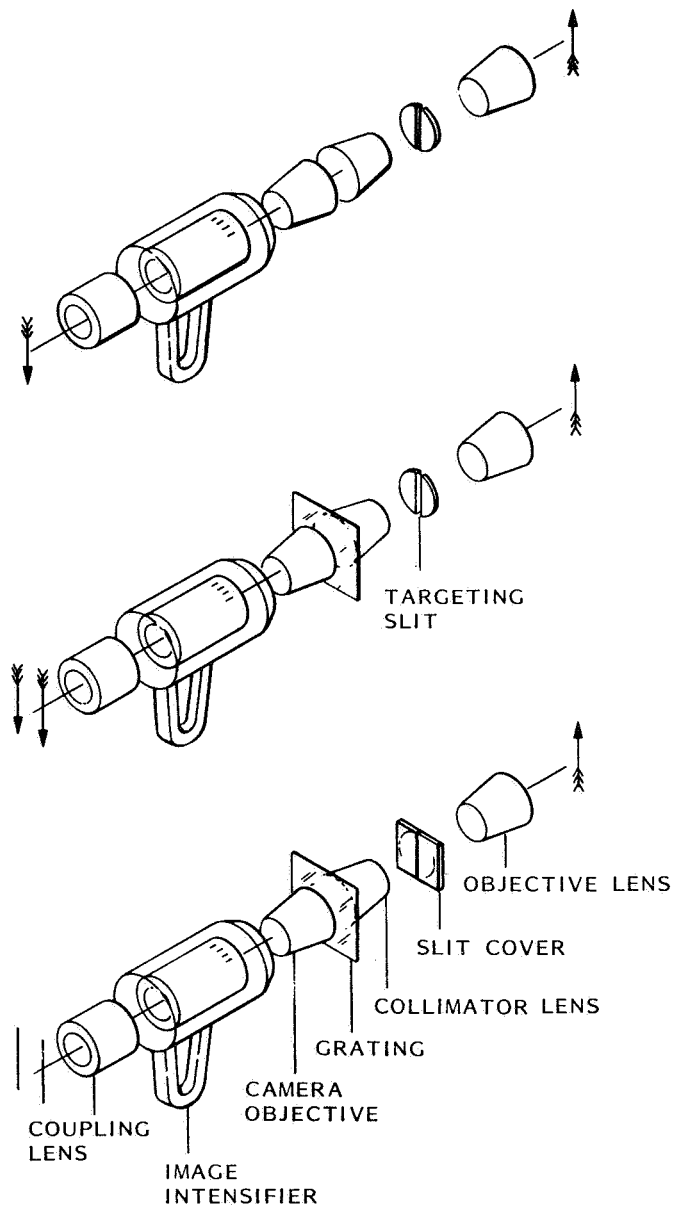


Fig. 7. Image intensified slit spectrograph for shuttle glow observations. Top is shown with straight through imaging configuration. Middle is shown in objective grating configuration. Bottom is shown in spectrometer configuration.

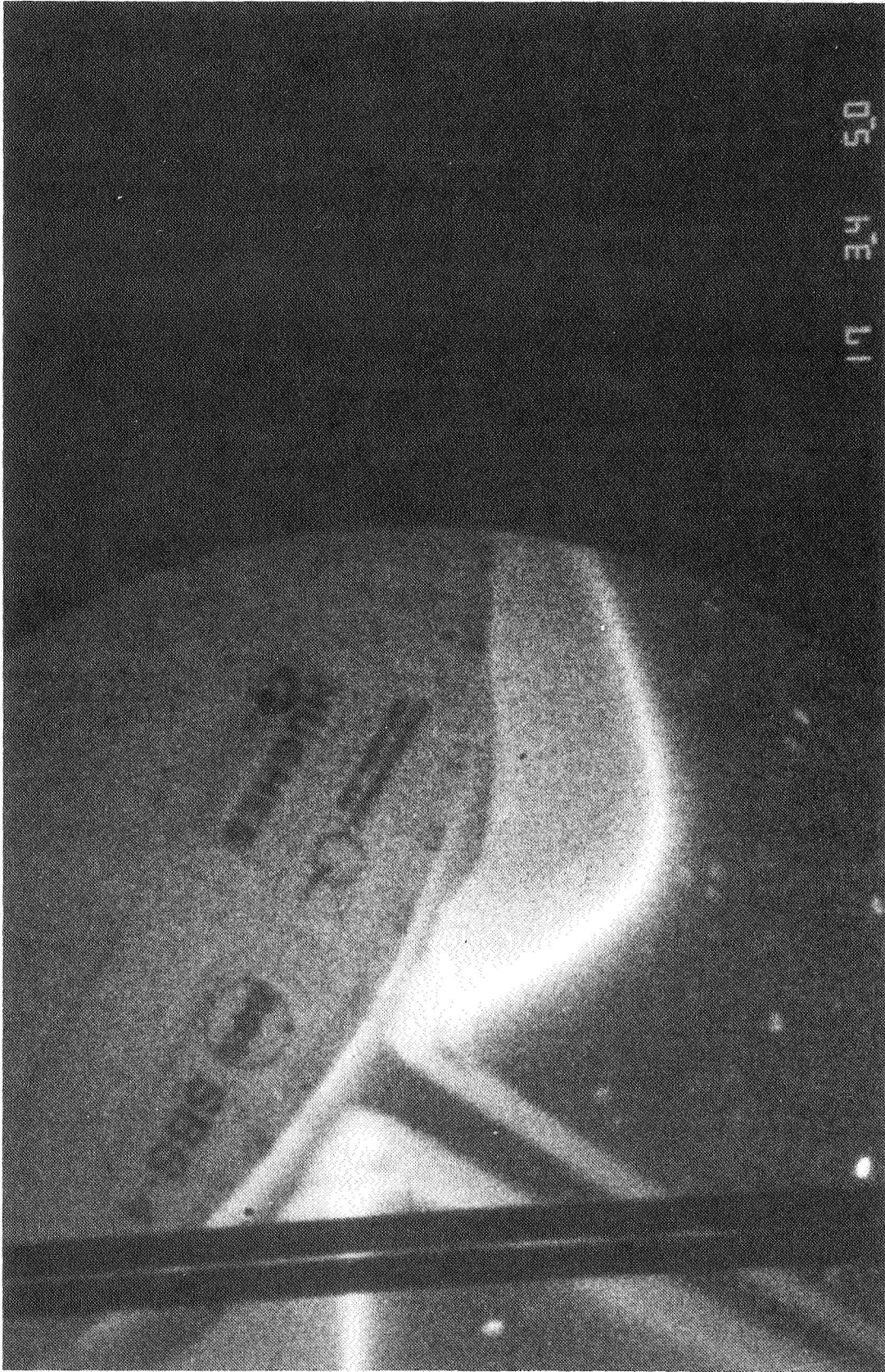


Fig. 8. Straight through imaging looking at the shuttle tail, port engine pod, and bulkhead. Photograph taken at 17:34:50.

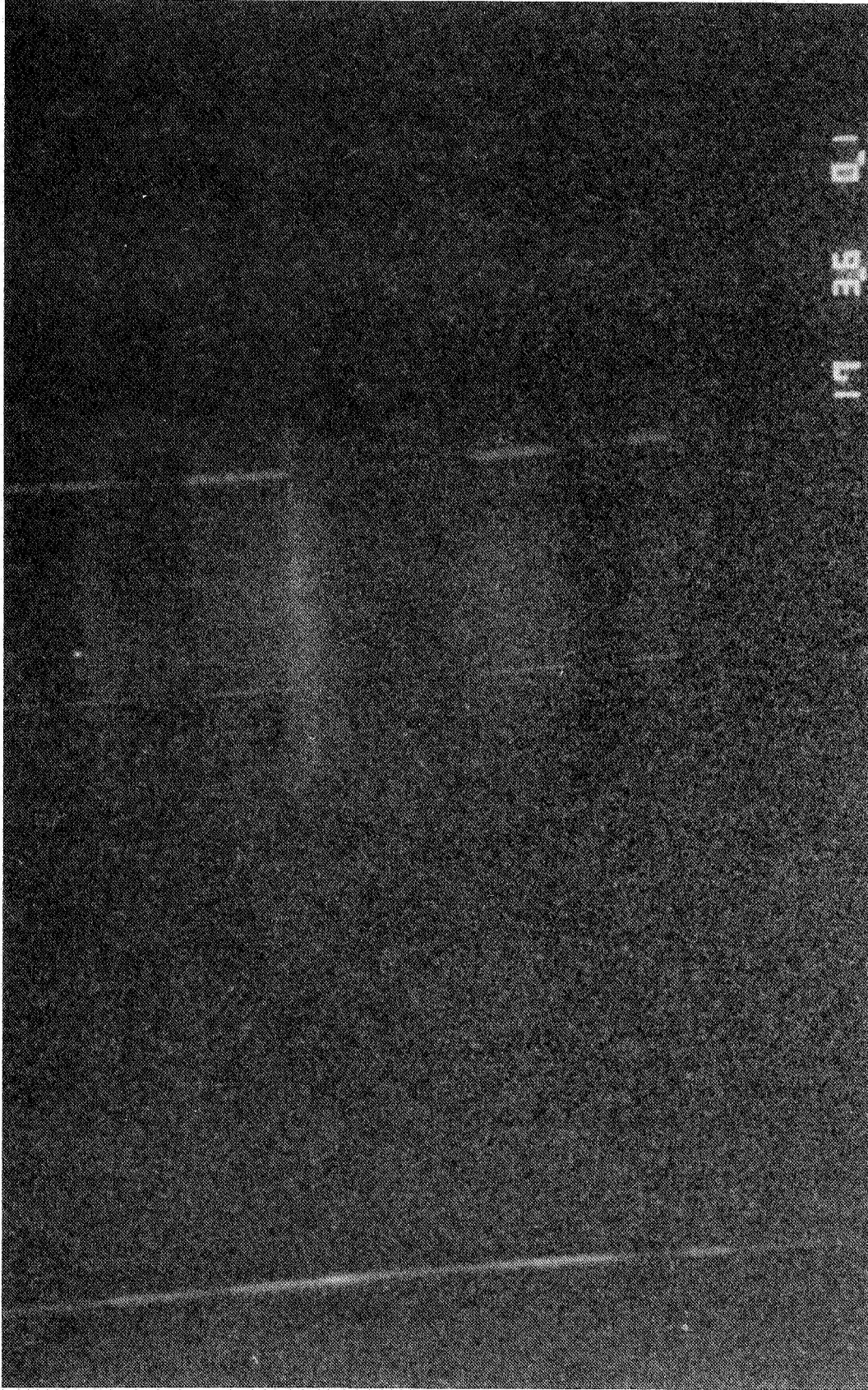


Fig. 9. Same image as Figure 3 except that grating and slit has been included. By comparison with Figure 3 the objects can be identified. Orbiter skin produces line spectra of scattered airglow. Continuum spectra is produced by vehicle glow.

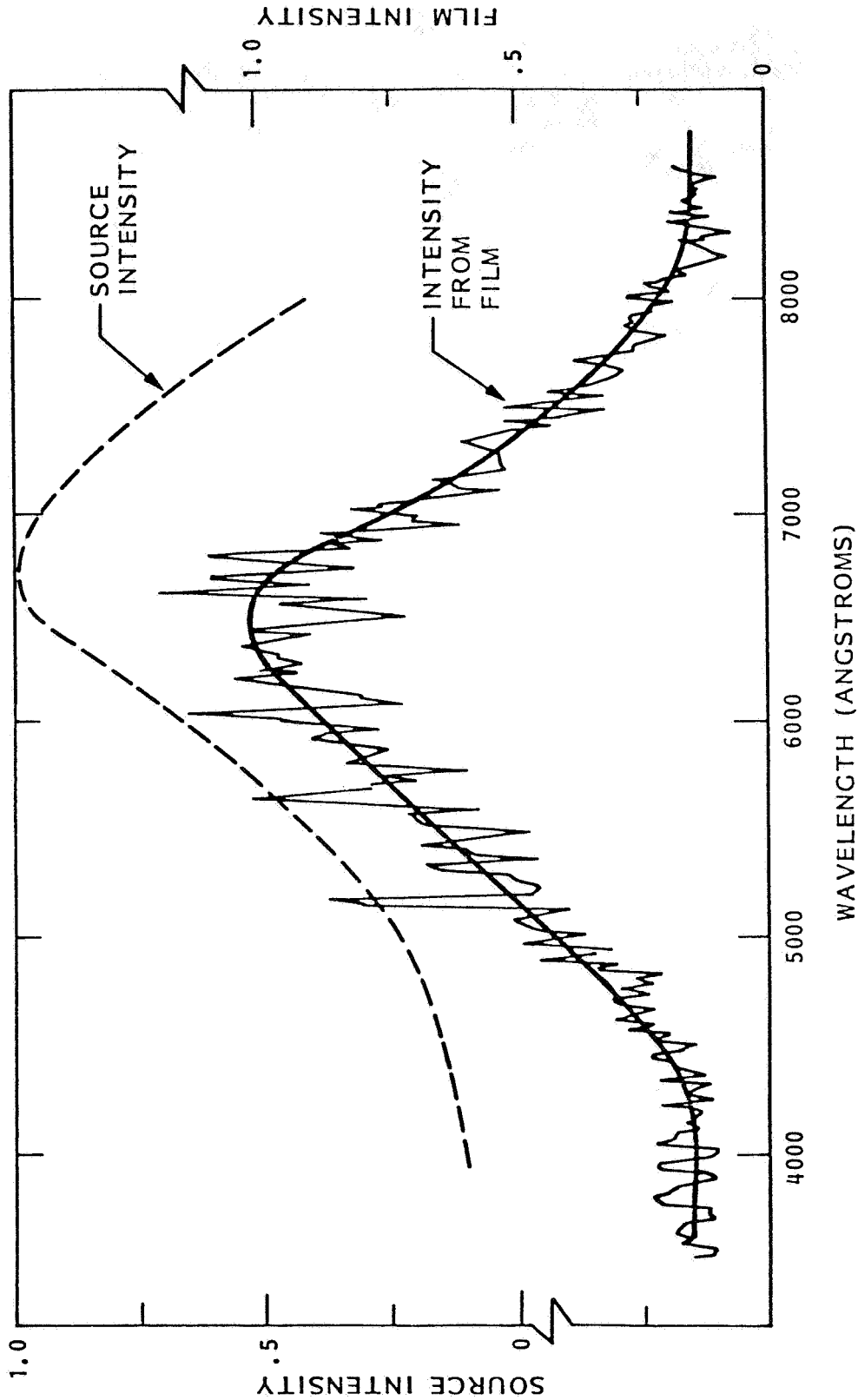


Fig. 10. (Bottom) Six line average tracing of spacecraft glow identified in Figure 2. The tracing has been corrected for the calibrated D-Log-E response of the film. The noise character in the data is primarily due to ion scintillations in the image intensifier which have accumulated in the image over the 30-second exposure. (Top) Corrected spectrum of spacecraft glow where the instrument response has been applied to the curve drawn through the data shown in the bottom of the figure.

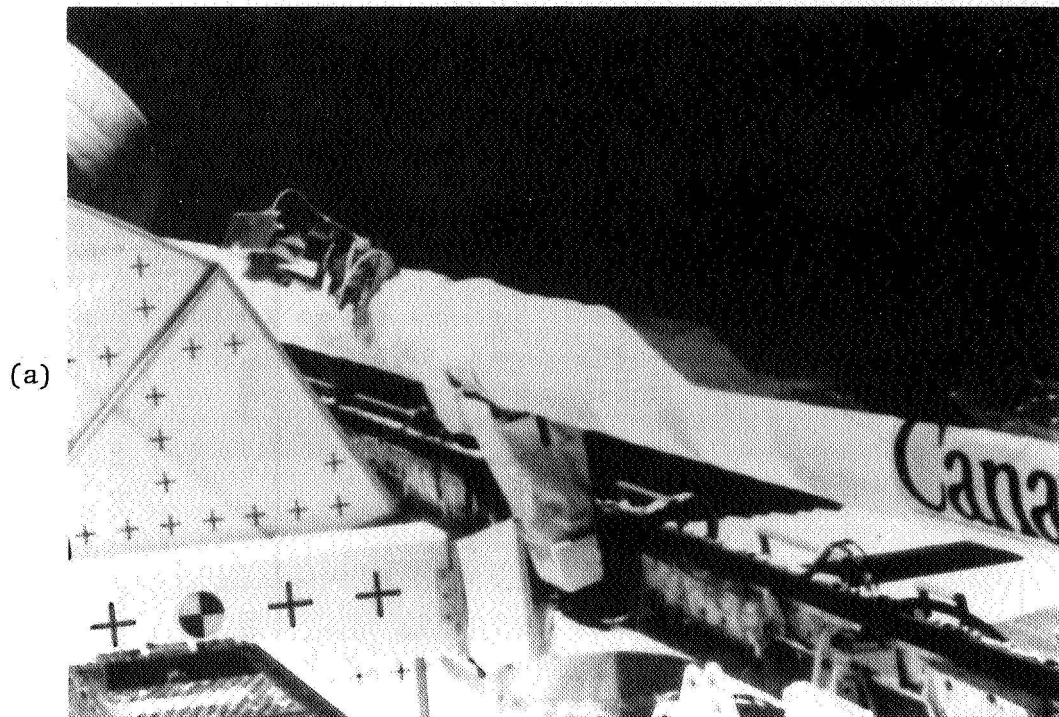


Fig. 11. (a) The material samples mounted on the remote manipulating system (RMS) arm on the shuttle. The order of the samples is kapton, aluminum oxide, black chemglaze, aluminum oxide, and kapton. (b) Material samples glowing in the ramming atmosphere.

RELATIVE GLOW INTENSITIES

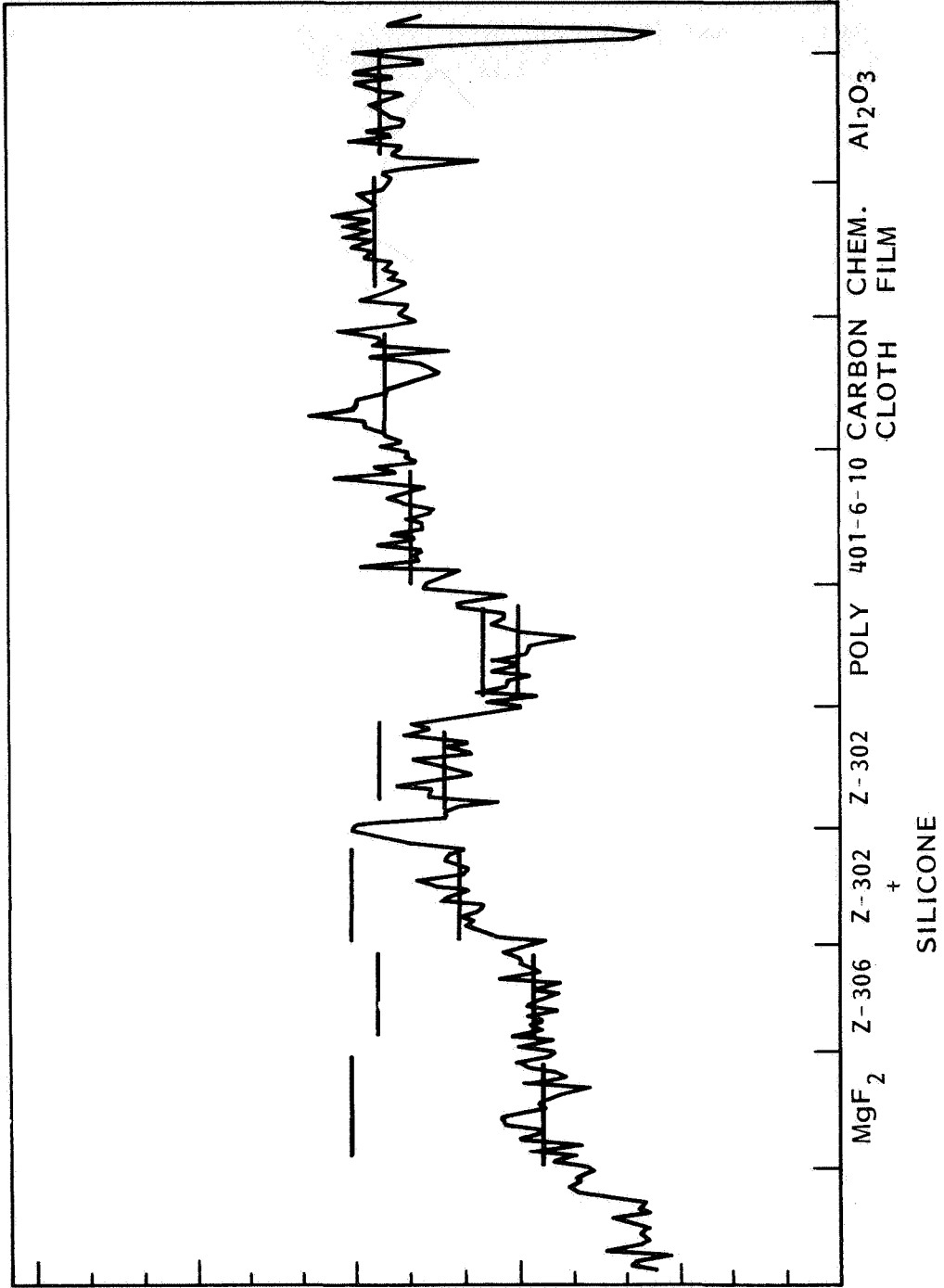


Fig. 12. Microdensitometer tracings of the nine glow samples on mission 41-D.

JET LOCATIONS

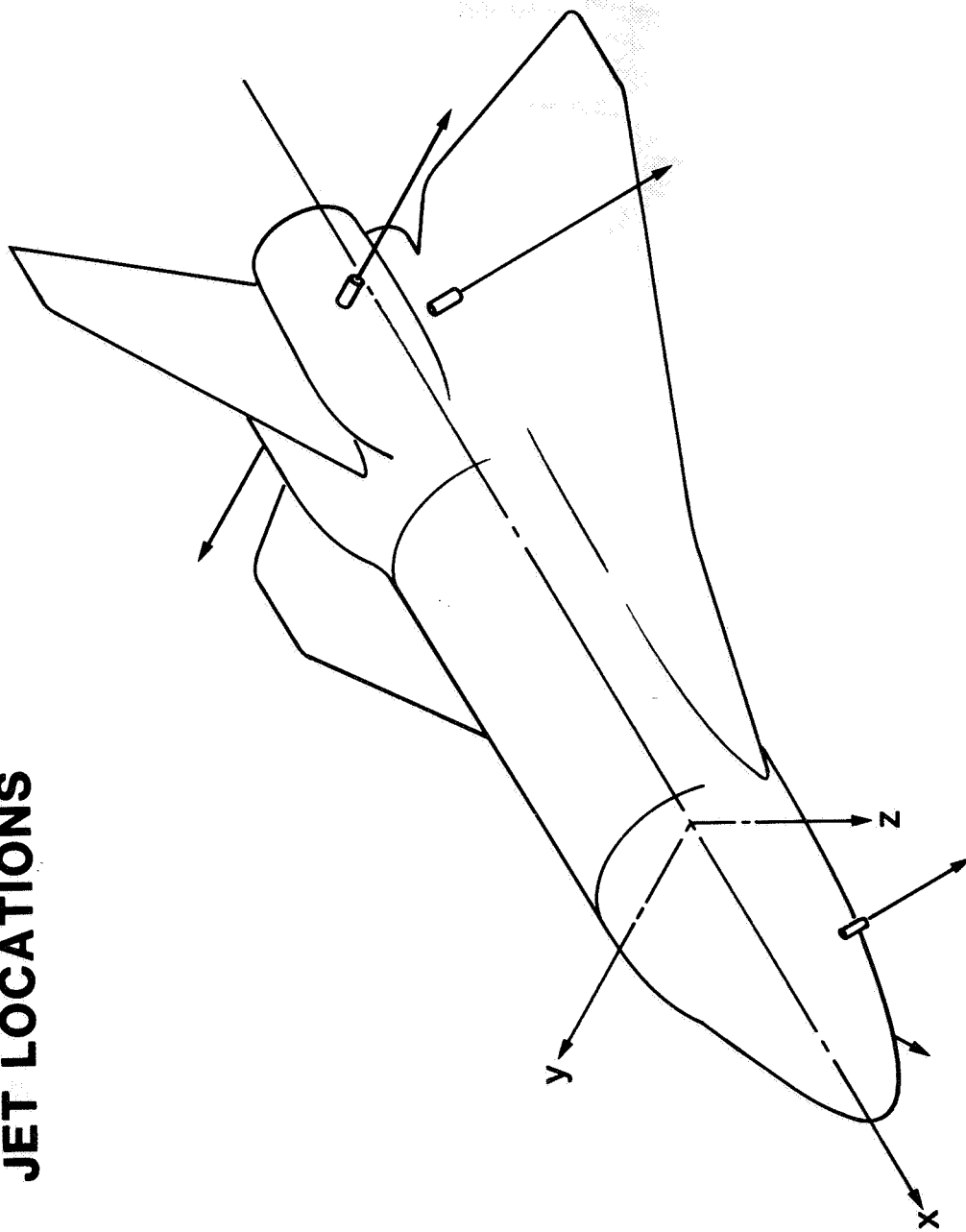
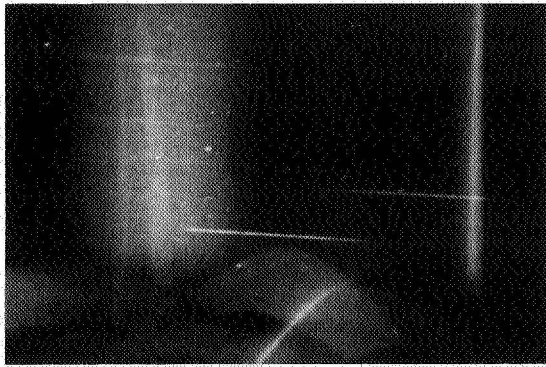
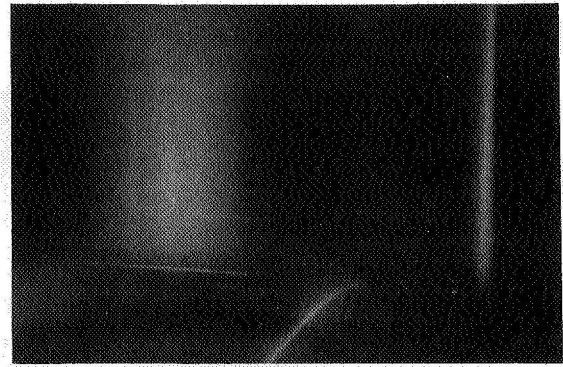


Fig. 13. A schematic sketch of the location of the thrusters on the Orbiter.

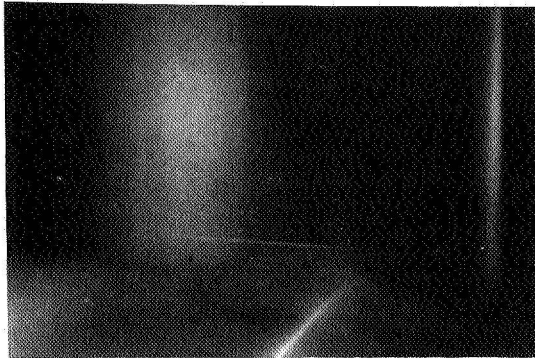
THRUSTER FIRINGS



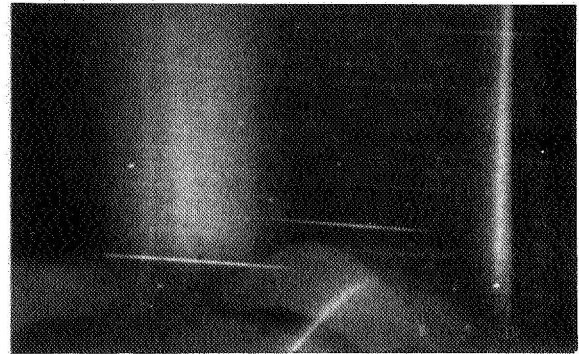
BACKGROUND



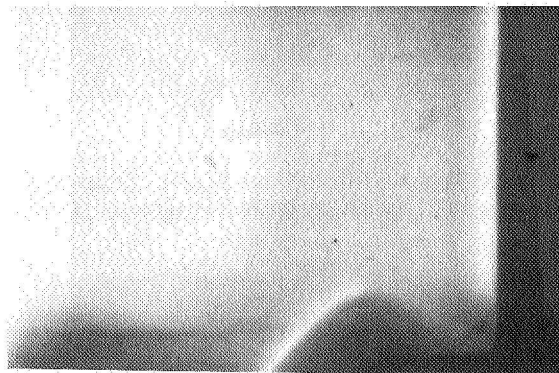
FORWARD JETS



TAIL YAW JET 1



TAIL YAW JET 2



TAIL DOWNWARD JETS

Fig. 14. The effect of firing thrusters during the exposures. Top left, no thrusters fired.

THRUSTER FIRING DECAY

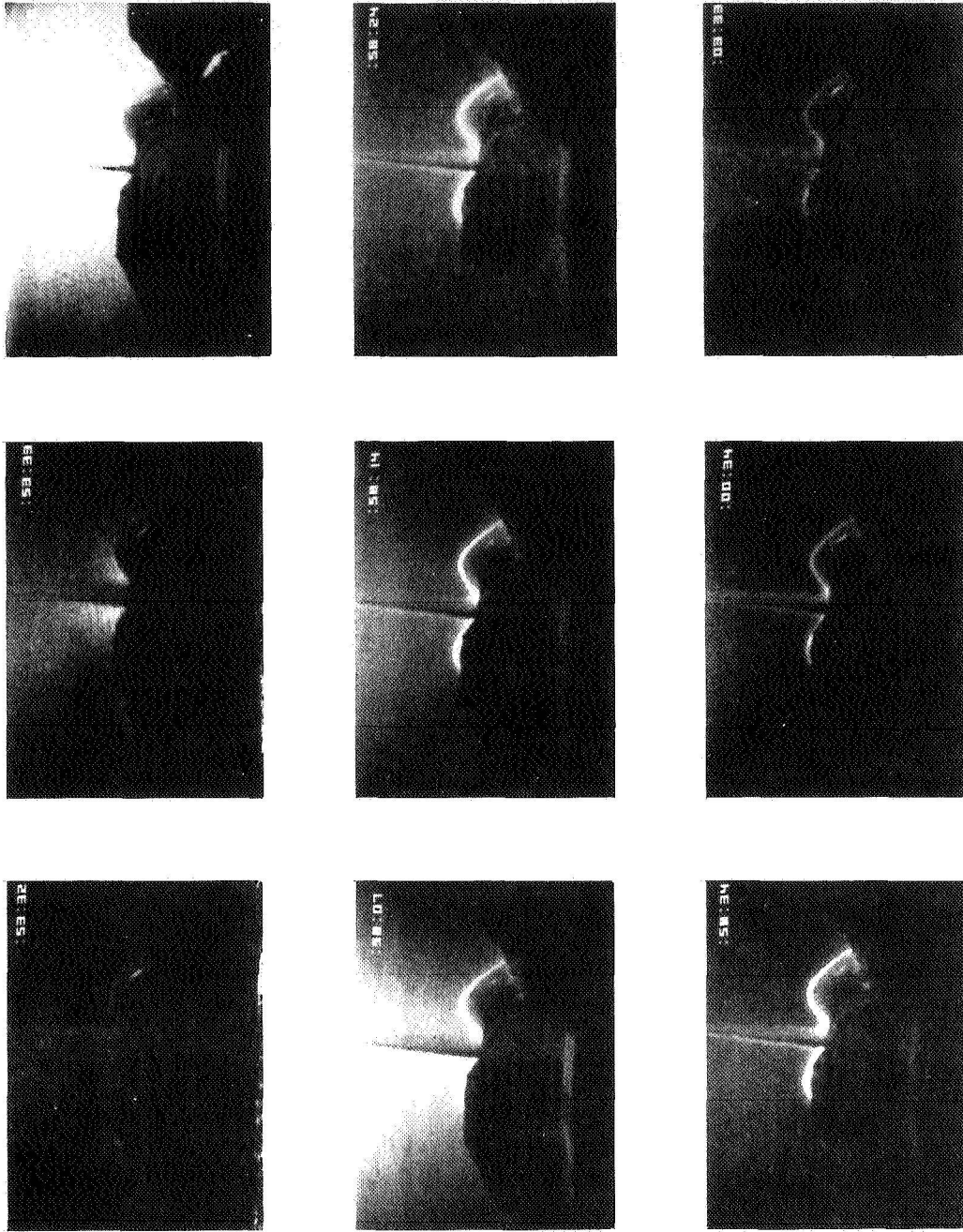


Fig. 15. Collage of television monitor photographs of the thruster firing as recorded by the Orbiter bulkhead closed-circuit television cameras. Time counter in seconds and hundredths of seconds. Note that glow on engine pods is enhanced after jet firing.

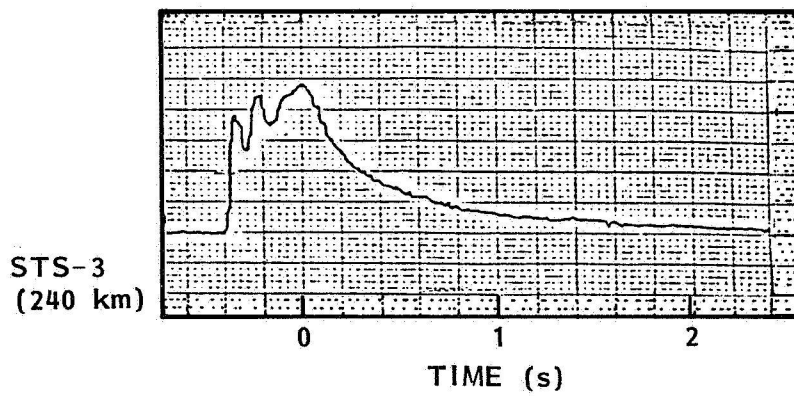
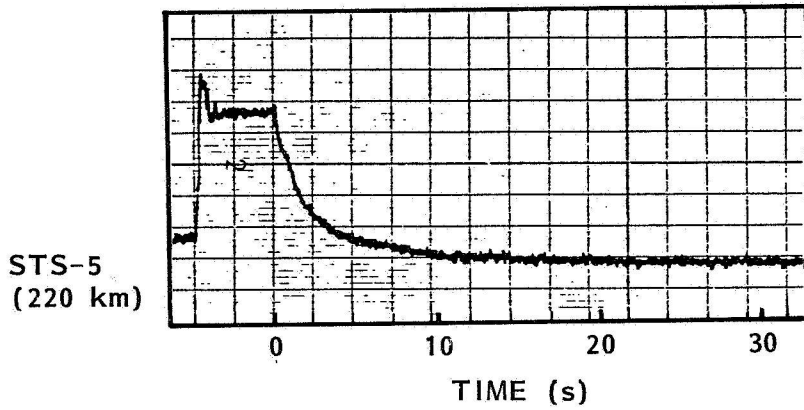


Fig. 16. The function of the thruster glow intensity on the engine pods as a function of time after a thruster firing. The data were taken with the Orbiter bulkhead video cameras. Intensity is in arbitrary units.

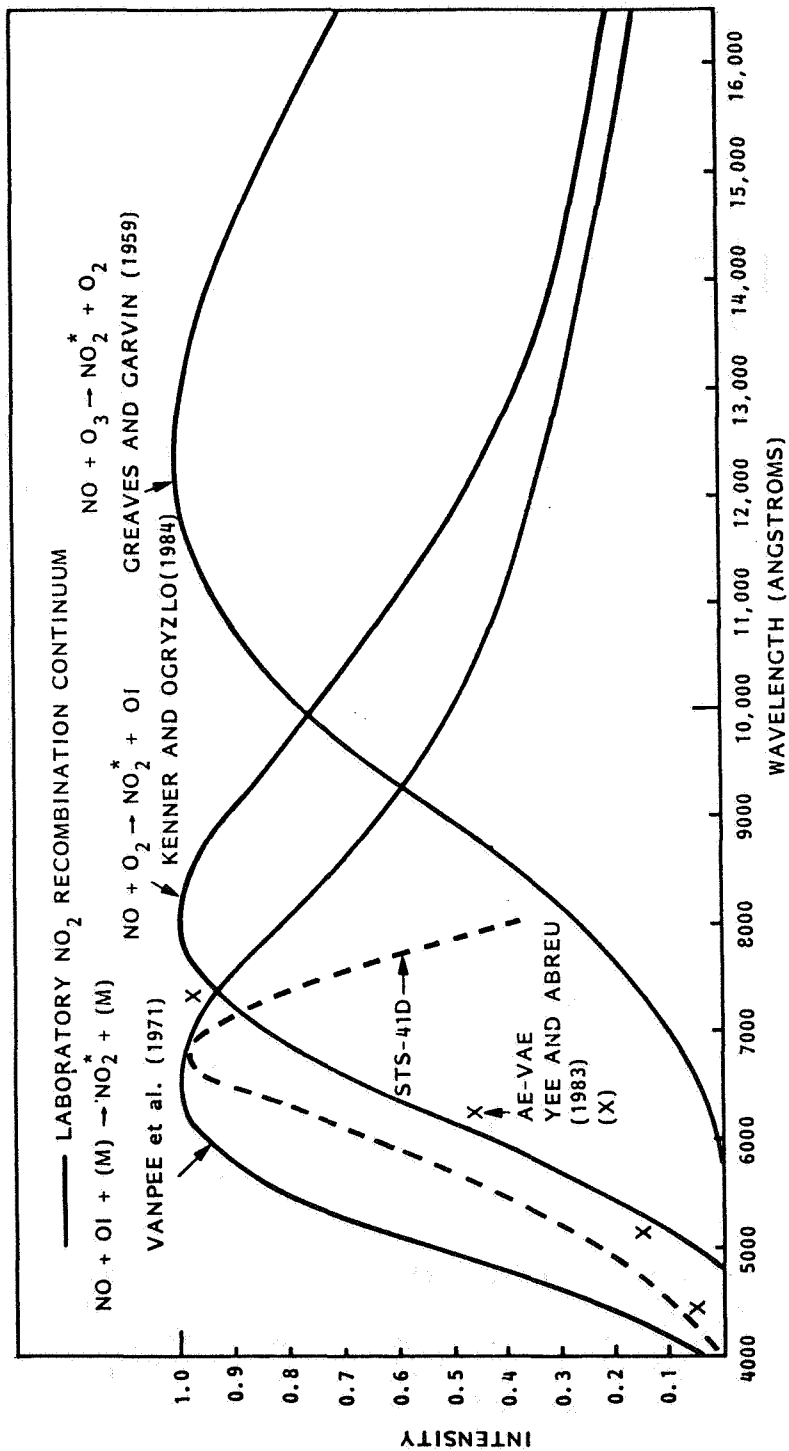


Fig. 17. The spectrum of the spacecraft glow compared with that of the laboratory experiments of Fontijn et al. [1964] and Paulsen et al. [1970]. A spectral blend produced by spectrally e-folding the measured spectrum with lifetime data of Schwartz and Johnston [1969] is also plotted.

SPACE SHUTTLE RAM GLOW: IMPLICATION OF NO₂ RECOMBINATION CONTINUUM

Gary Swenson and Steve Mende

Lockheed Palo Alto Research Laboratory

Stu Clifton

Space Science Laboratory
NASA Marshall Space Flight Center

Abstract. The ram glow data gathered to date from imaging experiments on space shuttle suggest the glow is a continuum (within 34 Å resolution); the continuum shape is such that the peak is near 7000 Å decreasing to the blue and red, and the average molecular travel leading to emission after leaving the surface is 20 cm (assuming isotropic scattering from the surface). Emission continuum is rare in molecular systems, but the measured spectrum does resemble the laboratory spectrum of NO₂(²B₁) recombination continuum. The thickness of the observed emission is consistent with the NO₂ hypothesis given an exit velocity of ~2.5 km/sec (1.3 eV) which leaves ~3.7 eV of ramming OI energy available for unbonding the recombined NO₂ from the surface. The NO₂ is formed in a 3-body recombination of OI + NO + [M] = NO₂ + [M], where OI originates from the atmosphere and NO is chemically formed on the surface from atmospheric NI and OI. The spacecraft surface then acts as the [M] for the reaction. Evidence exists from orbital mass spectrometer data that the NO and NO₂ chemistry described in this process does occur on surfaces of spectrometer orifices in orbit. Surface temperature effects are likely a factor in the NO sticking efficiency and, therefore, glow intensities.

Background

The AE-E satellite was equipped with a Visual Airglow Experiment (VAE) which observed atomic and molecular features in the Earth's airglow layer. Backgrounds in the photometer filter channels were found to have a variability with ram angle. This recognition of a ram background in the AE instrument was first cited by Torr et al. [1977]. These data were reported by Yee and Abreu [1982, 1983]. The data displayed a detectable level of luminosity in the near UV channels of the instrument (3371 Å), with increasing luminosity towards the red wavelengths (7320 Å). The background in all filter channels, when plotted, described a bright ram source, increasing in brightness toward the red wavelengths. The analysis presented suggested the glow extended well away from the spacecraft alluding to the probability that the emitter is a metastable. OH Meinel bands were reported as being a likely candidate species for emission, since the general red character and emission lifetime seemed to fit the evidence. The Yee and Abreu [1982] analysis had found a strong correlation between the ram emission intensity and altitude. The emission intensity closely followed the atomic oxygen scale height above 160 km altitude. Atomic oxygen then is

the probable aeronomical constituent to be a chemical catalyst for whatever process is occurring. Slinger [1983] was among the first to report the OH hypothesis. Langhoff et al. [1983] discussed the simplification of OH to the infrared glow spectrum implied by OH chemistry possibilities.

The DE-B spacecraft was equipped with a high resolution Fabry-Perot Interferometer (FPI). In this instrument, a 7320 Å filter was utilized in series with the Fabry-Perot etalon. Abreu et al. [1983] reported on the background with ram effect associated with this channel. A ram glow was reported and the deduced etalon spectrum showed similarity with the OH spectrum observed in nightglow from the atmospheric limb. The available evidence from these two spacecraft seems to favor the OH hypothesis for the observed glows.

Glow observations have been reported by a number of investigators from shuttle missions STS -3, -5, -8 and -9. Banks et al. [1983] reported glow from Orbiter television and still camera pictures around aft spacecraft surfaces while documenting glows associated with an electron accelerator experiment on STS-3. Mende [1983] and Mende et al. [1983,1984a,b] have documented ram glows associated with STS -5, -8, and 9 using an intensified camera. On the later missions (STS-8 and -9), objective grating imagery of spacecraft glow from the vertical stabilizer depicted a red structureless glow [Mende et al., 1984b]. The spectral resolution is on the order of 150 Å. On the STS-8 mission it was observed that glows from surface samples including aluminum, kapton, and black chemglaze (a polyurethane black paint typically used in low light level detection instrument baffles) were not equally bright. The surface characteristic and/or the material makeup clearly was shown to affect the glow brightness.

High spectral measurements of the ISO spectrometer on Spacelab 1 show the presence of a red dominated glow [Torr and Torr, 1984]. There are a number of observed emission features which may be part of the natural aurora airglow background environment and therefore may not be part of the shuttle glow.

There is a proposed plasma process for glow production [Papadopoulos, 1983] which involves a two-stream instability between incoming ram and reflected ions. The ion instability sets up an electrostatic wave, which in turn heats the ambient electrons. The pumped-up electrons can in turn excite in situ and ramming constituents. Pumping the electrons to 20+ eV will allow $e + X$ reactions. The energy is sufficient to excite N_2 to 2nd positive, and possibly ionize to 1st negative. A lot of UV emissions could arise with this process whereas the chemical processes postulated are energetically limited to be red and infrared emitters. N_2 first negative (1,0) at 3914 Å and N_2 2nd positive band at 3371 Å are spectral features expected for this physical process. Detailed calculations have been made by Kofsky and Barrett [1983] regarding the ion instabilities and likely excitation emissions.

Green [1984] recently reviewed the ram glow data and theory for the shuttle environment. The review described the two classes of mechanisms, one being molecular emission from surface collisions and another due to the plasma critical velocity effect. In his discussions, vibrationally excited CO, OH or electronically excited N_2 were postulated as most likely candidates and chemically plausible with the evidence at hand.

More recently, shuttle glow spectrum was reported from STS 41-D with 34 Å resolution by Mende et al. [1984c] and Swenson et al. [1985]. These data show the shuttle ram glow to be an emission continuum within the instrument resolution.

The current evidence strongly suggests the glow associated with the ramming atmosphere is a result of NO_2 in recombination [Swenson et al., 1985]. The natural atmosphere is reacting with the 8 km/sec vehicle to produce the phenomenon. The purpose of this presentation is to review the evidence and our current interpretation of the physical processes leading to the glow.

NO_2 Recombination Chemistry

The picture of spacecraft glow that has evolved includes the optical observations from the space shuttle and Explorer series satellites. We have recently assembled a theory that's consistent with the observations of the shuttle glow spectrum. The theory basically involves the fact that NO forms and sticks on orbiting surfaces (more efficiently on cold ones). NO will react very quickly in 3-body recombination with OI to form NO_2 . The surface monolayer of NO is exposed to fast atmospheric OI on ram spacecraft surfaces. Since NO_2 forms with ramming OI, the 5 eV OI also contains enough energy to unbind the formed NO_2 from the surface. NO_2 leaving the surface at 2.3 km/sec can account for the observed e-fold in the stand-off luminous glow from the space shuttle. The bottom part of Figure 1 shows the OI interacting with surface sticking NO to form NO_2 . The excited NO_2 which exits the surface gives the red glow.

Wall catalytic formation of NO was observed by Reeves et al. [1960] with laboratory experiments involving NI and OI. Their experiments showed that $\text{N}(\text{S}) + \text{O}(\text{P}) = \text{NO}(\text{B}^2\pi)$ forms on the wall and the NO gas phase is formed followed by emission, i.e., $\text{NO}(\text{B}^2\pi) = \text{NO}(\text{X}^2\pi) + h\nu$ (beta bands). In their experiments, emission from the excited gas product coming off the wall was observed.

Spectrum of Shuttle Glow

An experiment was operated on several space shuttle missions to provide spatial and spectral distributions of the ram glow associated with the space shuttle Orbiter. The most recent data featured resolved spectrum and imagery of the glow with spectroscopic resolution of 34 \AA FWHM between 4000 \AA and 8000 \AA [Swenson et al., 1985]. The spectrum of the glow on the shuttle tail pod could be clearly separated from reflected light from the Orbiter. The spectrum was taken at 290 km altitude from the ram surface. The spectrum noise was dominated by the ion scintillation in the image intensifier which produces a grain over the entire image of the 30-sec exposure.

In Figure 2, the spectrum from STS 41-D is plotted and compared with laboratory spectrum of Fontijn et al. [1964] and Paulson et al. [1970]. The laboratory spectrum was produced from 3-body recombination of $\text{NO} + \text{OI} + (\text{M}) = \text{NO}_2 + (\text{M})$. Continuum emission is not common in molecular systems. NO_2 certainly has the ingredients of composition from the ambient source to be the candidate emitter. The spectrum isn't a perfect fit to the laboratory spectrum by any means, but we attribute this to the temperature at which the spacecraft reaction is taking place as opposed to the laboratory experiments. The laboratory spectrum is typically formed with a recombinant temperature of $\sim 300 \text{ K}$ whereas the 5 eV ramming OI characterizes a $60,000 \text{ K}$ effective recombinant temperature.

It is well established that NO_2 can take on a number of spectral

shapes dependent on the recombinant species and the available internal energy of the recombinant such as found with O_3 (see Figure 3). Figure 3 shows the laboratory recombination spectrum for NO_2 for 3-body curve as well as the spectrum for 2-body recombination with NO and O_3 where the O_3 is vibrationally excited to different states. The laboratory spectra, again, are all-low temperature spectra. For comparison, we have shown the measured STS 41-D spectrum, which we contend is spectrally different as a result of the ramming OI energy. Golomb and Brown [1975] found laboratory evidence for thermal effects on the spectral shape of the OI recombination spectrum at low temperature (200-350° K) range. They found the intensity of the blue portion of the continuum to decrease with increasing temperature.

Mass Spectrometer Evidence

What evidence do we have that NO forms and sticks on orbiting surfaces in the thermosphere? The best evidence is that reported by the mass spectrometer investigations and what has been observed in NI , NO , and NO_2 . Engebretson and Mauersberger [1979] described in detail the response of NO with respect to thermal and orbital parameters for their instrument on AE-C satellite. It's been known since mass spectrometers first flew that most of the atmospheric NI entering the mass spectrometer orifice converts to NO with wall collisions and in fact, a large percentage of the NI signal is deduced from the NO (mass 30) signal in the instruments (see Engebretson and Mauersberger, [1979] and the references cited therein). It's been well established in laboratory experiments that the NI and OI wall reaction form the gas phase NO . Engebretson and Mauersberger [1979] then reported a most interesting phenomenon. They reported that NO was absorbed on the spectrometer walls (with efficiencies higher at low wall temperatures). The top part of the chemistry shown in Figure 1 reflects what has been observed in the mass spectrometer orifice. They observed the gas phase NO , and from temperature and altitude geometry, they deduced that a significant amount of NO was sticking to the wall. The UV emission from surface catalyzed NO in the gas phase has been observed in the laboratory and should be observable on an orbiting ram surface with the proper instrument [Reeves et al., 1960]. Only the NO beta bands are observed in the laboratory (temperatures ~300° K) surface-catalyzed excitation type experiments. What will happen on the spacecraft surface with OI at 5 eV producing the NO is uncertain.

What about the link between the top (NO) chemistry and the bottom (NO_2) chemistry depicted in Figure 1? Engebretson and Mauersberger also noted NO_2 formed in the orifice (most efficiently at low wall temperatures). In fact, Engebretson (private communication) indicates that this NO_2 is observed in the open ion source configuration of the type used with AE-C but is not as prevalent in closed ion source instruments. This implies that without a source of energetic OI, the $NO+OI = NO_2$ (gas phase) chemistry does not take place or that wall collision chemistry acts to destroy the NO_2 after it does form.

Surface temperature has been found to be a very important parameter in the effective surface sticking efficiency and NO_2 formation rate in the studies performed by Engebretson and Mauersberger [1979]. The colder surfaces are more efficient for NO to stick, and therefore we could expect a more intense NO_2 emission but lesser NO beta band emission

since it is the gas phase NO which emits the beta bands. The warmer surfaces then would tend to emit less NO₂ (red) emission, but more NO (blue beta band) emission.

Source Continuity Considerations

Does the source availability account for the luminosity observed in the red glow? At 250 km we observe ~6 kilorayleighs of visible glow when viewing normal to a ram surface (interpreted from e-folding considerations of spacecraft tile surface glows). In other words, ~6.10⁹ photons/cm² sec are observed. The atomic nitrogen population of ~10⁷ [Engebretson et al., 1980] with a spacecraft velocity of 8.10⁵ cm/sec yields a nitrogen flux of 8.10¹² to the surface. The efficiency of producing an NO₂ recombination photon would necessarily be ~1%. This is not unreasonable in NI,OI chemistry. Engebretson and Mauersberger [1979] reported a wall loss probability of NI at >10% per wall collision. If we assume that loss always results in an NO production, an NO monolayer sticking to the surface would be very quickly replaced after an NO molecule is lost from the surface due to ramming OI.

Lifetime and Energy Considerations

What about lifetime and e-folding considerations in the observed luminosity? The lifetime of NO₂ in fluorescence is ~70 microseconds according to Schwartz and Johnston [1969]. It was previously reported by Yee and Dalgarno [1983] that the effective e-folding distance an average molecule travels prior to emission is ~20 cm. (This has been reverified on several STS-9 images at Lockheed.) If we assume $x = t*v$ [Yee and Dalgarno, 1983], where $x = 20$ cm, we would infer that the exit velocity from the surface would be ~2.5 km/sec if NO₂ were the emitter. This corresponds to an effective exit temperature of 10,000^o K (1.28 eV). This is ~25% the ram energy of OI; considerably higher than the expected surface temperature of near 300^o K. In the process of producing the NO₂ then, total thermal accommodation of the OI does not occur. In summary, the lifetime and energy considerations are reasonable with NO₂ being the emitter. That leaves ~3.7 eV of the initial ramming OI for unbonding the NO₂ from the surface. We expect from the experimental observations of NO and NO₂ variations observed between surface temperatures of 300^o K and 400^o K by Engebretson and Mauersberger [1979] that the surface bond energy for NO is very small.

Other Considerations and Summary

The mass spectrometer orifice modulation of a surface monolayer of NO fits with the glow observations in principle. If NO can form on an instrument surface, it can also form on other surfaces including the spacecraft skin. It is well understood that the surfaces of the mass spectrometer orifice and that of the shuttle surface are very different. To date, we only have spectrum of the shuttle glow since glows of other emitting material samples have been from small areas at high altitudes and consequently weak to the observing instruments [Mende et al., 1984a,c]. The observed surface samples have been a mixture of insulator

and conductor type materials, from all of which a glow emanates. When observing the stand-off glows from these small samples, we do note the e-folding distance is about the same as it is on the Orbiter skin. This suggests to us that the glow is originating from the same chemistry as we observe on the Orbiter. It is this link that lends further credibility to the link between the chemistry observed in the mass spectrometer orifice [Engebretson and Mauersberger, 1979] and that postulated as shuttle ram surface chemistry here [Swenson et al., 1985].

Some further comments regarding the spacecraft glow are warranted.

1. Conjecture has been that a "dirty" space shuttle is responsible for the glow and that because it is dirty, that type of vehicle is not good for remote studies. We notice that whether data are taken on day 1 or day 9 of a space shuttle mission, the glow intensity seems to be about the same. On the contrary then, the phenomenon is a natural one characteristic of all spacecraft. The edge-on view of between 2 and 12 meters of stabilizer and ohms pod surface presents a lot of area to produce glow for cabin or Spacelab module instruments such as the handheld imager. The subtleties of surface temperature and surface type certainly influence the glow intensity. Our theory supports ram glow as a natural phenomenon and by nailing down the physical process, we can extend models to other spacecraft.
2. Not all materials glow to the same degree. However, when observing the stand-off distance of other materials, we note that the e-folding distance of intensity from the surface is about the same for all. This supports the same chemistry cited in Figure 1 as likely happening on all surfaces, but the NO sticking efficiency may be important in glow production. Material type is a key to minimizing the effect.
3. The glow originating from AE-C, we believe, results from the same chemistry we have cited as being responsible for the glow on the space shuttle. The confusion in comparison, especially from the difference in intensity as a function of angle from the ram direction, very likely relates to the fact that a large portion of the AE-C glow was originating from the instrument baffle as well as from the surrounding spacecraft surface. The baffle glow was not included in the original analysis.

There are certainly some puzzles reported in the literature that do not fit our hypothesis. Torr and Torr [1984] report N₂ 1st Pos spectrum in apparent ram data in a shuttle-based spectrometer. It is possible that their measurement is contaminated by dayglow or some other natural phenomenon since the experiment was operated during a daylit orbit. It cannot be dismissed however that they possibly observed a baffle or extended ram glow. The Dynamics Explorer B data in the Fabry-Perot channel suggests structure in a narrow region of spectrum of that satellite [Abreu et al., 1983]. Some of the structure was consistent with OH emission spectrum and some was not. The ram glow we attribute to NO₂ in recombination is the near surface glow which e-folds 15-20 cm from the surface.

References

- Abreu, V. J., W. R. Skinner, P. B. Hays, and J. H. Yee, Optical effect of spacecraft-environment interaction: Spectrometric observations by DE-B satellite, AIAA-83-CP838, AIAA Shuttle Environment and Operations Meeting, 178, 1983.

- Banks, P. M., P. R. Williamson, and W. J. Raitt, Space shuttle glow observations, Geophys. Res. Lett., 10, 118, 1983.
- Engebretson, M. J., and K. Mauersberger, The impact of gas-surface interactions on mass spectrometric measurements of atomic nitrogen, J. Geophys. Res., 84, 839, 1979.
- Engebretson, M. J., J. A. Defreese, and K. Mauersberger, Diurnal, seasonal, and nighttime variations of atomic nitrogen in the equatorial thermosphere, J. Geophys. Res., 85, 2165, 1980.
- Fontijn, A., C. B. Meyer, and H. I. Schiff, Absolute quantum yield measurements of the NO-O reaction and its use as a standard for chemiluminescent reactions, J. Chem. Phys., 40, 64, 1964.
- Golomb, D., and J. H. Brown, The temperature dependence of the NO-O chemiluminous recombination, J. Chem. Phys., 63, 5246, 1975.
- Greaves, J. C., and D. Garvin, Chemically induced molecular excitation: Excitation spectrum of the nitric oxide-ozone system, J. Chem. Phys., 30, 348, 1959.
- Green, B. D., Atomic recombination into excited molecular-A possible mechanism for shuttle glow, Geophys. Res. Lett., 11, 576, 1984.
- Kenner, R. D., and E. A. Ogryzlo, Orange chemiluminescence from NO₂, J. Chem. Phys., 80, 1, 1984.
- Kofsky, I.L., and J. L. Barrett, Optical emissions resulting from plasma interactions near windward directed spacecraft surfaces, AIAA-83-CP838, AIAA Shuttle Environment and Operations Meeting, 198, 1983.
- Langhoff, S. R., R. L. Jaffee, J. H. Yee, and A. Dalgarno, The surface glow of the Atmospheric Explorer C and E Satellites, Geophys. Res. Lett., 10, 896, 1983.
- Mende, S. B., Measurement of vehicle glow on the space shuttle, AIAA-83-CP838, AIAA Shuttle Environment and Operations Meeting, 79, 1983.
- Mende, S. B., O. K. Garriott, and P. M. Banks, Observations of optical emissions on STS-4, Geophys. Res. Lett., 10, 122, 1983.
- Mende, S. B., P. M. Banks, and D. A. Klingelsmith, III, Observation of orbiting vehicle induced luminosities on the STS-8 mission, Geophys. Res. Lett., 11, 527, 1984a.
- Mende, S. B., G. R. Swenson, and K. S. Clifton, Preliminary results of the Atmospheric Emissions Photometric Imaging Experiment (AEPI) on Spacelab 1, Science, 225, 191, 1984b.
- Mende, S. B., G. R. Swenson, K. S. Clifton, R. Gause, L. Leger, and O. K. Garriott, Space vehicle glow measurements on STS 41D, Submitted to J. Spacecraft and Rockets, 1984c.
- Papadopoulos, K., On the shuttle glow, SAI Report 84-147-WA, 1983.
- Paulsen, D. E., W. F. Sheridan, and R. E. Huffman, Thermal and recombination emission of NO₂, J. Chem. Phys., 53, 647, 1970.
- Reeves, R. R., G. Manella, and P. Harteck, Formation of excited NO and N₂ by wall catalysis, J. Chem. Phys., 32, 946, 1960.
- Schwartz, S. E., and H. S. Johnston, Kinetics of nitrogen dioxide fluorescence, J. Chem. Phys., 51, 1286, 1969.
- Slanger, T. G., Conjectures on the origin of the surface glow of space vehicles, Geophys. Res. Lett., 10, 130, 1983.
- Swenson, G. R., S. B. Mende, and K. S. Clifton, Ram vehicle glow spectrum: Implication of NO₂ recombination continuum, Geophys. Res. Lett., 12, 97, 1985.

- Torr, M. R., P. B. Hays, B. C. Kennedy and J. C. G. Walker,
 Intercalibration of airglow observations with the Atmospheric
 Explorer Satellites, Planet. Space Sci., 25, 173, 1977.
- Torr, M. R., and D. G. Torr, Atmospheric spectral imaging, Science, 225,
 169, 1984.
- Vanpee, M., K. D. Hill, and W. R. Kineyko, AIAA J. (Am. Inst. Aeronaut.
 Astronaut.), 9, 135, 1971.
- Yee, J. H., and A. Dalgarno, Radiative lifetime analysis of the
 spacecraft optical glows, AIAA-83-CP838, AIAA Shuttle Environment and
 Operations Meeting, 191, 1983.
- Yee, J. H., and V. J. Abreu, Optical contamination on the Atmospheric
 Explorer-E satellite, Proceedings of the SPIE, 338, 120, 1982.
- Yee, J. H., and V. J. Abreu, Visible glow induced by
 spacecraft-environment interaction, Geophys. Res. Lett., 10, 126,
 1983.

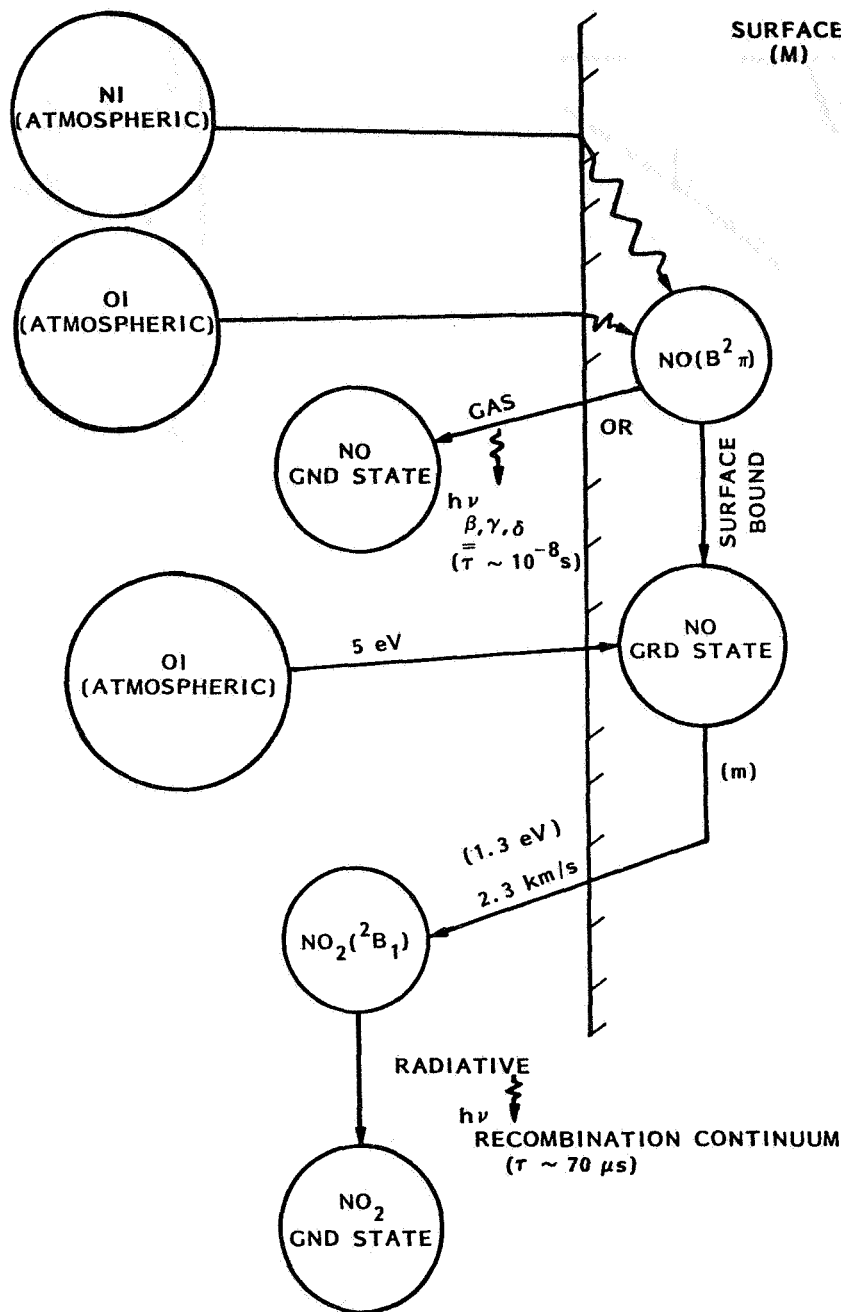


Fig. 1. A schematic representation of the chemistry believed to be responsible for spacecraft ram glow. Starting at the top, the ramming OI and NI intercept a spacecraft surface and form NO, some of which sticks to the surface and some of which escapes in the gas phase. The NO which sticks to the surface is subjected to ramming OI which forms a 3-body recombination with the surface [M] to create NO₂. The escaping NO₂ radiates the red continuum observed on ram surfaces. [See Swenson et al., 1985.]

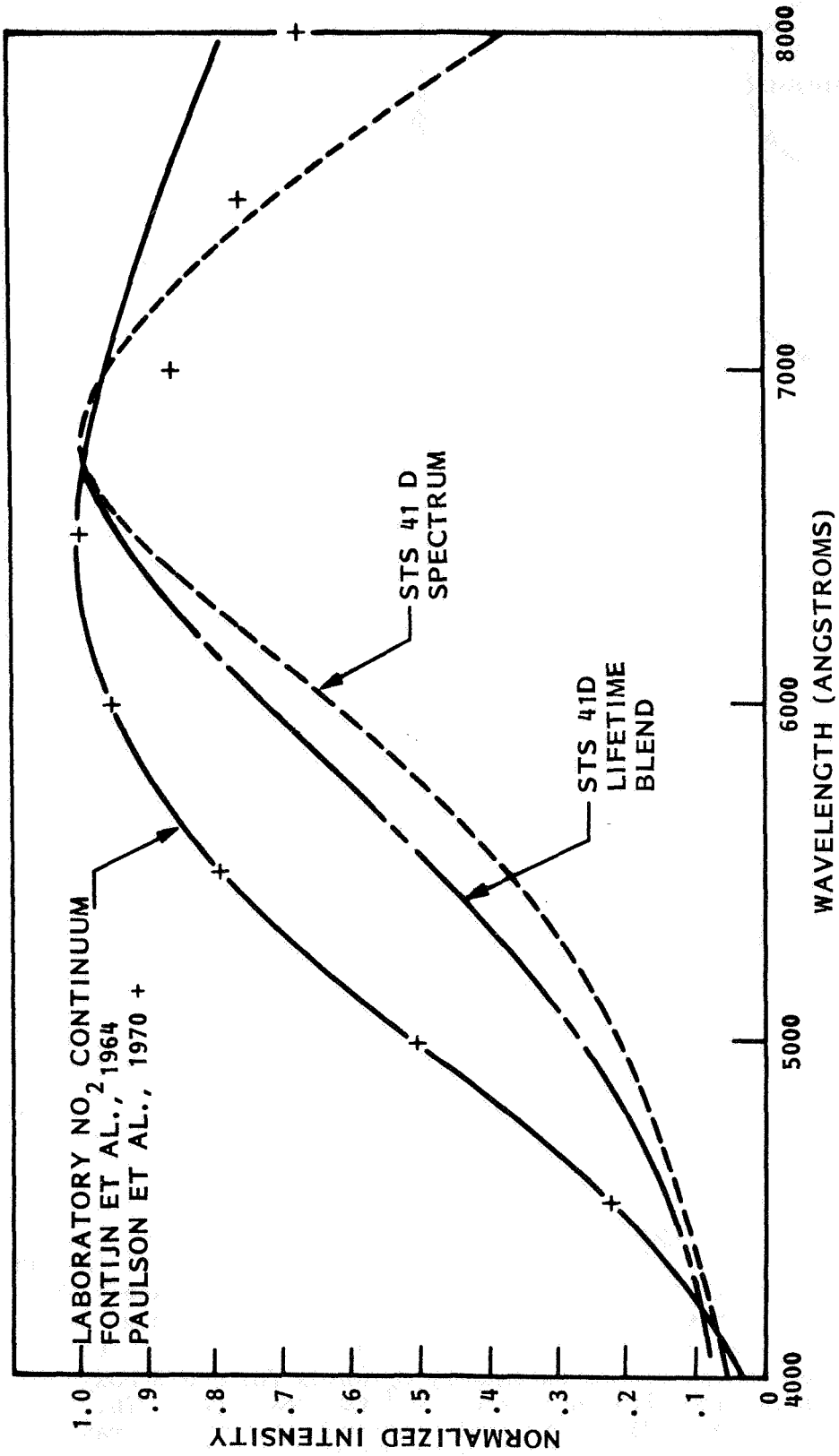


Fig. 2. The spectrum of spacecraft glow compared with that of the laboratory spectrum measured in laboratory experiments by Fontijn et al. [1964] and Paulsen et al. [1970]. A spectral blend produced by spectrally e-folding the measured spectrum with lifetime data of Schwartz and Johnston [1969] is also plotted.

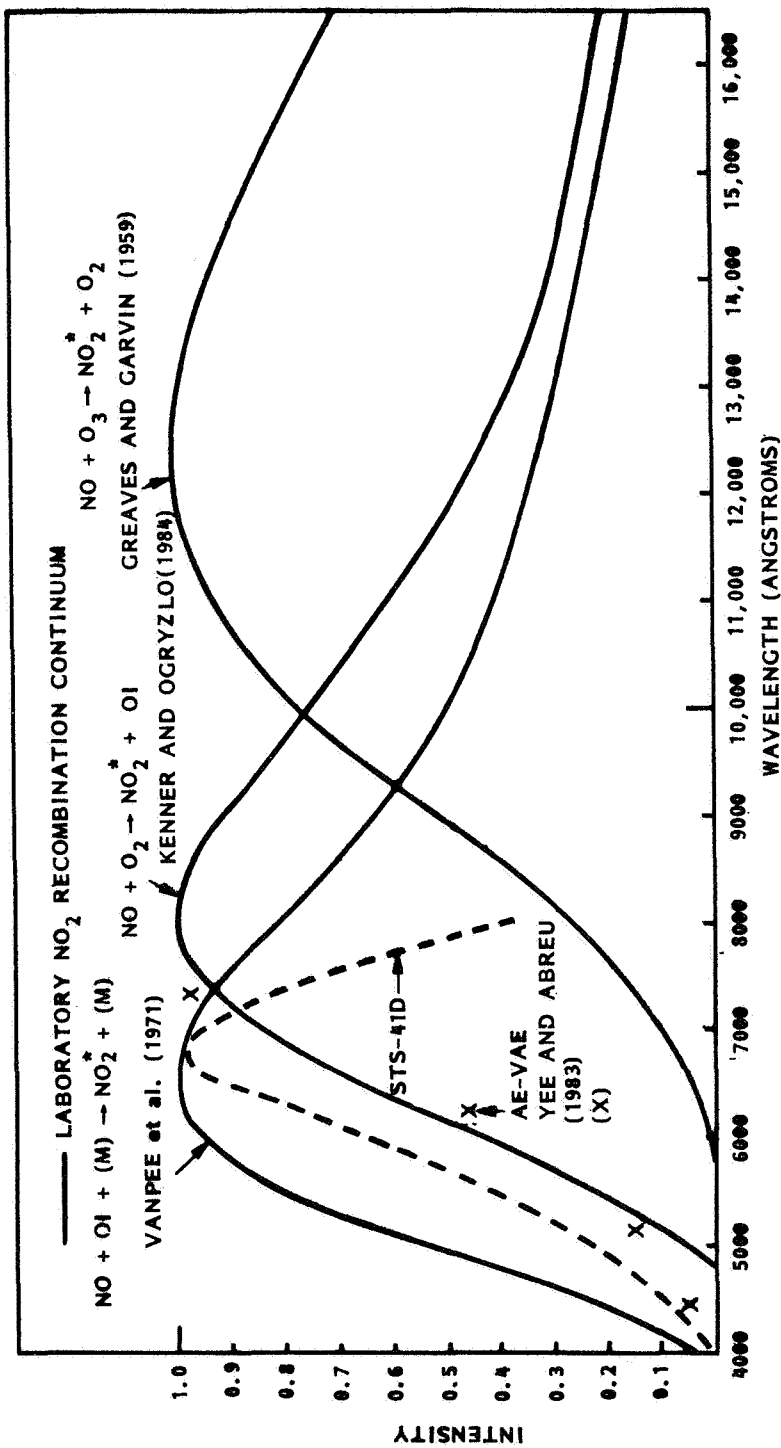


Fig. 3. The NO₂ recombination spectrum for 3-body recombination [Vanpee et al., 1971], and for 2-body recombination with upper state O₃ [Kenner and Ogryzlo, 1984], as well as vibrationally excited O₃ [Greaves and Garvin, 1959]. The STS 41-D spectrum is plotted as a dashed curve and the Atmosphere Explorer data are plotted [Yee and Abreu, 1983]. It is noted that the laboratory spectrum of recombination can take on a large range of spectral shape dependent on the state of the recombinant constituents.

AE AND DE MASS SPECTROMETER OBSERVATIONS RELEVANT TO THE SHUTTLE GLOW

Mark J. Engebretson

Department of Physics, Augsburg College

Abstract. Recent work by Swenson et al. [1985] has suggested that NO_2 may be responsible for the observed continuum glow near surfaces of the space shuttle. This report will review the observations of atomic nitrogen (N) at shuttle altitudes using mass spectrometers, giving special attention to the surface reactions of N relevant to the production of NO_2 on spacecraft surfaces. We will present data from two semi-open source mass spectrometers, the OSS instruments on the Atmosphere Explorer-C and -D satellites, and the closed source Neutral Atmospheric Composition Spectrometer (NACS) on the Dynamics Explorer-2 satellite, to show the similar behavior of NO in each case and the contrasting behavior of NO_2 . Although signals of NO and NO_2 are highly dependent on surface temperature and surface composition, it appears that direct exposure of ion source surfaces to rammed gas is a necessary condition for the production of large amounts of NO_2 . We will also present evidence that elevated surface temperatures can significantly reduce the production of NO_2 , likely by causing more rapid desorption of NO from these surfaces.

Introduction

The first comprehensive study of N densities in the thermosphere was presented by Mauersberger et al. [1975], using data from the Open Source Neutral Mass Spectrometer (OSS) on the Atmosphere Explorer-C satellite [Nier et al., 1973]. It is standard practice to use the mass spectrometer signal of mass 32 (O_2) as a measure of ambient atomic oxygen because of ion source surface adsorption of O and subsequent recombination into O_2 (see, for example, Hedin et al., 1973). A similar process was discovered to occur in the case of atomic nitrogen: observations from the Open Source Neutral Mass Spectrometer (OSS) on the Atmosphere Explorer-C satellite indicated that the mass 30 (NO) signal and the direct signal of atomic nitrogen (mass 14) exhibited identical variations with local time, latitude, and season, once the relatively large source background of NO was subtracted out. Approximately 95% of the N atoms detected appeared as NO or NO_2 , the dominant spectral peak of which is also at mass 30. These observations suggested that highly reactive N atoms entering the ion source of a mass spectrometer were likely to adsorb on metal surfaces and/or to react chemically with the dominant adsorbed species, atomic oxygen.

A recent study of data from the Neutral Atmospheric Composition Spectrometer (NACS) on the Dynamics Explorer-2 satellite [Carignan et al., 1981] has confirmed that with this instrument also the mass spectrometer signal of NO provides a quantitative measure of thermospheric N densities [Engebretson and Nelson, 1985].

Temperature Dependence

As part of the analysis of NO signals it was found that the level of background NO in the mass spectrometer ion source could be correlated with the temperature of the ion source walls. When data were taken on successive orbits, the background level of mass 30 decreased significantly after the first orbit, reaching stable levels on the third and subsequent orbits, but reverting to earlier levels after one or more orbits of experiment inactivity.

Shown in Figures 1 and 2 are logarithmic plots of source densities of mass 30 (NO), 40 (Ar), 14 (a product of electron bombardment of N_2), and 4 (He) as a function of time for two spinning orbits, 1630 and 1632, run November 21, 1981. The NACS instrument was off during orbit 1629, but on during successive perigee passes during orbits 1630-1633. Note that, at the beginning of orbit 1630 the mass 30 background was nearly $8 \times 10^8 \text{ cm}^{-3}$, while on orbit 1632 it was a factor of 10 lower at comparable altitudes. All other signals shown appear to be nearly identical on both orbits.

This contrast between "cold" and "warm" orbits, with ion source surface temperatures of approximately 300 K and 450 K, respectively, is characteristic of data from each of the satellite mass spectrometers studied here. Table 1 shows representative data for masses 30 and 46 from elliptical orbit passes of AE-C and DE-2 for such "cold" and "warm" orbits. In each case there are significantly lower signals of masses 30 and 46 on the downleg of these orbits when ion source surfaces are warmed up. Near the end of each pass, however, there is considerably less variation between "cold" and "warm" passes, consistent with the closer agreement in surface temperature near the end of each pass.

It is also clear in Table 1 that the abundance of NO_2 on the downleg of an orbit is dependent on temperature effects. Data from both AE-C and DE-2 instruments indicate that NO_2 signals are even more sensitive than NO signals to variations in surface temperature. Figures 3 and 4 show data from the OSS mass spectrometer on AE-C for two orbits specially programmed for a study of the variation of NO and NO_2 with surface temperature history. During this period in late 1975 the AE-C satellite was operated only one day a week, for two full circular orbit passes at 310 km altitude. Orbit 8530 was run after the usual 30-min OSS warmup. Orbit 8536 was preceded by a 4-hour warmup, thus simulating operations during two previous perigee passes in elliptical orbit operations.

The sharp early morning rise characteristic of thermospheric N densities is evident in Figure 3, a plot of net mass 30 signals from orbit 8536, but is obscured in the data from the beginning of orbit 8530 (Figure 4). Comparison of the two figures indicates that NO_2 accounts for most of the excess mass 30 signal observed on orbit 8530 (NO_2 produces 2.7 times as much signal at mass 30 as at mass 46). It is also important to note that although the ratio of NO_2 to NO appears to drop throughout orbit 8530, indicating the gradual desorption of an adsorbed species, the spin modulation evident on both orbits suggests that much of the NO_2 observed must be attributed to a relatively fast production process.

Ram Effects

The method of using mass 30 signals to measure thermospheric N worked successfully with other satellite mass spectrometers as well. Signals of masses 30 and 14 on the AE-D OSS instrument also were proportional, and the use of a gold-plated ion source on the AE-D instrument appeared to reduce considerably the dependence of the net NO signal on surface temperature effects. The NACS instrument on DE-2 also used a gold-plated ion source, but the closed source design of this instrument prohibited direct access of any molecules or atoms to the ionization chamber, hence excluding any direct measurements of N atoms.

A comparison of NO and NO₂ observations from the AE-C, AE-D, and DE-2 mass spectrometers is presented in Table 2. The ion source surfaces of the AE-C instrument are made of nichrome, while those of the AE-D and DE-2 instruments are gold plated. The AE-C and -D ion sources are of an open source design, with ram acceptance angles of 30 and 12 degrees, respectively, while the DE-2 ion source is closed, necessitating typically 100 wall collisions and complete thermal accommodation of all gas molecules before they will be analyzed by the mass spectrometer. Table 2 shows that the open source instruments produce large amounts of NO₂, with the fraction increasing as the satellite proceeds toward higher altitudes. The AE-D data at 700 km indicate nearly 100% of the mass 30 signal is due to NO₂. Although the DE-2 NACS instrument also uses a gold-plated source, the DE-2 data indicate the reverse effect: the fraction of NO₂ decreases to less than 3% as the satellite passes toward higher altitude. We attribute this striking difference to the closed source geometry of the DE-2 instrument, and infer that the thermal accommodation of the ramming gas (much of which is thermospheric O) significantly reduces the probability of converting adsorbed NO into NO₂.

Further analysis of the surface chemical processes reported here is contained in papers by Engebretson and Mauersberger [1979] for the Open Source Neutral Mass Spectrometer (OSS) instruments on the Atmosphere Explorer satellites, and Engebretson and Nelson [1985] for the Neutral Atmospheric Composition Spectrometer (NACS) instrument on the Dynamics Explorer-2 satellite.

Summary of Observations

Data from three satellite mass spectrometers have shown that odd nitrogen molecules are formed in abundance on the surfaces of mass spectrometer ion sources as a result of the impact of thermospheric O and N atoms. The adsorption and desorption of NO and NO₂ from these surfaces appears to vary considerably with surface temperature. Heating of ion source surfaces appears to significantly reduce the concentration of these species, especially NO₂. Comparison of data from open and closed source instruments with gold-plated surfaces indicates that adsorbed NO is much more likely to be converted to NO₂ by ramming O atoms than by less energetic (thermalized) O atoms.

Implications for Shuttle Glow

The large mass spectrometer background and small spin modulation we

have observed suggest that NO and NO₂ will likely form long-lasting monolayers on various satellite and/or shuttle surface materials. Production of NO₂ is likely to be greatly enhanced on cold surfaces exposed to ramming thermospheric gas. Although our experience is clearly limited to two metallic surfaces, we consider it likely that the simple gas-surface reactions reported here will take place on other spacecraft surfaces as well. The optical observations and modeling of Swenson et al. [1985] and the mass spectrometric observations reported here make NO₂ a likely candidate for the source of the glow observed near the ram-oriented surfaces of various spacecraft.

It is intriguing to consider the use of a mass spectrometer to verify the presence of NO and NO₂ on surfaces other than those within the mass spectrometer's ion source. Although the large signal of odd nitrogen from mass spectrometer ion source surfaces makes this a difficult task, a beam inlet system, which is essentially an extension of the open source geometry used in the Atmosphere Explorer satellite mass spectrometers, may provide a feasible way to complement existing optical detection systems.

Acknowledgments. This research was supported by the Dynamics Explorer Guest Investigator Program through NASA Grant NAG 5-349 to Augsburg College.

References

- Carignan, G. R., B. P. Block, J. C. Maurer, A. E. Hedin, C. A. Reber, and N. W. Spencer, The neutral mass spectrometer on Dynamics Explorer B, Space Sci. Instrum., 5, 429-441, 1981.
- Engebretson, M. J., and K. Mauersberger, The impact of gas-surface interactions on mass spectrometric measurements of atomic nitrogen, J. Geophys. Res., 84, 839-844, 1979.
- Engebretson, M. J., and J. T. Nelson, Atomic nitrogen densities near the polar cusp, Journal of Geophysical Research, in press, 1985.
- Hedin, A. E., B. B. Hinton, and G. A. Schmitt, Role of gas-surface interactions in the reduction of Ogo 6 neutral particle mass spectrometer data, J. Geophys. Res., 78, 4651-4668, 1973.
- Mauersberger, K., M. J. Engebretson, W. E. Potter, D. C. Kayser, and A. O. Nier, Atomic nitrogen measurements in the upper atmosphere, Geophys. Res. Lett., 2, 337-340, 1975.
- Nier, A. O., W. E. Potter, D. R. Hickman, and K. Mauersberger, The open-source neutral-mass spectrometer on Atmosphere Explorer-C, -D, and -E, Radio Sci., 8, 271-281, 1973.
- Swenson, G. R., S. B. Mende, and K. S. Clifton, Ram vehicle glow spectrum: Implication of NO₂ recombination continuum, Geophys. Res., Lett., 12, 97-100, 1985.

9/25/84

ORBIT NO. : 1630
 PROCESSED : 7/17/83
 MAF KEY : D 81325 56817325 81325 58785299 B NACS COMP2001

DE-B NACS
 MASS : 30 40 14 4
 SYMBOL : \$ A N 4

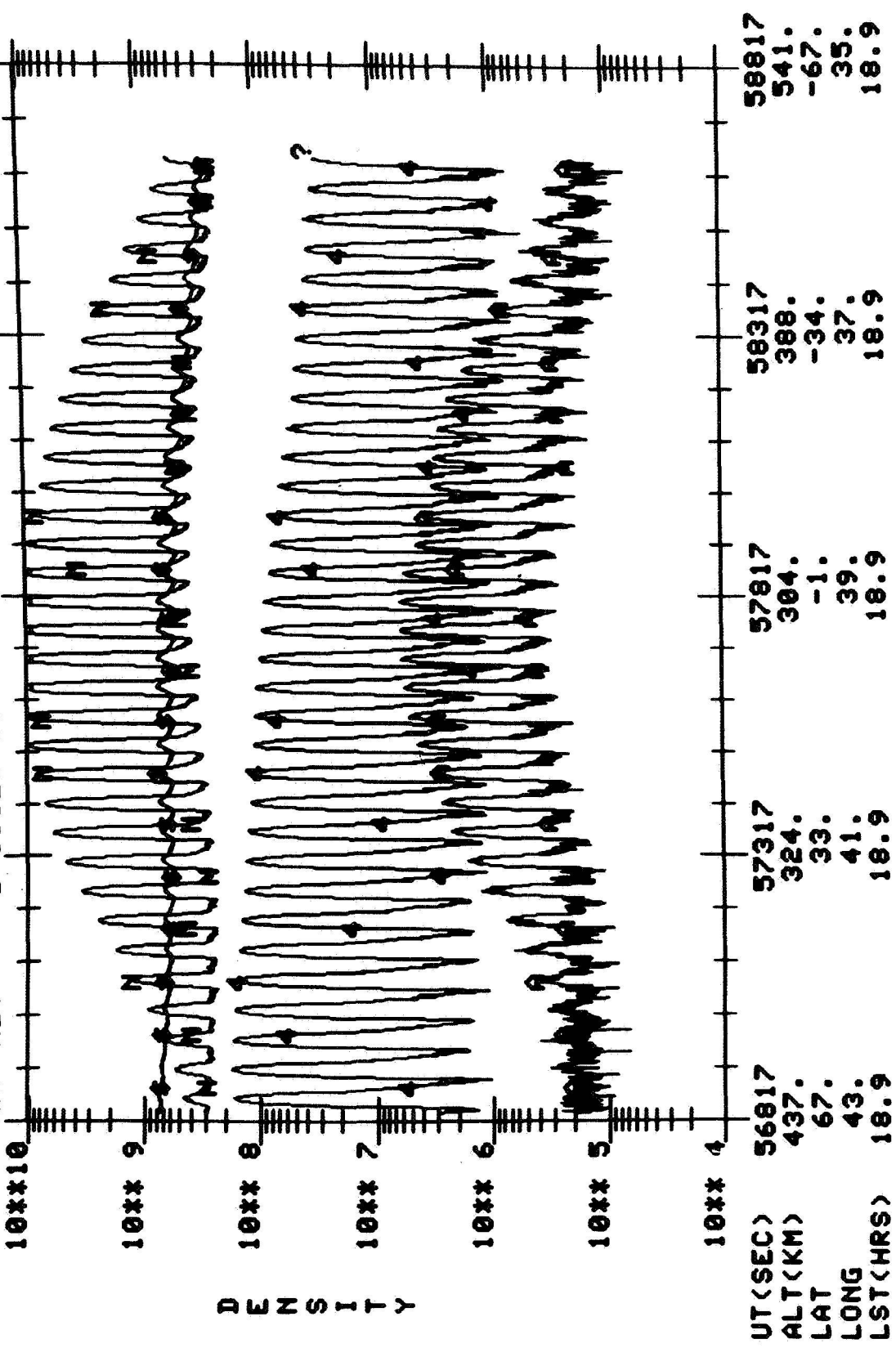


Fig. 1. Ion source number densities of NO, Ar, N₂, and He measured by the Neutral Atmospheric Composition Spectrometer (NACS) on orbit 1630 of the Dynamics Explorer-2 satellite, plotted as a function of universal time (UT). The NACS instrument was off during the previous orbit.

9/25/84

DE-3 NACS

ORBIT NO. : 1632 MASS : 30 40 14 4
 PROCESSED : 9/10/84 SYMBOL : \$ A N 4
 MAF KEY : D 01325 68433169 01325 70393143 B NACS COMP2001

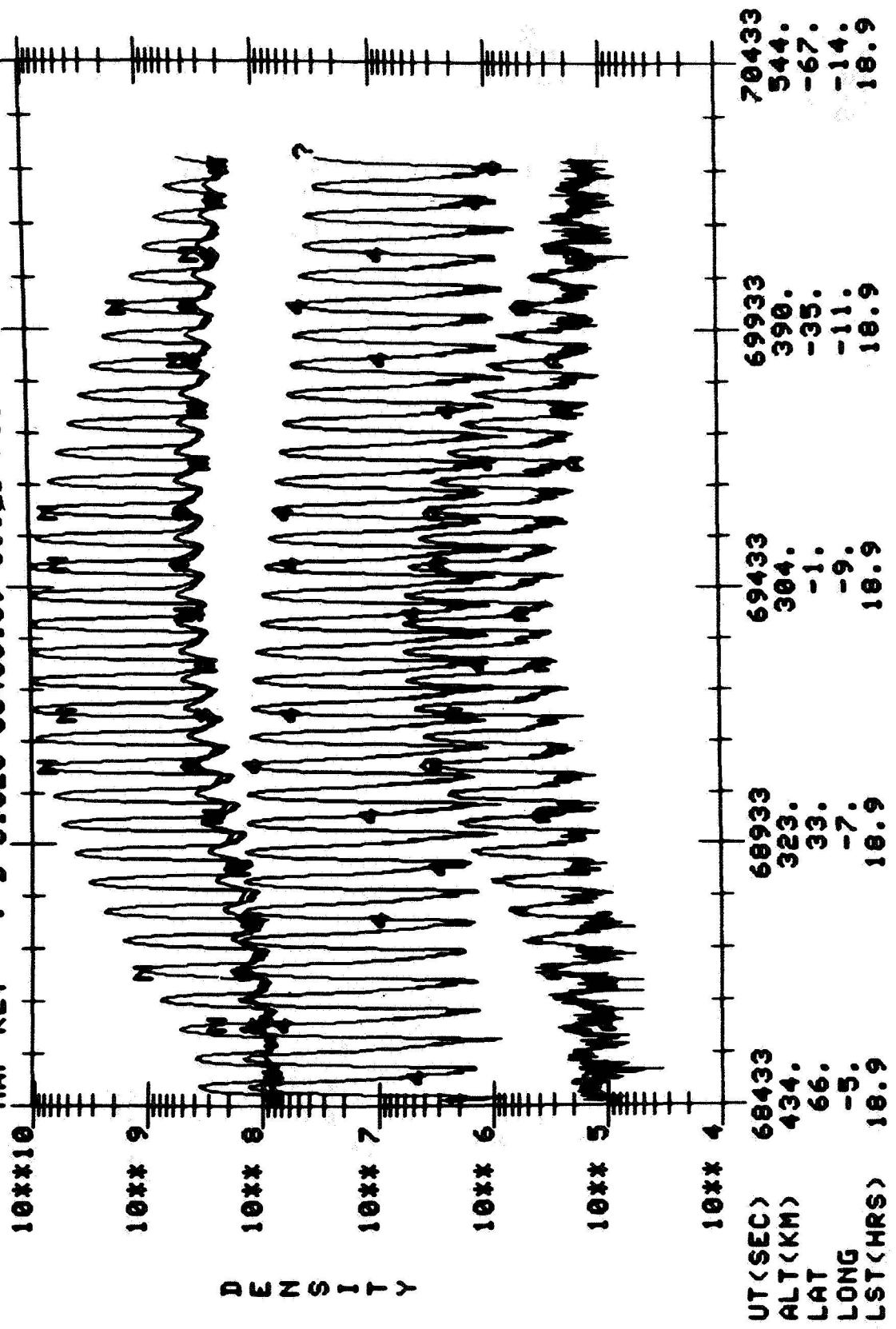


Fig. 2. Ion source number densities of NO, Ar, N2, and He for orbit 1632 of DE-2, as in Figure 1. The NACS instrument was on for two successive perigee passes prior to this orbit.

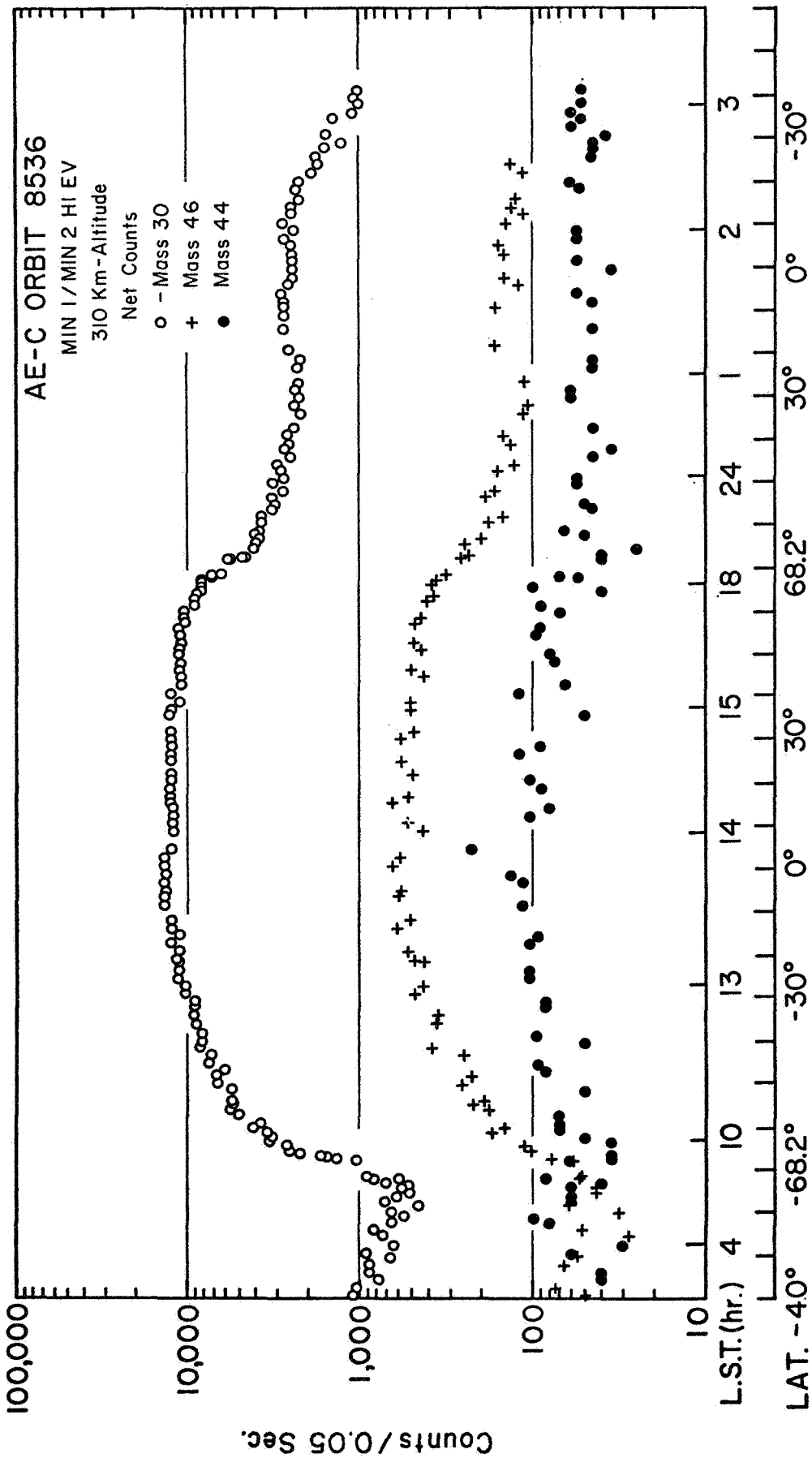


Fig. 3. Net (forward facing minus backward facing) counts of masses 30, 44, and 46 measured by the Open Source Neutral Mass Spectrometer (OSS) on orbit 8536 of the Atmosphere Explorer-C satellite, plotted as a function of time during a full orbit pass. This orbit was preceded by a 4-hour warmup.

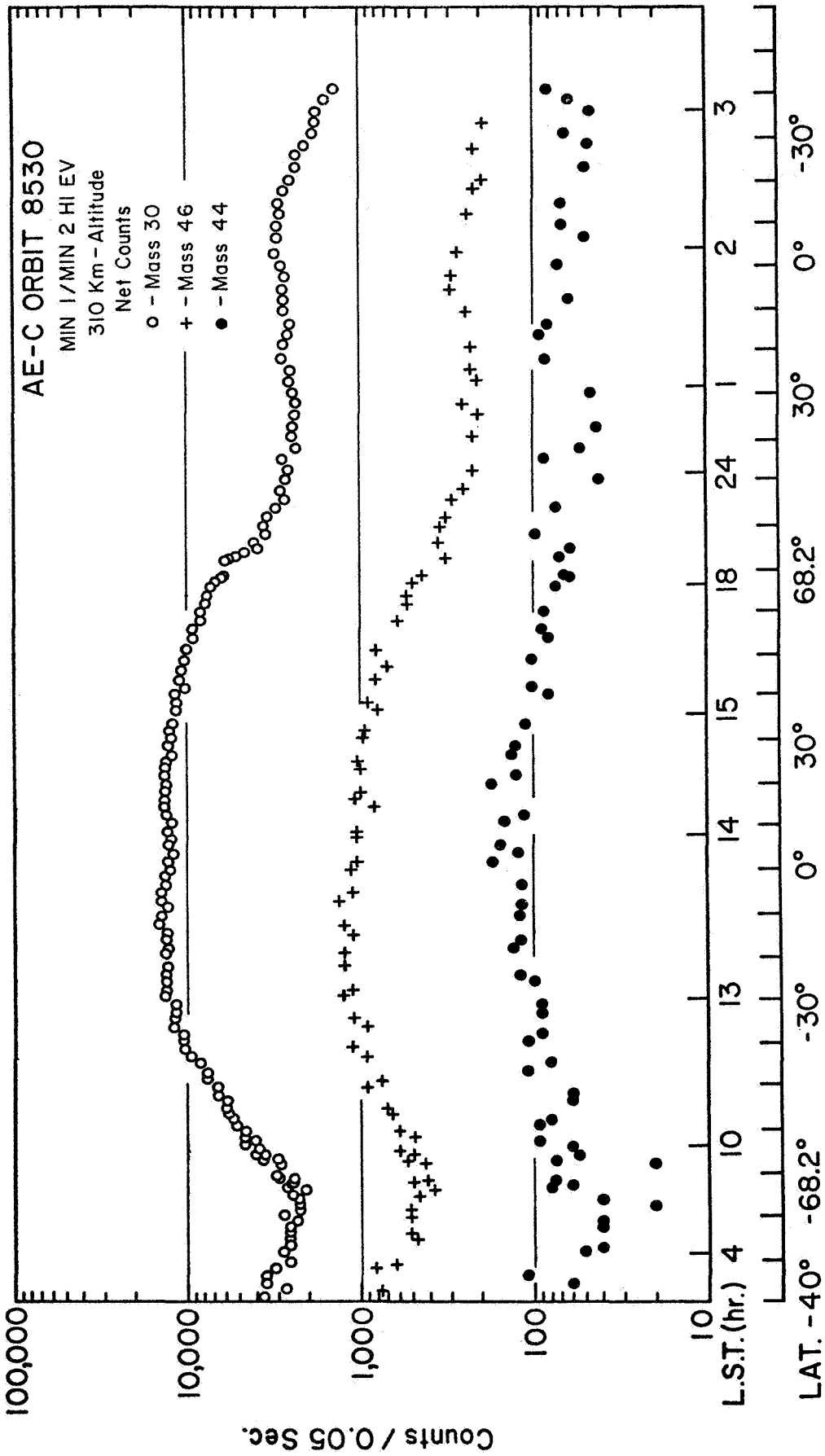


Fig. 4. Net counts of masses 30, 44, and 46 for orbit 8530 of AE-C, as in Figure 3. This orbit was preceded by a standard 30-min warmup.

TABLE 1. TYPICAL ORBIT COUNT RATES OF MASSES 30 AND 46 FROM ELLIPTICAL DESPUN ORBITS OF THE AE-C AND DE-2 SATELLITES

Altitude	AE-C			DE-2		
	Mass 30	Mass 46	30/46	Mass 30	Mass 46	30/46
"COLD" orbits						
500	1,800	500	3.6			
300	17,500	2,000	8.8	29,200	3,130	9.3
Perigee						
300	17,000	1,000	17.0	12,900	1,200	10.8
500	2,850	310	9.2			
700	1,450	260	5.6			
"WARM" orbits						
500	320	36	8.9			
300	7,800	430	18.1	9,900	161	61.7
Perigee						
300	12,400	670	18.5	13,800	330	41.3
500	2,000	230	8.7	3,500	30	115
700	1,060	200	5.3	2,050	15	137

TABLE 2. RATIOS OF SIGNALS OF MASSES 30 AND 46 FOR THREE SATELLITE MASS SPECTROMETERS. INTENSITY RATIOS ARE DETERMINED AT THE GIVEN ALTITUDES ON THE UPLEG OF ELLIPTICAL ORBITS UNDER SUNLIT CONDITIONS.

	AE-C	AE-D	DE-2
Source material	nichrome	gold	gold
Geometry	open (30°)	open (12°)	closed
Altitude	N(30) / N(46)		
300 km	18	4.6	41
400	13	3.6	56
500	8.7	3.6	92
600	6.6	3.5	120
700	5.3	2.7	137

THE ATMOSPHERE EXPLORER AND THE SHUTTLE GLOW

A. Dalgarno, J-H. Yee, and M. LeCompte

Harvard-Smithsonian Center for Astrophysics

Abstract. Recent analyses of the Atmosphere Explorer data are discussed in which it is demonstrated that the satellite glows have two components, one at high altitudes which is consistent with excitation in single collisions of atmospheric oxygen atoms with the vehicle surface and the other at low altitudes which is consistent with double collisions of nitrogen molecules. Contrary to an earlier suggestion, the low-altitude data are not consistent with single collisions of oxygen molecules.

The separation of the two components strengthens the conclusion that the high-altitude glow arises from vibrationally excited OH molecules produced by a formation mechanism that is different from that leading to the normal atmospheric OH airglow. The spectrum is consistent with association of oxygen and hydrogen atoms at sites on the surface into the vibrational levels of OH. The low-altitude glow is consistent with the Green mechanism but there are difficulties with it.

The shuttle glows are different and have the spectral appearance of emission from NO₂. The characteristics of the shuttle glows and the satellite glows will be contrasted and a tentative resolution of the differences in the Atmosphere Explorer and shuttle glows will be offered.

Discussion

Much detailed information about the glows resulting from the interaction of spacecraft with the atmospheric environment has been acquired from studies of the data provided by the Visible Airglow Experiment onboard the Atmosphere Explorer satellites [Hays et al., 1973]. Figure 1 illustrates the glow intensity at 732 nm as a function of altitude [Yee and Abreu 1982, 1983]. Above 160 km the intensity is directly proportional to the ambient number density [O] of atomic oxygen. Yee and Abreu [1982, 1983] suggested that the glow was produced by oxygen-containing metastable molecules released from the surface after energetic collisions with oxygen atoms and they drew attention to laboratory studies of OH, NO and NO₂ surface luminosities. The shuttle glow intensity appears to increase with diminishing altitude and may also be proportional to [O] [Banks et al., 1983; Mende et al., 1983, 1984a,b, 1985].

Yee and Abreu [1982, 1983] analyzed the variation of the glow intensity with the angle of attack and obtained a distribution $\cos^3\phi$ with some emission persisting to an angle of 120°. In laboratory studies of the dissociative absorption probability, the variation with ϕ depends upon the interacting species and the nature of the surface. A variation as $\cos^3\phi$ happens to be consistent with a one-dimensional barrier model of desorption which has received experimental support from studies of the interaction of the light molecule H₂ with Cu surfaces

[Balooch et al., 1974]. For the heavier molecule N_2 on a W(110) surface, in contrast, the dissociative absorption probability depends only weakly on angle [Auerbach et al., 1984] as apparently does the shuttle glow intensity [Mende et al., 1984a,b].

The efficiency with which the glow is produced on the AE satellites for each collision of an oxygen atom was found to increase during the satellite lifetimes indicating that surface processing was occurring [Yee et al., 1984]. The shuttle does not remain in orbit long enough for time-dependent effects on the luminosity to be detectable though direct shuttle-based measurements have demonstrated a substantial erosion of various materials and the glow intensity depends upon the surface material [Mende et al., 1984b, 1985].

The observation of a glow at angles greater than 90° on the AE satellites was attributed to the surface release of excited molecules with a finite radiative lifetime [Yee and Abreu, 1982, 1983]. The distribution with ϕ is consistent with a decay length of 10 m. Because the analysis did not take account of the Maxwellian velocity distribution of the impacting atoms, the derived value of 10 m should be regarded strictly as an upper limit. The corresponding radiative lifetime probably lies between 10 ms and 1 ms.

The shuttle glow can be analyzed more directly in that the glow is seen to be spatially extended. A careful analysis of the photographs of the glow yielded a decay length of 20 cm and suggested that the mechanisms of the AE and shuttle glows are different [Yee and Dalgarno, 1983, 1985].

The measured intensity ratio of the AE glow in the band passes centered at 732 nm and 656 nm is 2.15 between 170 and 175 km and 2.25 between 140 and 145 km [Yee and Abreu, 1982, 1983; Langhoff et al., 1983], close to the OH intensity ratio observed in the night airglow. Together with the inferred radiative lifetime, the similarity of the intensity ratios led Slanger [1983] to suggest vibrationally-excited OH as the molecule responsible for the AE luminosity. Further data obtained over a wavelength range extending to 280 nm [Yee and Abreu, 1983] gave a spectrum which differs from that of the airglow but Langhoff et al. [1983] showed that the OH identification could be retained by postulating OH formation through a surface association mechanism that populates all the vibrational levels at nearly uniform rate. Their model reproduced satisfactorily the shorter wavelength data but it yielded a 732 nm/656 nm intensity ratio between 5.6 and 7.4. They suggested tentatively that the discrepancy with the measured ratio of 2.15 was due to the uncertainties in the line positions of transitions originating in the high vibrational levels for which no laboratory data exist.

Additional support for the OH identification was obtained from measurements with a Fabry-Perot interferometer onboard the Dynamics Explorer DE-B satellite [Abreu et al., 1985]. Two lines were detected whose positions, corrected for the Doppler shift arising from the moving satellite, coincide with lines of OH. A third line was detected which could also be due to OH. Although persuasive, we note that the lines also coincide in position within the accuracy of the measurements with three lines of the first positive system of N_2 .

The spectrum of the shuttle glow [Mende et al., 1983, 1984a,b 1985] is different from the AE glow. It appears to be without structure and is very similar to the NO_2 recombination continuum [Swenson et al.,

1985]. Emission from NO_2 has been the subject of many laboratory studies [Fontijn et al., 1964; Paulsen et al., 1970; Kenner and Ogryzlo, 1984; Kuwabara et al., 1984]. Swenson et al. [1985] suggested that NO, produced by the ramming N_2 and O, remains on the surface where it reacts further with the ambient oxygen atoms. A more efficient mechanism may utilize the ambient NO molecules and N atoms and N_2O may be formed as well as NO_2 . The excited NO_2 molecules have a lifetime of about 80 μs at 500 nm [Schwartz and Johnston, 1969]. To be consistent with the derived spatial extent of 20 cm [Yee and Dalgarno, 1983], the NO_2 must be released with a velocity of 2.5 km s^{-1} corresponding to a kinetic energy of about 1.4 eV.

An alternative theory of the spacecraft glow has been advanced by Papadopoulos [1984]. According to it, energetic electrons are produced by a plasma interaction and the glow is caused by electron impact excitation. The plasma phenomenon determines the spatial extent of the glow. We have extended an earlier study by Kofsky [1984] of the expected spectrum. As Kofsky [1984] pointed out, the most intense emissions appear in the ultraviolet, a region not yet observed on the space shuttle. Weaker emissions occur in the visible and infrared but the behavior of the spectrum below 600 nm is quite different from both the shuttle and the AE spectra.

The plasma mechanism leads to a glow intensity which increases with the ambient electron density. The AE glow has been analyzed. No correlation was found between its intensity and the electron density [Yee et al., 1984].

Below 160 km, the intensity of the AE glow is no longer proportional to $[\text{O}]$ and the spectrum is different [Yee and Abreu, 1982, 1983]. Slanger [1983] remarked that the enhancement in the glow intensity above that obtained by extrapolating the contribution from atomic oxygen was directly proportional to the number density $[\text{O}_2]$ of ambient molecular oxygen, but a more detailed study by Yee et al. [1985] of a larger data base concludes instead that the glow intensity can be represented by the expression

$$I_\lambda = k_o(\lambda)[\text{O}] + k_{\text{N}_2}(\lambda)[\text{N}_2]^2 \quad (1)$$

where $[\text{N}_2]$ is the number density of ambient molecular nitrogen. The variation as the square of $[\text{N}_2]$ could be alternatively a variation as the product of any pair of the molecules N_2 , O_2 and NO which have similar scale heights in the altitude range of the observations. A variation as $[\text{N}_2]^2$ indicates a mechanism involving the successive collisions of two molecules and is consistent with the mechanism suggested by Green [1984] for the shuttle glow. However if it is to make a significant contribution to the shuttle glow, its efficiency must be several orders of magnitude greater on the shuttle than the values derived for the AE satellites. A possible objection to the Green mechanism is the success of the ion mass spectrometric measurements of atomic nitrogen [Engbretson and Mauersberger, 1979] on the AE satellites which argues that little dissociation of N_2 occurred. If N_2 is not dissociated by impact with the surface, the shuttle glow mechanism may be modified by invoking ambient N or NO in place of the dissociated N_2 .

Table 1, reproduced from Yee et al. [1985], gives the derived relative intensities from the process involving O and from the process

involving N_2 . The N_2 mechanism gives rise to a spectrum decreasing rapidly in intensity at the shorter wavelengths, and its increasing importance at low altitudes is responsible for the steeper glow spectrum below 160 km. At longer wavelengths, the spectrum bears some similarity to the spectrum measured on the Spacelab 1/shuttle mission degraded to match the resolution of the AE photometer [Torr and Torr, 1985]. The spectrum resulting from the Green mechanism is not available and it is unclear how well it might reproduce the observations.

The discrepancy between the model value of the 732 nm/656 nm intensity ratio and the value corresponding to the oxygen mechanism, shown in Table 1, is substantial. It can be removed by postulating an additional source of emission in the spectral region between 600 and 700 nm. A plausible candidate is the shuttle glow mechanism.

A microdensitometer trace of the objective grating spectrum of the glow on the tail of the shuttle STS-8 gave an intensity per unit wavelength near 700 nm of about 450 R/Å corresponding to a total glow intensity of 1MR [Mende et al., 1984a]. The shuttle glow intensity is enhanced by the oblique geometry of the observations. Corrected to a direction normal to the shuttle surface, we estimate an intensity between 10 and 20 R/Å. For the AE satellite the intensity is reduced further by the curvature of the satellite surface to between 5 and 10 R/Å corresponding to a total of 150 R if the shuttle mechanism is operating on the AE satellite. The baffle of the AE airglow photometer extrudes 8 cm above the surface, and bearing in mind the short decay length of the shuttle glow, we estimate that of the total 150 R only 30 R would be detected. The total measured intensity is 60 R and we suggest that half the measured high-altitude glow on the AE surfaces arises from the mechanism that has been attributed to OH and half from the shuttle mechanism that has been attributed to NO_2 . Table 2 compares the resultant relative intensities with those measured above 160 km. The agreement is close. A more quantitative study is in progress.

We believe the OH mechanism also operates on the shuttle but is weak compared to the NO_2 mechanism in the visible. It may be detectable between 1 and 2μ if the calculations of Langhoff et al. [1983] are appropriate.

Acknowledgments. This research was supported in part by the Air Force Geophysics Laboratory under contract F19628-88-0034, by the Aeronomy Program of the National Science Foundation under Grant ATM-84-07314, and by NASA Grant NAGW-496 to the University of Michigan.

References

- Abreu, V. J., W. R. Skinner, P. B. Hays, and J-H. Yee, Optical effects of spacecraft-environment interactions: Spectrometric observations by DE-B satellite, J. Spacecraft and Rockets, 22, 177-180, 1985.
- Auerbach, D. J., H. E. Pfnur, C. T. Rettner, J. E. Schlaegel, J. Lee, and R. J. Madix, Kinetic energy and angular dependence of activated dissociative absorption of N_2 on W(110): Observed insensitivity to incidence angle, J. Chem. Phys., 81, 2515-2516, 1984.

- Balooch, M., M. J. Cardillo, D. R. Miller, and R. E. Stickney, Molecular beam study of the apparent activation barrier association with the absorption and desorption of H on Copper, Surf. Sci., 46, 358-392, 1974.
- Banks, P. M., P. R. Williamson, and W. J. Raitt, Space Shuttle glow observation, Geophys. Res. Lett., 10, 118-121, 1983.
- Engebretson, M. J., and K. Mauersberger, The impact of gas-surface interactions on mass spectrometric measurements of atomic nitrogen, J. Geophys. Res., 84, 839-844, 1979.
- Fontijn, A., C. B. Meyer, and H. I. Schiff, Absolute quantum yield measurements of the NO-O reaction and its use as a standard for chemiluminescent reactions, J. Chem. Phys., 40, 64-70, 1964.
- Green, B. D., Atomic recombination into excited molecular nitrogen-A possible mechanism for Shuttle glow, Geophys. Res. Lett., 11, 576-579, 1984.
- Hays, P. B., G. Carignan, B. C. Kennedy, G. G. Shepherd, and J. C. G. Walker, The Visible-Airglow Experiment on Atmospheric Explorer, Radio Science, 8, 369-377, 1973.
- Kenner, R. D., and A. E. G. Ogryzlo, Orange chemiluminescence from NO₂, J. Chem. Phys., 80, 1-6, 1984.
- Kofsky, I. L., Spectroscopic consequences of Papadopoulos' discharge model of spacecraft ram glows, Radio Science, 19, 578-586, 1984.
- Kuwabara, S., K. Kuwata, I. Nishiyama, and I. Hanazaki, Acoustically oscillating emission from NO₂* produced by infrared photosensitized reaction in SF₆+NO₂, Chem. Phys. Lett., 106, 540-543, 1984.
- Langhoff, S. R., R. L. Jaffe, J-H. Yee, and A. Dalgarno, The surface glow of the Atmosphere Explorer C and E satellites, Geophys. Res. Lett., 10, 896-899, 1983.
- Mende, S. B., O. K. Garriott, and P. M. Banks, Observations of optical emissions on STS-4, Geophys. Res. Lett., 10, 122-125, 1983.
- Mende, S. G., P. M. Banks, and D. A. Klingel Smith, Observation of orbiting vehicle induced luminosities on the STS-8 mission, Geophys. Res. Lett., 11, 527-530, 1984a.
- Mende, S. B., G. R. Swenson, and K. S. Clifton, Preliminary results of the Atmospheric Emissions Photometric Imaging Experiment (AEPI) on Spacelab 1, Science, 225, 191-193, 1984b.
- Mende, S. B., G. R. Swenson, K. S. Clifton, R. Gause, L. Leger, and O. K. Garriott, Space vehicle glow measurements on STS 41-D, J. Spacecraft and Rockets, submitted, 1985.
- Papadopoulos, D., On the Shuttle glow (the plasma alternative), Radio Science, 19, 571-577, 1984.
- Paulsen, D. E., W. F. Sheridan, and R. E. Huffman, Thermal and recombination emission of NO₂, J. Chem. Phys., 53, 647-658, 1970.
- Schwartz, S. E., and H. S. Johnston, Kinetics of nitrogen dioxide fluorescence, J. Chem. Phys., 51, 1286-1302, 1969.
- Slanger, T. G., Conjectures on the origin of the surface glow of space vehicles, Geophys. Res. Lett., 10, 103-132, 1983.
- Swenson, G. R., S. B. Mende, and K. S. Clifton, Ram vehicle glow spectrum: Implication of NO₂ recombination continuum, Geophys. Res. Lett., 12, 97-100, 1985.
- Torr, M., and D. G. Torr, A preliminary spectroscopic assessment of the Spacelab 1/Shuttle optical environment, J. Geophys. Res., 90, 1683-1690, 1985.

- Yee, J-H., and V. J. Abreu, Optical contamination on the Atmospheric Explorer-E Satellite, SPIE Proceedings, 338, 120-129, 1982.
- Yee, J-H., and V. J. Abreu, Visible glow induced by spacecraft-environment interaction, Geophys. Res. Lett., 10, 126-129, 1983.
- Yee, J-H., and A. Dalgarno, Paper AIAA-03-2660-OP, Radiative lifetime analysis of the Shuttle optical glow, Environment and Operations Meeting, 191-197, 1983.
- Yee, J-H., and A. Dalgarno, Radiative lifetime analysis of the Shuttle optical glow, J. Spacecraft and Rockets, submitted, 1985.
- Yee, J-H., V. J. Abreu, and A. Dalgarno, Characteristics of the spacecraft optical glow, Geophys. Res. Lett., 11, 1192-1194, 1984.
- Yee, J-H., V. J. Abreu, and A. Dalgarno, The Atmosphere Explorer optical glow near perigee altitudes, Geophys. Res. Lett., submitted, 1985.

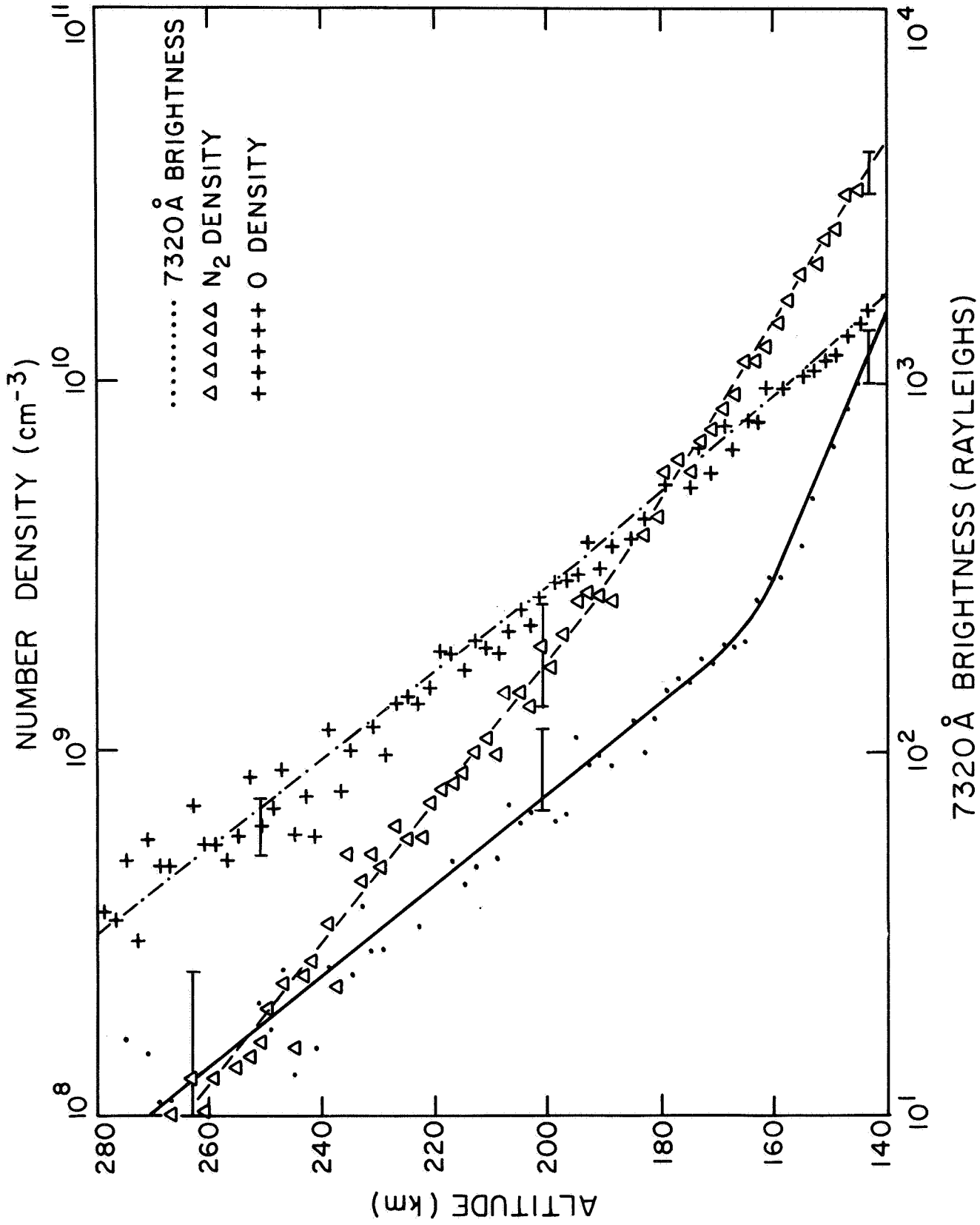


Fig. 1. The Atmosphere Explorer glow at 732 nm in Rayleighs as a function of altitude.

TABLE 1. INTENSITY RATIOS*

(nm)	Theoretical	Empirical			
	O-H recombination	O-mechanism		N ₂ -mechanism	
		(i)	(ii)	(i)	(ii)
732	1.00	1.00	1.00	1.00	1.00
656	0.18-0.13	0.71	0.68	0.09	0.08
428	0.05-0.03	0.02	0.02	0.06	0.06
337	0.06-0.02	0.05	0.04	0.21	0.17
280	---	0.08	0.03	0.19	0.08

* (i) $k(\lambda)/k(732)$ (ii) $\frac{k(\lambda)}{\Delta(\lambda)} \frac{\lambda(732)}{\Delta(732)}$

TABLE 2. AE GLOW SPECTRUM

	OH*	NO ₂	I _{OH} +I _{NO₂}	K _o
	(Langhoff et al., 1983)	(Swenson et al., 1985)		(Yee et al., 1985)
7320 Å	1.000	1.00	1.000	1.000
6563 Å	0.159	1.00	0.580	0.679
4278 Å	0.030	0.05	0.040	0.021
3371 Å	0.022	-	0.012	0.036

ORBITER GLOW OBSERVATIONS AT HIGH SPECTRAL RESOLUTION

David J.W. Kendall and Richard L. Gattinger

Herzberg Institute of Astrophysics
National Research Council of Canada

Edward J. Llewellyn and Ian C. McDade

Institute of Space and Atmospheric Studies
University of Saskatchewan

Steven B. Mende

Lockheed Palo Alto Research Laboratory

Abstract. An experiment flown on mission STS 41-G as part of the Canadian complement of experiments was designed to obtain relatively high resolution spectra of the Orbiter glow phenomenon over limited spectral regions centered on prominent upper atmospheric emissions. Observations were carried out successfully at altitudes of 360 km and 230 km although those at the lower altitude were limited by degradation of the image intensifier. Definitive glow results were obtained at the end of a thruster firing which showed the spectrum to be a continuum at a resolution of approximately 0.4 nm centered at a wavelength of 630 nm. Results at other wavelengths in the absence of any firings strongly suggest that the Orbiter glow is a continuum throughout the spectral region 550 nm to 760 nm. A discussion is presented that considers the reaction $\text{NO} + \text{O}_2^*$ as being a possible candidate for the mechanism producing the shuttle glow.

Introduction

In 1984, an opportunity arose to fly a complement of experiments onboard the shuttle to be performed by a Canadian payload specialist. One of the experiments accepted for flight was given the acronym OGLow and consisted of an imaged intensified camera system onto which was attached a series of filters or a transmission grating spectrograph. The filters were selected to be centered on prominent atmospheric emissions of interest to the WAMDII (Wide Angle Michelson Doppler Imaging Interferometer) instrument that will be flown onboard the shuttle in 1989 [Shepherd et al., 1985]. The purpose of the OGLow experiment was to obtain relatively high spectral resolution images of the Orbiter glow phenomenon and of the selected atmospheric emissions in order to provide knowledge of these emissions from above the atmospheric source region and to provide quantitative values of the shuttle glow intensity and spectral shape at these wavelengths.

The OGLow experiment was flown successfully on mission 41-G in October 1984 and produced results both of the glow phenomenon and of atmospheric emissions. Further details on the instrument and the varied scientific objectives may be found in Kendall et al. [1985].

Observations

For the STS 41-G flight, narrow bandpass interference filters (0.4 nm) were employed with a central wavelength, for normal incidence, slightly longer than that of the atmospheric emissions. As the camera operated in a true imaging mode, this choice of central passbands afforded both spectral scanning [Shepherd et al., 1965] and some protection against wavelength shift due to temperature change. The specifications of the filters are listed in Table 1. For the observations of shuttle glow the Orbiter was positioned with the payload bay pointing in the nadir, with the velocity vector in the -Y direction with respect to the Orbiter body X,Y,Z coordinate axis system, and with the 100 km atmospheric layer bisecting the rear stabilizer as observed from the aft windows of the cabin. In this way it was possible to compare the shuttle glow directly with known atmospheric emissions.

For the atomic line emissions (557.7, 630.0, 731.9, and 777.4 nm) this procedure is straightforward as the limb enhancement may be readily calculated. However, for the molecular emissions (O_2 atmospheric band at 762.0 nm and the 8-3 OH Meinel band at 730.2 nm) the change of the filter capture fractions with the shift of passband, due to spatial scanning, must be considered. Studying the glow at the wavelengths of the atmospheric emissions also allows inversion of the emission profiles to determine boundary values for both temperature and species concentration [McDade and Llewellyn, 1984].

The crew activity plan for the mission afforded two opportunities to make shuttle glow measurements during two entire night passes. The first of these was on mission day 2, when the Orbiter was at an altitude of 360 km, and the second occurred on mission day 5 at an altitude of 230 km. An 8-second exposure photograph from day 2 with the 630.8 nm filter is shown in Figure 1 and fails to reveal an obvious shuttle glow. The dimensions of the Orbiter stabilizer, on the digitized image, were carefully measured and compared with those obtained from an image taken under non-glow conditions. In practice, the equations for the surfaces of the OMS pod and the upper stabilizer were determined using a least-squares fitting routine and then used to register subsequent images. The estimated error in this procedure is ± 2 cm. The extension of the ring pattern throughout the entire atmosphere attests to the extended nature of the airglow emission while the ring pattern across the tail demonstrates the albedo of the shuttle. The presence of albedo away from the bright ring is due to both scattered moonlight and other airglow emissions, notably the airglow continuum and the OH Meinel bands. Similar photographs were obtained with the other filters and failed to reveal any Orbiter glow. Unfortunately, the intensifier was damaged, with a consequent loss of sensitivity, at the end of this night pass.

By comparing the airglow limb brightness with that measured on the tail of the Orbiter, upper limits for the shuttle glow at 360 km can be determined. These values are presented in Table 2. It should be noted that while these values are expressed in terms of a continuum brightness, the present results cannot be used to conclude that the glow is in fact a continuum at this altitude.

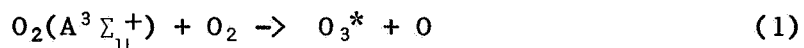
On mission day 5 the Orbiter was again positioned so that the velocity vector was in the -Y direction and the same observing program

was repeated. The only group of exposures, all taken with the 630.8 nm filter, that revealed a definitive glow were those taken after a thruster firing and before the induced glow had entirely disappeared. One of these exposures is shown in Figure 2. Through the cooperation of the entire shuttle crew it was possible to avoid exposures that included a thruster firing. A video tape, obtained from a payload bay CCTV camera operated during this entire night pass, indicates that there were only three vernier thruster firings that caused a noticeable shuttle glow during the observing period. The presence of this glow along the entire leading face of the stabilizer, except for the region shadowed by the OMS pod, indicates that at this resolution (0.4 nm) the thruster-induced glow is a continuum. As for the high altitude observations, upper limits for the spacecraft glow at 230 km have been determined. These values are also presented in Table 2. Due to the loss of sensitivity of the intensifier, these upper limits are significantly larger than those obtained for the high-altitude observations. Attempts to correlate the induced glow photographs with the video tape are continuing although it has been noticed that each vernier thruster firing appears in three distinct parts, each less intense than its predecessor. The final brightening is close to the stabilizer and it is probably this final part that is present in Figure 2.

The width of the induced glow has been determined from the digitized image of Figure 2 to be approximately 15 cm; this value is in reasonable agreement with the values reported by Yee and Dalgarno [1983] and Swenson et al. [1985]. If the continuum nature of the glow observed at 630.8 nm also extends to the rest of the emission spectrum, then it would appear that for instruments intended to look at narrow line emissions, e.g., WAMDII and WINDII, there is no major problem from the vehicle glow. For observations over an extended spectral range this may not apply.

Discussion

If the vehicle glow, both the normal ram glow and that induced from the thruster firing, is a true continuum, it is reasonable to suppose that it arises from a recombination that forms NO_2 as suggested by Swenson et al. [1985]. In Figure 3 the glow spectra of Swenson et al. have been replotted together with those of Torr and Torr [1985] when the ISO instrument, flown on Spacelab 1, was pointing directly into the velocity vector. These latter values have been normalized to unity at the longest wavelength, i.e., 800 nm. The continuum from $\text{NO} + \text{O}$ [Fontijn et al., 1964; Paulsen et al., 1970] and that from $\text{NO} + \text{O}_3$ [Greaves and Garvin, 1959] have also been included in the figure. Here the values have been normalized to unity for the maximum intensity within the plotted spectral region. Recently Kenner and Ogryzlo [1984] have presented observations of an orange chemiluminescence from NO_2 and these are also included in the figure. It is readily apparent that while none of these spectra exactly match the shuttle glow observations, those from Kenner and Ogryzlo [1984] are in closest agreement. This is particularly true when the uncertainty in the longer wavelength glow measurements is recognized. These latter investigators concluded that the orange glow was due to the reaction of NO with vibrationally excited O_3^* , where the latter species was formed according to the reaction:



and where the $O_2(A^3\Sigma_u^+)$ state was formed through the heterogeneous recombination of oxygen atoms on a nickel mesh. In their analysis, Kenner and Ogryzlo [1984] concluded that the primary losses of vibrationally excited ozone were due to wall quenching and through reaction with NO. However, if the measurements of the loss of vibrationally excited ozone with oxygen atoms are considered [West et al., 1976, 1978], it appears that the analysis of Kenner and Ogryzlo [1984] could be in error. An alternate possibility is that the excited ozone state referred to by Kenner and Ogryzlo is a low lying electronic state as conjectured by McGrath et al. [1983]. In the following analysis, we have considered both the Kenner and Ogryzlo scheme and a direct reaction between NO and O_2^* as suggested by Harteck and Reeves [1964]. In their analysis Kenner and Ogryzlo derived the expression:

$$I \text{ (orange glow)} = \frac{k[O_2^*][O_2][NO]}{[M]} \quad (2)$$

where the effective rate constant $k = 5 \times 10^{-13} \text{ cm}^3 \text{ molecule}^{-1} \text{ sec}^{-1}$ and each of the other terms have their usual meaning. The concentration of excited oxygen molecules close to the nickel screen for essentially zero flow conditions, would be given by:

$$[O_2^*] = \frac{\xi [O]}{k_1[O] + k_2[O_2] + A} \quad (3)$$

where ξ is the efficiency of the surface recombination; $k_1[O]$ represents the loss rate of O_2^* through O; $k_2[O_2]$ is the loss rate through O_2 ; and A is the radiative loss. For the model atmosphere shown in Table 3, the concentration of O_2^* is equal to $\xi \times 10^{11}$ at all altitudes. If the surface layer of O_2^* does not build up during the flight, then the production rate would equal the loss rate from the surface. Thus the production rate of orange glow emitters is equal to $2 \times 10^3 \xi [NO]$ at 200 km and $3.6 \times 10^4 \xi [NO]$ at 300 km. Hence the surface brightness over the entire spectrum at 200 km is $260 \xi \text{ kR}$ and $9.3 \xi \text{ R}$ at 300 km. For any reasonable value of the efficiency [Black and Slanger, 1981] this is unable to match the glow intensity reported by Mende et al. [1984] or the upper limits obtained here.

An alternative approach is to consider the direct reaction of O_2^* and NO as postulated by Harteck and Reeves [1964]. In this case we have a production rate expression given by:

$$I \text{ (orange glow)} = \frac{\xi [O]k_3[NO]}{k_1[O] + k_2[O_2] + A} \quad (4)$$

Under these conditions at 200 km, the surface brightness is equal to $9 \times 10^{24} \xi k_3$ and $1 \times 10^{22} \xi k_3$ at 300 km. If k_3 is gas kinetic and $\xi = 10^{-4}$ the effective surface brightness is 90 kR at 200 km and 100 R at 300 km. These values do not contradict the presently available measurements although it should be noted that the glow forming reaction is in the gas phase. The surface simply provides a source of O_2^* and an opportunity for the effective NO concentration to be doubled. The high speed of the emitting molecules is simply due to the mechanics of the collision. The

thruster glow would of course follow both this reaction and the normal NO + O reaction. This latter reaction would deplete [O] so that the normal shuttle glow would be enhanced; the loss of O₂* through collisions with O is decreased. However, after the thruster firing, the O₂* concentration on the shuttle surface would be reduced and the vehicle glow could be reduced, at least for a short time. As Ogryzlo and Slanger (private communications, 1985) have noted, different materials have different efficiencies as catalysts for the surface recombination of oxygen atoms, so that it is to be expected that vehicle glow is material dependent.

An alternative hypothesis has been presented by Swenson et al. [1985] who suggested that the glow recombination reactions essentially followed the surface formation of an NO monolayer. However, the departure of the observed glow spectrum from that of NO + O allows us to question that mechanism. A mechanism in which oxygen atoms adsorbed on the surface react with impacting NO molecules and then are extracted from the surface has been suggested by Thrush et al. [1968]. Although such a mechanism could indeed shift the NO₂ spectrum to longer wavelengths, Kenner and Ogryzlo [1984] have shown that such a process is unnecessary for the formation of the orange glow. It should also be noted that a potential source of enhanced NO concentration could be the reaction between incident N atoms and O₂* molecules residing on the surface.

Acknowledgments. We wish to acknowledge the assistance provided by B.H. Long, G.R. Swenson, and G.J. Buttner in the present work. This experiment has been supported by the Canada Centre for Space Science of the National Research Council of Canada; the Lockheed Palo Alto Research Laboratory; and the Universities Space Research Association.

References

- Black, G., and T.G. Slanger, Production of O₂(a' Δg) by oxygen atom recombination on a pyrex surface, J. Chem. Phys., 74, 6517-6519, 1981.
- Fontijn, A., C.B. Meyer, and H.I. Schiff, Absolute quantum yield measurements of the NO-O reaction and its use as a standard for the chemiluminescent reactions, J. Chem Phys., 40, 64-70, 1964.
- Greaves, J.C., and D. Garvin, Chemically induced molecular excitation: Excitation spectrum of the nitric oxide-ozone system, J. Chem. Phys., 30, 348-349, 1959.
- Hartek, P., and R.R. Reeves, Formation and reaction of the excited O₂(A³Σ_u⁺) molecule, Disc. Faraday Soc., 37, 82-86, 1964.
- Kendall, D.J.W., R.L. Gattinger, R. Wlochowicz, M. Garneau, G.J. Buttner, S. Mende, G.R. Swenson, E.J. Llewellyn, W.A. Gault, G.G. Shepherd, B.H. Solheim, and L.L. Cogger, OGLow - An experiment to measure Orbiter and Earth optical emissions, Canad. Aeronaut. Space J., in press, 1985.
- Kenner, R.D., and E.A. Ogryzlo, Orange chemiluminescence from NO₂, J. Chem. Phys., 80, 1-6, 1984.
- McDade, I.C., and E.J. Llewellyn, Atomic oxygen concentrations in the auroral ionosphere, Geophys. Res. Lett., 11, 247-250, 1984.
- McGrath, W.D., J.M. Maguire, A. Thompson, and J. Trocha-Grimshaw, The production of electronically excited ozone by flash irradiation, Chem. Phys. Lett., 102, 59-63, 1983.

- Mende, S.B., P.M. Banks, and D.A. KlingelSmith, III, Observations of orbiting vehicle induced luminosities on the STS-8 mission, Geophys. Res. Lett., 11, 527-530, 1984.
- Paulsen, D.E., W.F. Sheridan, and R.E. Huffman, Thermal and recombination emission of NO₂, J. Chem. Phys., 53, 647-658, 1970.
- Shepherd, G.G., C.W. Lake, J.R. Miller, and L.L. Cogger, A spatial spectral scanning technique for the Fabry-Perot spectrometer, Appl. Opt., 4, 267-272, 1965.
- Shepherd, G.G., W.A. Gault, D.W. Miller, Z. Pasturczyk, S.F. Johnston, J.W. Haslett, D.J.W. Kendall, and J.R. Wimperis, WAMDII: Wide Angle Michelson Doppler Imaging Interferometer for Spacelab, Appl. Opt., in press, 1985.
- Swenson, G.R., S.B. Mende, and K.S. Clifton, Ram vehicle glow spectrum: Implication of NO₂ recombination continuum, Geophys. Res. Lett., 12, 97-100, 1985.
- Thrush, B.A., C.J. Halstead, and A. McKenzie, Chemiluminescence in gases: Reactions yielding electronically excited sulfur dioxide, J. Phys. Chem., 72, 3711-3714, 1968.
- Torr, M.R., and D.G. Torr, A preliminary spectroscopic assessment of the Spacelab 1/shuttle optical environment, J. Geophys. Res., 90, 1683-1690, 1985.
- West, G.A., R.E. Weston, and G.W. Flynn, Deactivation of vibrationally excited ozone by O(³P) atoms, Chem. Phys. Lett., 42, 489-493, 1976.
- West, G.A., R.E. Weston, and G.W. Flynn, The influence of reactant vibrational excitation on the O(³P) + O₃⁺ bimolecular reaction rate, Chem. Phys. Lett., 51, 429-433, 1978.
- Yee, J.H., and A. Dalgarno, Radiative lifetime analysis of the shuttle optical glow, AIAA-83-CP838, AIAA Shuttle Environment and Operations Meeting, 191-196, 1983.

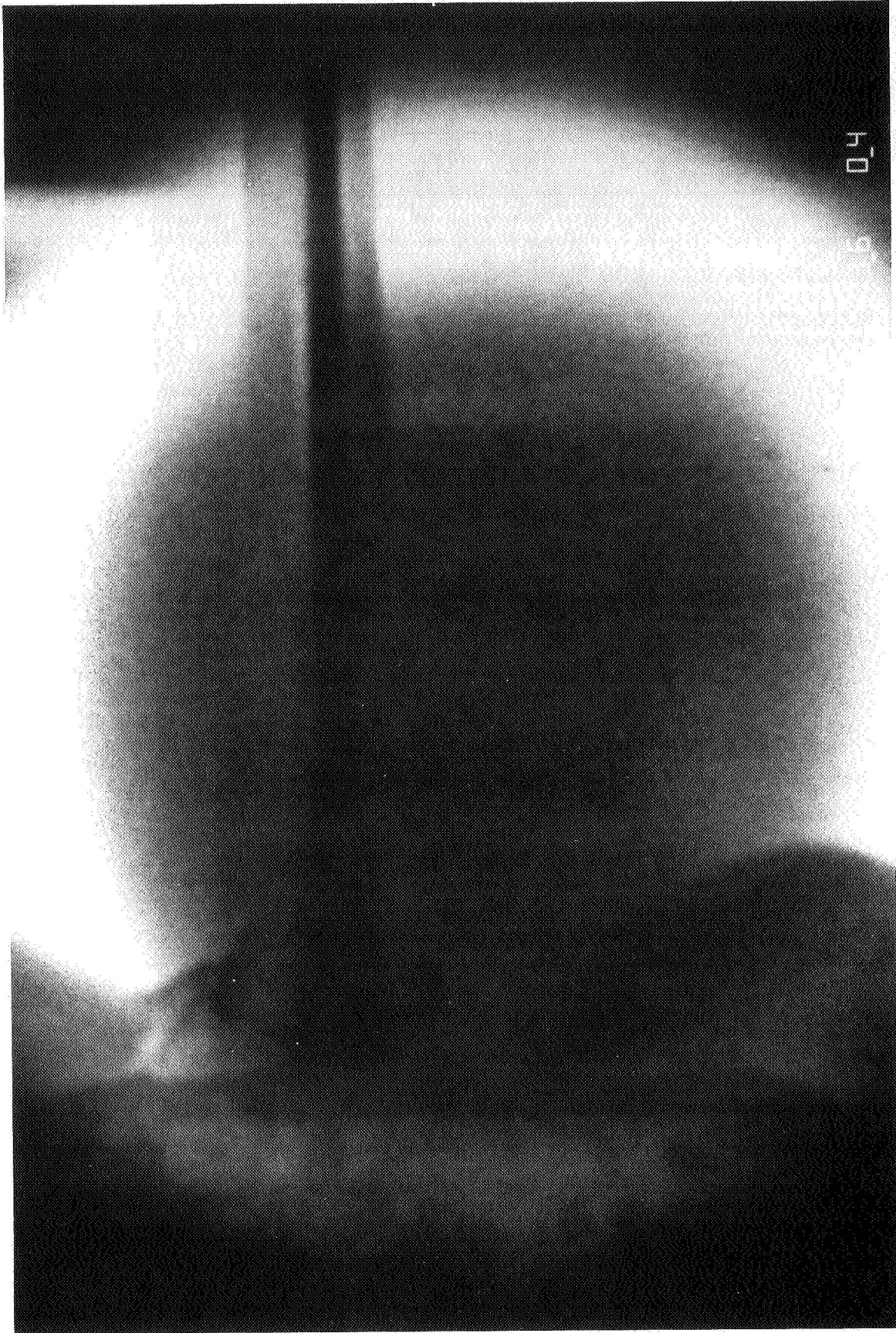


Fig. 1. Ram glow photograph of the rear stabilizer taken with the 630.8 nm filter at 360 km altitude; exposure time 8 sec.

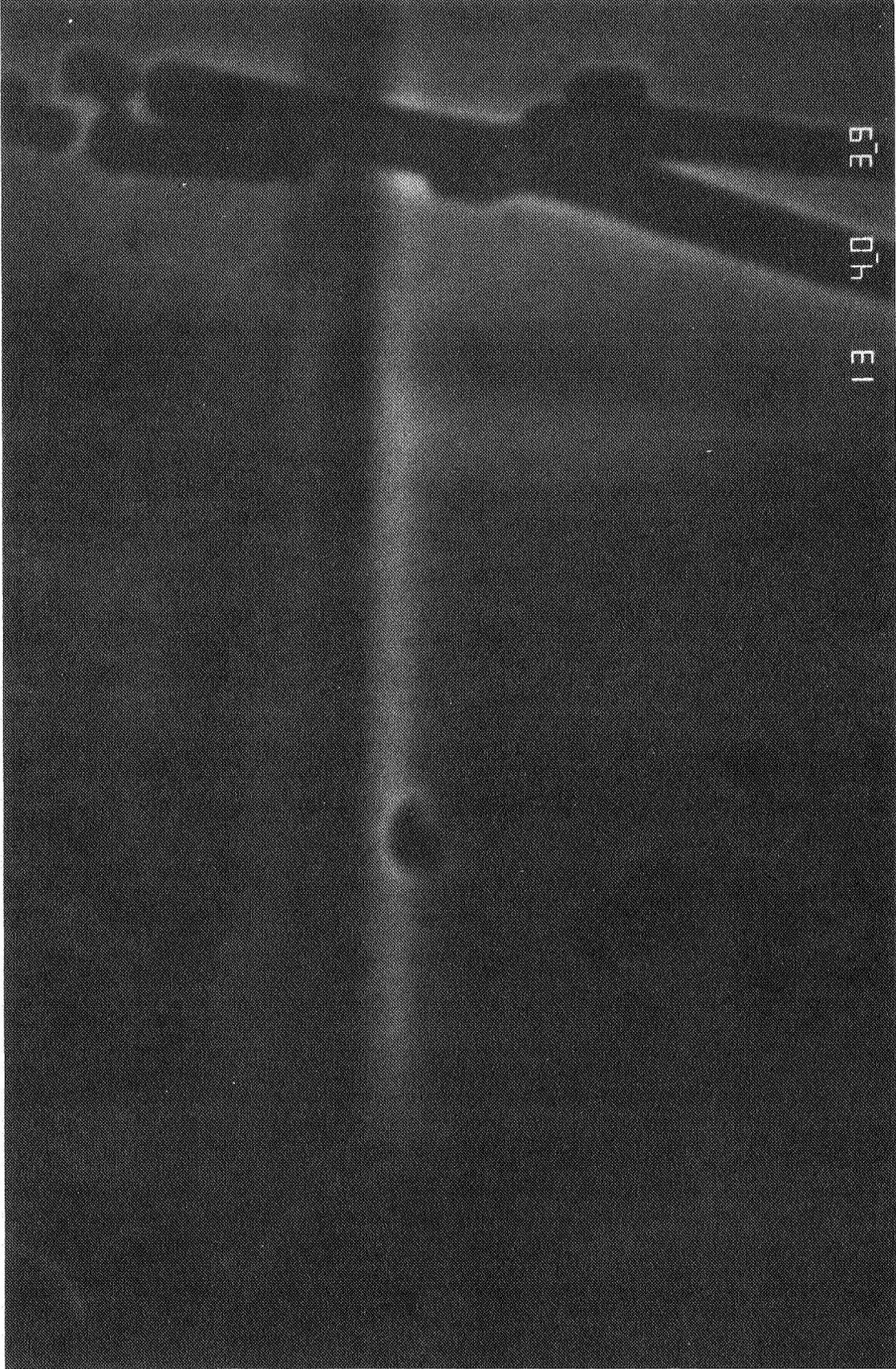


Fig. 2. Ram glow photograph of the rear stabilizer taken with the 630.8 nm filter at 230 km altitude following a thruster firing.

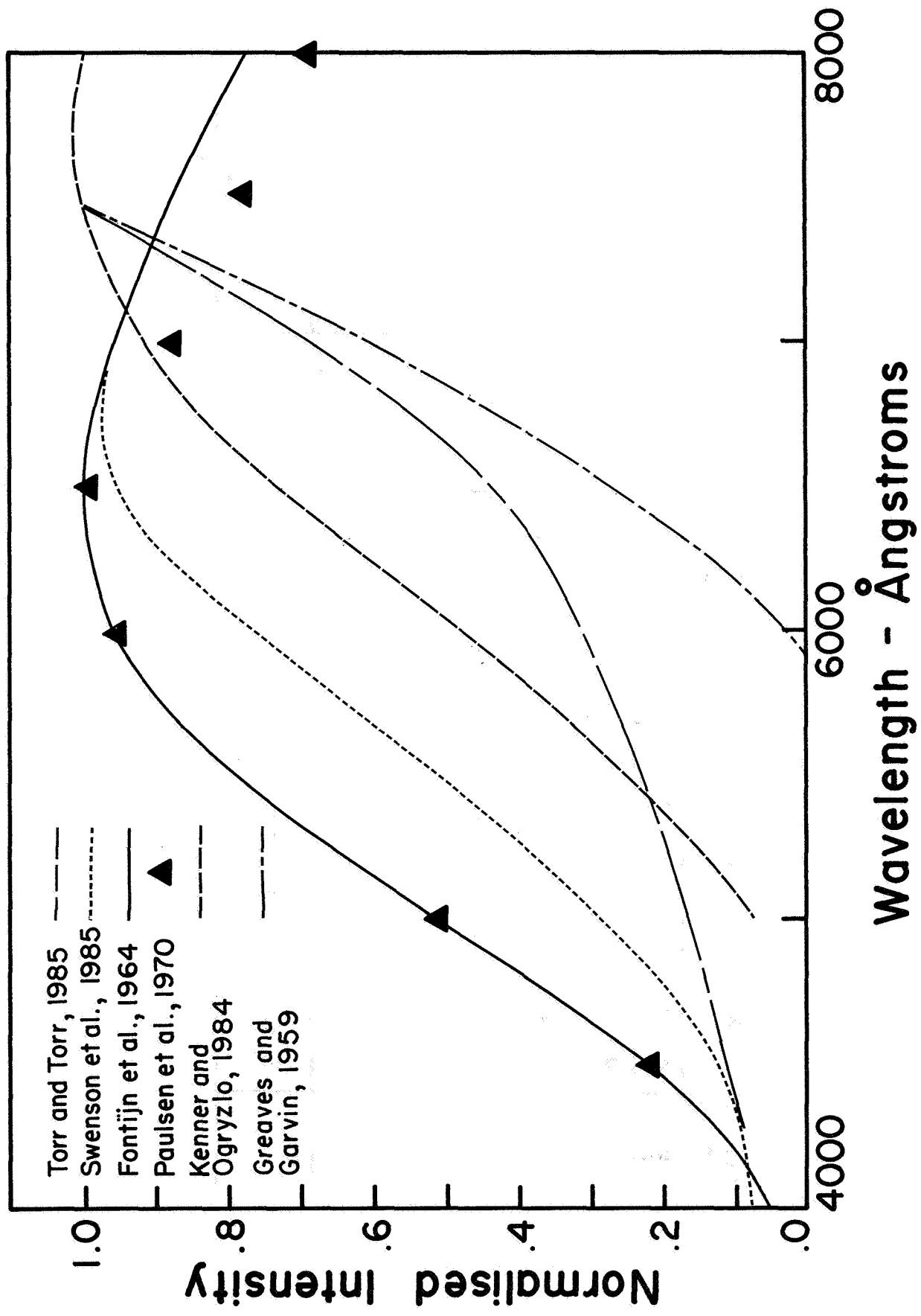


Fig. 3. Comparison of Orbiter glow and NO₂ continuum spectra.

TABLE 1. FILTER SPECIFICATIONS

Filter No.	Emission	Wavelength nm	Center Wavelength nm	Bandwidth nm	Peak Transmittance percent
F1	$0 \ ^1D - ^1S$	557.735	558.30	0.40	44
F2	$0 \ ^3P - ^1D$	630.031	630.78	0.31	58
F3	Meinel $Q_1(1)$ $OH(8,3)$ $Q_1(2)$ $Q_1(3)$	727.840 728.638 729.780	730.08	0.38	52
F6	$0^+ \ ^2D - ^2P$	731.984 mean-doublet	733.18	0.40	52
F4	Atm $PQ(11)$ $O_2(0-0)$ $PP(11)$	763.959 764.071	764.24	0.41	47
F5	$0 \ 3s^5S - 3p^5P$	777.194 777.417 777.539	778.42	0.40	51

TABLE 2. UPPER BOUNDS FOR SHUTTLE GLOW INTENSITY ON MISSION 41-G

Wavelength nm	Glow Intensity (R/A)		
	360 km	230 km*	222 km (STS-8)
557.7	<40	<100	150
630.0	<50	<200	300
730.2	<75	<200	400
762.0	<90	<300	550

* These values have been modified from those presented at the workshop by reason of more recent analysis.

TABLE 3. MODEL ATMOSPHERE FOR GLOW ANALYSIS

Altitude km	[O] cm ⁻³	[NO] cm ⁻³	[O ₂] cm ⁻³	[M] cm ⁻³
200	3 x 10 ⁹	5 x 10 ⁵	4 x 10 ⁸	6 x 10 ⁹
300	4 x 10 ⁸	10 ³	6 x 10 ⁶	5 x 10 ⁸

NEUTRAL MASS SPECTROMETER MEASUREMENTS IN THE SHUTTLE BAY
ENVIRONMENT

E. Miller

Space Science Laboratory
NASA Marshall Space Flight Center, Huntsville, AL

G. Carignan

Space Physics Research Laboratory
University of Michigan, Ann Arbor

Abstract. A neutral mass spectrometer, flown as part of the Induced Environment Contamination Monitor (IECM), is briefly described. Results from STS-2, -3, -4, and Spacelab 1 are qualitatively summarized. The gases observed were, for the most part, those with molecular weights below 45 amu with sources attributable to instrument background, shuttle-induced environment, and the ambient atmosphere. The most abundant gases were H₂O, N₂, and He. Heavier gases consisted primarily of fluorocarbons.

Introduction

A neutral mass spectrometer was flown as part of the Induced Contamination Monitor (IECM) on shuttle flights STS-2, -3, -4, and Spacelab 1 [Miller, 1983a,b, 1984] (Figure 1). It will also fly on Spacelab 2. The mass spectrometer covered the mass range from 2-150 amu with a nominal resolution of 1 amu over the range. The instrument field-of-view was collimated by a three-stage skimmer to 0.1 sr (Figure 2). Gas entering at angles greater than 10° to the view axis are skimmed into a matrix of zirconium oxide getters where active atoms and molecules are pumped providing the collimation. Nonreactive gases such as helium and argon are not pumped by these getters and thus are not collimated.

In normal operation, a 600-s cycle format was employed during which each mass number from 2 to 150 amu was sampled for 2 s and during the subsequent 300 s, mass 18 (H₂O) was sampled continuously with a 2-s integration period. Other formats, selectable by the astronauts, reduced the integration period to 0.2 s and/or truncated the mass range to 2-50 amu. With both options selected the mass range from 2-50 was sampled each 10 s. The instrument was sealed in an ultra-clean vacuum prior to launch and opened to the environment after the shuttle was in orbit.

The IECM was mounted in the payload bay such that the view axis of the mass spectrometer was along the -Z axis. On STS-2, -3, and -4, with the bay doors open, there was very little shuttle surface in the entire 2π front hemisphere, so that virtually all arriving contaminant gases were scattered from atmospheric gases. Interpretation of the arriving flux in terms of its source strength or column density thus involves consideration of the scattering cross section of the 8 km/s collisions between contaminants and the atmosphere. On STS-4, the IECM was grappled by the Remote Manipulator Arm and a survey was made with

the instrument axis looking back in toward the bay and wing surfaces. On Spacelab 1 the IECM was located well below the sill line so that much of the aft bulkhead and instrument surfaces were within the uncollimated field-of-view.

The IECM and the mass spectrometer functioned well on all four flights. There were some anomalies and minor problems, but for the most part, operation was nominal. The quantitative interpretation of the mass spectrometer measurements was expected to be difficult and it has been. The major limitation of the spectrometer measurements has been the relatively large background of previously pumped gases over the zirconium oxide getters. Despite the difficulties and the limitations of the system, some success has been achieved in characterizing the gaseous environment in the vicinity of the shuttle.

Results

A qualitative summary of the measurements will be presented here describing the interpretation of the gaseous contributors to each of the mass numbers from 2-44 and a few others at greater mass number.

Mass 2--Molecular hydrogen that is almost entirely background of the zirconium oxide getters. No significance can be attached to the mass 2 measurement.

Mass 3--Statistically insignificant (SI).

Mass 4--Helium. This is the best measurement made by the instrument. There is virtually zero background contribution at mass 4. Helium is not collimated or otherwise affected by the getters and so the instrument field-of-view is 2π sr. Atmospheric helium is observed and its quantification is in good agreement with model values on all flights. Helium is also a major contaminant of the shuttle (10^{-9} torr on Spacelab 1) and is observed even in the wake [Naumann et al., 1985].

Mass 5--SI.

Mass 6--SI.

Mass 7--SI.

Mass 8--SI.

Mass 9--SI.

Mass 10--SI.

Mass 11--Small but statistically significant; possibly borane.

Mass 12--All carbon bearing molecules contribute to this peak.

Mass 13--Mostly a product of dissociative ionization of CH_4 . This peak together with 14, 15, and 16 is used to separate methane from other contributors to these mass numbers.

Mass 14--A complex sum of doubly and dissociatively ionized N_2 , doubly ionized CO , and dissociatively ionized CH_4 . Its abundance is heavily modulated by angle of attack because of the N_2 contribution and is also modulated by methane producing events.

Mass 15--Almost exclusively from methane; a very small fraction from the 15 isotope in nitrogen compounds. It is the mass of choice for quantifying the methane source density because it is uncontaminated by atomic oxygen and is almost equally sensitive of methane as the mass 16 peak.

Mass 16--Methane and atomic oxygen. Ambient atomic oxygen does not survive the many surface collisions before ionization. It combines to form CO , CO_2 , and O_2 . The contribution to the mass 16 peak is thus indirect through dissociative ionization of oxygen bearing molecules. Methane is a substantial background gas over the zirconium oxide getters. It also appears to be catalytically produced in the instrument from some effluent associated with thruster firings. It is postulated that it is formed on the getter surfaces by conversion of unoxidized or partially oxidized thruster fuel, monomethyl hydrazine.

Mass 17--Dissociatively ionized H_2O , i.e., OH^+ . The amplitude of the mass 17 peak is about 40 percent of the mass 18 peak due to water.

Mass 18--Water. The density of H_2O ; in the ion source is the sum of the instrument background and contaminant H_2O from various shuttle sources. In most observation geometries, the contaminant H_2O observed is the consequence of scattering by the ambient atmosphere into the instrument orifice, giving source densities of about $10^7/\text{cm}^3$ and column densities of $10^{12}/\text{cm}^2$.

Mass 19--A statistically significant but unknown contaminant. It is possibly an ionization product of a fluorine compound, but the associated spectral peaks have not been identified.

Mass 20--Mostly doubly ionized argon with a small contribution from the oxygen 18 isotope in H_2O . A small impurity in the neon 22 used for calibration is observed during calibrations.

Mass 21--Statistically insignificant except during calibration using isotopically labeled neon. Neon 22 was used for the calibration; contributions at masses 20 and 21 resulted from impurities and, in the case of mass 21, a slight cross-talk from the large mass 22 peak.

Mass 22--Doubly ionized CO_2 , except during calibration when the isotopically labeled neon 22 caused count rates in excess of $2 \times 10^6/2 \text{ s}$ at mass 22.

Mass 23--SI.

Masses 24, 25, 26, and 27--Small, but measurable, products of an instrument contaminant of unidentified origin.

Mass 28--Molecular nitrogen (ambient and contaminant) and carbon monoxide which is a relatively large instrument background over the zirconium oxide getters and other metal surfaces. At small angles of attack the mass 28 peak is dominated by streaming ambient molecular nitrogen, and the quantitative interpretation of the peak yields reasonable values for ambient density. During the contamination survey taken on STS-4 with the IECM looking into the payload bay the fluxes of molecular nitrogen appear to be about half that of water. This would lead to a column density for N_2 contaminant of $1.0 \times 10^{12}/cm^2$. The survey also showed that the major N_2 contamination source was in the vicinity of the aft bulkhead (Figure 3).

Mass 29--Mostly N_2 with one atom of nitrogen 15.

Mass 30--Probably NO with large peaks observed during thruster firings.

Mass 31--Not analyzed.

Mass 32--Molecular oxygen mostly of atmospheric origin through the recombination of atomic oxygen. The level of molecular oxygen contamination is very low, probably below the instrument background.

Mass 33--SI.

Mass 34--Not analyzed; partly O_{16-018} .

Mass 35--SI.

Mass 36--An unknown minor contaminant, possibly HCl, plus a small component of argon 36.

Masses 37, 38, 39, 41, and 42--Small but statistically significant peaks characteristic of propene.

Mass 40--Argon. Analysis of the mass 40 peak at low angles of attack yields reasonable values for ambient argon densities. There is an argon contaminant on at least some of the flights. The STS-3 door closing event showed a steep rise in mass 40.

Mass 44-- CO_2 . Mostly instrument background with some small contribution from the shuttle that is too low with respect to background to quantify.

Masses 50, 81, and 100--Fractionation spectrum of C_2F_4 (tetrafluoroethene) observed on Spacelab 1 flight.

Masses 85, 87, 101, 103, 125, and 137--Fractionation spectrum of freon 114, $C_2Cl_2F_4$ from a known $6.2 \text{ cm}^3/\text{day}$ leak in the Spacelab cooling loop on Spacelab 1.

Masses 67 and 69--The principal peaks of electron impact-ionized Freon 21, CHCl_2F , are presumably from a leak in the shuttle cooling loop. Strong signatures of Freon 21 were observed on STS-4 during the contamination survey and during the payload bay door cycling events.

References

- Miller, E. R. (editor), STS-2, -3, -4 Induced Environment Contamination Monitor (IECM) Summary Report, NASA TM-82524, 1983a.
- Miller, E. R., Update of Induced Environment Contamination Monitor Results, presented at AIAA Shuttle Environments and Operations Meeting, Washington, D.C., 1983b.
- Miller, E. R. (editor), Induced Environment Contamination Monitor - Preliminary results from the Spacelab 1 flight, NASA TM-86461, 1984.
- Naumann, R. J., G. R. Carignan, and E. R. Miller, Space Shuttle molecular scattering and wake vacuum measurements, Journal of Vacuum Science and Technology, in press, 1985.

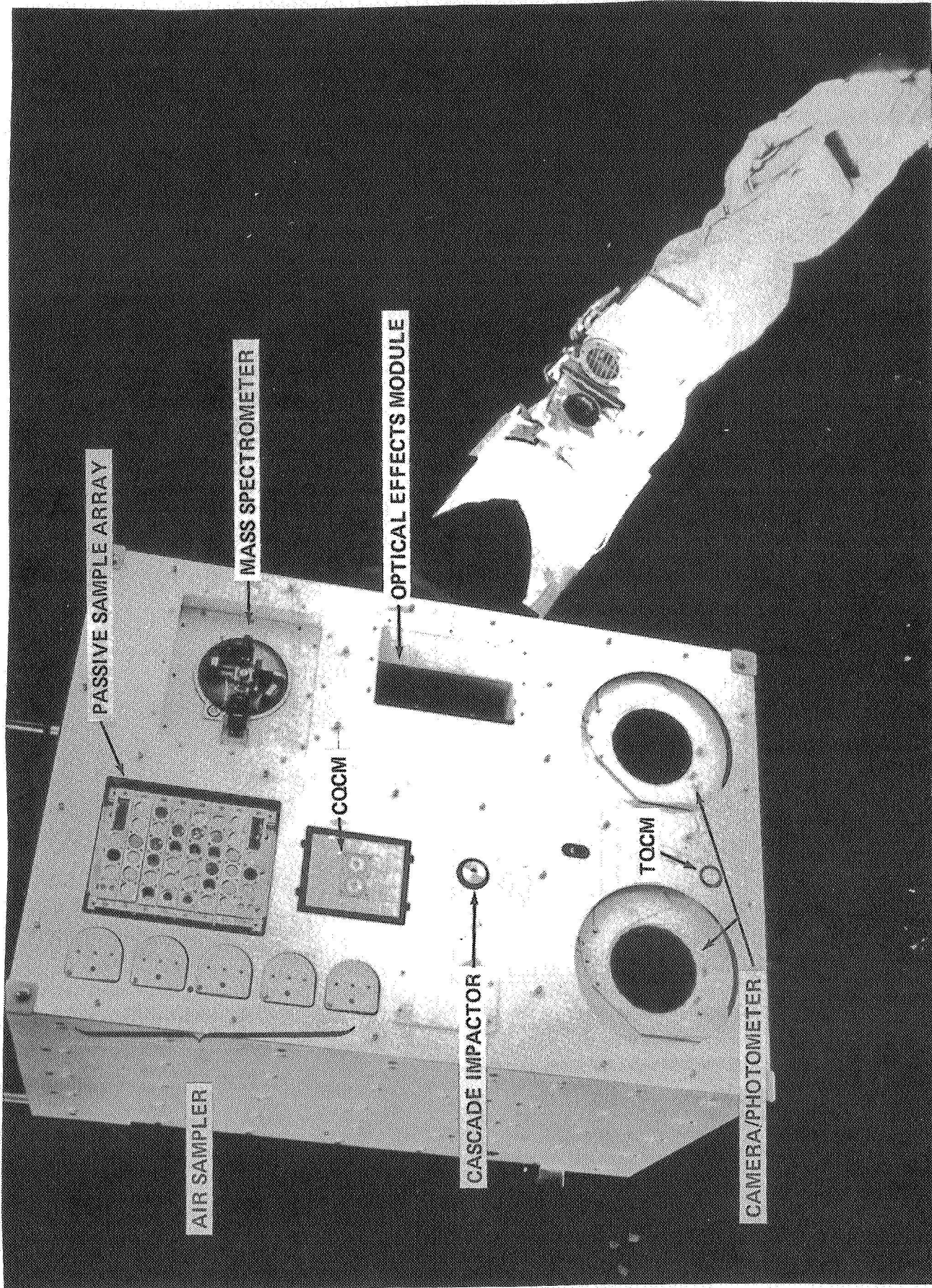


Fig. 1. IECM during remote contamination survey.

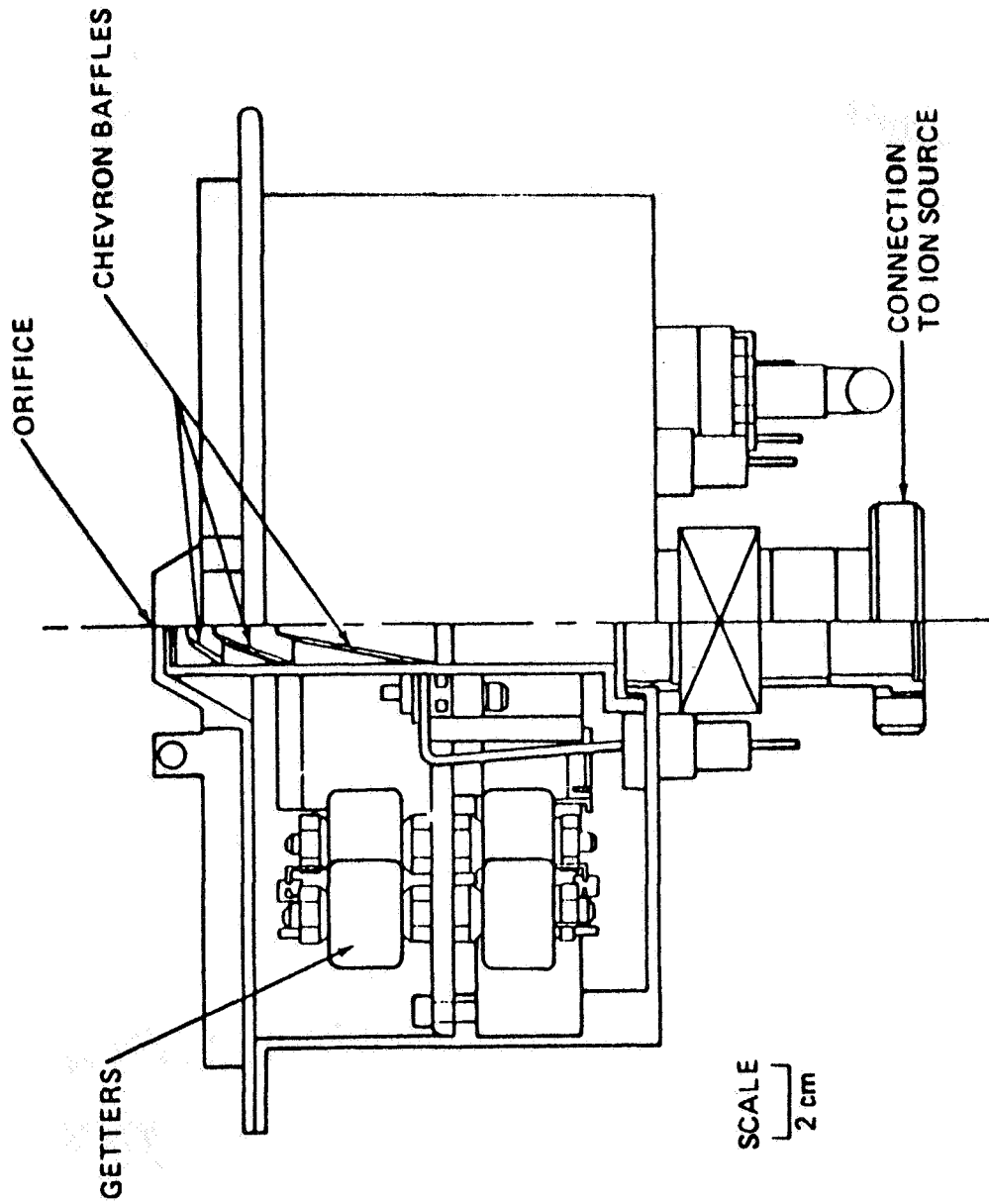


Fig. 2. Mass spectrometer collimator.

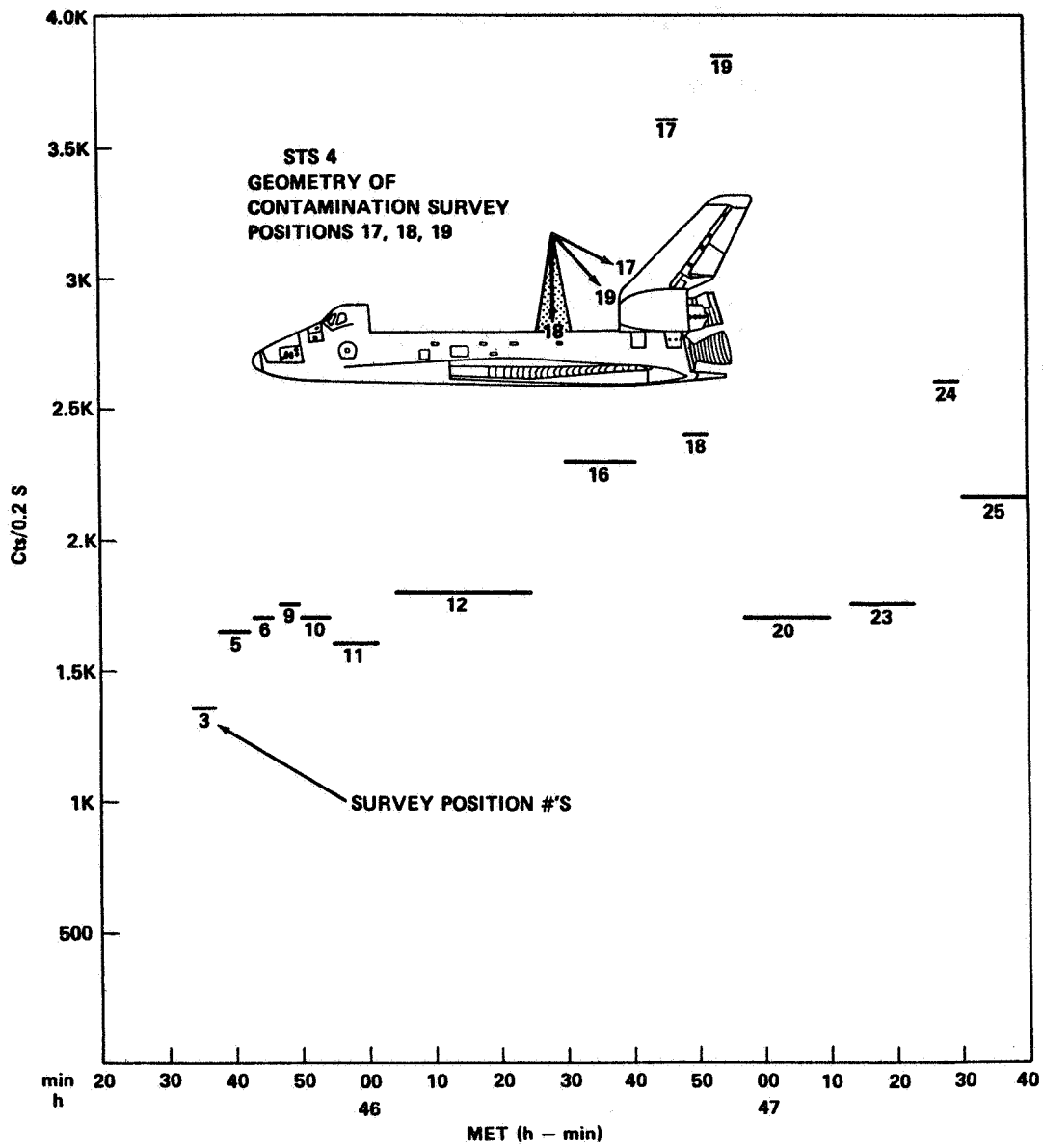


Fig. 3. Mass 28 during the remote contamination survey on STS-4.

SPECTRAL IDENTIFICATION/ELIMINATION OF MOLECULAR SPECIES IN SPACECRAFT GLOW

B. D. Green, W. J. Marinelli, and W. T. Rawlins

Atmospheric Sciences Group, Physical Sciences Inc.

Abstract. We have developed computer models of molecular electronic and vibrational emission intensities. Known radiative emission rates (Einstein coefficients) permit the determination of relative excited state densities from spectral intensities. These codes have been applied to the published spectra of glow above shuttle surfaces [Swenson et al., 1985] and to the Spacelab 1 results of Torr and Torr [1985]. The theoretical high-resolution spectra have been convolved with the appropriate instrumental slit functions to allow accurate comparison with data. The published spacelab spectrum is complex but N_2^+ Meinel (A \rightarrow X) emission can be clearly identified in the ram spectrum. N_2 First Positive emission does not correlate well with observed features, nor does the CN Red System. Spectral overlay comparisons are presented. The spectrum of glow above shuttle surfaces, in contrast to the ISO data, is not highly structured. Diatomic molecular emission has been matched to the observed spectral shape. Source excitation mechanisms such as (oxygen atom)-(surface species) reaction product chemiluminescence, surface recombination, or resonance fluorescent re-emission will be discussed for each tentative assignment. These assignments are the necessary first analytical step toward mechanism identification. Different glow mechanisms will occur above surfaces under different orbital conditions. Effective remedial actions can only be planned once the glows have been characterized.

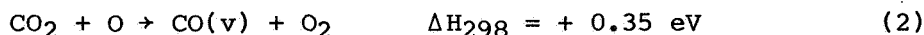
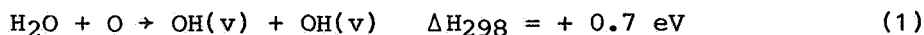
Introduction

While it is clear that a more extensive database is required in order to characterize spacecraft glows, considerable insight into potential mechanisms can be gained by careful analysis of existing data to extract all the information contained therein. We present here our preliminary spectral analyses of the published ISO data on Spacelab 1 [Torr and Torr, 1985] and the spectrum from Lockheed's hand-held spectrophotometer on STS 41-D [Swenson et al., 1985]. Spectral predictions are made for various molecular electronic and vibrational emission bands and compared with the data. The particular emitters were chosen as likely candidates in a kinetic review of the shuttle local environment. This review considered various classes of mechanisms that could occur both above and on shuttle surfaces. Because glows have been observed over a variety of surfaces, chemical reactions with the surface materials were not highlighted in this review. They will be considered in a future paper [Green et al., 1985a]. Our comparison of spectral predictions with observations clearly eliminates many potential radiators (such as N_2 First Positive and CN Red Systems), clearly identifies other features as far-field

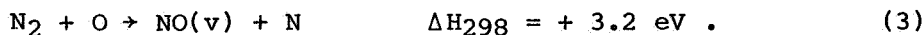
atmospheric emissions (such as N_2^+ Meinel and First Negative), and suggests other potential radiators (such as vibrational overtones of CO and NO in addition to OH). We will present these comparisons after our kinetic review.

Potential Chemical Excitation Mechanisms

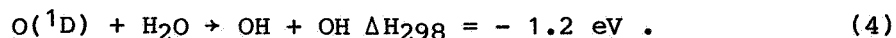
The variety of chemical processes that could be occurring in the local shuttle environment is shown schematically in Figure 1. As the ambient atmospheric O and N_2 enter the local shuttle cloud (at a relative velocity 8 km/s), they can strike gas-phase contaminants and react with or collisionally excite them. A major portion of the atmospheric flux reaches the surface where it can excite or react with adsorbed species on shuttle surfaces. If the atmospheric N_2 strikes a bare surface site it can dissociate on impact [Green, 1984]. Atomic oxygen, if slowed by gas-phase collisions, can also be adsorbed. Surface recombination and desorption could then give rise to emissions. Finally, the ambient atmospheric species can react with surface materials. In the gaseous contaminant cloud, the prevalent species have been measured to be H_2O and CO_2 [Miller, 1983; Narcisi et al., 1983], although He, O_2 , Ar, freons, cleaning agents and other species have also been detected in trace amounts. H_2O is dominantly attributable to outgassing and the flash evaporator system releases. The most likely gas phase reactions are



and in the reflected atmospheric shocklayer:



Even though all these processes are endothermic, in the ram velocity vector the kinetic energies involved in the collisions are sufficient ($5.2 \pm 1 \text{ eV}$) to permit the reactions to proceed. In particular, the reverse reaction (1) is reasonably fast ($k_{-1} = 1.8 \times 10^{-12} \text{ cm}^3/\text{s}$), while the forward reaction involving O^* is extremely rapid ($k_4 = 9.9 \times 10^{-11} \text{ cm}^3/\text{s}$):



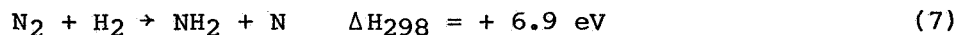
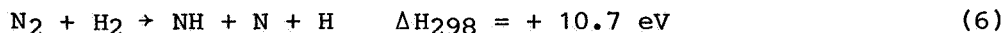
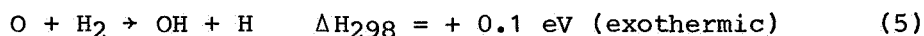
Thus, the possibility exists for creating vibrationally excited CO and OH from these gas-phase reactions. In addition to reaction, processes 1 and 2 could simply lead to vibrationally excited H_2O and CO_2 (resulting in infrared emission). These vibrational excitation cross sections have been measured to be large [Dunn et al., 1975] at somewhat lower translational energies (4-6 km/s). Radiance levels can be estimated from these cross sections, contaminant levels, and atmospheric fluences to be less than 100 kR in the infrared. Overtone emission in the visible will be much weaker and should make negligible contributions to visible glow spectra. Gas-phase chemical reactions do not occur at a sufficient rate to generate significant glow

intensities. For contaminant column densities of $2 \times 10^{12} \text{ cm}^{-2}$ and assuming (1) rate constants 0.01 gas kinetic and (2) that 1% of the product molecules are excited and emit in the visible, total glow intensities of hundreds of Rayleighs are predicted. Stated in another manner, only 1% of the incoming ambient flux undergoes collisions with the H_2O contaminant cloud. However, if the column densities were considerably higher due to ram pressure build up, then gas-phase chemical reactions could contribute to the glow. The spatial extent of the glow for these processes would reflect the contamination concentration gradients above the surfaces.

An additional gas-phase glow has been observed during/after thruster firings. The thruster equilibrium exhaust concentrations are calculated as 33% H_2O , 31% N_2 , 17% H_2 , 13% CO , and 4% CO_2 , with traces of H , O_2 , and monomethylhydrazine- NO_3 . However, radicals will be produced in high concentrations during the thruster firing and will persist in this environment. Likely candidates are OH and NH_2 . NH_2 has a structured emission spectrum in the yellow region of the visible. During thruster firings exhaust species leave the nozzle at an average velocity of $3.5 \times 10^5 \text{ cm/s}$. If the thruster exhaust is directed into the ram, large collisional energies can result. For example, the reaction



could occur at collisional energies of up to 6.5 eV. Under these conditions up to 15 quanta of vibrational energy in NO could be excited. Additional processes such as



can occur. Due to the high concentrations of neutrals released in a typical RCS thruster firing (10^{25} molecules in 80 ms), hundreds of kilorayleighs of radiance could easily arise, even assuming only one collision in 10^6 leads to a visible photon. In summary, gas-phase chemiluminescent reactions can easily account for observed bright flashes associated with thruster events. If thruster effluents are trapped above ram surfaces, these concentration enhancements could give rise to detectable chemiluminescent glows. Outgassing/offgassing contamination levels appear to be sufficiently small so that gas-phase reactions of these species cannot explain observed radiance levels in the visible. The relative importance of various processes contributing to the glow may change in other spectral regions.

All of these gas-phase species will be adsorbed to some extent on shuttle surfaces. Self-contamination has long been recognized as a problem [Scialdone, 1972] because the mean free path between collisions is large enough for molecules from localized contamination sources to be collisionally backscattered over large areas of the shuttle. Mass spectrometric observations in the cargo bay detect remote thruster firings, refrigerant, and He leaks. The degree of adsorption of a given species is surface-specific. However, H_2O , the

most prevalent gas-phase contaminant, is notorious for being easily physisorbed on a host of surfaces. Carbon dioxide, carbon monoxide, nitrogen, and hydrogen are also likely to be present in order of decreasing concentration. These physisorbed species are dynamically moving over surface sites, creating a surface consisting of both occupied and bare bonding sites. The molecules in the ambient flux continuously strike the shuttle surface sites. For a polished surface, there are 10^{15} sites/cm² and at 250 km; an ambient oxygen atom will strike a surface site once a second on average. For rougher surfaces, the number of surface sites can be much greater. Ambient O or N₂ may not react or collisionally desorb these species with unit efficiency. Thus, if contaminant/effluent molecules are adsorbed on tile surfaces, it may take minutes or even hours for the ambient flux to "clean" the surface. Contaminant mobility on the surface will allow "creep" from non-ram surfaces to replenish the physisorbed species concentration on ram surfaces. In analogy with the gas phase, reactions 1-3 and 5-7 may occur. The energy of physisorption will also have to be overcome, making the reactions slightly more endothermic. Nevertheless, there is still sufficient kinetic energy in collision that chemiluminescent reactions or collisional excitation could occur.

If N₂ in the atmospheric flux strikes a bare surface site, there is often enough energy in the collision to dissociate the N₂ with the product N atoms remaining physisorbed on the surface. Atomic oxygen in the ram flux may not be adsorbed as readily since the energy of the collision is not channeled into potential energy and must be dissipated through other channels. If reflected oxygen atoms undergo numerous collisions with contaminant species, they may remain in the vicinity of the surface and be adsorbed. Thus, the relative concentration of O and N on the surfaces is not obvious. The nitrogen and oxygen atoms on the surface can then recombine to excited molecular states. This class of mechanisms was first suggested by Green [1984] and reviewed thoroughly by Green et al. [1985b]. Recombination can give rise to N₂, O₂, and NO. All these species have been observed in heterogeneous recombination in the laboratory by varying mole fractions of N and O [Halstead, 1985]. There appears to be no obvious preference for recombination partner; i.e., N₂ recombination is not excluded in the presence of O atoms.

The above chemical mechanisms can produce chemiluminescent excitation up to the level of reactant kinetic energies (as modified by reaction exo/endothermicities). Plasma excitation mechanisms, on the other hand, involve energetic (~100 eV) electrons which could excite higher molecular electronic states and even dissociate or ionize species. Thus, significant spectral differences are expected (as demonstrated below).

Spectral Comparisons

In order to quantify emission levels, we have developed at PSI spectral synthesis codes which predict very high-resolution molecular electronic and vibrational spectra for a host of molecules and band systems. These "basis functions" are then convolved with the appropriate slit function for each application. The emission from various states and species can be combined to give a composite spectrum.

Least-squares fitting is used to adjust the individual state populations to achieve a "best" fit. The relative emitting state populations are the end product of this analysis.

As an example of the code's capability, the 220-400 nm section of the ISO ram spectrum [Torr and Torr, 1985] is plotted in Figure 2, along with synthetic spectral prediction for N_2^+ First Negative bands. The best fit was achieved for a rotational temperature of 2000 K and 18 Å resolution. This resolution is lower than quoted, yet spectra at the nominal 6 Å resolution do not match the observed fluorescence signature. The relative shapes and intensities of the $\Delta v = 0$ and 1 series (and even the marginal intensity of the $\Delta v = 2$ series) all agree well with the data. Five vibrational levels ($v' = 0-4$) were included in the fit, and the vibrational distribution derived is quite similar to the distribution expected for solar resonance fluorescence excitation of $N_2^+(X)$ as suggested by Torr and Torr, although the populations of levels 2-4 had to be increased somewhat above the resonance fluorescence distribution, and may indicate vibrational excitation in $N_2^+(X)$. There is no evidence for chemical glow processes such as NO(B) emission. Certainly, the $N_2^+(B)$ could not arise from a chemical source. A plasma process, on the other hand, would excite considerable N_2 Second Positive (C→B) emission. A laboratory UV spectrum of a beam plasma discharge is plotted in Figure 3. The discharge was conducted in pure N_2 at 4×10^{13} molecules/cm³ density. Strong Second Positive emission is evident and in fact, dominates the spectrum. Lyman-Birge-Hopfield and Fourth Positive bands are also observed weakly in the laboratory spectrum. Since these features are absent in the ISO spectrum, we conclude that the UV portion of the ISO spectrum is dominated by far-field atmospheric emission.

The complex visible portion of the published ISO ram spectrum is reproduced in Figure 4a. Assignment of features in this spectrum is more difficult but various atomic lines and N_2^+ Meinel (A→X) transitions are clearly identified (again presumably from resonance fluorescence excitation in the far-field atmosphere). Synthetic Meinel band predictions are shown in Figure 4b, as are the First Positive features. Agreement of the synthetic spectrum with the data is marginal--Meinel bands match observed spectral features but First Positive emission is clearly not a major component of the ISO spectrum. CN Red bands (A→X) were also synthesized and did not match the observed features. These features are in the correct spectral region but have the wrong shape. In light of the above kinetic discussion, overtone vibrational transitions for CO and NO were created. A synthetic spectrum of these transitions is shown in Figure 5. Because the molecular dipole moment functions are not well known, there are large uncertainties in the spectral intensities. The band positions are quite accurately known and the relative spectral shape should be accurate enough to provide insight. Hydroxyl, the most probable radiator, is not included at present. We are incorporating recent spectroscopic constants into our code at present [Langhoff, 1985]. A laboratory visible spectrum of an N_2/O_2 mixture during a beam plasma discharge is displayed in Figure 6. Much structured emission including O_2^+ First Negative, N_2 First Positive, and N_2^+ Meinel bands, is observed along with several atomic lines. The overlap with the ISO spectrum is again poor; no broad spectral features rise to the red as a result of plasma processes.

The Swenson et al. [1985] data are presented in Figure 7. Upon inspection of this broad spectrum, there are several striking features. The "noise" level is not constant but is much larger where there is spectral intensity. The "noise" spikes are often several resolution elements wide. Both these observations suggest that the "noise" features are real structure. Finally, the strongest "noise" spike falls at 520.0 nm, exactly where N(²D) atmospheric emission line occurs. Prompted by these observations, we felt that structure possibly existed in the broad continuum--that Mende's data were perhaps less noisy than they appeared. Nitrogen electronic spectra (including First Positive) were unable to match the broad spectral features for any vibrational or rotational distribution. However, in response to our kinetic analysis, we performed a least-squares fit of NO overtone vibrational bands to the observed spectrum. The NO emission series are more structured than the data; nevertheless, several spectral features are reproduced. The present calculations extend only to $v' = 19$; inclusion of higher vibrational levels of NO would tend to fill in the gaps in the computed spectrum. Inclusion of additional radiators such as OH may also improve the comparison. We feel that vibrational emissions are present at some level in this spectrum. The highly structured laboratory BPD spectrum of Figure 6 clearly does not agree with the Lockheed data.

Using a 20,000 K rotational temperature, together with the vibrational distribution for NO(v) obtained from our best fit to the Swenson et al. [1985] spectrum, we calculated the infrared emission spectrum. This spectrum is presented in Figure 8. If indeed NO (and CO or OH) is present in spacecraft glow, the infrared emission spectrum will be very bright. It will significantly interfere with remote observations of deep space or the Earth's atmosphere where infrared radiances are in the MegaRayleigh range.

Summary

Although this work is preliminary, spectral fitting analysis has suggested that chemical processes will play a role in observed glows. The two glow observations considered were quite different in spectral distribution. The alarming aspect of the ISO data is that even looking out of the payload bay and not observing any shuttle surfaces, a glow spectrum was obtained underlying far-field atmospheric emissions. A number of chemiluminescent mechanisms have been suggested as giving rise to vibrationally excited OH, CO, and NO dominantly, in addition to previously suggested surface recombination mechanisms. Vibrational overtone emissions may well be present in the glow data. Due to the variability of the shuttle's environment, it is likely that there will be conditions on-orbit when different chemical plasma mechanisms will dominate glow emission. Given this, it is not really surprising that the two spectra do not agree. Extension of the data base will allow the various physical regimes to be quantified, allow the key mechanisms to be identified, and permit meaningful remedial actions to be taken.

Acknowledgements. This work has supported by the Air Force Geophysics Laboratory and by Physical Sciences Inc. internal research funds.

References

- Dunn, M. G., G. T. Skinner, and C. E. Treanor, Infrared radiation from H₂O, CO₂, or NH₃ collisionally excited by N₂, O, or Ar, AIAA J. 13, 803-812, 1975.
- Green, B. D., Atomic recombination into excited molecular states - A possible mechanism for Shuttle glow, Geophys. Res. Lett. 11, 576-579, 1984.
- Green, B. D., E. Murad, and W. T. Rawlins, The nature of the glow and its ramifications on space based observations, to be presented at AIAA 20th Thermophysics Conference, VA (June), AIAA-85-0910, 1985a.
- Green, B. D., G. E. Caledonia, and T. D. Wilkerson, The shuttle environment - Gases, particles and glows, J. Space. Rockets (September), 1985b.
- Halstead, J., private communication, 1985.
- Langhoff, S., private communication, 1985.
- Miller, E., STS-2, -3, -4 Induced Environment Contamination Monitor (IECM) summary report, NASA TM-82524, February 1983.
- Narcisi, R. S., E. Trzcinski, G. Frederico, and L. Wlodyka, The gaseous environment around space shuttle, AIAA-83-2659-CP, Presented at Shuttle Environment and Operations Meeting, Washington, D.C., 1983.
- Scialdone, J. J., Self-contamination and environment of an orbiting spacecraft, NASA TN D-6645, May 1972.
- Swenson, G. R., S. B. Mende, and K. S. Clifton, Ram vehicle glow spectrum: Implication of NO₂ recombination continuum, Geophys. Res. Lett. 12, 97-100, 1985.
- Torr, M. R. and D. G. Torr, A preliminary spectroscopic assessment of the Spacelab 1/Shuttle optical environment, J. Geophys. Res. 90, 1683-1960, 1985.

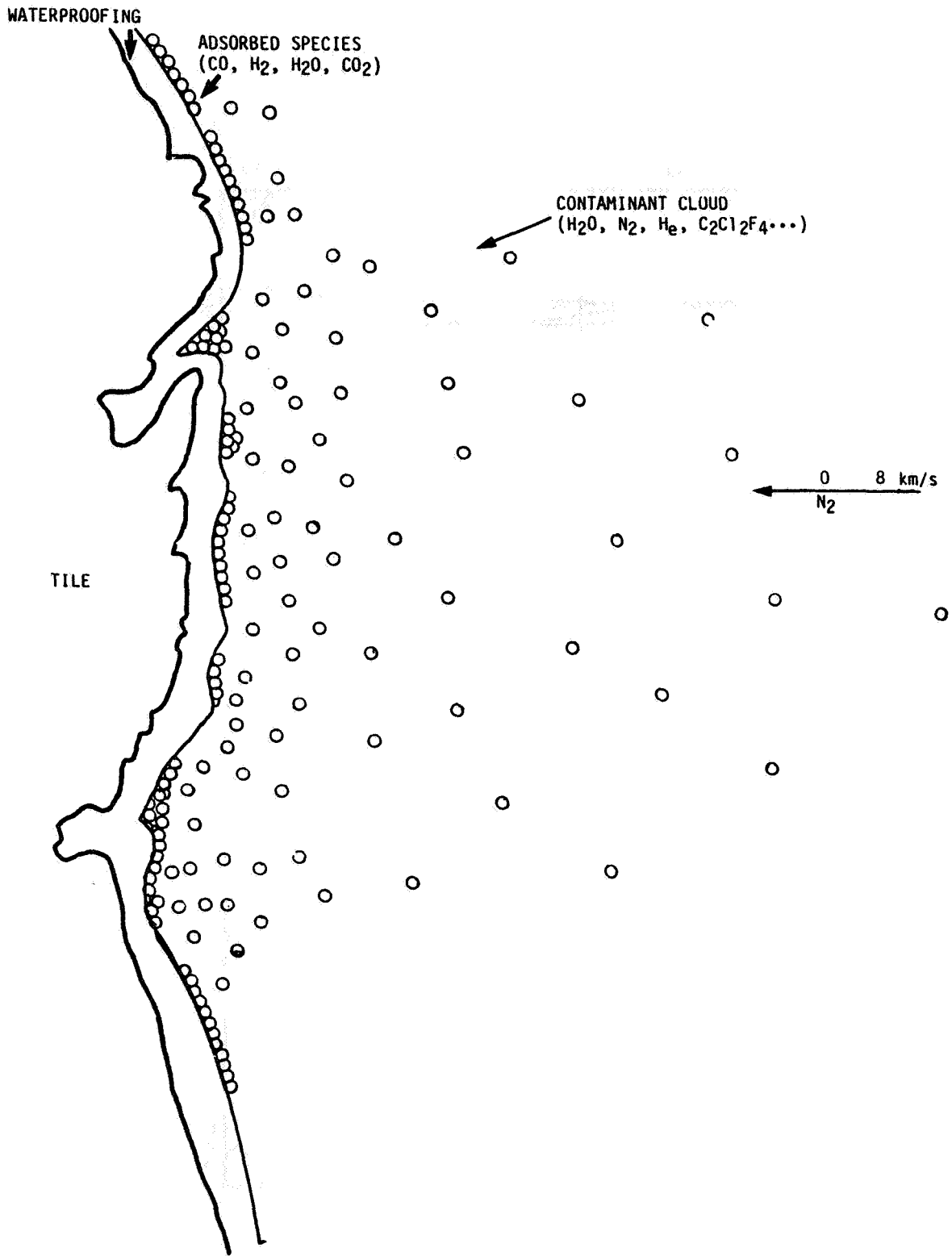


Fig. 1. Conceptual drawing of gas-phase/adsorbed species above shuttle surfaces.

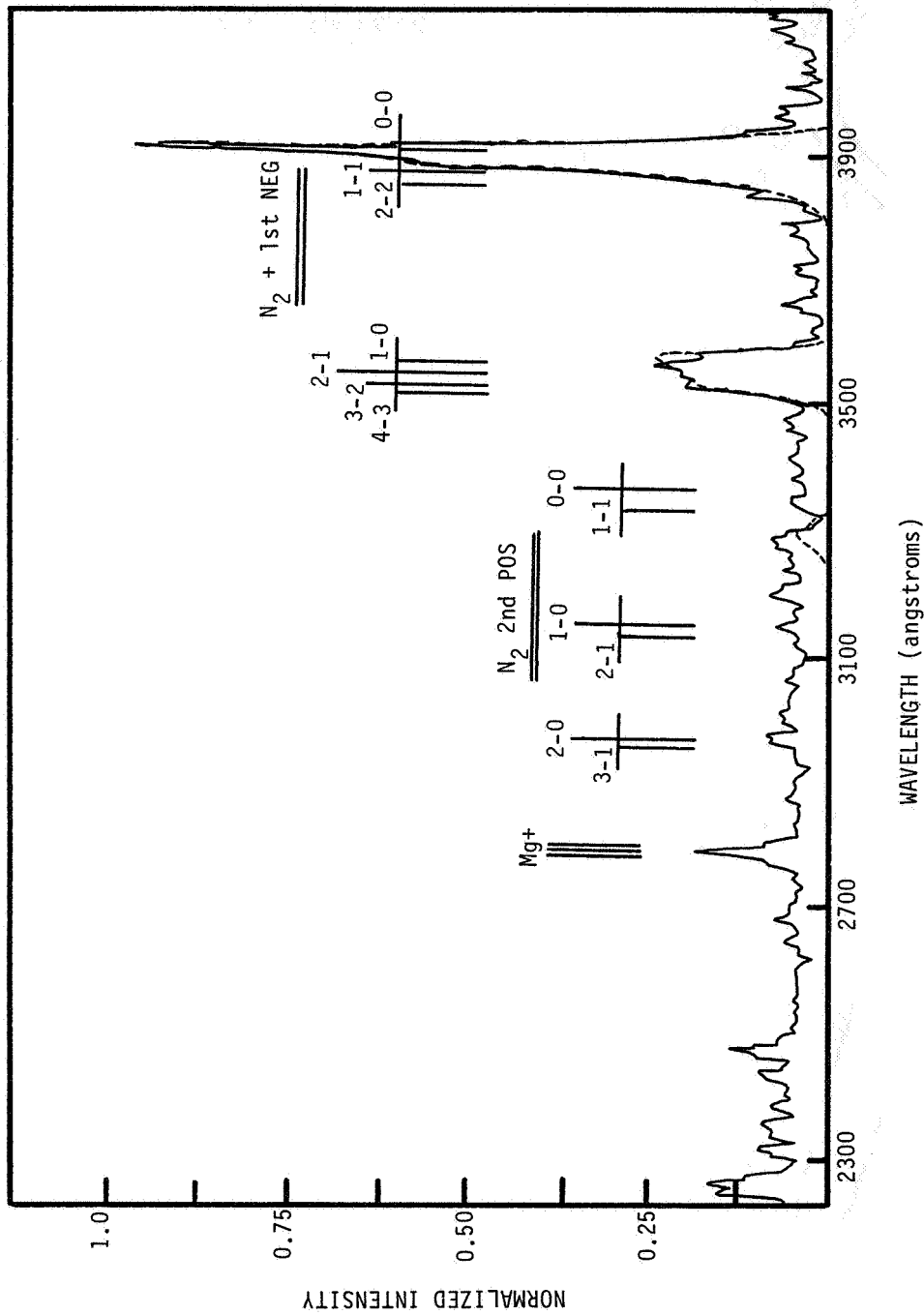


Fig. 2. Comparison of ISO ultraviolet data (solid line) from Spacelab 1 [Torr and Torr, 1985] with theoretical N_2^+ First Negative spectrum (dashed); $v' = 0-4$, rotational temperature 2000 K, 1.8 nm resolution.

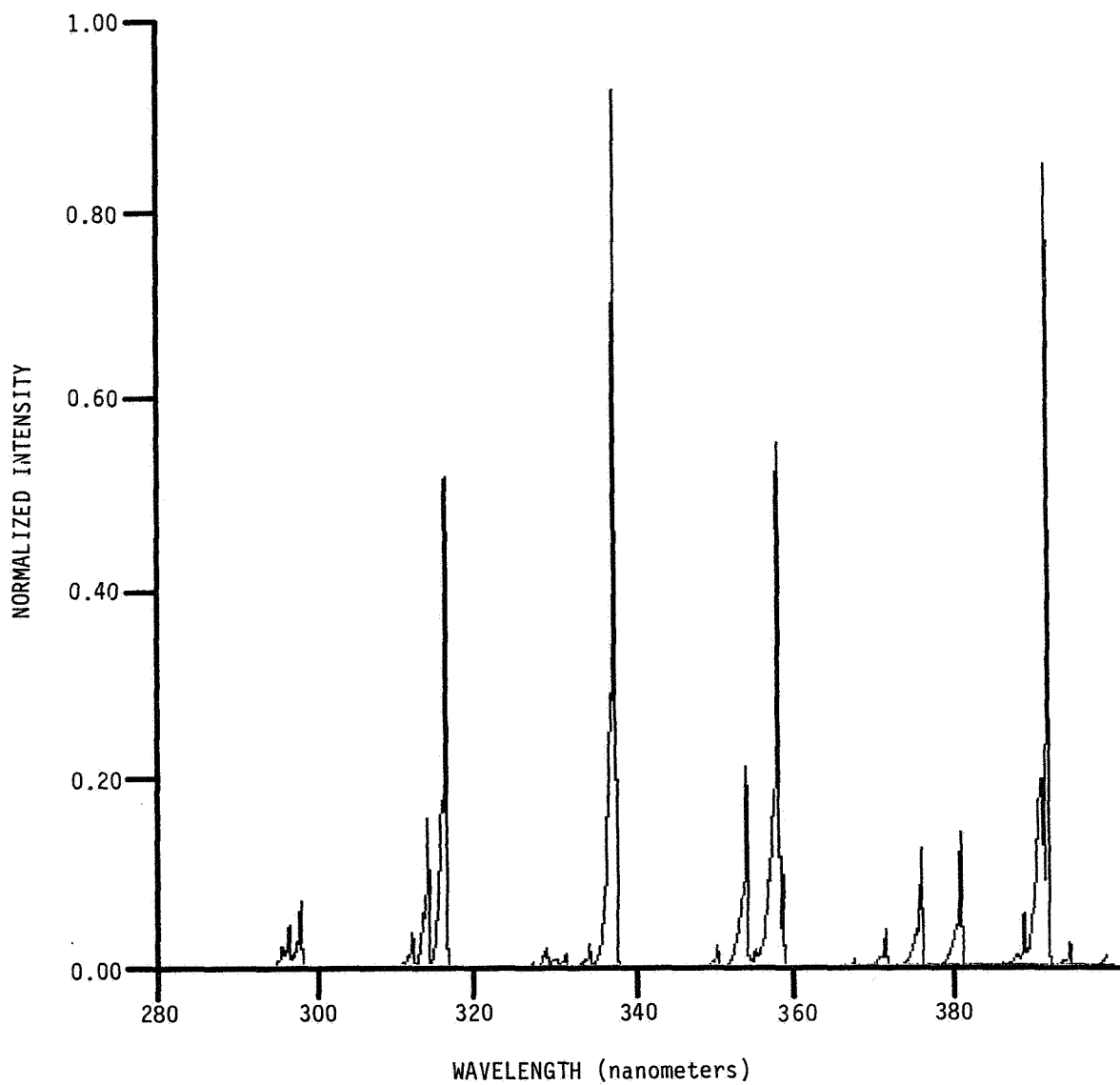


Fig. 3. Laboratory UV spectrum of a beam plasma discharge in N₂. This spectrum does not resemble ISO data; Second Positive features are clearly present.

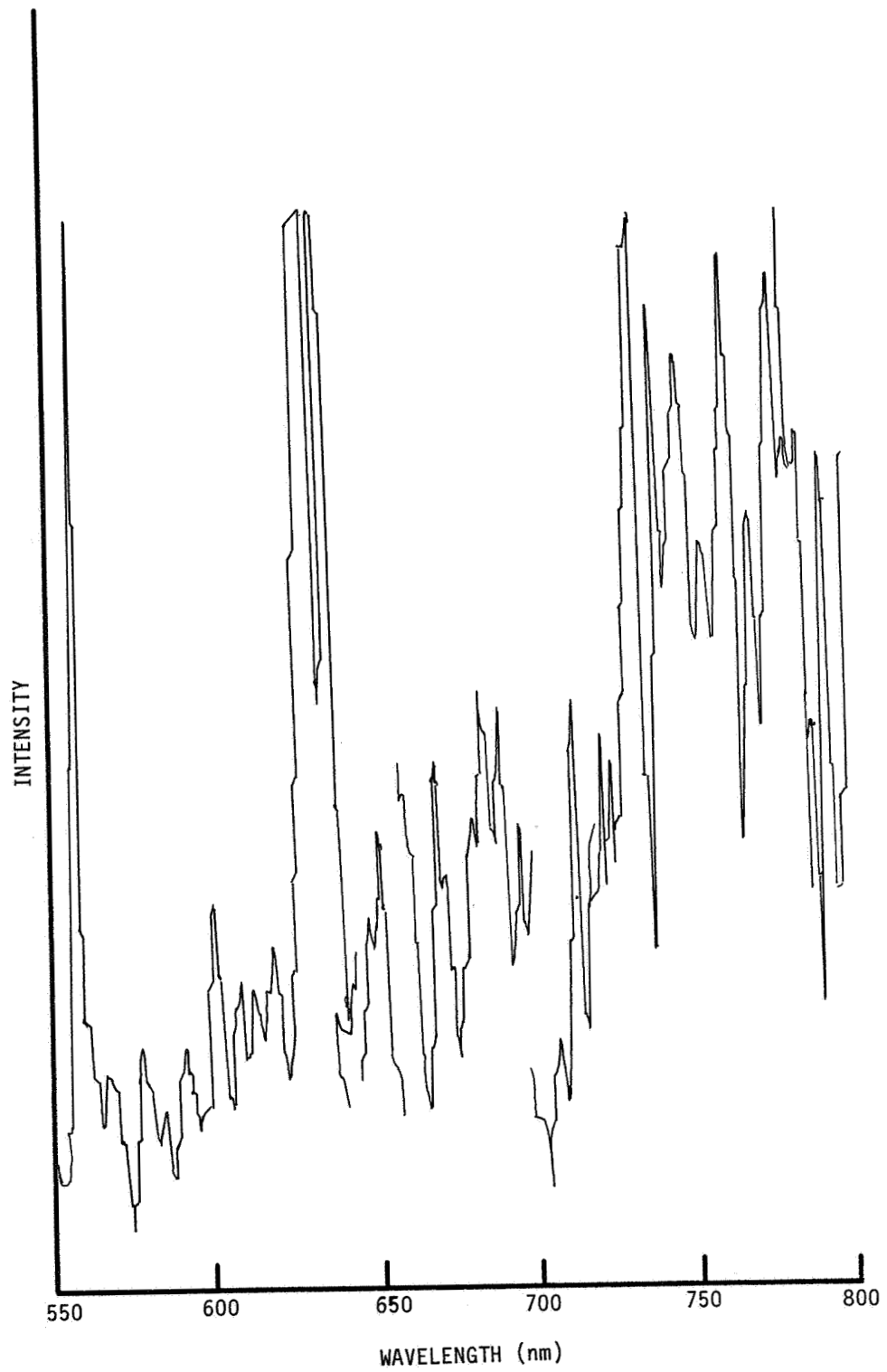


Fig. 4a. Visible data from ISO under near-ram conditions.

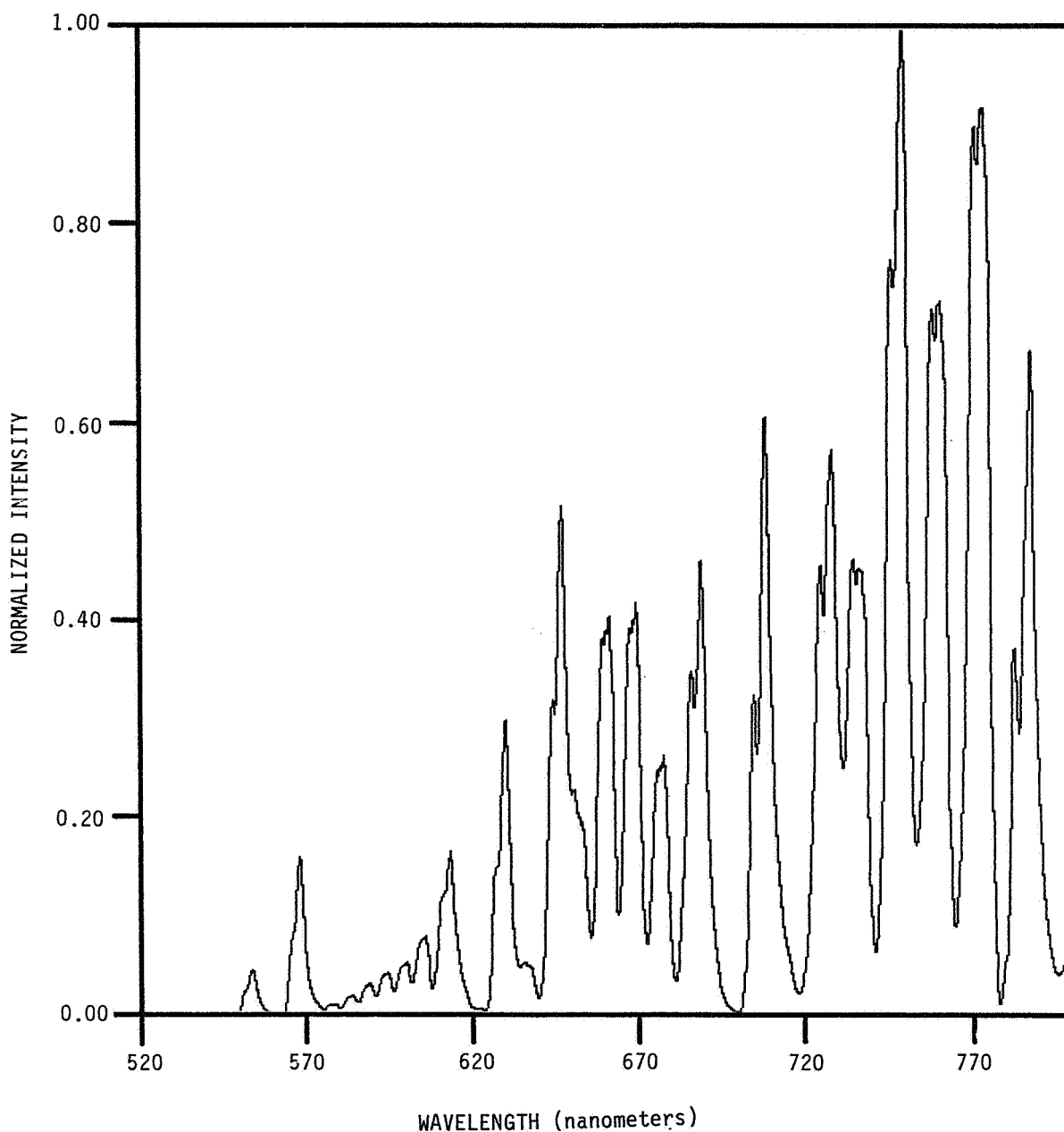


Fig. 4b. Synthetic spectrum of N₂ containing Meinel and First Positive transitions. This spectrum represents a best-fit to the data of Figure 4a, but clearly does not reproduce all the spectral features.

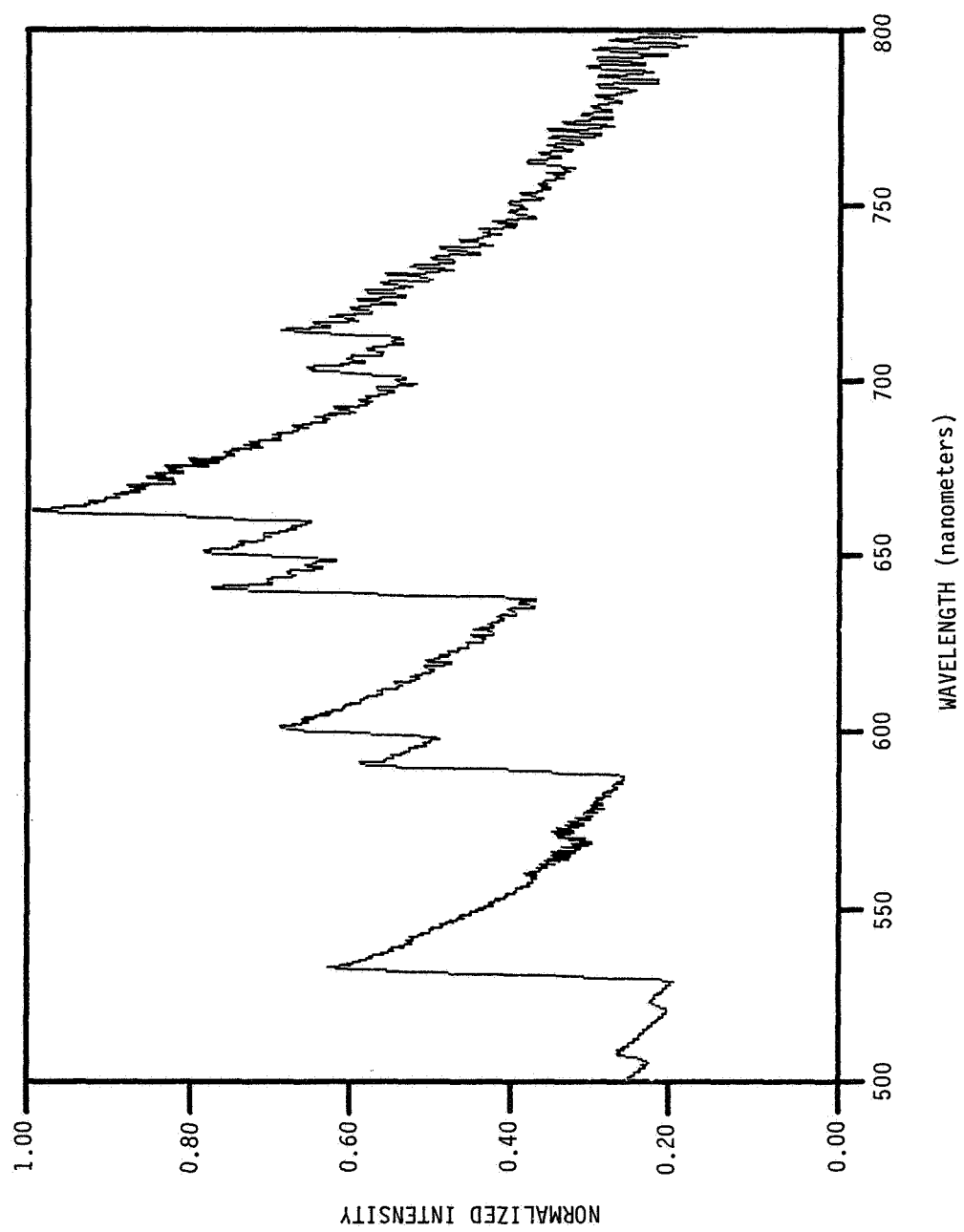


Fig. 5. Overtone emission from highly vibrationally and rotationally excited
NO showing visible emission features.

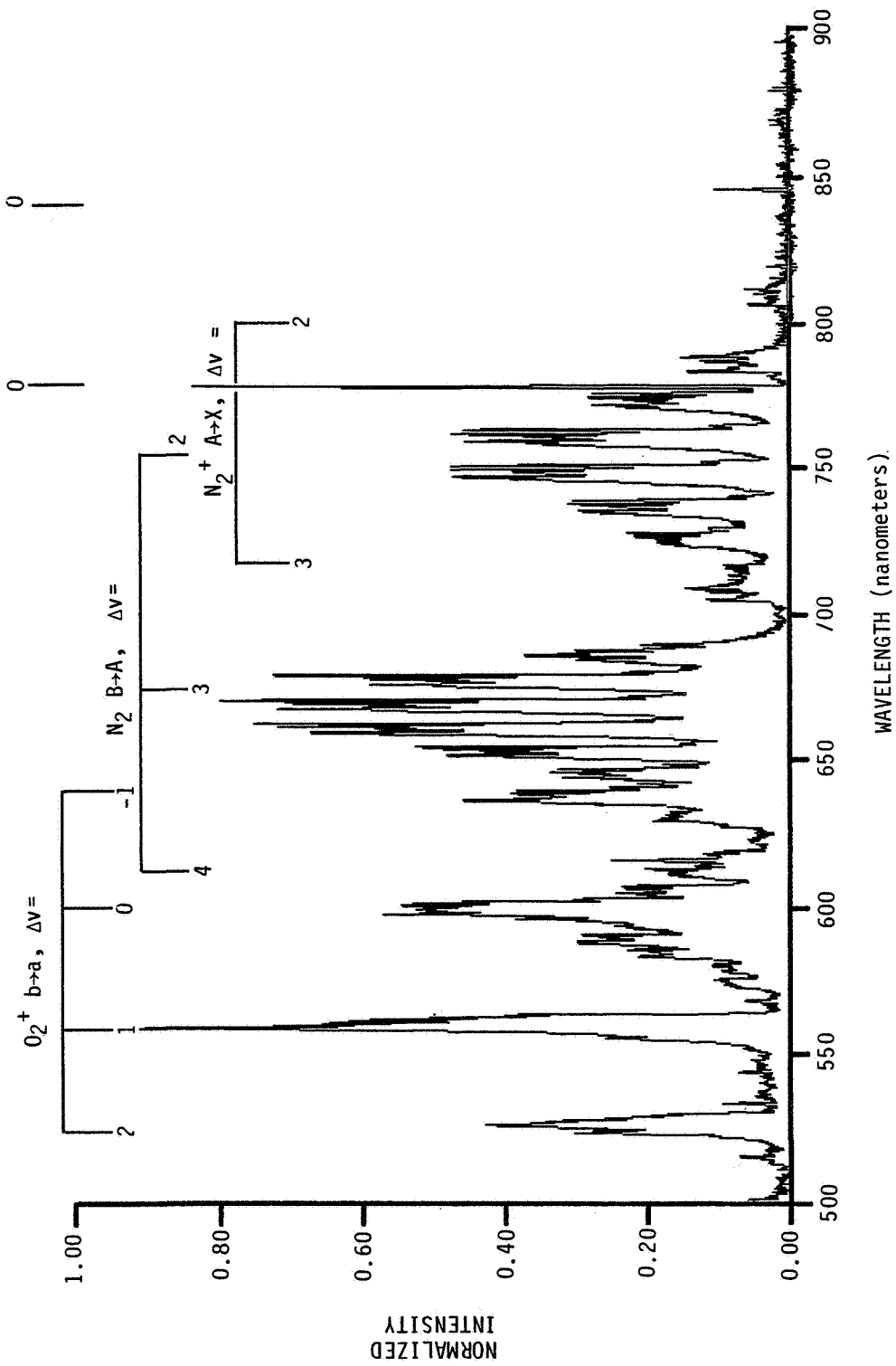


Fig. 6. Laboratory visible spectrum of a beam plasma discharge in N₂ and O₂ showing O₂ ionic, atomic line, and N₂ electronic transitions.

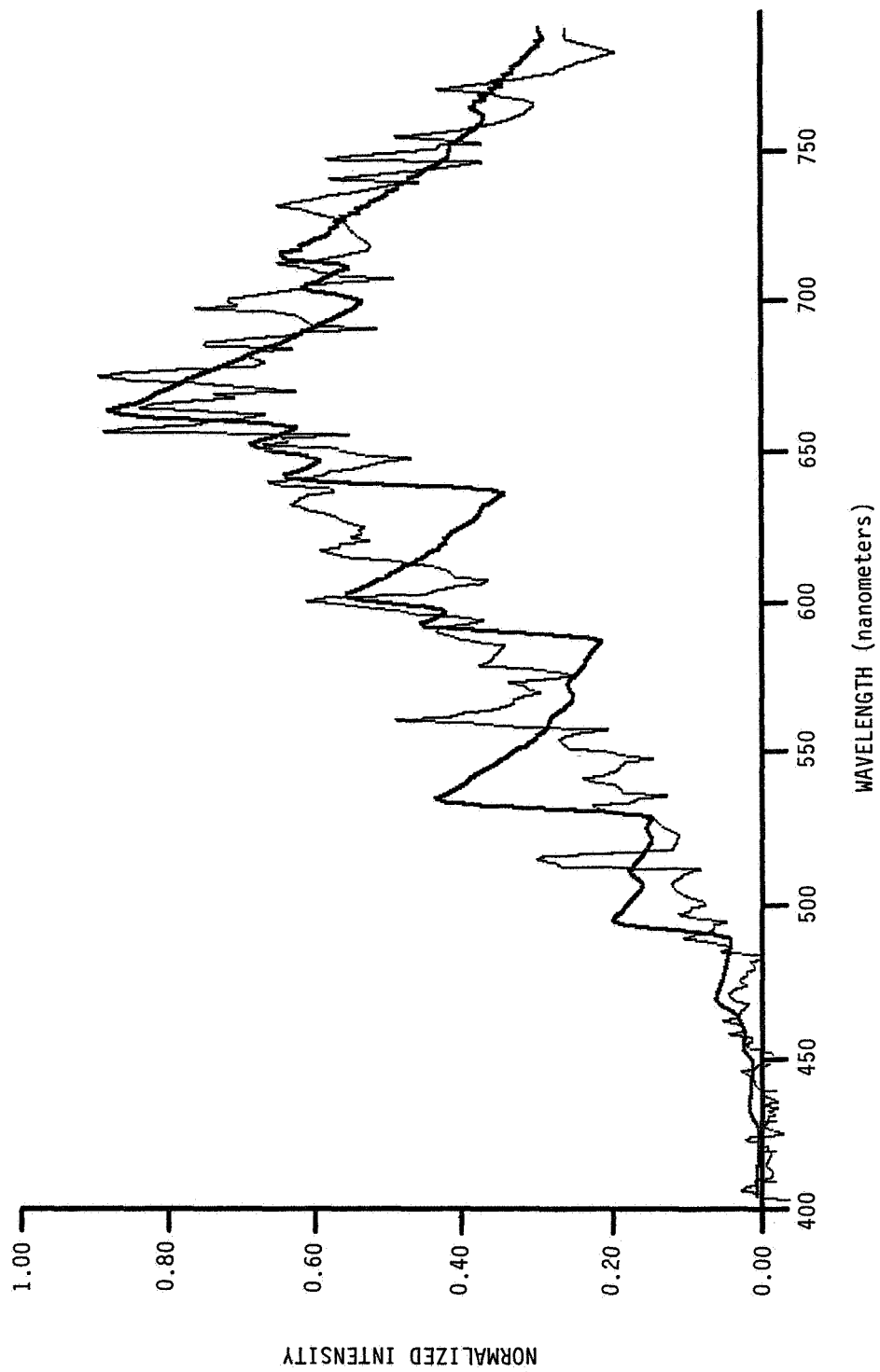


Fig. 7. Comparison of NO vibrational overtone transitions with response-corrected Lockheed glow data.

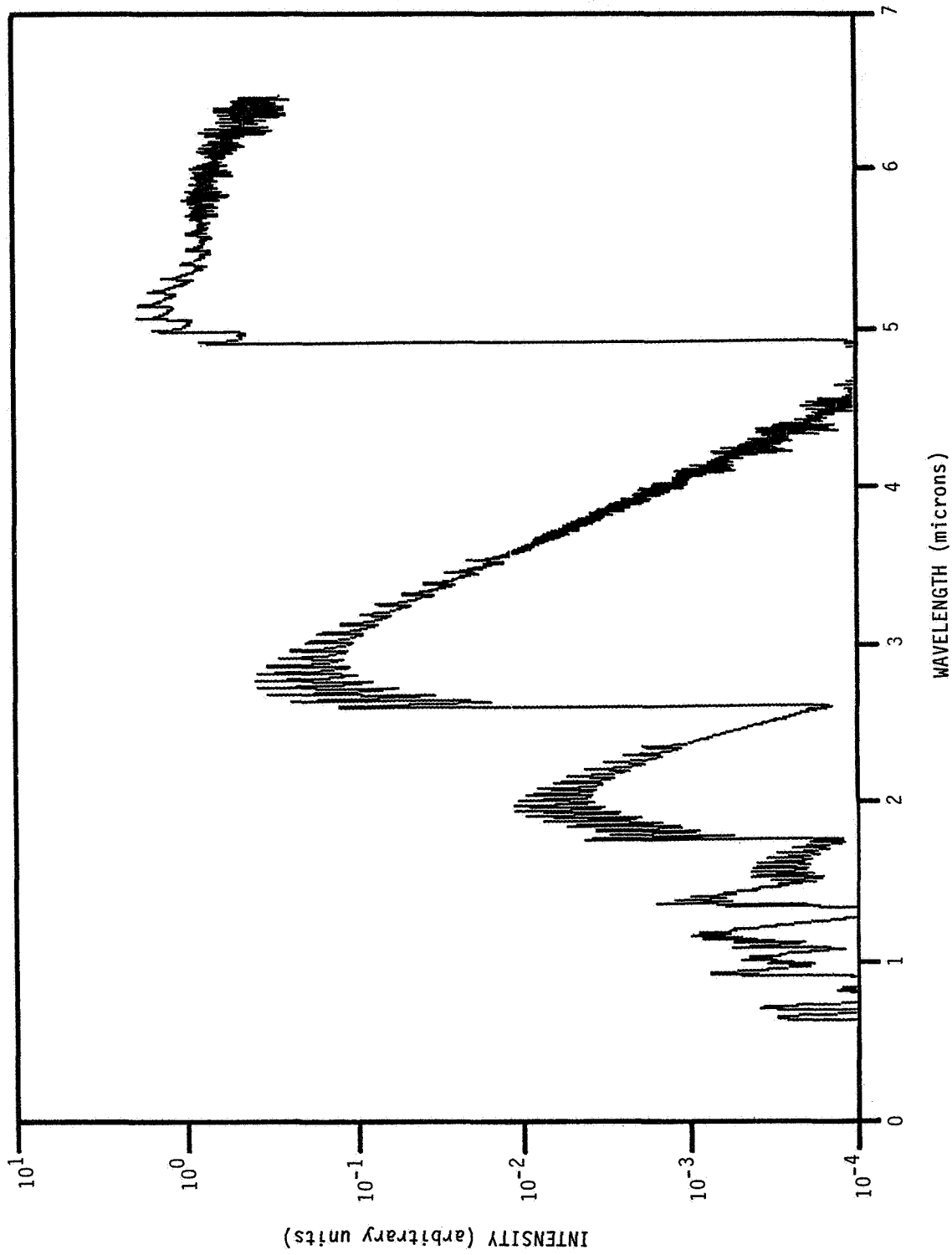


Fig. 8. Plot of NO vibrational emission between wavelengths 0.5 and 6.5 μm . NO emission is much stronger in the infrared.

THE UV-VIS OPTICAL ENVIRONMENT OF THE SHUTTLE

Marsha R. Torr

Department of Physics, Utah State University

Abstract. During the Spacelab 1 shuttle mission, spectroscopic measurements were made of the atmospheric emissions over a broad wavelength range extending from the extreme ultraviolet to the near infrared. These measurements were made under a variety of vehicle attitude and sunlight conditions. Superimposed on such spectra would be any features associated with the induced vehicle environment and its interaction with solar photons and the ambient neutral atmosphere and plasma. In this paper, we discuss various anomalies and unexpected features in the spectra from the perspective of possible shuttle-induced origins. The data indicate a dramatic cleanup of the vehicle environment over the course of the 10-day mission, a strong non-atmospheric red continuum underlying the spectra at night and at large angles to the velocity vector, and a variety of molecular band distributions which are not explained by our present understanding of the atmosphere.

Introduction

The phenomenon of glows associated with spacecraft surfaces directed into the velocity vector is now widely known. In the case of the shuttle at altitudes near 250 km, these glows are visible to the naked eye at night and are readily photographed with hand-held cameras [see Banks et al., 1983; Mende et al., 1983]. In addition, it has been recognized for many years that sensitive instruments directed into the velocity vector experience an intensity enhancement that increases significantly from the blue to the red and which is due to the interaction of the vehicle with the ambient environment [Torr et al., 1977; Yee and Abreu, 1983]. These effects are well covered in related papers in these proceedings.

Of major concern to those working at low light levels from space vehicles is whether these effects are due entirely to surface and near surface glow which can perhaps be avoided by looking at angles other than the ram or by operating at much greater altitudes, or whether an extended optical contamination exists around the vehicle. A clear understanding of the extent of the induced optical environment is of importance to investigations from space shuttle, Space Station, Space Telescope, and vehicles operating in the upper atmosphere in general.

At the First Shuttle Glow Workshop a year ago, we reported an initial data set obtained on the Spacelab 1 shuttle flight with the Imaging Spectrometric Observatory (ISO). These particular data were obtained in an observing sequence in which the field-of-view was directed tangentially away from the Earth and straight out of the payload bay (-Z axis) into the velocity vector. The data were acquired on the dayside of the Earth. From these data it was concluded that the wavelength region from 6000 Å to 8000 Å was densely populated with a number of bright overlapped bands. These bands were subsequently tentatively identified as N₂(1P) [Torr and Torr, 1985a] and were found to significantly exceed the brightness of these features expected from the ambient atmosphere.

It then becomes of obvious interest to know how these spectra obtained looking into the velocity vector compare with others obtained with different viewing geometries and under different conditions of solar illumination. In the following sections, we present a variety of preliminary spectra obtained in different orientations.

Results

Three spectra are shown in Figure 1, all taken with the field-of-view of the instrument looking tangentially away from the Earth and on the dayside, but with the field-of-view into the wake, at 90° to the wake, and into the velocity vector, respectively. The lower panel (into the velocity vector) is the spectrum shown at the workshop a year ago. All three spectra show bright bands in the red. However, it should be noted that the scales on the three spectra are quite different, so that the intensities are increasingly bright going from the bottom to the top of the figure. Thus, the surprising aspect of the data shown in this figure is that the ram data are significantly "cleaner" in the red portion of the spectrum. The sensitivity of the instrument drops by a factor of 3 from 6000 \AA to 8000 \AA . Thus, there is a tendency to amplify the noise at higher wavelengths in converting from counts to $R/\text{\AA}$. However, the integration periods are comparable in all three cases. The data taken with the field-of-view looking into the wake were taken on the first day of the mission, some 20 hours after launch. The data taken looking at 90° to the velocity vector were taken on the second day of the mission, approximately 40 hours after launch. The data into the velocity vector were acquired on day 10 of the mission and followed a very extended period of the payload bay being directed at the Sun (almost 24 hours). These results therefore suggest that there was a significant cleanup in the vehicle-induced environment over the course of the 10-day mission.

The data shown in Figure 2 were all taken looking at a tangent ray altitude of 250 km into the wake and on the first day of the mission. The comparison in this case is of different solar conditions; night, twilight, and day. In this case, relatively bright band features are again present in the red portion of the spectrum. Because so many of the contaminants are the same as the species occurring naturally in the atmosphere, the problem is to try to determine whether these features are due to the ambient upper atmosphere or due to the vehicle, or due to a distortion of the ambient environment by the vehicle. As was mentioned above, the viewing geometry in these three sequences is tangential to the Earth. In such a viewing configuration, naturally occurring features are considerably amplified because the slant path length of the atmosphere is longer than the vertical distance through the same emission layer. The slant path amplification factor at these altitudes would be approximately 30 for atmospheric features. Thus, the features appearing in the nightglow spectrum would correspond to vertical intensities of $1\text{-}2 R/\text{\AA}$ if they are of atmospheric origin. However, if the source is a glowing interaction region surrounding the vehicle, its intensity would not be expected to change in the same way with angle to the zenith.

In Figure 3, we show a comparison of the 250 km tangent ray altitude nighttime data shown in Figure 2, together with another nightglow spectrum taken with the field-of-view looking within 20° of the vertical.

The slant path factor difference in the obvious atmospheric features such as the $O(^1D)$ lines at 6300/6364 Å is evident. However, there is a major difference between the two spectra. We have been cautious in assigning any real significance to underlying continuum in the ISO data from Spacelab 1 for various reasons. Our observing sequences were designed with relatively few background measurements and even some of these were lost due to launch delay impacts. In addition, the vehicle testing associated with the mission required subjecting the payload to thermal extremes. In several cases, there was the possibility that the nearest instrument background measurement might not fully remove a changing thermal background component. As a result, residual backgrounds were removed from the data and the analyses have concentrated on the line and band spectra. However, in the case of the near vertical spectrum shown in Figure 3, the continuum apparent in this spectrum was repeated on seven consecutive nightside passes, all of which had relatively good instrument background corrections. We therefore believe that these data (and possibly the other spectra shown also) indicate a strong red continuum with a peak intensity of approximately 30 R/Å. This continuum cannot be atmospheric in its origin and is observed at night looking at an angle of almost 90° to the velocity vector.

Figure 4 shows a dayglow spectral survey covering 600 Å to 8000 Å. In this case the instrument was looking at a tangent ray height of 150 km and at an angle of 20° to the wake. Six consecutive such spectra were obtained over a full orbit with the vehicle sunlit. Considerable analysis has yet to be done on these data and only a few comments will be made here. The red visible wavelengths are dominated by the bright O_2 atmospheric bands which are explained by atmospheric sources. The $N_2(^1P)$ bands in this region might also be explained by atmospheric processes. The N_2^+ emissions are anomalous and are discussed in another paper in these proceedings. Throughout the spectrum there are features for which we do not yet have identifications. The N_2 Lyman-Birge-Hopfield bands have a highly anomalous vibrational and rotational distribution (Figure 5). It is likely that this is an atmospheric phenomenon, but we do not yet understand the excitation mechanism [Torr and Torr, 1985b], and have found the same features, similarly anomalous, in the nightglow [Torr et al., 1985].

Conclusions

In this paper we have presented a number of spectra measured from Spacelab 1 under a variety of conditions. The data indicate a significant reduction of the intensity of features in the red portion of the spectrum over the course of the mission, which could be associated with a significant reduction in the vehicle outgassing over the 10 days of the mission. The nighttime data indicate a strong underlying red continuum (30 R/Å) at large angles to the velocity vector. The spectra in general show evidence of highly anomalous N_2 and N_2^+ band systems. At the present time we cannot account for these in terms of our current understanding of the atmospheric/ionospheric processes. In addition, the spectra contain a number of features which we cannot yet identify. Thus, either we do not understand some very fundamental aspects of the terrestrial atmosphere, or the shuttle environment comprises an extended interaction region in which various collision processes are occurring in large numbers.

Acknowledgment. This work was supported by NASA Contract NAS8-33992.

References

- Banks, P. M., P. R. Williamson, and W. J. Raitt, Space Shuttle glow observations, Geophys. Res. Lett., 10, 118, 1983.
- Mende, S. B., O. K. Garriott, and P. M. Banks, Observations of optical emissions on STS-4, Geophys. Res. Lett., 10, 122, 1983.
- Torr, M. R., and D. G. Torr, A preliminary spectroscopic assessment of the Spacelab 1/Shuttle optical environment, J. Geophys. Res., 90, 1683, 1985a.
- Torr, M. R., and D. G. Torr, The N₂ Lyman Birge Hopfield dayglow from Spacelab 1, Geophys. Res. Lett., submitted, 1985b.
- Torr, M. R., and D. G. Torr, A spectral survey of the dayglow at 150 km tangent ray height, Geophys. Res. Lett., submitted, 1985c.
- Torr, M. R., P. B. Hays, B. C. Kennedy, and J.C.G. Walker, Intercalibration of airglow observations with the Atmosphere Explorer Satellite, Planet. Space Sci., 25, 173, 1977.
- Torr, M. R., D. G. Torr, and J. W. Eun, A spectral search for Lyman-Birge-Hopfield band nightglow from Spacelab 1, J. Geophys. Res., 90, 4427, 1985.
- Yee, J. H., and V. J. Abreu, Visible glow induced by spacecraft-environment interaction, Geophys. Res. Lett., 10, 126, 1983.

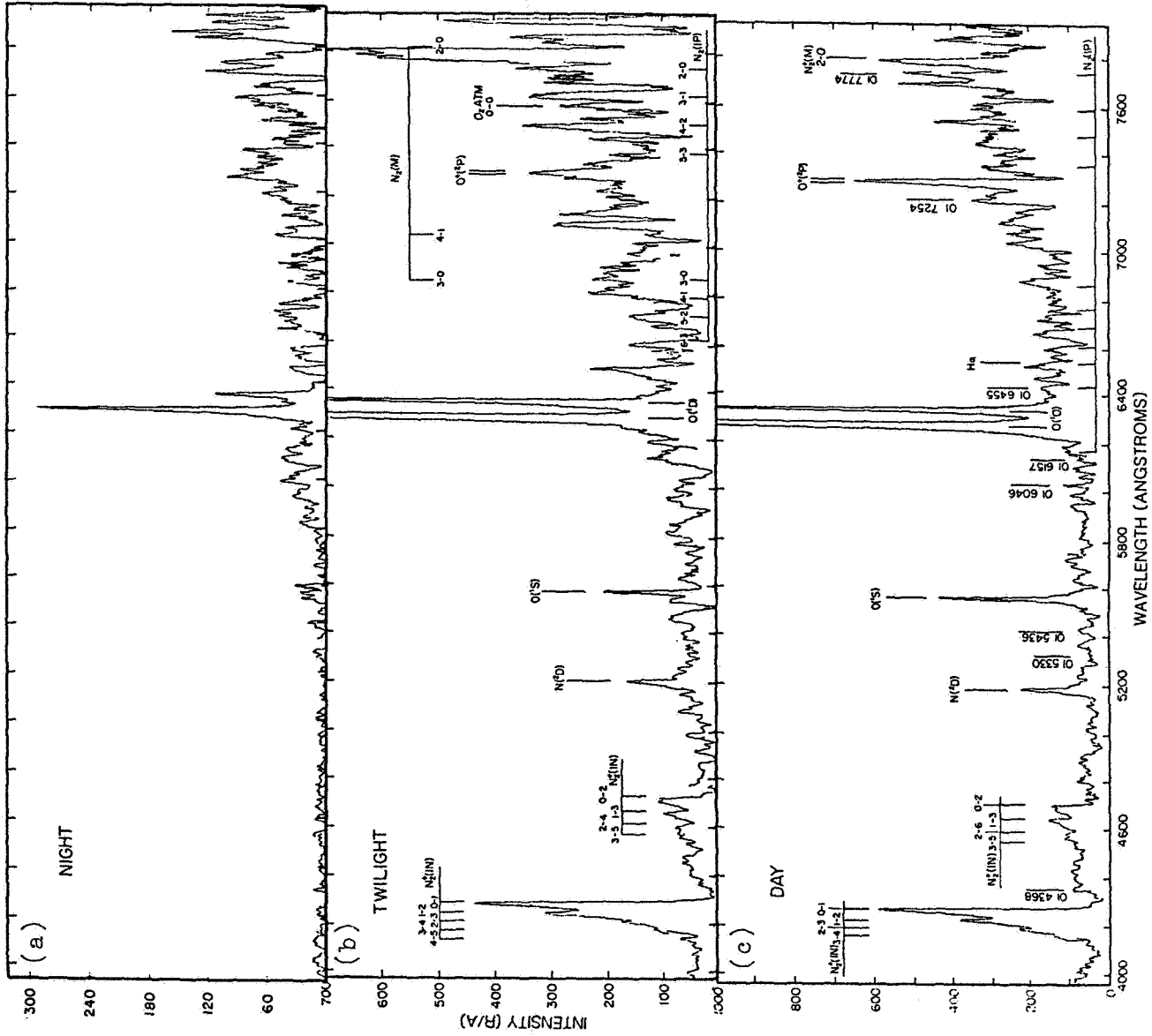


Fig. 2. Visible spectra looking into the wake (a) nightside, (b) twilight, and (c) dayside.

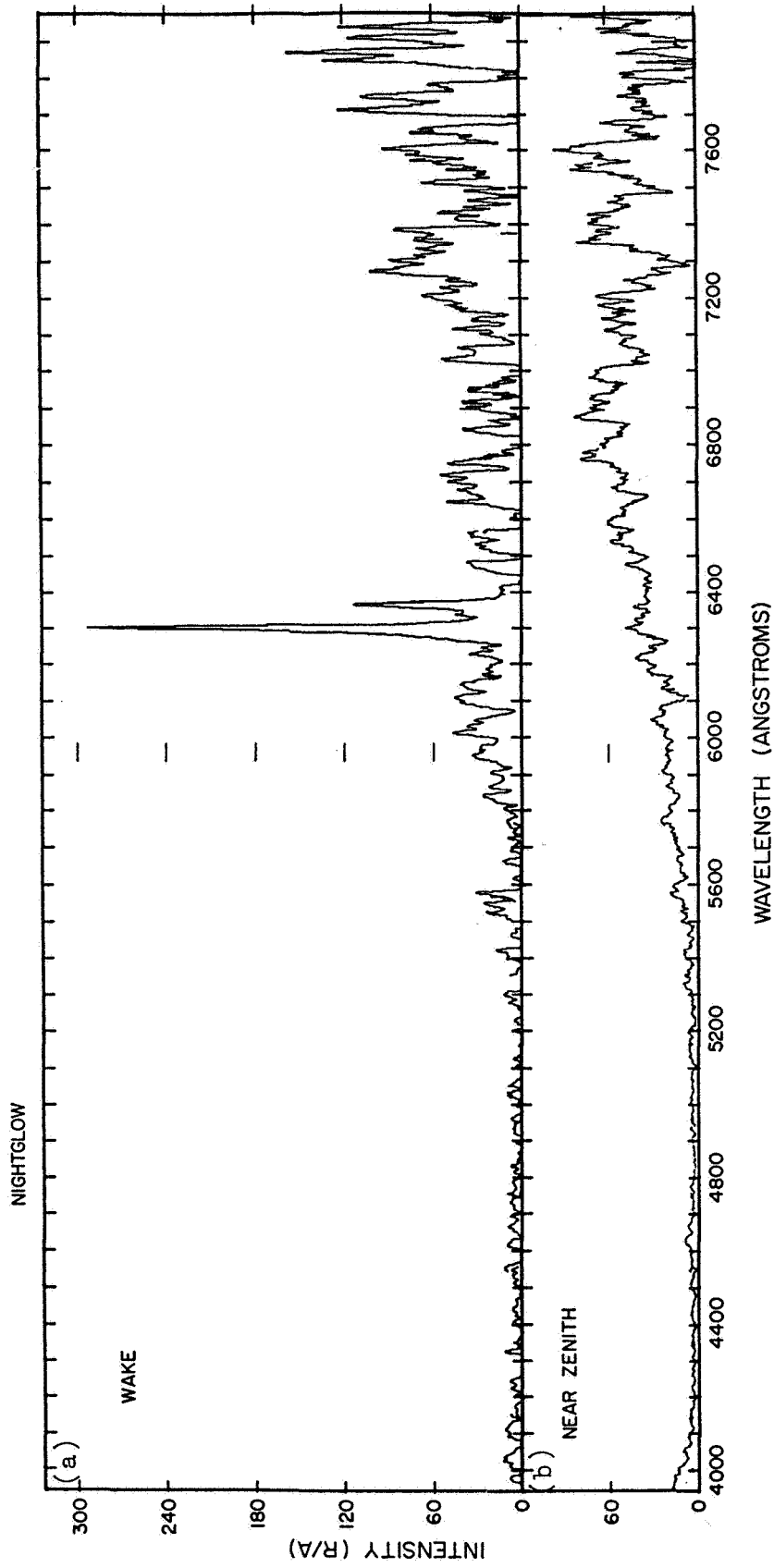


Fig. 3. Visible spectra taken on the nightside (a) looking at a 250 km tangent ray height (i.e., same spectrum as 2a) and (b) looking close to the vertical.

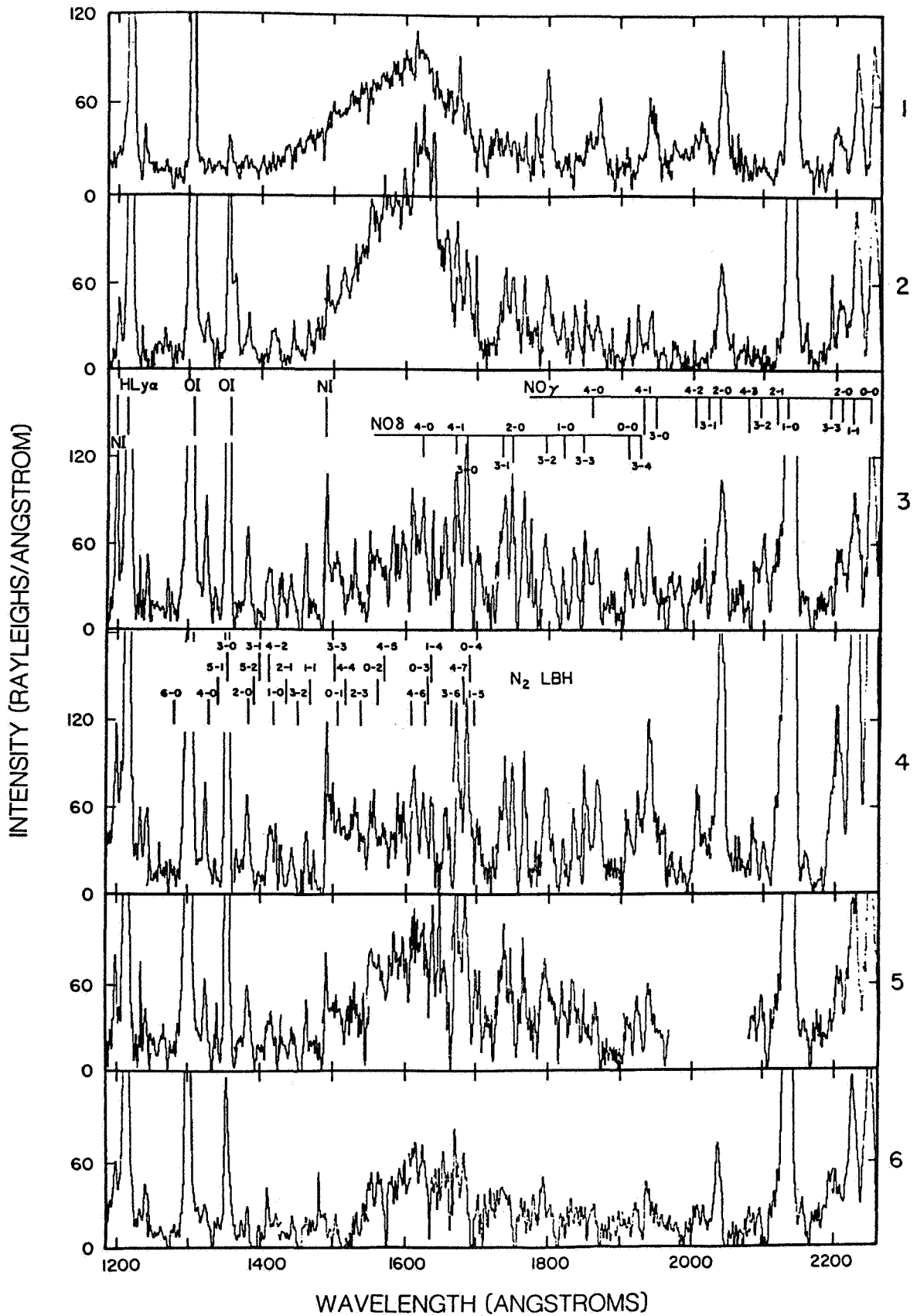


Fig. 5. Far ultraviolet spectra of the dayglow for a 150 km tangent ray height. The six consecutive spectra correspond to changing latitude and solar zenith angle conditions [from Torr and Torr, 1985b].

ENHANCED N_2^+ IN THE SHUTTLE ENVIRONMENT

D. G. Torr, A. Khoyloo, and Marsha R. Torr

Department of Physics
Utah State University
Logan, Utah

Abstract

Observations were made of the N_2^+ first negative and Meinel emission bands with the Imaging Spectrometric Observatory (ISO) on Spacelab 1. These observations have revealed the presence of N_2^+ emissions which exceed those expected on the basis of current ionospheric models by up to a factor of 10. If the emission is of terrestrial origin, large unidentified ionospheric sources of N_2^+ ions must exist. On the other hand, if the source is local to the shuttle environment, a mechanism must be found which is capable of generating emissions of such unexpectedly large intensity. We suggest charge exchange of ambient ionospheric O^+ ions with shuttle environmental N_2 , followed by resonance scattering of sunlight, as a candidate. However, this model implies that a cloud of N_2 gases must surround the vehicle in concentrations in excess of 10^{11} cm^{-3} with a scale length of tens of meters. In addition, the N_2^+ residence time must be of the order of 10 sec.

INVESTIGATION OF VEHICLE GLOW IN THE FAR ULTRAVIOLET

Supriya Chakrabarti and Timothy Sasseen

Space Sciences Laboratory, University of California, Berkeley

Abstract. To date, all vehicle glow observations have been conducted in the visible and near infrared wavelength regions. As the Space Telescope's wavelength coverage extends to the far ultraviolet range and current plasma theory of the spacecraft glow phenomena predicts bright glow intensities, we have begun a study of the ram glow effects in the 800-1400 Å region. The data were collected between March 21-28, 1979, from 600 km altitude near local midnight by the University of California, Berkeley's extreme ultraviolet spectrometer on board the polar orbiting STP78-1 satellite. Data from several nighttime orbits obtained outside the South Atlantic Anomaly region and within $\pm 30^\circ$ magnetic latitude range were separated into forward (south viewing) and backward (north viewing) bins. Each of these bins was subdivided into three directional categories: (1) up (zenith angles $30-80^\circ$), (2) side (zenith angles $80-100^\circ$), and (3) down (zenith angles $120-150^\circ$). The maximum ram glow effects are expected in the side viewing directions. Our data indicate possible effects of ram glow signatures in the 800-1400Å wavelength region.

Introduction

An unexpected optical phenomenon was discovered during the third flight of the space shuttle. Color photographs and low light level TV experiments showed that the Orbiter "glows" in the dark [Banks et al., 1983]. The glow phenomenon was found to be associated with the interaction of the ambient atmosphere with the Orbiter body and has since been referred to as shuttle glow, vehicle glow, or spacecraft glow.

The emission intensity was found to depend on the angle between the spacecraft velocity vector and either the line of sight vector or the surface being viewed. The brightest signal was observed from the spacecraft surface facing the direction of its motion, thus allowing the hypothesis that the emissions are due to the interaction of the ambient atmosphere with the spacecraft. Thruster firing was also found to emit light in the visible and near infrared region [Banks et al., 1983; Mende et al., 1983].

Similar observations were made earlier [Torr et al., 1977] from the Atmosphere Explorer C (AE-C) satellite. The investigators found that very large intensities of emissions (up to 2.5 kR at 7320Å at midnight) are due to the interaction of the satellite with the atmosphere. Banks et al. [1983] deduced an intensity of 10 kR for the glow while Mende et al. [1983] reported the intensity of the glow to be 300-400R. This huge difference in intensity can be attributed to both the difference in altitude of the two flights and the angle of attack.

Yee and Abreu [1983] examined AE-E photometric data and found that the emissions are brightest in the red and are considerably weaker shortward of 4000Å. They suggested that the glow has a diffuse or continuum spectrum. Later space shuttle experiments [Mende et al., 1983, 1984a,b; Swenson et al., 1985] have confirmed that the spectrum is diffuse in nature. They also found that the spectrum is consistent with the orange-red color found in the photographs and peaks near 7000Å.

Several mechanisms responsible for producing the emissions have been proposed. Yee and Abreu [1983] found a strong correlation between the glow emissions and atomic oxygen density above 160 km altitude. No correlation was found between the emission intensity and the molecular nitrogen density. Moreover, below 160 km, the glow intensity was found to be uncorrelated with O density. Although the authors did not propose any specific excitation mechanism, their data strongly suggest one involving atomic oxygen.

Slanger [1983] proposed that the emissions are due to the OH Meinel band system. This proposed mechanism was supported by the altitude distribution of the glow as observed by Yee and Abreu [1983] and the lifetime of these emissions. However, later spectroscopic observations

[Mende et al., 1984a] indicated that OH cannot be the primary source of these emissions.

The Imaging Spectrometric Observatory (ISO) experiment on the Spacelab 1 missions has studied the shuttle glow phenomenon using high resolution ($2 - 3\text{\AA}$) spectrometers in the far ultraviolet (FUV) to near infrared region [Torr and Torr, 1984]. These observations indicated the presence of N_2 emissions in the glow spectrum. It is possible that this glow spectrum contains day-glow emissions and therefore, an independent verification of the N_2 emissions in the glow spectrum will also be needed.

Another proposed mechanism to explain the shuttle glow effects involves hot electrons causing plasma discharge [Papadopoulos, 1984]. Support for this hypothesis was provided by the observation of the N_2^+ first negative system by the ISO experiment and from the observations of NO 2150 \AA emissions from the AE-D satellite. However, the absence of the N_2 second positive system in the ISO spectrum and the dependence of the glow intensity on the surface materials [Mende et al., 1984a] argue against this possibility. One interesting aspect of this mechanism is that it predicts glow emissions in both the blue and the ultraviolet (UV). Unfortunately, no systematic study of the glow has been conducted in the UV.

Torr et al. [1977] have suggested that the emissions are produced by the recombination of NO with O on the interior surface of their instrument. NO 2150 \AA glow emissions observed spectroscopically from the AE-D satellite were found to have a brightness of $\sim 2 - 3\text{kR}$ at 140 km altitude (A. I. Stewart, private communication, 1985). Recent spectroscopic measurements [Swenson et al., 1985] have indicated a continuum spectrum of the glow emission which is similar to the recombination continuum of NO_2 obtained in the laboratory.

Most of the glow studies have been conducted at altitudes equal to or less than 300 km. Yee and Abreu [1983] have reported observation of the glow to altitudes greater than 400 km, at least at 7320 \AA . This raises a potential concern for the Space Telescope; therefore, it is important that glow intensities be measured at the Space Telescope altitude (590 km) and all wavelengths covered by it. Unfortunately, from existing data, no experiment can provide answers to all of these questions.

We flew a spectrometer onboard an Air Force satellite at 600 km. The primary purpose of the experiment was to study the airglow emissions in the Earth's upper atmosphere. The experiment was conducted near solar maximum during 1979-1980, a condition likely to be experienced by the Space Telescope. In this report, we summarize our observations of possible glow-like phenomena in the 800-1400 \AA wavelength range.

Instrument and Orbital Operations

The instrument consists of a 0.5-mm-wide rectangular entrance slit, a concave reflection grating, and two redundant position-sensitive extreme ultraviolet (EUV) detectors lying on the Rowland cylinder. It has been described in full detail by Bowyer et al. [1981]. At any given time, a 650 \AA -wide window is observed every 0.2 second out of the full 300 to 1400 \AA operating range of the instrument.

The combination of slit dimension, grating size, spin, and telemetry rate of the spacecraft provides a triangular working field-of-view of $18^\circ \times 9^\circ$. The instrument has a full width at half maximum (FWHM) resolution of 8 \AA and a peak sensitivity of 0.1 counts $\text{sec}^{-1} \text{R}^{-1}$ per wavelength bin at 550 \AA .

The satellite was placed in a 600 km altitude, Sun-synchronous, polar circular orbit lying essentially in the noon-midnight plane. The spectrometer was housed in the spinning wheel of the spacecraft in the so-called cartwheel configuration. The spectrometer's line-of-sight is oriented at 120° from the spin axis. As the wheel rotates at 11 rpm, the instrument's line-of-sight sweeps out a cone, alternately viewing the Earth and space and never looking closer than 30° to the Sun.

Results

Our instrument is housed in a spinning platform which enables us to study the dependence of the emissions with the angle of attack. However, since the emissions are considerably weaker in

the EUV than in their red counterpart, we report here on only the spectra obtained in the side viewing direction (zenith angles between 80° and 100°) where the vehicle glow effects are expected to be strongest. Only nightside data obtained within $\pm 40^\circ$ magnetic latitude are considered in this study. All data obtained during a South Atlantic Anomaly (SAA) pass were discarded from this analysis.

The sketch shown in Figure 1 demonstrates how the spectra were selected for the forward (ram) and backward (wake) viewing directions. Also shown is the observing geometry for the up (zenith angles between 30° and 50°) and down (zenith angles between 120° and 150°) directions.

A large number of individual side viewing observations were selected according to the rules outlined earlier to yield an average forward looking and an average backward looking spectra as shown in Figure 2. Several bright features are present in these spectra and are indicated. Also shown are 1σ count statistics for each wavelength bin.

It is evident that the spectra are dominated by emissions from neutral hydrogen and neutral oxygen. These emissions and their morphology have been discussed by Chakrabarti et al. [1984], Chakrabarti [1984], and Abreu et al. [1984]. The hydrogen emissions are excited by multiple scattering of solar Lyman α emissions generated by geocoronal hydrogen atoms. The OI emissions, on the other hand, are excited by radiative recombination of ionospheric O^+ ions and show strong latitudinal dependence. To find the spectral characteristics of the glow emissions in this wavelength range, the spectrum obtained in the wake was subtracted from that obtained in the ram direction. The resulting spectrum is shown in Figure 3.

Discussion

The residuals in the spectrum shown in Figure 3 are positive for most of the detected features shown in Figure 2. This implies that the HI and OI emission features are brighter in the ram direction than in the wake viewing direction. The geocoronal hydrogen Lyman α emissions have been studied extensively [see for example, Meier and Mange, 1973] and have been found to depend primarily on the solar zenith angle. Because our observations were made near equinox and the satellite is in a noon-midnight orbit, any possible solar zenith angle effects are nullified due to the accumulation of spectra obtained in the north and south hemispheres. Figure 1 shows that the closest altitude where the line-of-sight crosses the auroral zone is ≥ 700 km. Thus, the observed ~ 1.5 kR Lyman α excess intensity in the forward viewing direction is not likely to be due entirely to an auroral source. Any spatial variation of the intensity distribution giving rise to the observed effect must also be time varying at roughly 15 minutes or less. Otherwise, the accumulation of forward and backward viewing spectra from every latitude point along the spacecraft orbit will cancel out such an effect. Another mechanism which can produce such asymmetry in the Ly α intensity is the contribution of interplanetary Ly α emissions. Such a mechanism can produce up to 1000R intensity difference (R. R. Meier, private communication, 1985). It is also possible that the interplanetary hydrogen emissions contribute to the observed directional dependence of the Ly α signal. However, there still remains a portion of the excess Ly α signal in the forward viewing direction.

We now are faced with the question: is it possible that we are observing the spacecraft glow effects produced by hydrogen atoms? We need $\sim 1.5 \cdot 10^5$ photons sec^{-1} along the line-of-sight to produce the required intensity. MSIS predicts $5.3 \cdot 10^4$ H atoms per cubic centimeter for our observing condition. If the Ly α glow extends only 20 cm, then it would be unlikely that a kilorayleigh glow could be produced from $\sim 10^{-5}$ production efficiency. The Lyman β "glow", on the other hand, has an intensity of ~ 10 R which has a greater probability of being produced by an atmospheric interaction. Although no conclusions can be drawn from these data, it is possible that some of these hydrogen emissions are excited by the spacecraft glow phenomenon.

We observe that two OI emissions at 911 and 1356Å are brighter in the ram direction. The intensities are ~ 15 R and might be produced by vehicle interaction. However, the OI 1304Å emission does not show the same directional dependence, and argues against it.

From energy arguments, one can rule out collision excitation mechanism for the hydrogen emissions. The Lyman α and β emissions need > 10 eV energy for their excitation which is larger

than that attainable by the 7 km/sec satellite velocity. These emissions are most likely due to recombination of protons at the satellite surface. Hydrogen recombination continuum at 912 Å provides support to this hypothesis.

We did not observe any N₂ LBH emissions in the individual spectra shown in Figure 2. However, the residual spectrum shown in Figure 3 contains a slight indication of the (6,0) band at 1273 Å. Taking these data at their face value then implies that we are observing an excess of ~400 R of total LBH emissions in the forward viewing direction. Very bright N₂ LBH emissions of unexplained origin have been observed in several experiments [for a review on this subject see Meier and Conway, 1983]. These emissions were found to be limited to the summer and north hemisphere. We searched for such emissions in our data and have not found them [Chakrabarti et al., 1984].

In summary, we have studied the dependence of the EUV and FUV emissions at 600 km. Our data show that several of these emissions are brighter in the ram direction than in the wake. It is possible that the ram glow phenomena are contributing to the observed excess intensity in the EUV. Further studies using higher sensitivity instruments will be needed to completely understand these effects.

Acknowledgments. We acknowledge helpful discussions with Gary Swenson, Robert Meier, John Clarke, Ian Stewart, and Stuart Bowyer. This work was supported by NASA Contract NAS8-32577.

References

- Abreu, V. J., A. Dalgarno, J. H. Yee, and S. Chakrabarti, The OI989 Å tropical nightglow, Geophys. Res. Lett., **11**, 569, 1984.
- Banks, P. M., P. R. Williamson, and W. J. Raitt, Space Shuttle glow observations, Geophys. Res. Lett., **10**, 118, 1983.
- Bowyer, S., R. Kimble, F. Paresce, M. Lampton, and G. Penegor, A continuous readout extreme ultraviolet spectrometer, Appl. Opt., **20**, 477, 1981.
- Chakrabarti, S., EUV (800-1400 Å) observations of tropical nightglow, Geophys. Res. Lett., **11**, 565, 1984.
- Chakrabarti, S., R. Kimble, and S. Bowyer, Spectroscopy of the EUV (350-1400 Å) nightglow, J. Geophys. Res., **89**, 5660, 1984.
- Green, B. D., Atomic recombination into excited molecular - A possible mechanism for Shuttle glow, Geophys. Res. Lett., **11**, 576, 1984.
- Meier, R. R., and P. Mange, Spatial and temporal variations of the Lyman alpha airglow and related atomic hydrogen distributions, Planet. Space Sci., **21**, 309, 1983.
- Meier, R. R., and R. R. Conway, On the N₂ Lyman-Birge-Hopfield band nightglow, J. Geophys. Res., **88**, 4929, 1983.
- Mende, S. B., O. K. Garriott, and P. M. Banks, Observations of optical emissions on STS-4, Geophys. Res. Lett., **10**, 122, 1983.
- Mende, S. B., P. M. Banks, and D. A. Klingelsmith, III, Observation of orbiting vehicle induced luminosities on the STS-8 mission, Geophys. Res. Lett., **11**, 527, 1984a.
- Mende, S. B., G. R. Swenson, and K. S. Clifton, Preliminary Atmospheric Emissions Photometric Imaging Experiment, Science, **225**, 191, 1984b.
- Papadopoulos, K., On the Shuttle glow (the plasma alternative), Radio Sci., **19**, 571, 1984.
- Slanger, T. G., Conjectures on the origin of the surface glow of space vehicles, Geophys. Res. Lett., **10**, 130, 1983.
- Swenson, G. R., S. B. Mende, and K. S. Clifton, Ram vehicle glow spectrum: Implication of NO₂ recombination continuum, Geophys. Res. Lett., **12**, 97, 1985.

- Torr, M. R., Optical emissions induced by spacecraft-atmosphere interactions, Geophys. Res. Lett., 10, 114, 1983.
- Torr, M. R., and D. G. Torr, Atmospheric spectral imaging, Science, 225, 169, 1984.
- Torr, M. R., P. B. Hays, B. C. Kennedy, and J. C. G. Walker, Intercalibration of airglow observations with the Atmosphere Explorer Satellites, Planet. Space Sci., 25, 173, 1977.
- Yee, J. H., and V. J. Abreu, Visible glow induced by spacecraft-environment interaction, Geophys. Res. Lett., 10, 126, 1983.

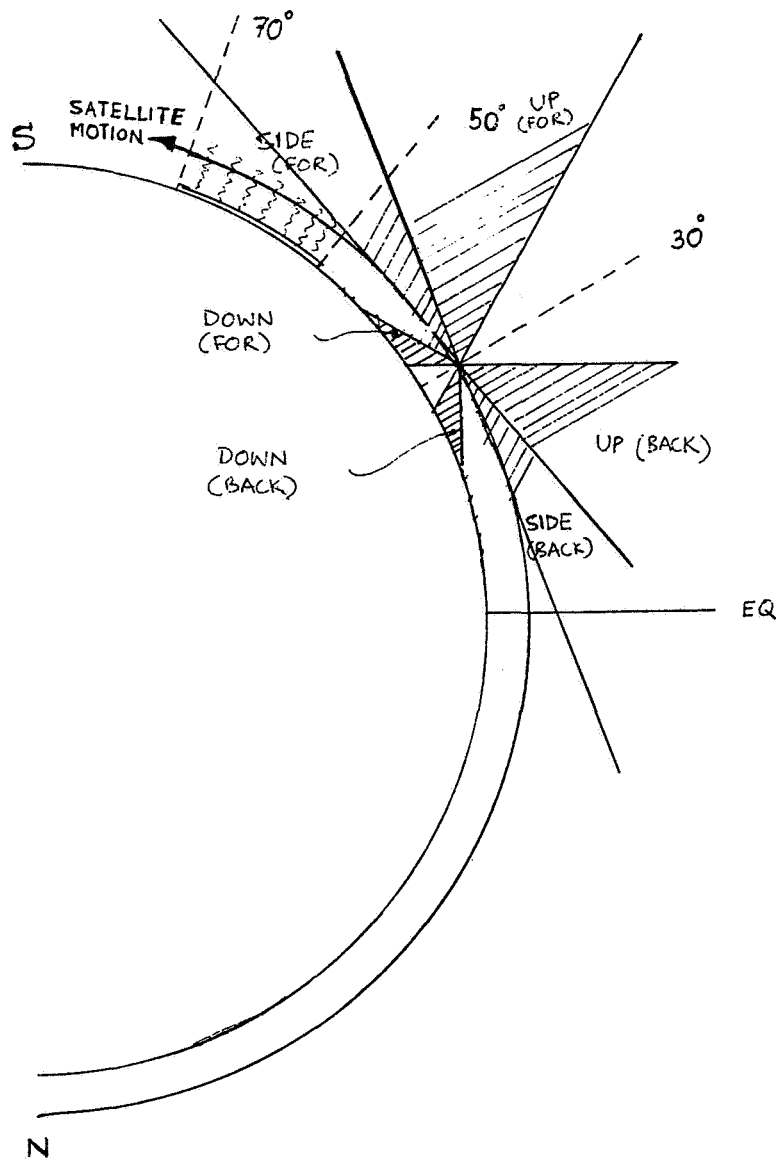


Fig. 1. The observing geometry for a nightside pass is shown. The satellite motion is indicated with an arrow from the north to the south pole at 600 km altitude. Boundaries of the up, side, and down looking directions chosen for this study are shown with hatches for a satellite location of 30° south latitude.

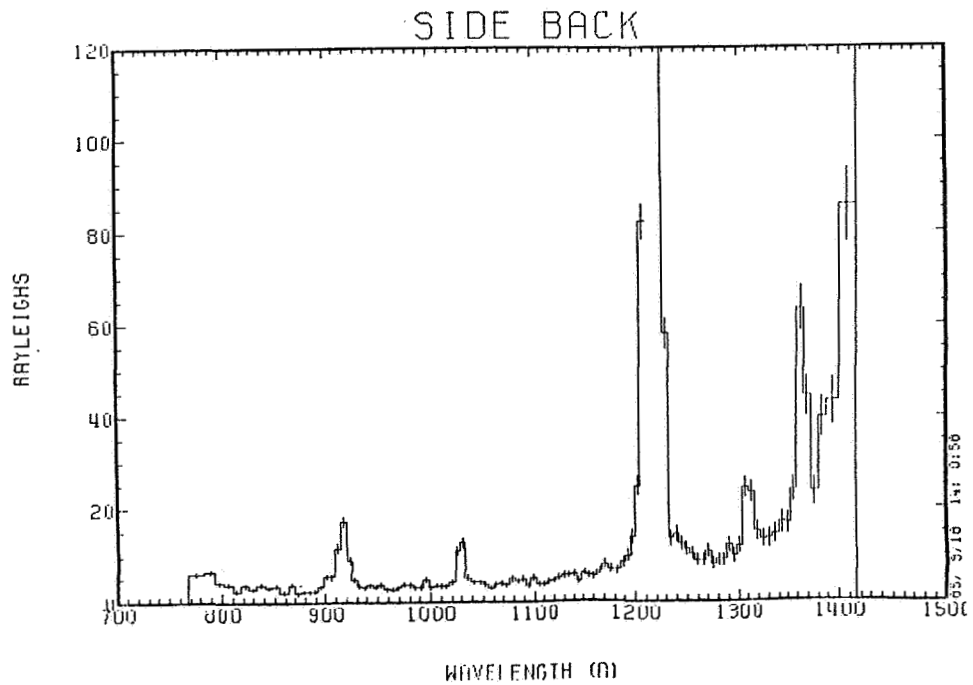
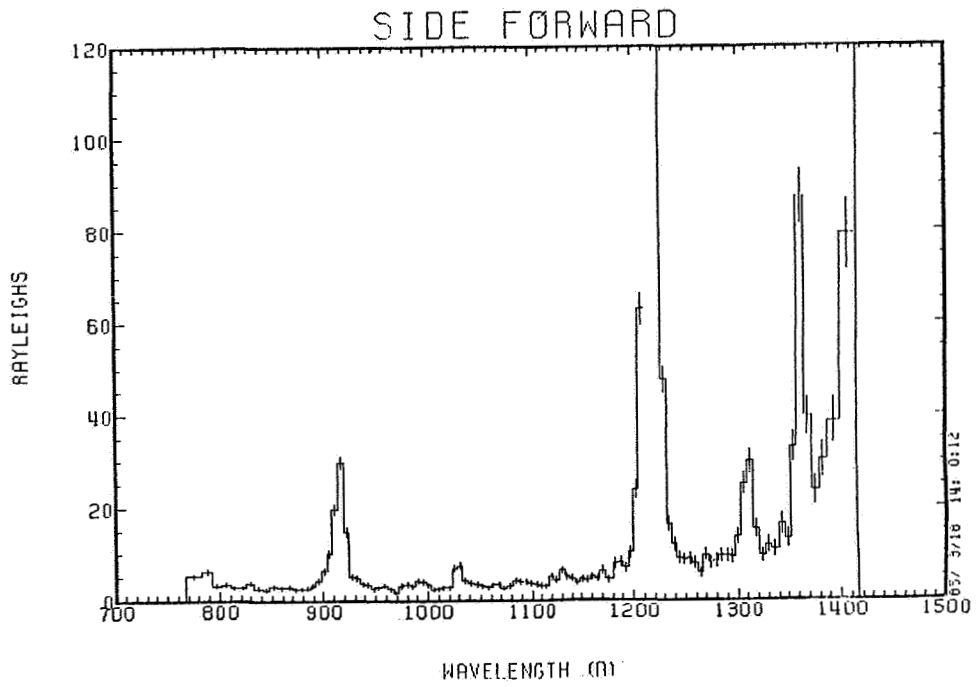


Fig. 2. Side viewing spectra obtained while the satellite was within $\pm 30^\circ$ magnetic latitude range are shown for the forward and backward looking directions. The viewing geometry is shown in Figure 1.

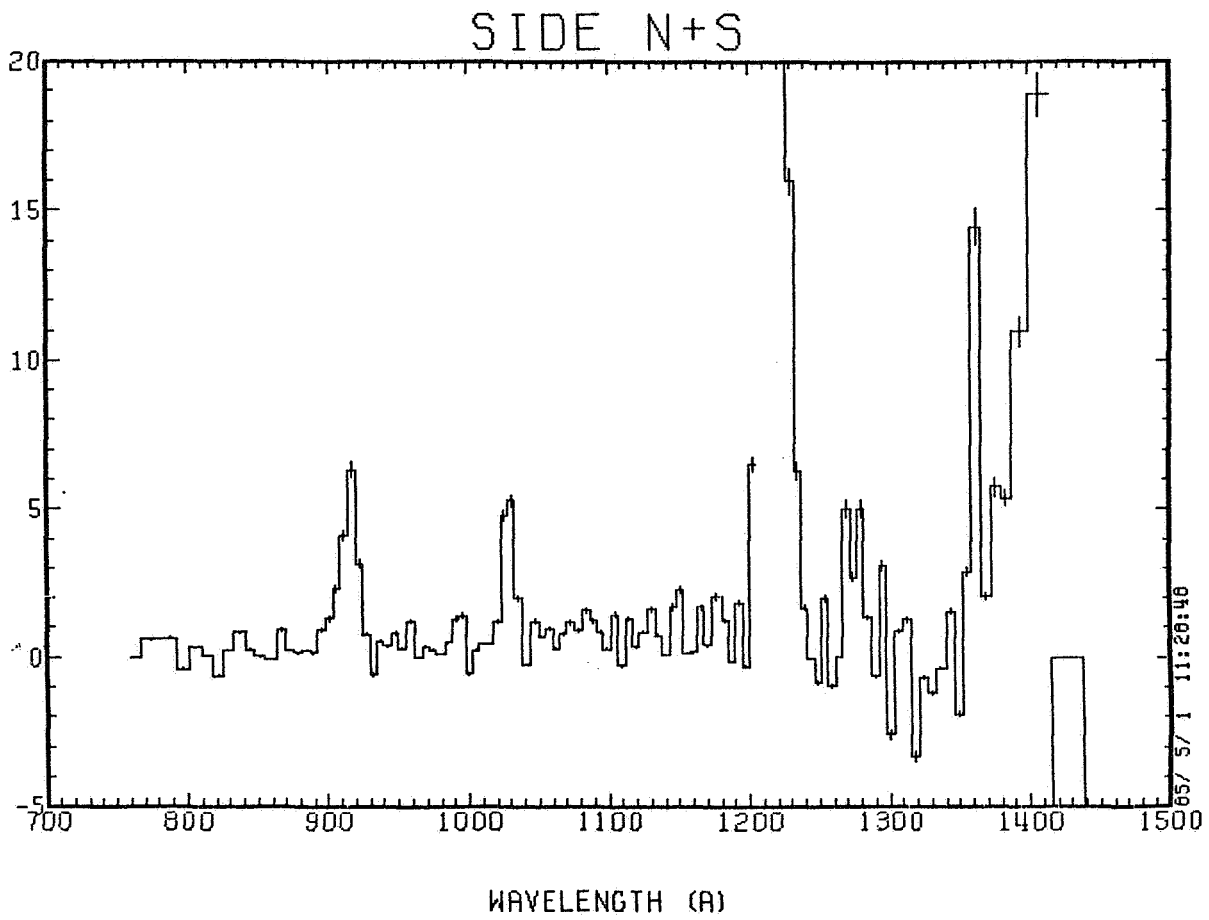


Fig. 3. The spectrum obtained by subtracting the backward looking spectrum from the forward viewing spectrum.

THEORETICAL CALCULATIONS

SPACECRAFT-INDUCED PLASMA ENERGIZATION AND
ITS ROLE IN FLOW PHENOMENA

K. Papadopoulos* and R. A. Smith

Science Applications International Corporation
McLean, Virginia

Abstract. Plasma instabilities induced by orbiting vehicles can cause many important phenomena ranging from electron and ion heating and suprathermal electron tail energization, to enhanced ionization and optical emissions. We outline the basic collective processes leading to plasma energization near plasma sheaths and in regions of neutral gas streaming through plasma, and discuss the role of the induced collective effects in producing the optical emission spectra.

*Permanent Address: University of Maryland, College Park, Maryland.

Introduction

As has been emphasized before [Papadopoulos, 1983, 1984], the glow problem is a strongly interdisciplinary one involving aeronomic chemistry, surface physics, and plasma physics. Its understanding requires a coherent experimental, theoretical, and modeling effort, involving all of the above disciplines in a coupled and dynamic fashion. Previous presentations in the workshop emphasized the aeronomical and surface aspects of the interaction [e.g., Kofsky and Barrett, 1985; Dalgarno et al., 1985; Tolk et al., 1985]. It is the purpose of the present paper to outline the plasma physics aspects of the interaction. The correlation of the glow behavior with the modification of the plasma environment in the vicinity of the Orbiter, as observed by the plasma diagnostics package (PDP) [Shawhan and Murphy, 1983], led us [Papadopoulos, 1983] to conjecture that plasma energized by the Orbiter plasma interaction could play a central role in directly producing or mediating the observed glow. This conjecture is strongly supported by the fact that processes relying on surface recombination are unable to account for glow generated far away from the shuttle surface due to thruster or "shuttle surfaces" firing. We review next the observed plasma environment as modified by the Orbiter-ionosphere interaction, followed by a discussion of the induced plasma processes and their role in exciting or influencing the glow spectra.

Implications of the Plasma Environment Near the Orbiter

The plasma environment in the vicinity of the Orbiter under ram conditions is substantially modified over the ambient. Measurements taken by the PDP indicate [Murphy et al., 1983]:

- (i) A region near the vehicle which exhibits a density enhancement of at least a factor 2-5 over ambient, reaching values of 10^7cm^{-3} ;
- (ii) A flat suprathermal electron tail above 10 eV, substantially enhanced during thruster operation, with a field-aligned component much flatter than its perpendicular counterpart [see also McMahon et al., 1983];
- (iii) An intense electrostatic broadband noise about the lower hybrid frequency;
- (iv) Elevated electron temperatures ($\sim 6000 \text{K}$) were observed [Raitt, 1985];
- (v) Ion fluxes with up to 30 eV energies, sometimes coincident with single or counterstreaming ion beams, were observed [Stone et al., 1983];

(vi) Large amounts of NO^+ , CO_2^+ and H_2O^+ , O^+ were observed, being on occasion the dominant ions [Grebowsky et al., 1983; Murad, 1985];

(vii) A gas layer up to 100 times higher than the ambient neutral density was observed.

It is important to notice that the plasma effects were strongly intensified during thruster operations. This intensification correlates very well with the observed glow behavior.

The presence of enhanced low (~ 1 eV) and high (≥ 10 eV) energy charged particle fluxes can play a central role in the glow emission and its spectrum because they can:

- (i) affect the gas and surface chemistry,
- (ii) interact with the ambient neutrals and excite a variety of emissions due to vibration and rotational excitation as well as due to ionization,
- (iii) interact directly with the surface and produce emissions in a fashion similar to plasma etching.

Physics of Plasma Energization

In discussing the physics involved in the plasma energization one should first identify the available free energy sources, and then examine the time scale and the form of the energy deposition. The most interesting situations occur when the energy deposition occurs on a collisionless time scale owing to plasma instabilities. We discuss two situations below. The first occurs near the orbiter surface, and will be associated with surface glow or etching processes. The second occurs over a larger volume, is independent of the presence of a surface, except for creating a dense stream of neutral gas [Rantanen et al., 1985], and will be associated with volume and thruster glow.

Surface Interactions

The phenomena that arise in the neighborhood of bodies moving in a plasma are very complex and their complete solution is beyond the scope of this brief paper. It is sufficient for our purposes to accept that an electric field $E(\underline{r})$ arises near the surface due to the different mobility of the electrons and ions. The plasma sheath thus formed slows down the electrons while accelerating the ions to neutralize the charge on the surface [Alpert, 1983]. The field created due to the difference of the electron and ion densities is of the order of 10-20 Debye lengths (λ_D), which corresponds to 10-20 cm at shuttle altitude. The expected potential is of the order of 2-5 V. For our purposes it is sufficient to accept an electric field $E \approx 10$ V/m, over a distance of 20 cm. In the presence of a

magnetic field $B_0 \approx 1/3$ G the electrons will drift with respect to the ions with a velocity $V_D = cE_{\perp}/B_0$ (Hall current), because $r_e \ll 20\text{cm} \ll r_i$, where r_e , r_i are the electron and ion gyroradii. The value of V_D is given by

$$V_D = 3 \times 10^6 E[\text{V/m}] \text{ cm/sec} \quad (1)$$

Since the ion sound speed $C_S \approx 3-4 \times 10^5$ cm/sec, $V_D \gg C_S$, resulting in an unstable configuration. The relevant instability is the modified two stream instability [McBride et al., 1972] or the lower hybrid drift instability [Huba and Papadopoulos, 1977]. In the electrostatic limit the dispersion relation in the electron reference frame is given by

$$\frac{\omega_{LH}^2}{(\omega - \underline{k} \cdot \underline{V}_D)^2} + \frac{\omega_{LH}^2}{\omega^2} \left[\frac{k_z^2}{k^2} - \frac{M}{m} \right] = 1 \quad (2)$$

where $\omega_{LH}^2 = \omega_i^2 / (1 + \omega_e^2 / \Omega_e^2)$ is the lower hybrid frequency, ω_i , ω_e are the ion and electron plasma frequencies, Ω_e is the electron cyclotron frequency, k_z is the wavenumber along the magnetic field and M, m are the ion and electron mass. The lower hybrid electrostatic waves heat electrons and ions with a time scale of ω_{LH}^{-1} , which corresponds to less than 10^{-4} sec for our conditions. The instability has been extensively studied in the laboratory and by computer simulations. The electron heating rate is given by

$$T_e = \frac{1}{n_e} \eta^* j^2 - \left[\frac{\partial T_e}{\partial t} \right]_{\text{mom}} - \left[\frac{\partial T_e}{\partial t} \right]_{\text{rot}} - \left[\frac{\partial T_e}{\partial t} \right]_{\text{vib}} - \left[\frac{\partial T_e}{\partial t} \right]_{\text{ion}} \quad (3)$$

where η^* is the value of the anomalous resistivity, and $(\partial T_e / \partial t)_{\text{mom}}$, $(\partial T_e / \partial t)_{\text{rot}}$, $(\partial T_e / \partial t)_{\text{vib}}$, and $(\partial T_e / \partial t)_{\text{ion}}$ are loss rates due to collisions, rotational excitation and deexcitation, vibrational excitation and deexcitation, and

impact ionization, respectively. Depending on the rate η^*j^2 and the abundance of molecular species in the neutral environment a variety of emissions from UV to IR can arise. A quantitative analysis of such a situation is presently under study and will be reported in the future. A proper analysis requires use of the kinetic equation instead of Eq. (3). It is interesting to note that the energy dissipation rate Q is given by

$$Q = \eta^*j^2$$

$$= 10^{-3} \left[\frac{\eta^*}{\eta} \right] \left[\frac{n_e}{10^6} \right] \left[\frac{V_D}{10^7} \right] \left[\frac{N}{10^{11}} \right] [T_e(\text{eV})]^{1/2} \text{erg/cm}^3 \text{sec} \quad (4)$$

where η is the resistivity due to the ion-neutral collisions and N is the neutral density. Notice that even for $\eta^* = \eta$ and the canonical problem parameters the energy deposition rate ($\sim 10^9$ eV/cm³-sec) is much larger than the 10^8 eV/cm³-sec associated with the observed orange glow [Kofsky, 1984].

Volume Interactions

These are phenomena associated with interaction of neutral gas streaming through an ambient magnetized plasma. The role of the spacecraft surface is simply to generate a high density neutral gas plume moving with the spacecraft. In this sense the physics of the volume generated glow is similar to the glow due to thruster operation far away from surfaces. An analysis of such interactions can be found in Formisano et al. [1982] and Papadopoulos [1983, 1984]. In contrast to these analyses, we consider here the situation where the conditions for a discharge are not satisfied, owing to lack of sufficient ion reflection. In this case an ion beam moving with the shuttle speed can be generated by charge exchange. This is due to the fact that in a charge-exchange collision each particle retains its original kinetic energy. The density n_b of such a beam will be given by

$$\frac{dn_b}{dt} = \nu_{cx} n_o - \frac{n_b}{\tau} \quad (5)$$

where n_0 is the ambient plasma density, ν_{cx} is the charge-exchange collision frequency which we take as $\nu_{cx} \approx 10 \text{ sec}^{-1}$, and τ is the confinement time of the charge-exchange-generated ions, which move with the shuttle, in the Orbiter vicinity. Since these ions will be lost once their trajectory deviates from straight line, we take $\tau \approx 1/\Omega_i$, i.e., the ion gyrotime. For O^+ , $\Omega_i \approx 200 \text{ sec}^{-1}$. Therefore in steady state

$$\frac{n_b}{n_0} \approx \frac{\nu_{cx}}{\Omega_i} \approx 5 \times 10^{-2} \frac{N}{10^{11}} . \quad (6)$$

A streaming ion beam with a density ratio $\alpha \equiv n_b/n_0 \approx 10\%$ will be formed. In the presence of such a beam the electrons will drift with respect to the ambient ions with velocity U_e by building a polarization field in order to maintain charge neutrality (Figure 1). The dispersion relation of the configuration of Figure 1 is

$$\frac{\omega_{LH}^2}{(\omega - \underline{k} \cdot \underline{U})^2} + \frac{(1-\alpha)\omega_{LH}^2}{\omega^2} + \frac{\omega_{LH}^2}{(\omega - \underline{k} \cdot \underline{U}_e)^2} \left[\frac{k_z^2}{k^2} \frac{M}{m} \right] = 1 . \quad (7)$$

This system results in the following interactions:

Counterstreaming cross-field ion-ion instability. For $k_z = 0$, flute mode, the third term on the r.h.s. of Eq. (7) disappears and we have the classic counterstreaming ion-ion instability across B_0 . The nonlinear behavior of such a system was elucidated as early as 1971 by Papadopoulos et al. [1971]. The ion beam excites hybrid waves which result in collisionless momentum coupling of the ion streams as well as ion heating. The electrons behave adiabatically in the linear stage but are heated by ExB drifts transverse to the flow and B direction. The momentum coupling between the ion streams results in a snowplowing behavior and enhances plasma density in the shuttle vicinity to the point where

$$\frac{n_b}{n_o} = \nu^* \tau_o \quad (8)$$

In Eq. (8) ν^* is the anomalous momentum coupling rate and τ_o is the ion residence time. From Papadopoulos et al. [1971] and Lampe et al. [1975], $\nu^* = 0.5(n_o/n_b)^{1/3}\omega_{LH}$. The value of τ_o is now different from $\tau \approx 1/\Omega_i$, because the shuttle moving ions are hot. Since we have a finite area $\tau_o = L/V_i$ where V_i is the thermal speed. Taking $V_i \approx U \approx 8$ km/sec; $\tau_o \approx 10^{-3}$ sec. From Eq. (8) we find

$$\frac{n_b}{n_o} = \left[\frac{\omega_{LH}\tau_o}{2^{4/3}} \right]^{3/4} \approx \frac{1}{2} (\omega_{LH}\tau_o)^{3/4}$$

which for $\omega_{LH} \approx 5 \times 10^4$ gives $n_b/n_o \approx 10$. As noted earlier, this is of the order of magnitude density enhancement observed by the PDP.

Beam lower hybrid electron-ion instability. For $(1-\alpha) \ll (k_z^2/k^2) M/m$ the dominant terms in the r.h.s. of Eq. (7) are the first and the third. This is the beam lower hybrid-electron-ion instability discussed by Formisano et al. [1982] and Papadopoulos [1983, 1984]. The instability results in generating field-aligned suprathermal electron tails with density $n_T/\min(n_b, n_o) \approx 0.2$ in the energy range $\approx (1-6) \times \frac{1}{2}MU^2$, i.e., $\approx 5-30$ eV. These electrons can produce additional ionization as well as contribute to emission from the N_2 first positive system.

Modified two stream instability. For $\omega_{LH} \approx k \cdot U_e$ the first term in Eq. (7) is negligible, and for $\alpha \ll 1$ the dispersion relation is similar to the dispersion given by Eq. (2). This is the modified two stream instability which results in electron heating of the order $T_e \approx \frac{1}{2}MU_e^2 \approx \frac{1}{2}MU^2(U_e/U)^2$. Since from the zero current condition $U_e/U \approx \min(n_b, n_o)/(n_b+n_o) \approx 0.1-0.3$, the electron temperature will be given by $T_e \approx 0.5-1.5$ eV. This again allows for the excitation of various vibrational and rotational emissions.

Summary and Conclusions

We have presented an overview of the types of collective plasma interactions expected to operate in the vicinity of the space shuttle. The model can account for all of the observations of the plasma environment summarized in the section on Implications of the Plasma Environment Near the Orbiter. Quantitative models are currently developed for

the optical emissions caused by the plasma energization. It is obvious that the importance of plasma physics vs. aeronomy increases with altitude. The altitude at which this transition occurs is of critical importance and can be found only through active experimentation. At this stage we can summarize the status of the plasma hypothesis as following:

(i) Currents driven by the plasma sheaths in the Orbiter vicinity can increase the plasma temperature sufficiently to bring the molecular constituents to excited states resulting in optical emissions. The expected rate of energy deposition is more than sufficient to account for the observations. Whether and at which altitude radiation due to surface recombination dominates over electron-driven collisional process is an open question.

(ii) Both volume and thruster emissions can be explained by the interaction of neutral gas streaming through the ambient plasma. Surface recombination faces serious difficulties in accounting for these effects. We should note that the time profile of thruster-induced emissions is similar to that of the lower hybrid noise excited by thruster firing.

(iii) The plasma model can easily account for the recently observed 1 KR Lyman alpha emission at 600 km altitude associated with the ram direction of the STP78-1 satellite [Chakrabarti and Sasseen, 1985], as well as for the N_2 first positive observed by ISO [Torr and Torr, 1984].

(iv) A recent active experiment from the space shuttle in which 1 mole of N_2 gas was injected towards the ram direction by the SEPAC team [Obayashi et al. 1984] showed ionization enhancement by a factor of 10 or more in the Orbiter vicinity.

Acknowledgments. We gratefully acknowledge discussions with Drs. I. Kofsky, A. Drobot, and E. Murad. The work was supported by AFGL # F19628-85-C0024

References

- Al'pert, Ya., The Near Earth and Interplanetary Plasma, Vol. 2, Cambridge Univ. Press, 1983.
- Chakrabarti, S., and R. Sasseen, these proceedings, 1985.
- Dalgarno, A., J. H. Yee, and M. LeCompte, these proceedings, 1985.
- Formisano, D., A. Galeev, and R. Sagdeev, Planet. Space Sci., 30, 491, 1982.
- Grebowsky, J., M. Paro, H. Taylor, and I. Eberstein, AIAA Shuttle Environment and Operations, Paper #83-2597, p. 52, 1983.
- Huba, J., and K. Papadopoulos, Phys. Fluids, 21, 121, 1977 .
- Kofsky, I., Radio Science, 19, 578, 1984.
- Kofsky, I. and J. Barrett, these proceedings, 1985.
- Lampe, M., W. Manheimer, and K. Papadopoulos, NRL Memo Rpt. 3630, 1975.
- McBride, J., E. Ott, J. Boris, and J. Orens, Phys. Fluids, 15, 2367, 1972 .
- McMahon, W., R. Salter, R. Hills, and D. Delorey, AIAA Shuttle Environment and Operations, Paper #83-2598, p. 52, 1983.
- Murad, E., Planet. Space Sci., in press, 1985.
- Murphy, G.B., S. D. Shawhan, and J. S. Pickett, AIAA Shuttle Environment and Operations, 1983.
- Obayashi, T., et al., Science, 225, 142, 1984.
- Papadopoulos, K., et al., Phys. Fluids, 14, 849, 1971.
- Papadopoulos, K., in ESA-SP-195, p. 227, 1983.
- Papadopoulos, K., Radio Science, 19, 571, 1984.
- Raitt, J., Radio Science, in press, 1985.
- Rantanen, R., R. Swanson, and D. Torr, these proceedings, 1985.

Shawhan, S., and G. Murphy, Rep. AIAA-83-0253, Am. Inst. of
Aero. and Astr., 1983 .

Stone, N.H., U. Samir, K. H. Wright, D.L. Reasoner, and
S.D. Shawhan, Geophys. Res. Lett., 10, 1215, 1983.

Tolk, M., R. Albridge, R. Haglund, M. Mendenhall, and J.
Tully these proceedings, 1985.

Torr, M., and D. Torr, Science, 225, 169, 1984.

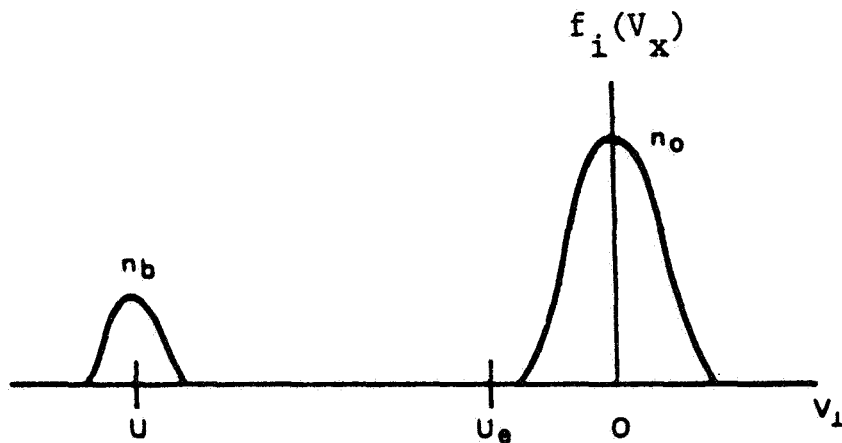


Fig. 1. Ion distribution function in the lab frame, with background ions of density n_0 and a charge-exchange-generated beam of density n_b . The electrons (not shown) drift at velocity U_e to maintain zero current.

SHUTTLE VERTICAL FIN FLOWFIELD BY THE DIRECT SIMULATION MONTE CARLO METHOD

J.E. Hueser and F.J. Brock

Old Dominion University

L.T. Melfi

NASA Langley Research Center

Abstract. The flow properties in a model flowfield, simulating the shuttle vertical fin, have been determined using the Direct Simulation Monte Carlo method. The case analyzed corresponds to an orbit height of 225 km with the freestream velocity vector orthogonal to the fin surface. Contour plots of the flowfield distributions of density, temperature, velocity and flow angle are presented. The results also include mean molecular collision frequency (which reaches 60 s^{-1} near the surface), collision frequency density (approaches $7 \times 10^{18} \text{ m}^{-3} \text{ s}^{-1}$ at the surface) and the mean-free-path (19 m at the surface).

Introduction

The glow that has been observed on shuttle flights has prompted much speculation about possible source mechanisms. A definition of the flowfield properties in the glow space should provide information which may assist in resolving the applicable physical mechanisms. The shuttle vertical fin was taken as a representative surface and a geometrically similar flow model was constructed. The flow properties were determined using the Direct Simulation Monte Carlo method [Bird, 1976]. The vertical fin was modeled as a disk having an 8 m radius, oriented with its surface-normal antiparallel to the freestream velocity vector, and embedded in an axisymmetric flowfield. The geometry and the computational cell distribution of the Monte Carlo flowfield are shown in Figure 1. The forward surface of the disk is located at $x = -0.01 \text{ m}$ and the flow is in the $+x$ direction. The boundary conditions along the forward ($x = -20 \text{ m}$) and outer flowfield boundaries correspond to the incident flux density of an equilibrium gas (atmosphere at orbit height) drifting at 7.76 km/s. The disk surface temperature was set at 150 K and a diffuse reflection law was used. Vacuum conditions were applied to the downstream side of the aft boundary ($x = 8 \text{ m}$). The freestream density $n = 0.4915 \times 10^{16} \text{ m}^{-3}$, temperature $T = 1090 \text{ K}$, and composition were taken from the properties of the atmosphere [Jacchia, 1977] at an orbit height of 225 km. The gas composition and molecular properties used are given in Table 1. The variable hard sphere molecular model [Bird, 1981] was used with a viscosity coefficient temperature exponent of 0.75.

Results and Discussion

The flowfield number density (m^{-3}) distribution is given by the contours displayed in Figure 1. The flowfield forward boundary ($x = -20 \text{ m}$) is only 2.5 disk radii upstream of the disk which yields a substantial discontinuity between flowfield properties at the forward boundary and freestream properties (the number density at the forward boundary is $1.7 \times 10^{16} \text{ m}^{-3}$ while the freestream density at the forward boundary is $0.49 \times 10^{16} \text{ m}^{-3}$). However, previous results with the Direct Simulation Monte Carlo method indicate that this boundary effect is rather localized and does not substantially influence the results in the vicinity of the disk. The density near the axis and near the forward surface of the disk (the centroid of the nearest cell to the surface is 8 cm upstream) is approximately $2.2 \times 10^{17} \text{ m}^{-3}$, a factor of 44 above the undisturbed freestream density. The density near the aft surface of the disk drops to nearly 10^{12} m^{-3} .

Contours of axial velocity (m/s), radial velocity (m/s) and flow angle (radians) are also given in Figure 1. These results imply that the flow is nearly axial for a few meters near the forward boundary and gradually approaches radial flow near the forward surface of the disk. There is a small region adjacent to the forward surface, near the axis, in which both velocity components are sufficiently small that the flow angle cannot be resolved unambiguously (see noise in flow angle contours). The axial velocity component would coincide with the undisturbed freestream speed well forward of the forward boundary of the flowfield.

The mean translational and internal temperature (K) distributions are given by the contours in Figure 2. The entire flowfield is highly non-equilibrium and thus temperature should be treated with caution. The translational temperature peak is outside (forward) of the flowfield. Both temperatures, of course, approach 150 K at the disk surface.

The mean collision frequency (s^{-1}) and collision frequency density ($\text{m}^{-3} \text{ s}^{-1}$) distributions are also given in Figure 2. Near the disk forward surface, for $r < 6 \text{ m}$, the collision frequency is approximately 63 s^{-1} and the collision frequency density is slightly larger than $6.7 \times 10^{18} \text{ m}^{-3} \text{ s}^{-1}$. The flow speed in this region is less than 5 m/s, implying that a molecule may experience several collisions before drifting out of the region.

In Figure 3 several of the flow parameters are displayed as functions of x only for $r = 0.95 \text{ m}$ (near the axis) and in Figure 4 for $r = 7.6 \text{ m}$ (near the outer edge of the disk), the disk surface is at $x = -0.01 \text{ m}$ in each subframe. Each displayed function is normalized by its maximum value before plotting. The normalization constants for each curve are written adjacent to the curve label above each subframe. The label definitions are:

ND = number density (m^{-3})
 CO = stream speed, mass average (m/s)
 TR = translational temperature (K)
 TI = internal temperature (K)
 VX = axial velocity component (m/s)
 VY = radial velocity component (m/s)
 FA = flow angle (0 corresponds to $-\pi$ and 1 to $+\pi$)
 LB = mean-free-path (m)
 NU = molecular mean collision frequency (s^{-1})
 NC = mean collision frequency density ($\text{m}^{-3} \text{s}^{-1}$)

Note the rapid increase in density and both collision frequencies (especially the collision frequency density, curve NC) as the flow approaches the surface, while the mean-free-path decreases rather linearly. The peak of the radial velocity increases by about an order of magnitude between the two figures and moves closer to the surface as r increases. For the outer radial cut (7.6 m) the flow angle approaches $\pi/2$ (0.75 on the ordinate) but along the inner radial cut is always less than $\pi/2$.

The surface parameters along the disk are plotted in Figure 5 as a function of r . The forward surface of the disk lies along the abscissa for the two subframes on the left, with the origin at 0.0 m and the outer edge at $r = 8$ m and similarly for the two subframes on the right, the aft surface of the disk lies along the abscissa. The upper left subframe gives flux density ($\text{m}^{-2} \text{s}^{-1}$) incident on the forward surface for each species (curves F1, F2, F3) and the total (sum over species, curve FD). All four curves are normalized by the peak value of the total flux density; thus, the ordinate gives the relative fraction of the total flux density produced by each species (F1, F2, & F3 correspond to species 1, 2, & 3). The maximum value of the incident flux density for the total and each species is written above the subframe adjacent to each curve label. The lower left subframe gives normalized plots of surface pressure (Pa) (curve PR), surface shear (curve SH), incident power density (W/m^2) (curve PI), and reflected power density (curve PR). The normalization constants for each curve are written adjacent to each curve label above the subframe. The two subframes on the right present the same parameters in the same way for the aft surface of the disk. Note that only species 3 (atomic oxygen) appears. It is quite probable that the lower relative abundance species would appear if the solution had been carried to a substantially larger flow time.

The peak total incident flux density (near $r = 0$) on the forward surface is $4.1 \times 10^{19} \text{ m}^{-2} \text{ s}^{-1}$ which is about 8% larger than the collisionless value ($3.8 \times 10^{19} \text{ m}^{-2} \text{ s}^{-1}$). On the aft surface (for this particular flow time) the peak total incident flux density is $2 \times 10^{14} \text{ m}^{-2} \text{ s}^{-1}$ (collisionless flow would yield a number orders of magnitude smaller). However, the properties along the aft surface must be regarded as approximate, preliminary estimates due to the very small sample size.

In the Monte Carlo model, each molecular encounter was counted for each molecule until it collided with the forward surface the first time. These data imply that in the mean the total collision probability for a molecule reaching the forward surface the first time is 0.07. If the flowfield length had been sufficiently large to contain the total disturbance produced in the freestream by the disk, this number would have increased, but probably by less than a factor of 2.

There is internal evidence from the Monte Carlo model implying a highly bimodal sample distribution near the forward surface, consisting of high-velocity freestream molecules flowing toward the surface and a low-velocity reflected stream flowing away from the surface. The axial width of the cells near the surface was selected to yield adequate spatial resolution. The total sample in these cells is large but probably consists principally of molecules from the low-velocity stream. Thus, molecules from the high-velocity stream are under sampled due to the small cell width and corresponding short transit time. This would influence the number of molecular encounters computed in the collision routine and thus influence the collision frequency, collision frequency density and mean-free-path. This situation clearly requires a detailed investigation, which is currently under way.

In a broader sense, there appears to be no unambiguous physical interpretation of mean values formed from the very different sample distributions of the two-stream flow encountered in the current problem. Although the primary flow properties are insensitive to this problem and are therefore regarded as an adequate definition of the flow, the collision frequencies should be used with caution.

References

- Bird, G. A., Molecular Gas Dynamics, Clarendon Press, 1976.
- Bird, G. A., Monte Carlo simulation in an engineering context, Rarefied Gas Dynamics, Progress in Astronautics and Aeronautics, Vol. 74, Part 1, edited by Sam S. Fisher, AIAA, New York, 1981, pp. 239-255.
- Jacchia, L. G., Thermospheric temperature, density, and composition: New models, Smithsonian Astrophysical Observatory Special Report 375, 1977.

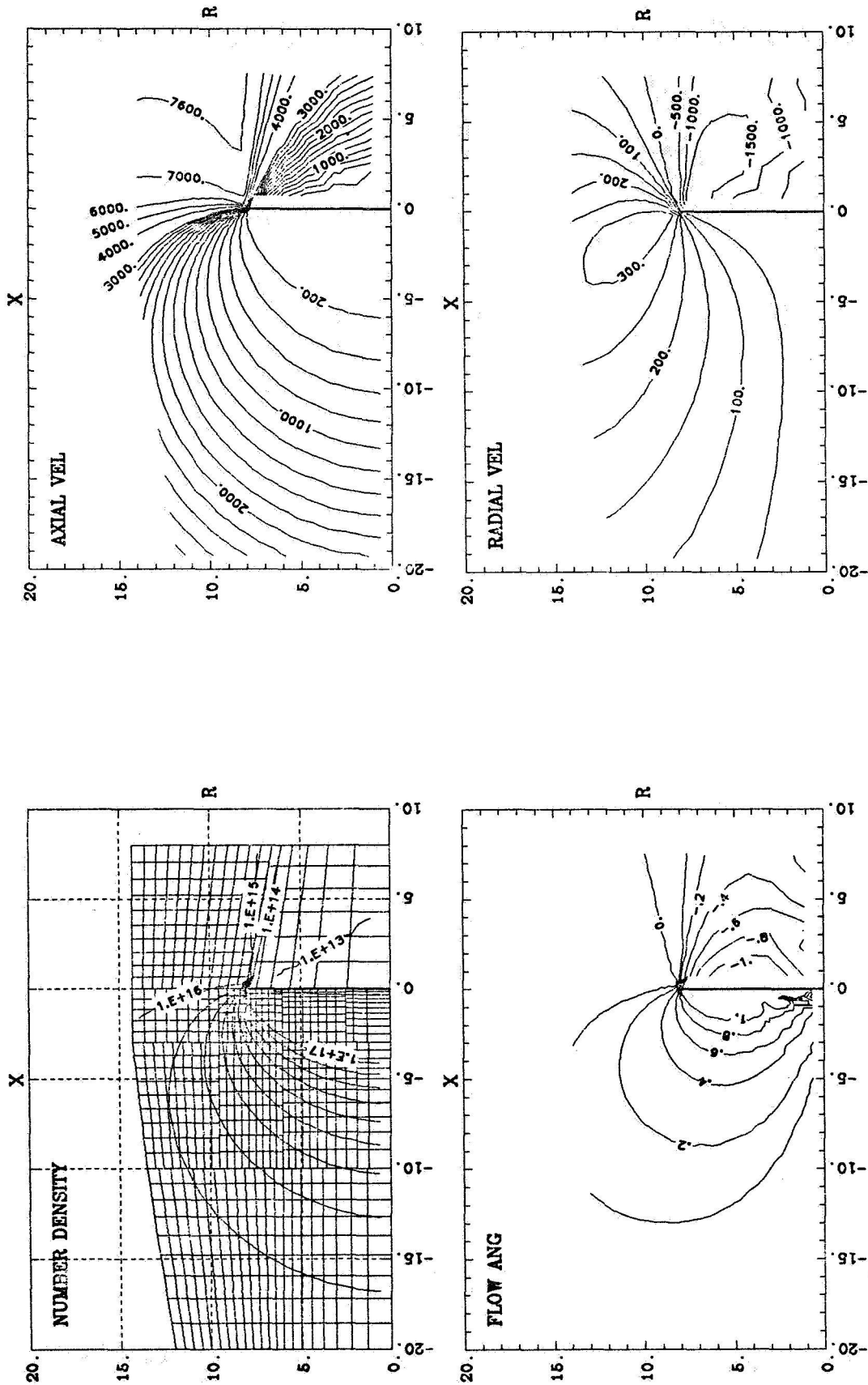


Fig. 1. Contours of flowfield properties, modeled shuttle fin.

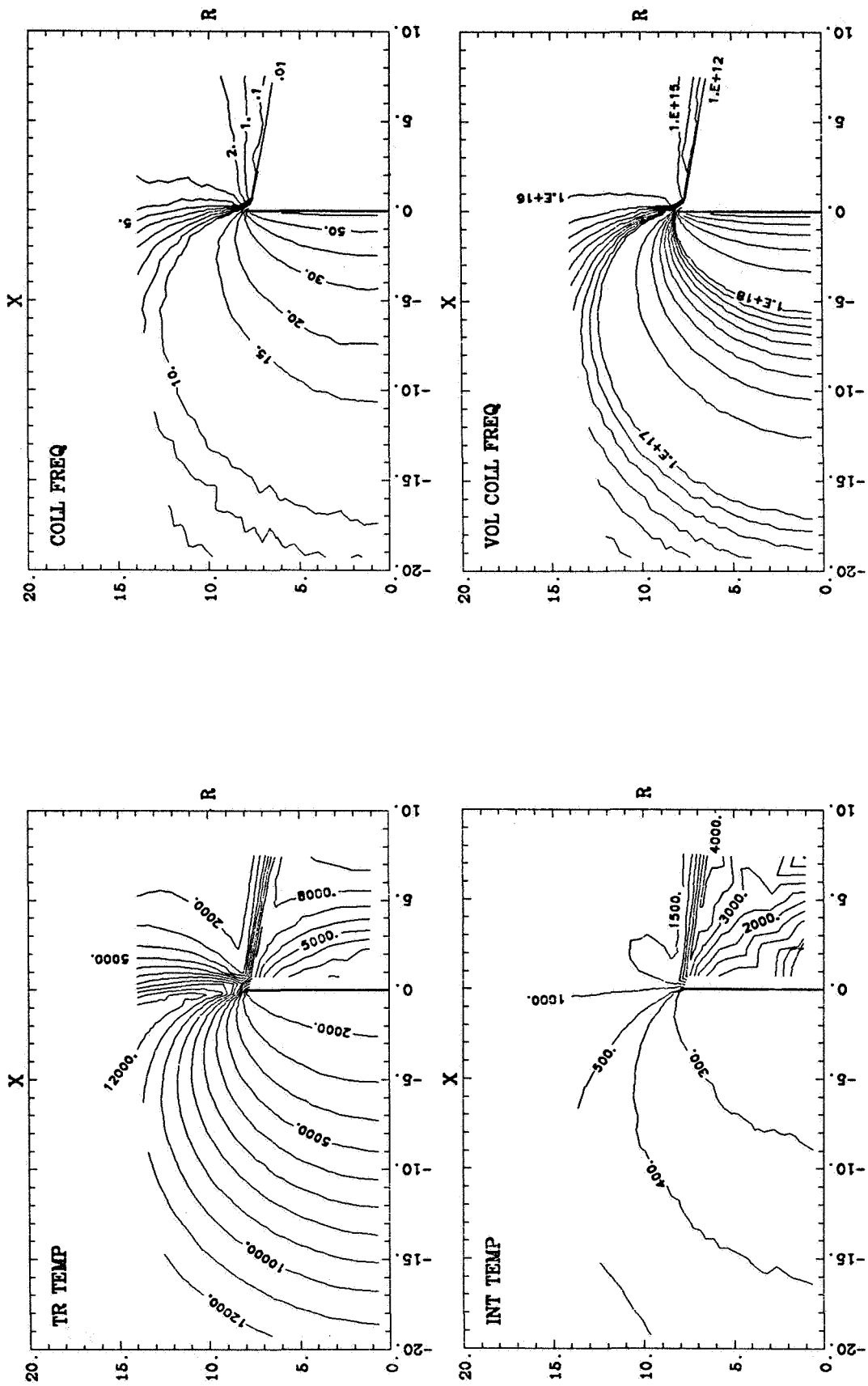


Fig. 2. Contours of flowfield properties, modeled shuttle fin.

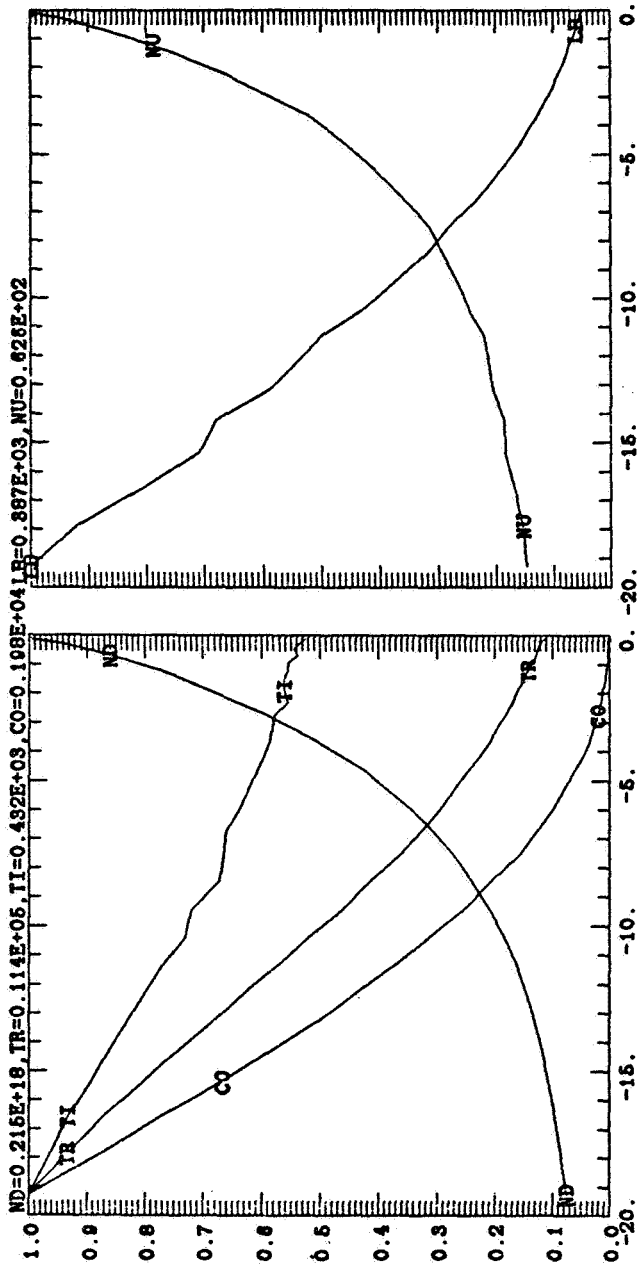
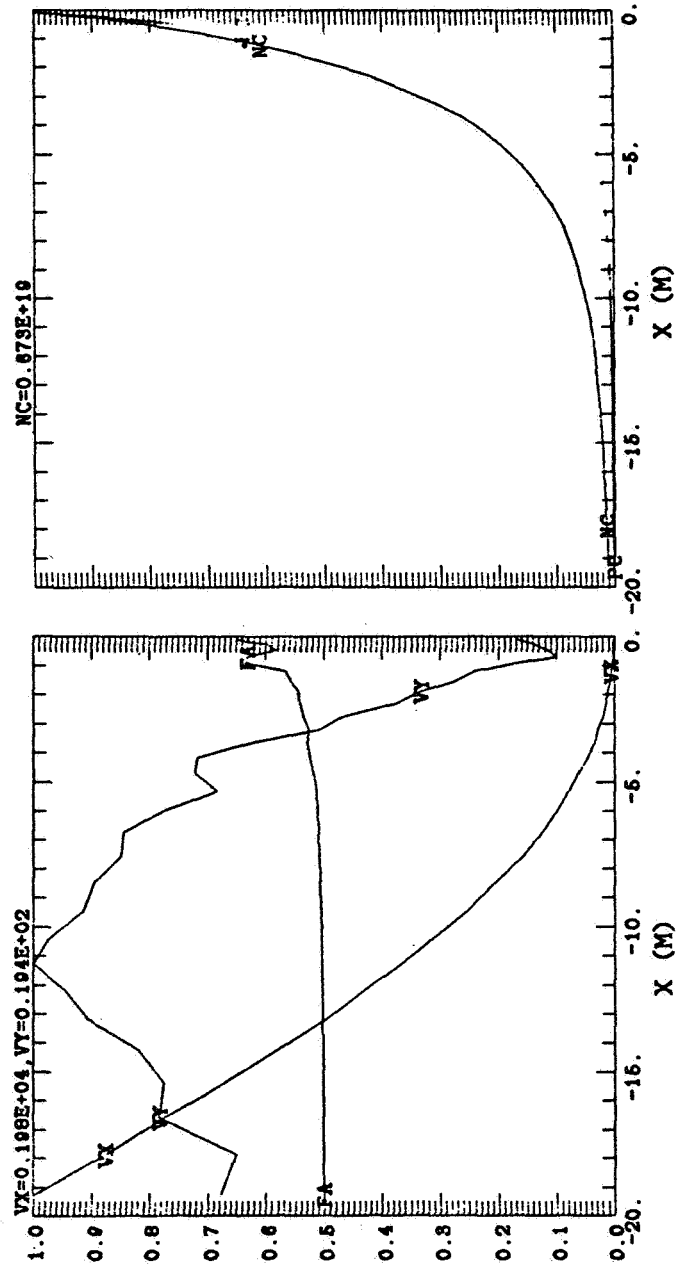


Fig. 3. Flow properties along a fixed radius, $r = 0.95$ meters. Normalization constants are given above each frame.



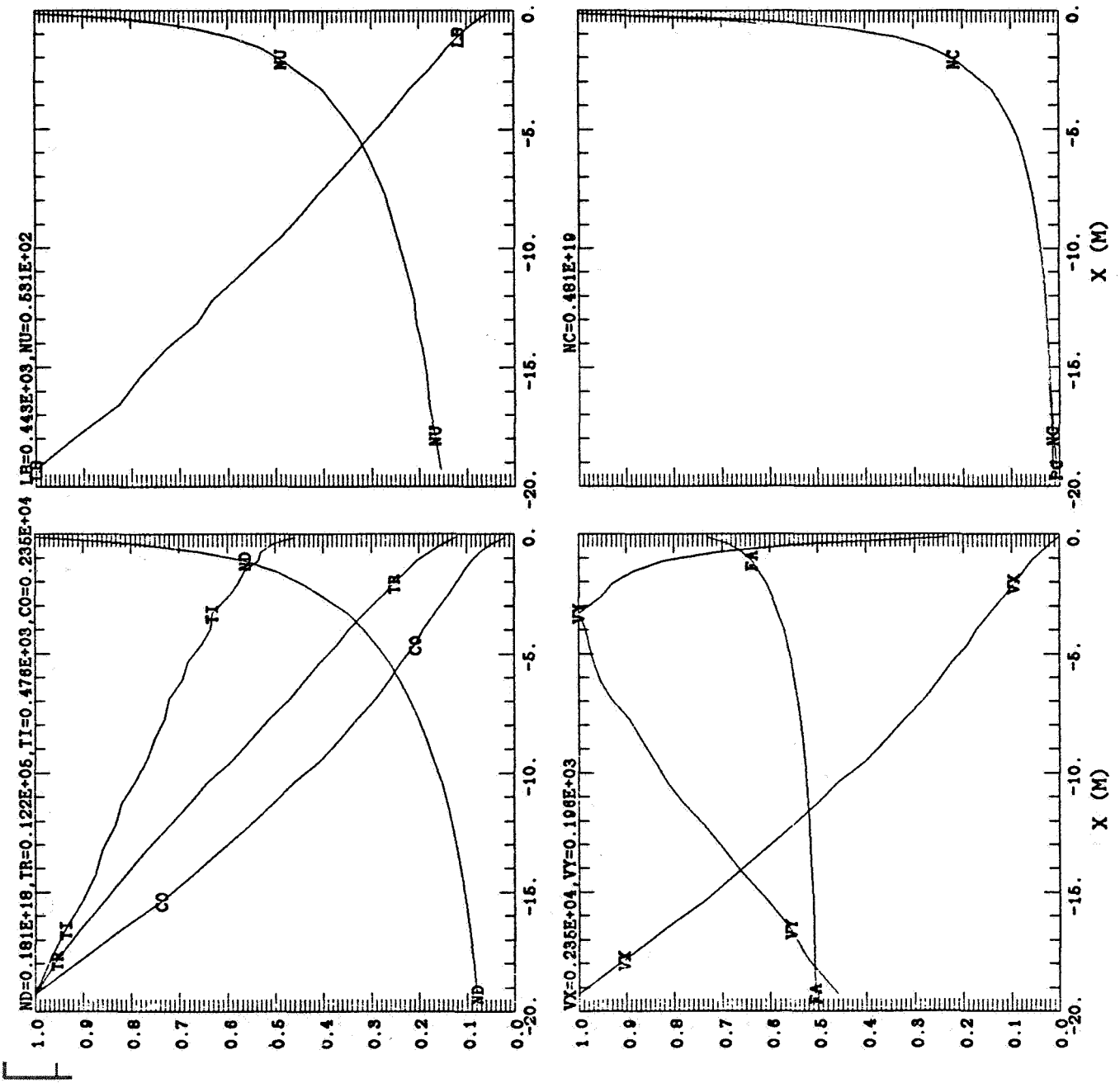


Fig. 4. Flow properties along a fixed radius, $r = 7.6$ meters. Normalization constants are given above each frame.

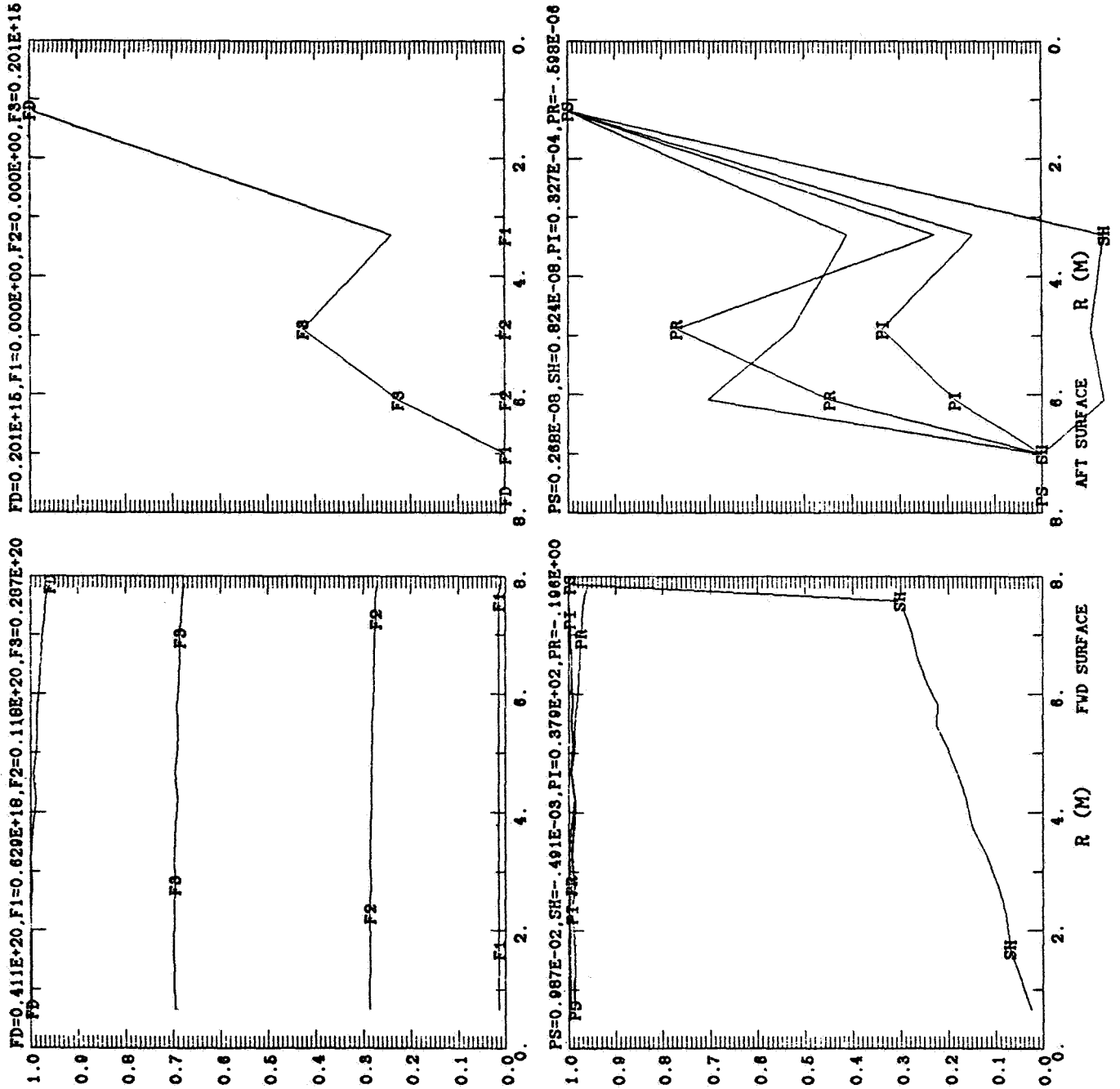


Fig. 5. Gas surface interaction properties. Normalization constants are given above each frame.

TABLE 1. COMPOSITION AND MOLECULAR PROPERTIES

Species	Relative Abundance	Molecular Mass (kg) $\times 10^{-25}$	Rotational Degrees of Freedom	Reference Diameter (m) $\times 10^{-9}$	Reference Temp. (K)	Characteristic Vib. Temp. (K)
1) O ₂	0.0142	0.531	2	0.2084	2880	2270
2) N ₂	0.2711	0.465	2	0.3105	2880	3390
3) O ₁	0.7113	0.265	0	0.2314	2880	-

A MECHANISM FOR THE LOCAL CONCENTRATION ENHANCEMENT
OF THE SHUTTLE ATMOSPHERE

Ray Rantanen

Science and Engineering Associates, Inc.

Roy Swanson

Boeing Aerospace Company

Doug Torr

Department of Physics, Utah State University

Abstract. Preliminary calculations suggest that collisions between instreaming atmospheric constituents and secondary backscattered molecules can generate unexpectedly large enhancements in neutral gas concentrations in the vicinity of the shuttle. This effect is a result of a rapid decrease in the mean free path length of the scattered components following the initial expected concentration enhancement. A study will be outlined for the theoretical investigation of this mechanism. The shape dependence of associated glow halos on vehicle configuration will be discussed.

Introduction

Scattering of the unidirectional flux of ambient gas molecules incident on Low-Earth Orbit (LEO) spacecraft surfaces results in an increased gas density on the ram facing surfaces and filling in of the rarefied wake region. The thermal component of the ambient atmosphere impinges on surfaces oriented parallel to the velocity vector and also contributes to the wake region.

The gas scattering dynamics determine line-of-sight column densities and may influence optical glow processes and the spatial extent of glow halos. The multiple scattering may lead to new approaches in atomic oxygen beam and glow simulation testing. These considerations in turn may impact space shuttle experiments, free flying space platforms, Space Station, and Strategic Defense Initiative systems.

The gas density increase on ram surfaces has been previously investigated by various authors (Bird, 1962; Melfi et al., 1981; Bareiss et al., 1975; Rantanen, 1977). The techniques employed include rarefied gas dynamics, direct simulation by Monte Carlo and three dimensional contamination configuration models. One such configuration model, SPACE II (Bareiss et al., 1981), is intended to calculate contamination related parameters. In its current form it does not calculate the density increase around shuttle due to backscattered ambient species re-emitted from the Orbiter surfaces. In the Monte Carlo modeling analyses of the shuttle, environment backscattering components are included and the results vary significantly from SPACE II.

The goal of the present study is to model shuttle gas flowfield densities and optical glow phenomena in a form applicable to shuttle, Space Station, and other space systems. By using and modifying existing models, a cost-effective approach may be easily applied to optimiza-

tion studies, attitude variations, configuration changes, and model verification. An approach using a multiple interaction density enhancement iteration algorithm to improve existing configuration models is presented here as is a glow halo shape simulation test procedure.

Considerations

From the shuttle frame of reference, the ambient gas molecules have velocities of about 8×10^5 cm/s $\pm 1 \times 10^5$ cm/s due to orbital motion superimposed on background thermal velocities. Gases impacting on the shuttle surfaces are thermally accommodated and are emitted at velocities near 5×10^4 cm/s for atomic oxygen and 4.0×10^4 cm/s for N_2 , for surface temperatures near 298° K.

Figure 1 schematically illustrates the details of physical interaction mechanisms for surfaces oriented perpendicular to and parallel to the velocity vector. The gas density increase on a surface perpendicular to the direction of orbital motion is due to the ram flux and backscattering of the surface re-emitted ambient species. A surface parallel to the velocity vector, Figure 1, is impinged upon by the thermal component of the ambient. As the gases are re-emitted, they collide with the ambient and with each other. Some are scattered back to the surface. The result is that the greatest gas density is at the trailing edge on a surface parallel to the flow.

The gases in the wake region, Figure 1, are the result of the thermal component of the ambient and those gases scattered back from the edges of the surface. These molecules collide at different energies than those on the ram side.

The mean free path for the undisturbed ambient gases is given by

$$MFP_A = \frac{1}{N_A \sigma_A}$$

where N_A = ambient density and
 σ_A = collision cross section of ambient species.

The mean thermal velocity of a molecule or atom emitted from a surface is low compared to the ambient impact velocities. If there was no gas density buildup on the ram side, the mean free path of an emitted gas would be

$$MFP_R = \frac{V_R}{N_A V_A \sigma_{AR}}$$

where V_R = re-emitted gas velocity,
 N_A = ambient density,
 V_A = ambient velocity, and
 σ_{AR} = collision cross section between ambient and re-emitted species.

If the cross sections are the same then the mean free path of the

re-emitted gases is less than the free stream ambient by the ratio of their respective velocities. However, in reality the flux of ambient gases impinging on the re-emitted gases is enhanced by the backscattered gases that were previously re-emitted, so that mean free path is further modified by these species. Calculations have been performed using a density iteration technique applied to the surfaces of circular disks moving in direct ram condition at an altitude typical of a shuttle orbit. If only the re-emitted gases are considered, the model calculations yield a density near the disk surface which is a factor of 32 greater than the free stream ambient. Because of backscattering, the model predicts densities near 50 to 60 times the free stream ambient.

Approach

The approach to modeling gas densities and resulting glow phenomena has four basic steps.

- a. Update gas kinetics for shuttle with eventual applications to Space Station and other space systems using SPACE II and TRASYS II.
- b. Utilize ground test simulation to aid in verifying, by visualization of gas density distribution profiles and variations with spacecraft size, configuration attitude and other factors.
- c. Use results of Monte Carlo analyses by other investigators as a baseline standard for testing the modeling approach.
- d. Correlate gas densities along viewing lines-of-sight with Imaging Spectrometric Observatory (ISO) data for glow model development and verification.

TRASYS II (Jensen et al., 1983) is used for developing the surface to surface or surface to a point density matrix around shuttle to allow more resolution for scattered and compressed gas algorithms than presently exists in SPACE II. A calculational technique is being developed which makes use of improved mass transport factors between surfaces and points and from points back to points so that backscattered gases can be added to the densities that exist as a result of gases emitted from the surface. The flux of gases at two points separated by a predetermined distance is calculated. The difference in flux between these two points then becomes the backscattered contribution from this region. A form factor is developed from this region back to the points between it and the surface.

Figure 2 shows preliminary results for the density, along the centerline axis of an 8-meter-radius disk and a disk of 1-meter-radius. The ratio of the calculated density to the free stream ambient density is plotted as a function of distance along the centerline upstream from the disks. The free stream ambient is 5×10^9 molecules or atoms/cm³. The mean free path (MFP) for a re-emitted molecule or atom is 40 meters when considering only interactions of the re-emitted molecule and the incoming ambient.

The density at a point for no interactions with the ambient is equivalent to the calculations utilized in the current SPACE II model.

$$D_o = \frac{RFLR \times MTF}{V_R}$$

where RFLR = surface emission rate of re-emitted ambient,
 MTF = mass transport function between the surface

and a point, and
 V_R = re-emitted velocity.

The density at an off surface point is assumed to be reduced exponentially by the factor $\exp(-x/\text{MFP})$. Then, after a primary reflection, the density, D_1 , at an external point is

$$D_1 = \frac{\text{RFLR} \times \text{MTF} \times e^{-x/\text{MFP}}}{V_R}$$

where x = distance from surface to the point.

The first iteration of the process described in the present approach is shown as curve D in Figure 2. The enhanced density at a point p from the backscattered, re-emitted species is given by

$$D_{Bp} = \sum_{p+1}^n \left[(\text{RFLR})(\text{MTF}_{n-1} e^{-\frac{x_{n-1}}{\text{MFP}}} - \text{MTF}_n e^{-\frac{x_n}{\text{MFP}}}) (\text{MTF}_{p,n}) \right] / V_B$$

where
 RFLR = surface emission rate,
 MTF_n = mass transport function between the surface and the point,
 x_n = distance from surface to a point,
 x_{n-1} = distance from surface to n-1, point,
 $\text{MTF}_{p,n}$ = mass transport function between point n and point p, and
 V_B = backscattered velocity.

The backscatter calculation is added to the density D_1 at each point along Z. Basically, D_1 attenuates the density and D_B adds to the density.

After the densities have been altered, the mean free path can be adjusted according to the backscattered flux calculated during the first iteration.

The updated mean free path is given by

$$\text{MFP} = \frac{V_R}{N_A V_{AO} + N_B V_{BO}}$$

where
 N_B = density addition due to backscattered gases, and
 V_B = velocity of backscattered gases.

For a point near the surface where the backscattered gas density is highest, the mean free path is 15 meters as opposed to 40 before the adjustment was made. The adjusted mean free path, as a function of distance from the 8-meter-disk for the surface re-emitted gases, is shown in Figure 3.

The incoming ambient mean free path near the surface is between 13 to 26 meters depending on its velocity which has been reduced via

collisions.

The next iteration would utilize the adjusted mean free path and the same calculational technique. Until the results of the first iteration processes are verified, via Monte Carlo modeling, the second iteration will not be performed.

The 1-meter-radius disk shows significantly less buildup upstream as compared to the 8-meter-radius disk. Sensitivity studies are underway to determine the influence of surface size, surface shape, velocity vector orientation, combinations of surfaces, and the parameters used in the calculations.

A technique for calculating the densities in the wake region via collisions at the outer edge of a surface is under development.

The modeling approaches will be incorporated into SPACE II when completed and the predicted results will be compared to Monte Carlo modeling of the shuttle orbiter. The gas densities along ISO experiment lines-of-sight will be calculated. Excitation mechanisms and corresponding cross sections will be applied to the different gas species. The resulting spectra will be compared to the ISO data and updated as required.

A simple but informative simulation technique has been developed to simulate the glow shape as a function of altitude, attitude, and spacecraft geometry to aid in visualization of the gas density distribution and to assist in modeling. Small particles are accelerated, via gravity, from the top of a silo onto targets at ground level and the density profile is photographed. Geometrical shapes, such as cylinders, cones, spheres, flats, and models of shuttle and the Space Station, have been used as targets. The target surfaces are textured to produce diffuse scattering. The re-emitted particles have a decreased velocity relative to the incoming particles which is determined by the particle surface material selection. Figure 4 shows the relative "glow shapes" observed thus far. Improved particle sizes and diffusers are planned for future tests.

Implications/Recommendations

The multiple collisions experienced by the incoming ambient gases and the resulting density profiles have an impact on glow mechanisms, predictions, and simulation testing.

The glow investigations to date have concentrated on surface-related excitations to explain the near surface visible glow. It is proposed that collision excitation mechanisms may occur at distances comparable to space vehicle dimensions. Some of the possible excitation processes may cause intense optical emissions at specific wavelengths.

The relatively high densities on the ram facing surfaces allows sufficient numbers of collisions between incoming ambient and the re-emitted ambient component to reduce the translational energies of the incoming molecules below orbital impact energies. This would seem to imply that simulation testing of materials may be successfully carried out with impact energies significantly lower than the 5 eV AO beam which is presently unobtainable at sufficient fluxes.

Besides the AO at appropriate energies and fluxes, other gases such as N₂ should be part of a simulated ambient atmosphere.

Simulation of the glow phenomenon in laboratory testing is impacted because of the multiple gases and complex collision process. Other excitation mechanisms should be available simultaneously such as

solar radiation and electrons. Impact excitation should be simultaneously simulated in an appropriate test configuration.

Models of the shuttle, Space Station, and other space system environments should be updated to include major aspects of the gas densities and glow emissions. The enhanced gas density profile affects the transport of contaminants to surfaces and to optical lines-of-sight.

The first time a systematic contamination evaluation and model was created was for Skylab. It did not, however, model the return flux phenomenon because of altitude (435 km) and a low ambient gas period.

On shuttle, the same modeling methodology derived from Skylab was adopted with the inclusion of return flux of contaminants scattered by ambient collisions.

The next evolutionary step in modeling gaseous space environments is the glow halo phenomenon. An adequate knowledge of contaminants exists and mathematical models are available to assess and minimize the problem. The erosion of materials by AO is understood well enough that hardened materials or coatings will result. Spacecraft glow remains as the phenomenon that is least understood. A comprehensive program of modeling, testing, and experiment is required to fill the understanding of glow phenomenon. This should include combinations of surfaces, gases, vehicle attitudes, day/night orbit conditions, sensors, and background levels and should be performed by shuttle, rockets, tethered systems free flying payloads or sources, and ground-based telescopes or combinations of these.

Acknowledgments. The authors are grateful to T. D. Gordon for his software support.

References

- Bareiss, L. E., R. O. Rantanen, E. B. Ress, and L. J. Leger, Preliminary evaluation of the contaminant induced environment for the Space Shuttle Orbiter, in NASA SP-379, 8th Conference on Space Simulation, 1975.
- Bareiss, L. E., F. J. Jarossy, J. C. Pizzacaroli, and N. L. Owen, Shuttle/Payload Contamination Evaluation Program, MCR-81-509, February 1981.
- Bird, G. A., Free-molecular flow field of a moving body in the upper atmosphere, Rarefied Gas Dynamics, Academic Press, 1962.
- Jensen, C. L., and R. G. Goble, Thermal radiation analysis system, MCR-73-105 (Rev. 5), June 1983.
- Melfi, L. T., J. E. Hueser, and F. S. Brock, Direct simulation Monte Carlo technique for modeling of the environment in the vicinity of the Space Shuttle Orbiter, SPIE, Paper 287-10, April 1981.
- Rantanen, R. O., Spacecraft contamination modeling, AIAA 12th Thermophysics Conference, AIAA No. 77-739, 1977.

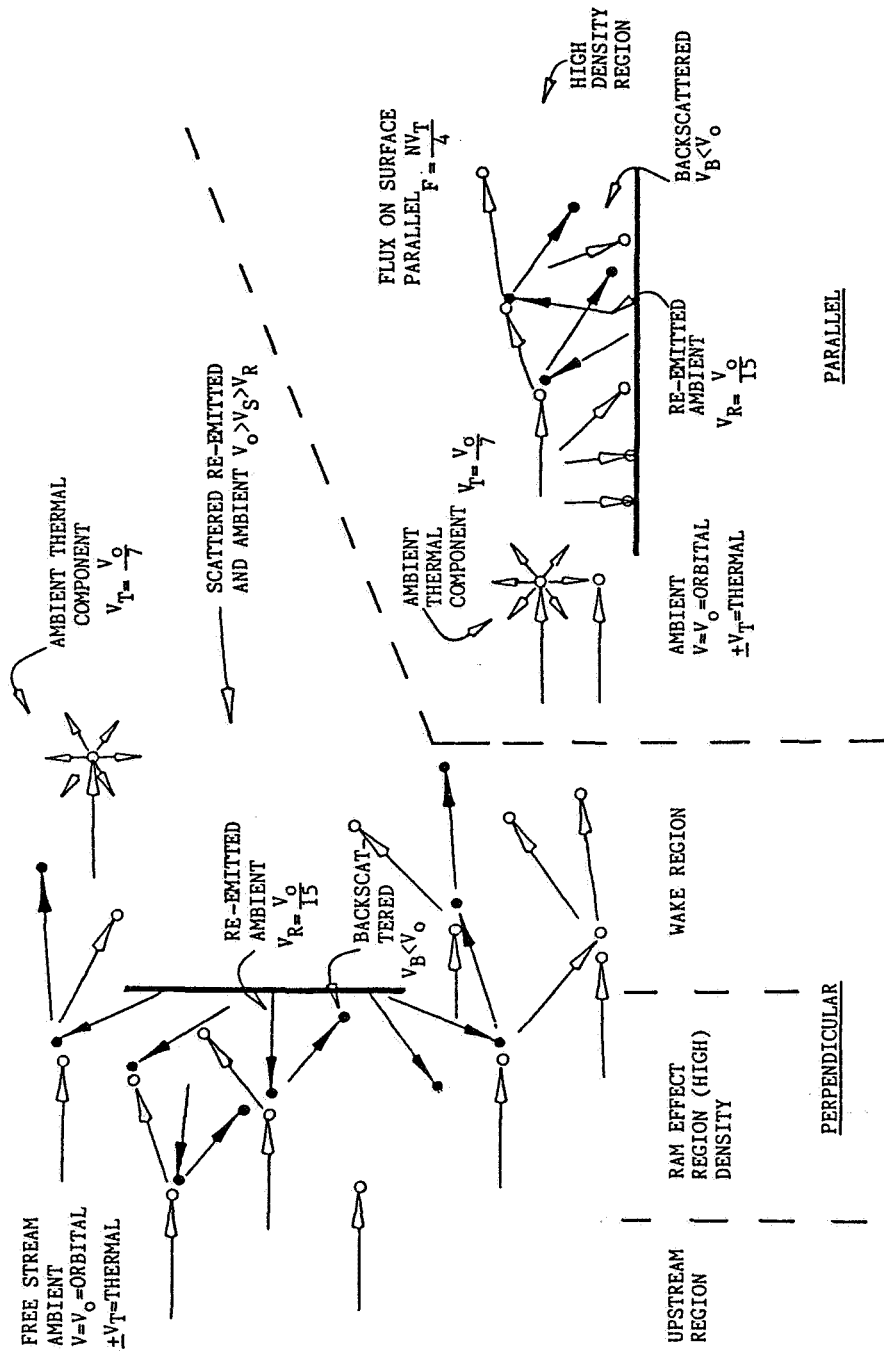


Fig. 1. Physical processes.

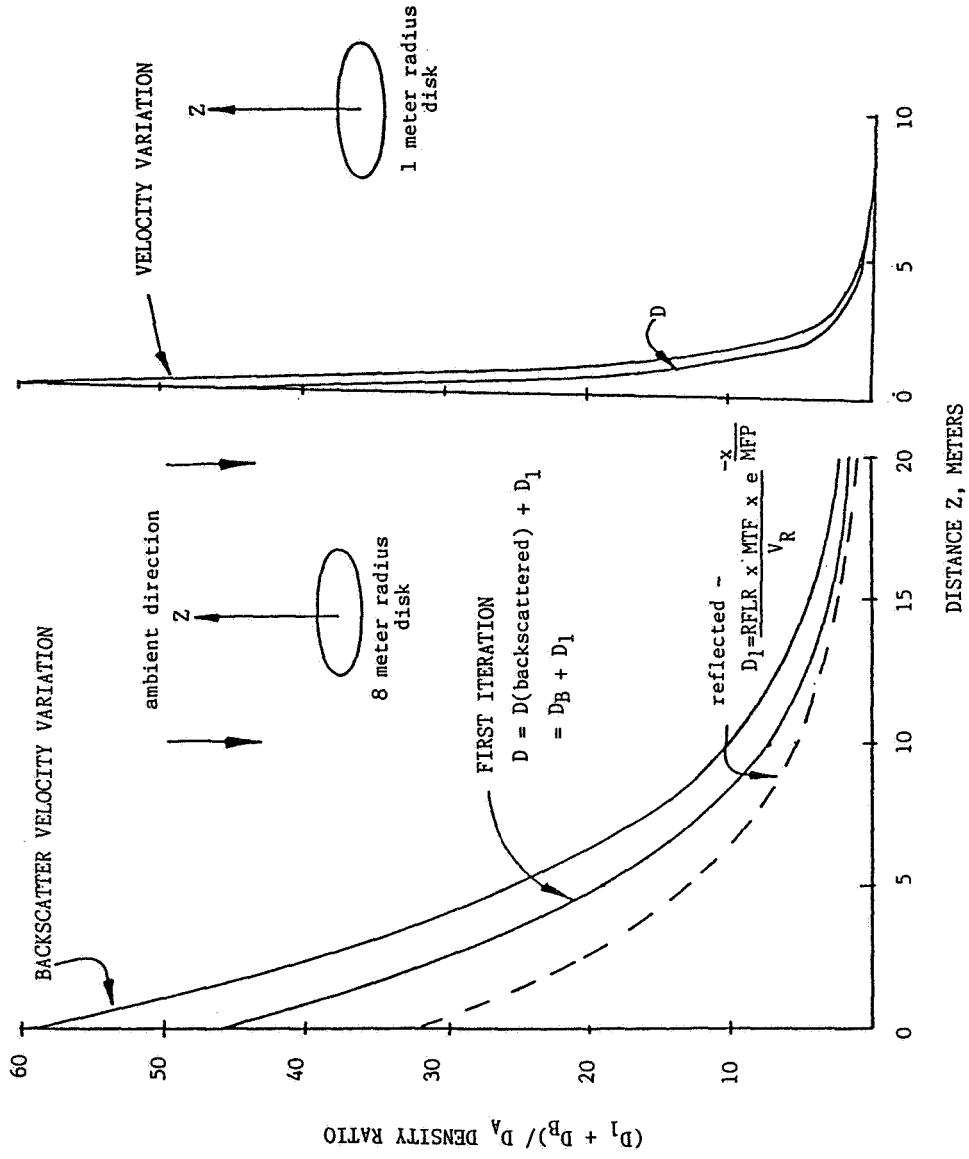


Fig. 2. Ratio of calculated density to ambient free stream density versus distance.

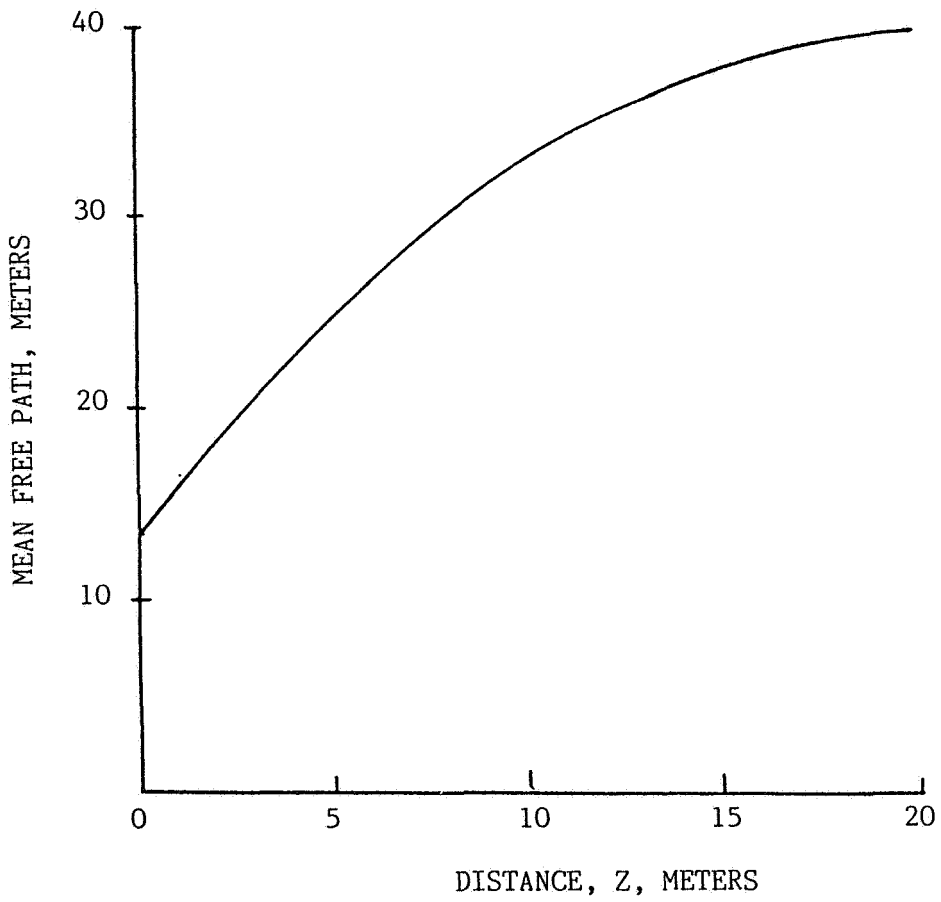


Fig. 3. Adjusted mean free path of surface re-emitted ambient.

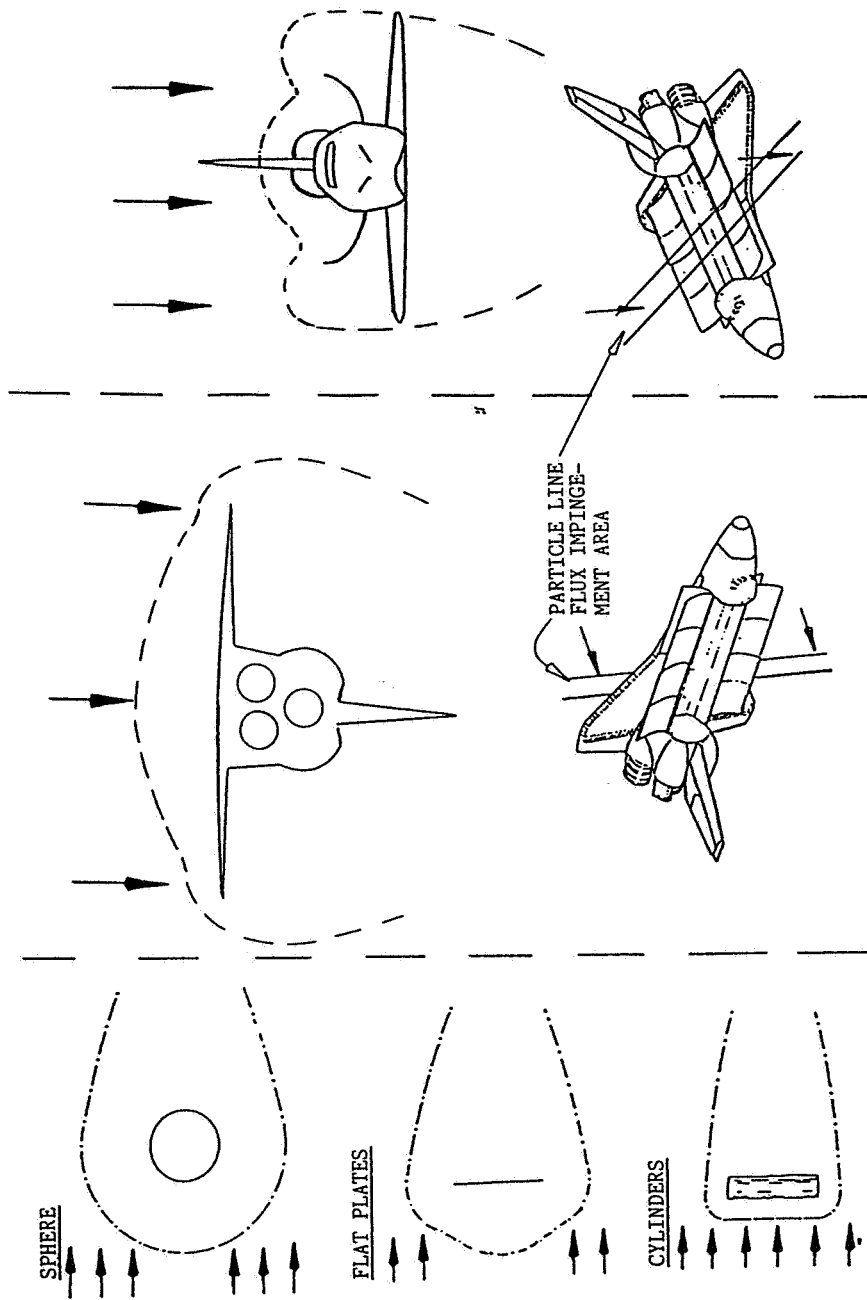


Fig. 4. Density shapes observed in simulation testing.

SURFACE-CATALYZED RECOMBINATION INTO EXCITED ELECTRONIC,
VIBRATIONAL, ROTATIONAL, AND KINETIC ENERGY STATES: A REVIEW

I. L. Kofsky and J. L. Barrett

PhotoMetrics, Inc., Woburn, MA

Abstract. Laboratory experiments in which recombined CO, CO₂, D₂O, OH, N₂, H₂, and O₂ molecules desorb from surfaces in excited internal and translational states are briefly reviewed. Unequilibrated distributions predominate from the principally catalytic-metal substrates so far investigated. Mean kinetic energies have been observed up to ~3x, and in some cases less than, wall-thermal; the velocity distributions generally vary with emission angle, with non-Lambertian particle fluxes. The excitation state populations are found to depend on surface impurities, in an as yet unexplained way.

Introduction

Several small-molecular species have been found to desorb after formation on laboratory surfaces with internal and kinetic energy distributions (and angular fluxes) markedly different from those that would result from their equilibration at the substrate's temperature. The observations for neutral molecules other than NO₂ and NO, which are reviewed separately in the accompanying paper by Barrett and Kofsky [these Proceedings] (with further data on NO* in Kofsky and Barrett [these Proceedings]), are listed in Table 1.

Discussion

This lack of equilibration, and a comparably common non-Boltzmann (statistical) distribution of desorption quantum states, are an at least qualitatively expected outcome of the dynamics of the surface reaction complex from which the molecular fragment originates [Polanyi, 1972; Tully, 1980; Kori and Halpern, 1983; Ceyer et al., 1983]. Indeed, our literature survey identified only one measurement of complete rotational and vibrational thermalization of a recombination product, OH on polycrystalline Pt [Talley et al., 1981] (item [14] in Table 1), curiously that very species initially considered responsible for spacecraft glow [by several groups]. This result was interpreted [Talley et al., 1981] as due to the rate of desorption of hydroxyl excited in Langmuir-Hinshelwood (among species present on the surface) reactions of O with H being small compared with the rate of collisional equilibration of the adsorbed radical with its substrate. We briefly touch on the more sophisticated theoretical arguments after reviewing the database of Table 1.

These quantum state-specific measurements were made using passive spectrometry, tuned laser and (to a lesser extent) electron beam induced fluorescence, and for the velocity distributions, time-of-flight and most recently laser Doppler methods [Cavanagh and King, 1984]. (Some qualitative reports of experiment results that were later verified have been omitted, as have gas-phase reactions of precursors formed on sur-

faces.) About half were performed in ultrahigh vacuum systems in which the surface crystal structure and its contamination (at the sub-monolayer level) could be characterized in situ by low-energy electron diffraction, Auger electron spectroscopy, and similar surface-science technologies. In the experiments indicated one reactant (or an impurity) was initially incorporated into the target surface, and in some others the atomic species was made to permeate through the sample from its back side; this of course does not mean that reactants from the beam also do not become adsorbed on, and in some experiments dissociated on, the substrate. (Molecules such as N_2 and NO have zero activation energy for dissociation on some transition metal crystal planes.) All but one set of the measurements (those of Harteck's group, [3], [11], [12], and [13] in Table 1) have been done within the last 6 years. The discipline and diagnostics have not yet developed to a stage at which all the internal quantum states of a desorbate as functions of its translational energy and angle of emission have been measured simultaneously.

The list refers to heterogeneous recombination involving species incident (or diffusing) at mean velocities <1 km/sec and thus kinetic energies $<1/2$ eV. Some of these combine (as mentioned) with surface dopants, in processes that might be referred to as selective chemical sputtering into molecular states, or alternatively as reactive scattering. It does not include non-associative molecule scattering [Asscher et al., 1985] or desorption [Cavanagh and King, 1984] experiments, many of which also provide evidence for nonequilibration and non-Lambertian (\cos^1 {angle θ to the normal}) effluent flux distributions. In addition it specifically omits physical sputtering, which refers to neutral or ionized incident particles with directed kinetic energy greater than the few tens eV threshold for dislodging atoms and complexes from the surface, some of which are ionized or in electronically excited states (reviewed in the context of spacecraft glows by Kofsky [1984]).

In this regard, most of the existing information about the ablative reactions with surface materials of 8 km/sec relative velocity atoms and molecules, such as those at orbital altitudes, comes from shuttle and other spacecraft exposure experiments/tests rather than the laboratory or theory. While the incident 5-eV oxygen atoms are well known to be associated with the mass loss and texturing of various types of exposed surfaces [Visentine et al., 1985], no connection between the rates of erosion and glow emission has been identified. Further, the role played by this kinetic energy in exciting spacecraft radiations is by no means established--the signal/noise of the measurements is insufficient to rule out the possibility that the glow off forward surfaces is due merely to the ram enhancement of densities of incident atoms and molecules. The mechanism might also involve O atom-associated (and perhaps off-surface induced plasma-associated) roughening of the surface to increase its concentration of sites where physisorption, chemisorption, and excitative-desorption can take place, and/or avoidance of "catalyst poisoning"--buildup of reaction-inhibiting species on the lattice--by impact of the moderately energetic neutral (and charged) particles. In that sense, and in cases that the incident particles accommodate on the surface to participate in Langmuir-Hinshelwood reactions, the low reactant energy database of Table 1 is relevant to the spacecraft glows issue.

Most of the recombination experiments in Table 1 were done on at least partially characterized surfaces of "catalytic" transition metals, in large part toward understanding the role of these (essentially, reducing)

substrates, rather than on materials of the type exposed on orbiting spacecraft--generally, insulators. On this limited subset, recombination with nonequilibrium and nonstatistical electronic, vibrational, and kinetic energy distributions (themselves desorption-angle dependent) of the product molecule is the rule rather than the exception. Translationally cold as well as hot desorbate beams have been seen, as well as rotationally cold streams from non-associative desorption [Cavanagh and King, 1981]. Although forward focusing from the macroscopically smooth laboratory surfaces (due to the parallel orientation of the surface barrier equipotentials) is common, flux distributions flatter than $\cos^1\theta$ can also occur [Cavanagh and King, 1984]. The angular distribution of the radiating species (and potentially, the not-yet measured polarization of rotational-band emission from the desorbate) is a further diagnostic of the surface interaction that could be applicable in investigations of spacecraft glows.

Note that while CO and O have been found to recombine on room temperature glass [Pravilov and Smirnova, 1981], the comparably exoergic NO + O surface reaction was not reported in connection with the several measurements of its gas-phase rate coefficient (references [6a-e] in Barrett and Kofsky [these Proceedings]).

Surface contamination by the Group V and Group VI elements S, O, and N--readily quantifiable by Auger electron or x-ray photoelectron spectroscopy--plays a part in several of the internal excitations of the desorbed molecules; no theoretical explanation of this effect, which presumably involves formation of an intermediate complex, appears to have been advanced. Similarly, interference with the recombination-desorption process by other molecules introduced into the flow of the surface has been observed [Hartek and Reeves, 1964; references in Barrett and Kofsky, these Proceedings]; indeed, interference and saturation of reactive sites are ubiquitous features of surface studies. Presumably these species occupy, or create, sites at which adsorption/excitative desorption occurs. Such an interference effect may be the reason for the "anomalously" rapid increase in intensity of the glow off Atmosphere Explorer at altitudes below 160 km (where atmospheric [O₂] is becoming comparable to [O]) reported by Yee and Abreu [1983].

Some Conclusions

A detailed classical trajectory model exists for the more exoergic Rideal-Eley (one participant incident from the gas phase) recombination of O with C adsorbed at three fold sites on the Pt (111) crystal face [Tully, 1980]. The theory predicts that of the ~6 eV exothermicity, statistically 2 eV appears in vibrational, 1 eV in rotational, and 2 eV in translational energy of the CO desorbate, with forward peaking; this result is largely independent of the applied gas-surface interaction potential (which was derived empirically). Experimentally no such high translational energies have been observed for any species/substrate combination; on the other hand even though most of the laboratory results have been interpreted as due to L-H rather than R-E reactions, a similarly large fraction of the available energy in internal excitation is commonly reported (as Table 1 shows). As the interaction potentials and binding energies of upper-atmospheric aeronomic species on the poorly-characterized and in many cases locally inhomogeneous and highly textured surfaces of exposed spacecraft materials are much less well understood, as

is the formation of complexes on them, similar ab initio calculations of the channeling of energy into radiative states of desorbate molecules are unlikely to provide quantitative predictions of glow brightnesses.

Existing information about quantum state-specific surface recombinations, in sum, indicates that when newly-formed molecules are desorbed from transition metals (and some glasses) a high probability exists that their internal energy is comparable to the reaction exothermicity, even when both participants were previously adsorbed on the surface; and that the degree of this excitation, and the surface reaction rate, often depends on the concentration of (oxidizing) surface contaminants, which themselves may be introduced from the incident beam. The database represented by Table 1, comparable NO-NO₂ surface reactions [Barrett and Kofsky, these Proceedings], non-associative desorption and scattering of various species (including in particular NO [Asscher et al., 1985]) from clean model surfaces, and related surface processes are far below the critical mass required for development of credible predictive theory (as is in general the case for catalysis [Somorjai, 1981]). Nonetheless some empirical extrapolation might be made to the largely insulating, rougher-surfaced materials exposed and as putative contaminants on low-Earth-orbiting spacecraft by applying the concepts developed to order the laboratory data (for example formation of complexes at desorption sites). Some further application of these ideas is in the accompanying paper on NO₂ and NO recombination [Barrett and Kofsky, these Proceedings]. Additionally, measurements analogous to those performed in the laboratory of the sensitivity of off-surface emission intensity to substrate temperature--which assesses the binding of reaction participants to the surface, and thus may identify precursor species--and angular distribution of the desorbate flux would complement those already proposed in understanding and scaling spacecraft glow excitation processes.

References

- Asscher, M., E. Pollak, and G. A. Somorjai, A model for vibrational and translational accommodation of NO molecules during scattering from a Pt (111) surface, Surf. Sci., 149, 146-156, 1985.
- Becker, C. A., J. P. Cowin, L. Wharton, and D. J. Auerbach, CO₂ product velocity distributions for CO oxidation on platinum, J. Chem. Phys., 67, 3394-3395, 1977. [6 in Table 1]
- Brennen, W., and P. McIntyre, Vibrational relaxation and electronic mutation of metastable nitrogen generated by nitrogen atom recombination on cobalt and nickel, Chem. Phys. Lett., 90, 457-460, 1982. [2]
- Cavanagh, R. R., and D. S. King, Rotational and spin-state distributions: NO thermally desorbed from Ru (111), Phys. Rev. Lett., 47, 1829-1832, 1981.
- Cavanagh, R. R., and D. S. King, Molecule-surface interactions and dynamics, J. Vac. Sci. Tech., A2, 1036-1037, 1984.
- Ceyer, S. T., W. L. Guthrie, T. H. Lin, and G. A. Somorjai, D₂O product angular and translational energy distributions from the oxidation of deuterium on Pt (111), J. Chem. Phys., 78, 6982-6990, 1983. [8]
- Comsa, G., R. David, and K. D. Rendulic, Velocity distribution of H₂, HD, and D₂ molecules desorbing from polycrystalline nickel surfaces, Phys. Rev. Lett., 38, 775-778, 1977. [9]

- Comsa, G., R. David, and B.-J. Schumacher, The angular dependence of flux, mean energy, and speed ratio for D₂ molecules desorbing from a Ni (111) surface, Surf. Sci., 85, 45-68, 1979. [10]
- Harteck, P., and R. R. Reeves, Formation and reaction of the excited O₂ (A³Σ_u⁺) molecules, Disc. Faraday Soc., 37, 82-86, 1964. [11]
- Kenner, R. D., and E. Ogryzlo, Orange chemiluminescence from NO₂, J. Chem. Phys., 80, 1-6, 1984. [13]
- Kofsky, I. L., Spectroscopic consequences of Papadopoulos' discharge model of spacecraft ram glows, Radio Sci., 19, 578-586, 1984.
- Kori, M., and B. L. Halpern, Vibrational energy distribution of CO in the oxidation of C on Pt, Chem. Phys. Lett., 98, 32-36, 1983. [7]
- Kori, M., and B. L. Halpern, Vibrationally excited CO₂ from the reaction of O atoms and adsorbed CO on platinum, Chem. Phys. Lett., 110, 223-229, 1984. [4]
- Mannella, G. G., and P. Harteck, Surface-catalyzed excitations in the oxygen system, J. Chem. Phys., 34, 2177-2180, 1964. [12]
- Mannella, G. G., R. R. Reeves, and P. Harteck, Surface catalyzed excitation with N and O atoms, J. Chem. Phys., 33, 636-637, 1961. [3]
- Polanyi, J. C., Some concepts in reaction dynamics, Accounts Chem. Res., 5, 161-168, 1972.
- Pravilov, A. M., and L. G. Smirnova, Chemiluminescence process in O(³P) + CO + M system, Kinet. Catal., 22, 416-419, 1981. [5]
- Somorjai, G. A., Chemistry in Two Dimensions: Surfaces, Cornell, Ithaca NY, 1981, p. 377.
- Talley, L. D., W. A. Sanders, D. J. Bogan, and M. C. Lin, Dynamics of hydroxyl radical desorption from a polycrystalline platinum surface, J. Chem. Phys., 25, 3107-3113, 1981. [14]
- Thorman, R. P., D. Anderson, and S. L. Bernasek, Internal energy of heterogeneous reaction products: Nitrogen atom recombination on iron, Phys. Rev. Lett., 11, 743-746, 1980. [1]
- Tully, J. C., Dynamics of gas-surface interactions: Reaction of atomic oxygen with adsorbed carbon on platinum, J. Chem. Phys., 73, 6333-6342, 1980.
- Visentine, J. T., L. J. Leger, J. F. Kuminecz, and I. K. Spiker, STS-8 atomic oxygen effects experiment, AAIA 23rd Aerospace Sciences Meeting, Paper #85-0415-CP, 1985.
- Yee, J. H., and V. J. Abreu, Visible glow induced by spacecraft-environment interaction, Geophys. Res. Lett., 10, 126-129, 1983.

TABLE 1. SURFACE RECOMBINATION WITH DESORPTION IN EXCITED STATES

<u>Species [Ref.]</u>	<u>Surface</u>	<u>Conditions*</u>	<u>Excitation state</u>	<u>Comments</u>
N ₂ [1]	Poly Fe	N permeates, 1150K	X, high v	T _v depends on S coverage
[2]	Poly Co, Ni	N in flow tube	W ³ A _u , v [≈] 11	Nitrides necessary
[3]	Co, Ni, Ag Cu	N and O flow	A?(B detected)	Probably W state, see [2]
		N only, low T _s	C (!) 1-2 mm out	Requires > dissociation energy
CO ₂ [4]	Pt/O	CO flow, 300-600K	2.6 eV of v ₃	Nonstatistical (first example), O pretreatment needed
[5]	Glass	CO and O flow	³ B ₂ (¹ B ₂)	Visible "continuum" measured
[6]	Poly Pt	CO flow, O ₂ gas, 300-1100K	T _k ≈3-4T _s	T _k decreases off normal, non- statistical, L-H process
CO [7]	Pt/C	O flow, 1400K	High v	Statistical but hot; L-H process
D ₂ O [8]	Pt 111	D ₂ and O ₂ flow, 440-913K	T _k ≈0.5T _s at 90°	Nonstatistical velocity, cos ¹ θ
H ₂ [9]	Poly Ni/1/2 S	H permeates, 940-1143K	T _k =1.7T _s at 0° ≈T _s at 90°	Nonstatistical velocity, with strong forward peaking
(HD, D ₂) D ₂ [10]	Ni 111/(S)	H permeates, 1143K	T _k ≈1.7T _s at 0° ≈0.65T _s at 90°	Ditto: cos ⁴ θ, distributions independent of S coverage
O ₂ [11]	Ni, Co, Glass	O flow	A, 0.1/recomb	Glass requires conditioning
[12]	Poly Ni	O flow	A (v=0 & 1), b	No OI lines
[13]	Poly Ni	O flow	A, a, b	Just as expected from O ³ P
OH [12]	Ni	O flow	A	Could be gas-phase artefact
([14]	Poly Pt	H ₂ +O ₂ , H ₂ +NO ₂ , H ₂ O flow, 1130K	T _v = T _r = T _s	All in equilibrium)

NO, NO₂ - Refer to the accompanying reports by Barrett and Kofsky [these Proceedings].

*T_s ≡ surface temperature ≈293K unless stated otherwise; T_k, T_v≡ kinetic, vibrational temperature.

INFRARED EMISSION FROM DESORBED NO₂* and NO*

I. L. Kofsky and J. L. Barrett

PhotoMetrics, Inc., Woburn, MA

Abstract. Infrared photons from the radiative cascade accompany both the gas-phase NO₂ "continuum" chemiluminescence (which originates from its ²B₂ and ²B₁ states) and the NO beta bands (B²Π → X²Π). When these upper electronic states are excited by recombination/desorption at surfaces of low-Earth orbiting spacecraft, similar IR emission spectra will be observed. The principal NO₂ features (other than the long-wavelength tail of its electronic transitions) are the ν₃ fundamental sequence near 6.2 μm and ν₁ + ν₃ intercombination bands near 3.6 μm; NO would emit the Δv = 1 and Δv = 2 systems above 5.3 and 2.7 μm. Because of the long radiative lifetimes of the upper vibrational states, the infrared radiances in projections parallel to the vehicle surface (which we estimate) are substantially less than those of the visible and ultraviolet glows.

Introduction

We estimate here spatial distributions and relative brightnesses of the infrared afterglows of visible-UV emissions from NO₂ and NO electronically excited in surface recombination reactions. The IR component of the glow off shuttle's silica identified as from NO₂* by Swenson et al. [1985] would consist of the long-wavelength transitions of the molecule's pseudo-continuum and more slowly emitted discrete vibrational bands of its lowest (X²A₁) electronic state. Recombination of N and O, which in experiments on transition-metal substrates appears to excite selectively and directly the ultraviolet-emitting NO B²Π state [Caubet et al., 1984], would result in similar cascade radiation in the even more slowly emitted vibrational bands of the lower (X²Π) state of NO.

NO₂

We proceed following the interpretation [Swenson et al., 1985] that the origin of the orange-red spectrally continuous (at 34Å FWHM resolution) radiation extending a few centimeters off shuttle's windward-directed SiO₂ tile surfaces is NO₂ electronically excited in reactions of NO with O. As pointed out by Kofsky and Barrett [1985], the shift of the peak photon intensity some 1000 cm⁻¹ to the red of the glow seen from homogeneous reactions in the laboratory and lower thermosphere can be interpreted as due to (weak) binding of the O atoms to the substrate, insofar as this shift is ~4000 cm⁻¹ when the O is bound in "vibrationally excited" O₃ [Kenner and Ogryzlo, 1984], ~7500 cm⁻¹ in O₃(001) [Braun et al., 1974], and 8000 cm⁻¹ in ground-state O₃ [Clough and Thrush, 1967] where its binding energy is 8500 cm⁻¹ or 1.05 eV. Alternatively, the shift to longer wavelengths might be interpreted as due to binding of the NO molecules to the surface (refer to Barrett and Kofsky [these Proceedings]), which would not materially affect the conclusions here.

In view of the only ~1/8-eV red shift, the surface-assisted excitation

reaction can be considered as chemically much more similar to the third (gaseous) body-stabilized $\text{NO} + \text{O}$ attachment reaction than the $\text{NO} + \text{O}_3$ rearrangement reactions, which involve breaking the $\text{O}-\text{O}_2$ bond. We nonetheless present also the appropriate literature information on the electronic- and vibrational-band emissions that result from the chemiluminescent ground-state ozone reaction, for reasons that will become apparent shortly. The infrared emission wavelengths and the total yields and spatial extents that we derived from the laboratory and theoretical database are summarized in Table 1, and for orientation some potential curves of NO_2 [Paulsen et al., 1970] are reproduced in Figure 1.

Virtually all the gas-phase $\text{NO} + \text{O}$ recombinations [Kaufman, 1973] but only 7% of the $\text{NO}_2 + \text{O}_3(\tilde{X}^1\text{A}_1)$ rearrangements [Clough and Thrush, 1967] proceed through the $^2\text{B}_1$ and $^2\text{B}_2$ states. The second column in Table 1 shows the fractions of the photons in the resulting pseudo-continua terminating on NO_2 's $^2\text{A}_1$ state that lie at wavelengths above $0.8 \mu\text{m}$. We derived these percentages from the measured chemiluminescence spectrums, which tail off toward $3 \mu\text{m}$ with generally upward curvature [Stair and Kennealy, 1967; Golde et al., 1973] from flat peaks near $0.64 \mu\text{m}$ [Paulsen et al., 1970; Fontijn et al., 1964] and $1.2 \mu\text{m}$ [Clough and Thrush, 1967]. In view of the aforementioned observed modest red shift of the glow off shuttle's tiles, very closely half of its electronic-band photons would be at wavelengths above $0.8 \mu\text{m}$, the nominal cutoff of the (S-20 response) image intensifier used in the spectrograph. As this longer-wavelength radiation originates from essentially the same distribution of upper states [Clough and Thrush, 1967], the spatial distribution of the near-infrared continuum emission would be similar to that in the orange-red glow. That is, the NIR surface radiances in photon units would be about equal to the visible radiances that have been measured [off silica; the spectral distributions could of course be different off other recombination substrates].

In laboratory gas-phase formation from reactions of NO with O the NO_2 molecules are left with average vibrational energy of about 7000 cm^{-1} after the electronic-band photon has been emitted, in states with ν_3 near 3 and $\nu_1 + \nu_3$ about 5 [Golde and Kaufman, 1974]. In the absence of collisions, as in the near-space environment, these decay by radiating the ν_3 fundamental bands near $6.2 \mu\text{m}$ [Stair and Kennealy, 1967; Clough and Thrush, 1969] and, with about a factor 10 less probability, a superposition of $\nu_1 + \nu_3$ (each $\Delta\nu = 1$) intercombination bands (with perhaps some ν_3 overtone) near $3.6 \mu\text{m}$ [Golde et al., 1973; Golde and Kaufman, 1974; Clough and Thrush, 1969]. Refer to columns 3 and 4 of Table 1, in which we have made an estimate of the broadening to shorter wavelengths of the emission in the complete (unquenched) radiative-relaxation cascade. Corrected for deactivation and artefactual population mechanisms in the laboratory, these bands have intensities proportional to that of the pseudo-continuum as well as the same temperature dependence, which indicates that they originate from upper vibrational states of the lower state of the electronic transitions. Further, the observation that the intensity ratio of the two infrared systems remains constant with concentration of the reactants suggests that they come from the same distribution of upper vibrational states. We estimated the number of photons emitted per recombination from the measured (from the integrated band strengths) radiative lifetimes in the 101 and 001 state listed in Table 1, with the reasonable assumptions that these lifetimes decrease as (vibrational quantum number) $^{-1}$ as

in harmonic-oscillator diatomic molecules and that all of the excitation is radiated in these two sequences. The estimates for $\text{NO} + \text{O}_3$ rearrangement reactions, which in totality result in a somewhat blue-shifted spectral intensity distribution within the $\nu_1 + \nu_3$ fundamental sequence [Golde and Kaufman, 1974], refer only to that 7% that proceed through the ${}^2\text{B}_1$ and ${}^2\text{B}_2$ electronic states and therefore produce (more easily measured, in the laboratory or spacecraft environment) visible and near-IR photons.

The ν_1 and ν_2 systems of NO_2 above 7.6 and 13.2 μm were below detection threshold in the laboratory experiments [Clough and Thrush, 1969; Stair and Kennealy, 1967], which is understandable in view of their low band strengths; we have included an estimate of the ν_2 fundamental intensity in Table 1. Clough and Thrush [1969] detected an unidentified weak peak near 2.5 μm , which appears also to be present (with ~10% of the amplitude of the underlying continuum) in the spectrum measured by Stair and Kennealy [1967] (this may be the unidentified feature reported in absorption in Herzberg's [1945] compilation).

Radiative lifetimes of the principal vibrational states are listed in the sixth column. Since lifetimes and vibrational spacings decrease with quantum number in the range excited, the longer-wavelength photons within each sequence arise from a narrower off-surface layer; furthermore the shorter-wavelength component in each of the two peaks is in general emitted after the longer wavelengths, that is, farther away from the vehicle. In view of the incomplete identification of NO_2 's upper vibrational states and lack of quantification of their transition probabilities and branching, only approximate predictions can be made of the characteristic emission distances and thus radiances in projections parallel to recombination surfaces. These lengths are listed in the seventh column of Table 1, where we have assumed that the NO_2^* molecules desorb with velocities that would result from thermal accommodation (which of course may not be the case; refer to the presentation by Kofsky and Barrett [these Proceedings]).

As the characteristic emission distance of the visible glows so far measured is about 5 cm [Kofsky and Barrett, 1985], these lengths indicate that at each altitude (i.e., incident particle flux) the maximum photon radiances viewing along windward-directed spacecraft surfaces are three orders of magnitude lower in the NO_2 intercombination-bands sequence near 3.6 μm and two orders of magnitude lower in the fundamental sequence centered at 6.2 μm . Since the vibrational-band radiation lengths are comparable to the dimensions of shuttle's surfaces, the outgoing beam has moderate divergence and thus in projections perpendicular to the surface the infrared photon radiances would be of the same order as the total radiances in the pseudo-continuum.

These estimates implicitly assume that the surface-catalyzed recombination proceeds through electronic states of NO_2 only, as in homogeneous $\text{NO} + \text{O}$ (+ M) reactions. Direct recombination into vibrationally excited states of ${}^2\text{A}_1$, as in the $\text{NO} + \text{O}_3$ reactions whose chemiluminescence we have also reviewed here, would of course lead to higher infrared/visible emission ratios. Similarly, selective depopulation of electronic states at the surface would increase the relative IR intensities. In such cases the infrared band sequences would be expected to remain those identified in Table 1, but with different spectral distributions within the peaks.

No direct evidence exists for recombination of NO on windward surfaces of low-Earth orbiting spacecraft. Nonetheless in view of the presence of N and O in the incident airstream, the observed recombination of these atoms into an electronically excited state on several polycrystalline metals (albeit not on teflon) at room temperature [Caubet et al., 1984; Reeves et al., 1960], and the fact that the emission bands observed in these laboratory experiments are capable of explaining the ultraviolet component of the Atmosphere Explorer ram glow reported by Yee and Abreu [1983] (refer to the spectrum in Figure 2, which shows features at the photometrically-observed 0.280 and 0.337 μm), we proceed with the exercise of calculating the cascade infrared radiances from NO^\dagger .

Surface recombination was found to produce directly the $\text{B}^2\Pi$ state only (in a process different from the accepted mechanism of the homogeneous reaction), as evidenced by the NO β ($\text{B}\rightarrow\text{X}$) progressions. No attempt was made to measure initial vibrational excitation of, or the rate of recombination into, the NO ground state. Note that if similar excitation takes place at exposed spacecraft material substrates this ultraviolet glow would extend outward less than 1 mm, as the B state's radiative lifetime is 3.2 μsec ; that is, in perpendicular-to-ram surface projections NO electronic radiation excited only at the optical sensor's surfaces would be detectable. We derived from the β -band intensities due to the surface and background gas measured by Caubet et al. [1984] the vibrational population distribution in NO $\text{X}^2\Pi$, which is given with an overview of the cascade radiation process and the radiative lifetimes of vibrationally-excited NO(X) in Table 2. The potential curves of NO are shown for orientation in Figure 3.

These laboratory data show that the average vibrational quantum number v_2^1 in the lower state is about 7. From this number and the branching ratios [Billingsley, 1976], we estimate that 5 fundamental-sequence (above 5.3 μm) and 1 overtone-sequence (near 2.8 μm) photons result from each surface-catalyzed recombination into the NO(B) state. Again due to anharmonicity of the ground electronic state, the longer-wavelength IR photons in each sequence are emitted closer to the surface than the shorter-wavelength photons. From the radiative lifetimes we find characteristic radiation lengths of about 1000 cm for each transition (taking the mean thermal molecular velocity as $\sqrt{(46/30)} \times 4 \times 10^4$ cm/sec), so that the volume from which the vibrational bands are emitted extends some 100 m forward of the vehicle. Thus the maximum near-parallel IR photon radiances would be many orders of magnitude lower than the UV (β -band) radiances at each ambient density. Since over that large distance the NO^\dagger beam would have substantial divergence even were it peaked strongly toward the surface normal (as discussed by Kofsky and Barrett [these Proceedings]), and at shuttle's operational altitudes little confinement due to collisions with the atmosphere, the IR radiances in perpendicular projections would be expected to be somewhat less than the UV photon radiances.

Over and above its assumption that N + O recombination into NO's B state can indeed take place on spacecraft ram surface materials, this derivation assumes that the initial vibrational-state population is the same as that observed under the laboratory conditions and, more impor-

tantly, that this reaction path is more probable than direct recombination into high vibrational states of NO's ground electronic state. This latter process, which would add to the off-surface infrared glow, can be readily investigated in the laboratory (or space environment) by laser-induced fluorescence methods.

References

- Billingsley, F. P., Calculated vibrational-rotational intensities for NO, J. Molec. Spec., 61, 53-70, 1976.
- Braun, W., M. J. Kurylo, A. Kaldor, and R. P. Wayne, Infrared laser enhanced reactions: Spectral distribution of the NO₂ chemiluminescence produced in the reaction of vibrationally excited O₃ with NO, J. Chem. Phys., 61, 461-464, 1974.
- Caubet, P., S. Dearden, and G. Dorthe, The specific production of NO (B²_{II}) from the recombination of NO on a nickel surface, Chem. Phys. Lett., 29, 480-483, 1984.
- Clough, P. N., and B. A. Thrush, Mechanisms of chemiluminescent reaction between nitric oxide and ozone, Trans. Faraday Soc., 63, 915-925, 1967.
- Clough, P. N. and B. A. Thrush, Vibrational emission by NO₂ in reaction of nitric oxide with ozone, Trans. Faraday Soc., 65, 23-31, 1969.
- Fontijn, A., C. B. Meyer, and H. I. Schiff, Absolute quantum yield measurements of the NO-O reaction and its use as a standard for chemiluminescent reactions, J. Chem. Phys., 40, 64-72, 1964.
- Golde, M. F., A. E. Roche, and F. Kaufman, Absolute rate constant for the O + NO chemiluminescence in the near infrared, J. Chem. Phys., 59, 3953-3959, 1973.
- Golde, M. F., and F. Kaufman, Vibrational emission of NO₂ from the reaction of NO with O₃, Chem. Phys. Lett., 29, 480-485, 1974.
- Herzberg, G., Infrared and Raman Spectra, Van Nostrand, New York, 1945, p. 284.
- Kaufman, F., The air afterglow revisited, in Chemiluminescence and Bioluminescence, edited by M. J. Cormier, D. M. Hercules, and J. Lee, Plenum, New York, 1973, p. 83.
- Kenner, R., and E. Ogryzlo, Orange chemiluminescence from NO₂, J. Chem. Phys., 80, 1-6, 1984.
- Kofsky, I. L., and J. L. Barrett, Spacecraft surface glows, Nucl. Inst. Meth., in press, 1985.
- Paulsen, D. E., W. F. Sheridan, and R. E. Huffman, Thermal and recombination emission of NO₂, J. Chem. Phys., 53, 647-657, 1970.
- Reeves, R. R., G. G. Mannella, and P. Harteck, Formation of excited NO and N₂ by wall catalysis, J. Chem. Phys., 32, 946-947, 1960.
- Stair, A. T., Jr., and J. P. Kennealy, Infrared chemiluminescence and vibrational luminescence in the NO-O-NO₂ reaction system, J. Chem. Phys., 64, 124-128, 1967.
- Swenson, G. R., S. B. Mende, and K. S. Clifton, Ram vehicle glow spectrum: Implication of NO₂ recombination continuum, Geophys. Res. Lett., 12, 97-100, 1985.
- Yee, J. H., and V. J. Abreu, Visible glow induced by spacecraft-environment interaction, Geophys. Res. Lett., 10, 126-129, 1983.

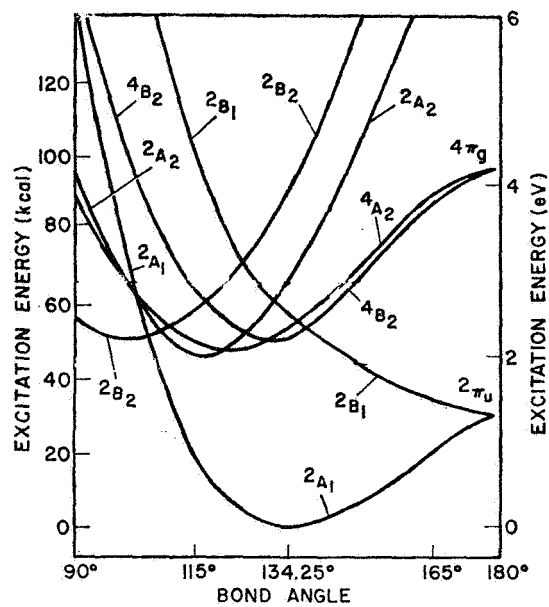


Fig. 1. Electronic energy as a function of bond angle for several low-lying states of NO_2 (from Paulsen et al. [1970]). The bond lengths are fixed at the equilibrium value for the 2A_1 state.

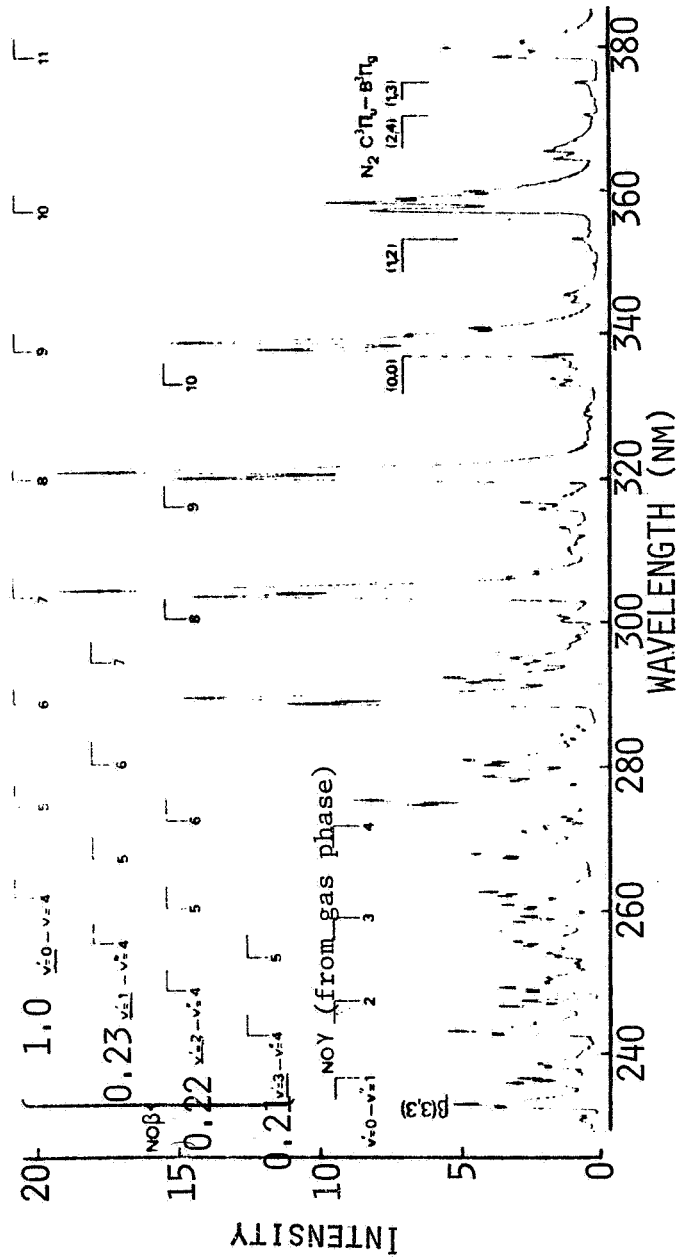


Fig. 2. NO chemiluminescence from N- and O-atom recombination at a polycrystalline Ni surface (from Caubet et al. [1984]). The relative initial vibrational-state populations in NO(B) are shown at upper left.

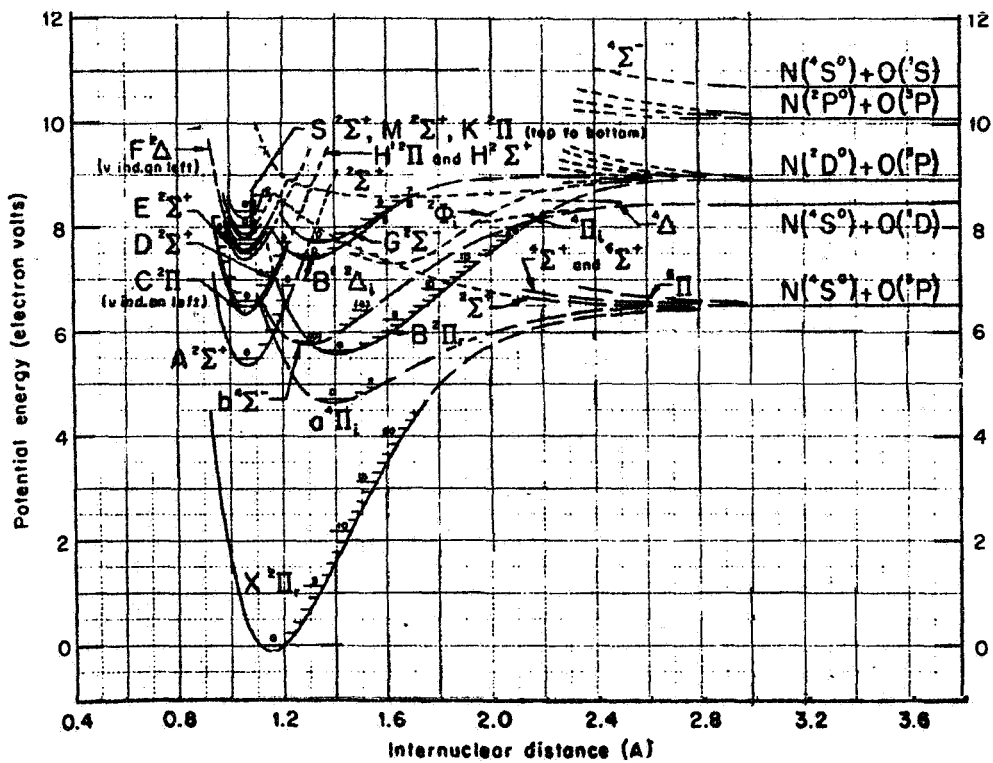


Fig. 3. Potential energy curves for NO.

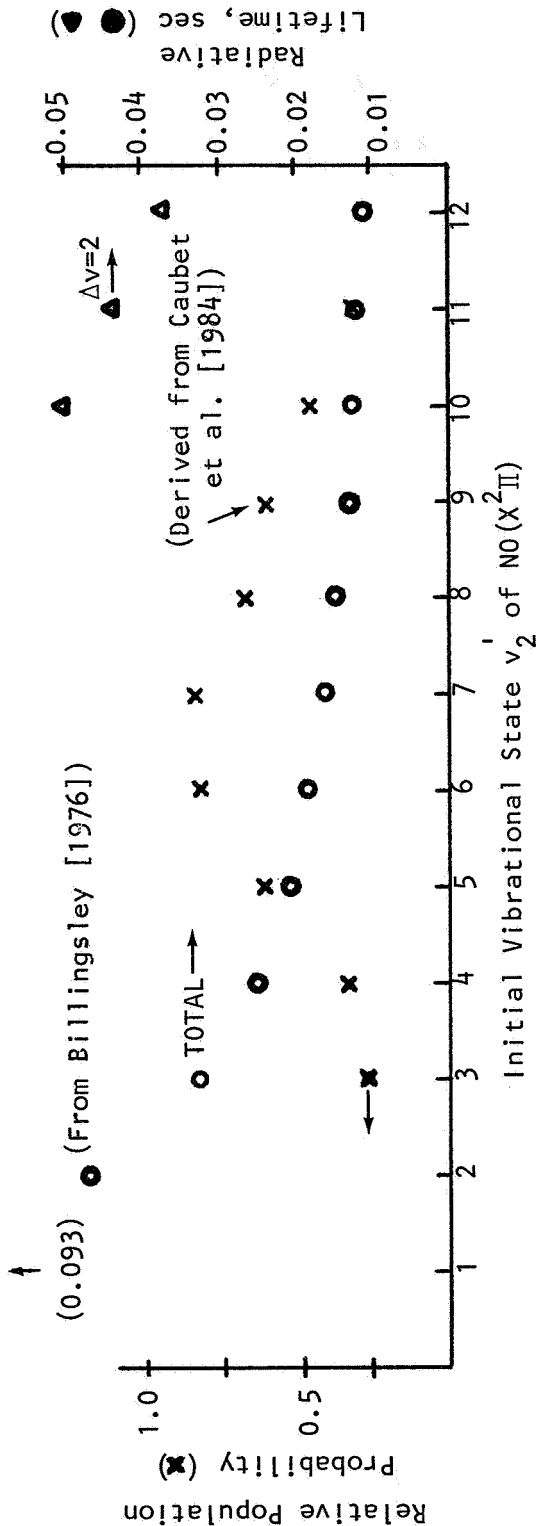
TABLE 1. NO₂ INFRARED RADIATIONS

<u>Gas-phase reaction</u>	<u>*</u>	<u>Wavelengths, μm +HWHM</u>	<u>Band</u>	<u>Photons/per electronic transition</u>	<u>Radiative lifetimes, sec</u>	<u>Lifetime x 4×10^4 cm/sec, cm</u>
NO + O + M	0.45	3.6 +0.35, -0.25	($\nu_1 + \nu_3$) each $\Delta v=1$ sequences, some $2\nu_3$	0.24 +0.1	0.0078 near 3.5 μm (101+000, 0.077)	300
NO + O ₃ (X)	0.93	3.55 +0.24, -0.13		0.37	~0.002 near 3.7 μm ($\nu_1 + \nu_3 \approx 4$)	60- 80
Both of above		6.2 +0.35 13.2 +1 7.6 2.5 +0.13	ν_3 fundamental ν_2 ν_1 unidentified	3 (0) 4 (0 ₃) $\sim 10^{-3}$ $\sim 10^{-2}$ $\sim 10^{-3}$	0.0066 (001+000)	250, to 60 at longer wavelengths

*Fraction of electronic-band photons at wavelengths $>0.8 \mu\text{m}$ in the gas-phase reactions.

TABLE 2. NO INFRARED RADIATIONS

Reaction Sequence	Wavelengths	Photons/ Reaction
$N + O \xrightarrow{\text{Surface}} NO(B, v_1^1);$	2.7 - 3.1 μm (overtone)	1
$NO(B) \xrightarrow{+ \beta \text{ bands}} NO(X, v_2^1);$	5.3 - 5.9 μm (fundamental)	5
$NO(X, v_2^1) \xrightarrow{+ \text{vibrational bands cascade}} NO(X, v_2^{-1}, -2)$		



THE NO-NO₂ SYSTEM AT LABORATORY SURFACES

J. L. Barrett and I. L. Kofsky

PhotoMetrics, Inc., Woburn, MA

Abstract. Experiments on formation and excitation of NO₂ and NO molecules at (and near) laboratory surfaces of varying degrees of characterization are reviewed. On some transition metals NO is desorbed in the B²Π state, from which it radiates the familiar β (B → X) bands. In contrast while an ONO intermediate is inferred from isotope interchange measurements on platinum, neither ground-state nor excited NO₂ has been found to be desorbed under the relatively limited number of laboratory conditions so far investigated.

Introduction

The spectral and spatial distributions recently measured viewing parallel to shuttle Orbiter's coated SiO₂ tiles have been suggested as being due to the pseudo-continuum radiation from NO₂ electronically excited at the surface [Swenson et al., 1985]. Experiment data on surface desorption of NO₂, and of NO*†, are summarized and briefly discussed here in the context of their relevance to spacecraft glows. Potential curves for the two species, and similar surface-catalyzed recombination information for other small molecules, are in the two accompanying papers by Kofsky and Barrett [these Proceedings].

Fluorescence of NO₂ using laser excitation shows that weakly absorbing features decay exponentially (that is, as single isolated states), with radiative lifetimes about 200 μsec [Donnelly and Kaufman, 1977; Cheshnovsky and Amirav, 1984]. In contrast strongly absorbing features decay nonexponentially with a range of lifetimes between 25 and 260 μsec (this is believed to result from Jahn-Teller coupling of the ²B₂ state with the ground ²A₁ state [Jackels and Davidson, 1976]). Thus desorption velocities close to wall-thermal would fit the few-cm outward extent seen off Orbiter's remote manipulator, and the lack of strong color gradients in the photographs of shuttle glow. As discussed in the review of infrared emission from NO₂ by Kofsky and Barrett [these Proceedings], the shift of Orbiter's glow spectrum roughly 1000 cm⁻¹ below the yellow-green afterglow that results from the well-characterized NO + O (+ M) reaction could be due to weak bonding of the participating O atom or NO molecule to the insulating surface.

Experiments

Table 1 summarizes experiments on and observations of the NO - NO₂ system at laboratory (in one case, instrument) surfaces. Items [7] and [8] refer specifically to N + O recombination on polycrystalline transition metals, and [1] references earlier work on the kinetics of NO on model substrates (which has some bearing on the issue at hand).

NO₂ and NO were identified as artefact species in one set of data from a satellite-borne neutral mass spectrometer with Au-NiCr surfaces [Enge-

bretson and Mauersberger, 1979], with the interpretation that NO_2 had been formed by reactions of inflowing O with adsorbed NO and then was desorbed over a characteristic time of ~11 sec; this appears longer than the decay time of the glow that can be inferred from the lag in brightness off one surface as Orbiter was rotated [Banks et al., 1983]. Other reaction mechanisms might also fit these data, and insufficient information is given about the densities of neutral and charged particles within the instrument to rule out gas-phase recombination with other reactive species formed in wall interactions (as in the kinetically complex process deduced by Kenner and Ogryzlo [1984], item [4] of Table 1). Artefacts from both associative and dissociative reactions are of course common features of mass spectra of the upper atmosphere. Note that the equivalent of an energized plasma is present in the instrument; no such stream of ions and electrons (from the induced suprathermal plasma [Papadopoulos, 1984], or the natural ionosphere) was incident on the laboratory recombination surfaces in Table 1.

In contrast under the admittedly limited range of controlled and defined laboratory conditions (items [1-4] of Table 1) no NO_2 has been found to be desorbed. Perhaps more important is the observation that in none of the several flow-tube measurements of the rate coefficient of the $\text{NO} + \text{O} (+\text{M})$ reaction (items [6a-e], among others) has wall-catalyzed recombination into excited states been reported as an experiment artefact requiring correction; unlike the transition metals of the experiments tabulated, and like most of shuttle's exposed surfaces, these walls are "dirty" insulators. Isotope interchange experiments on a Pt crystal face are interpreted as showing that an ONO complex forms, but then redissociates before desorbing [Dahlgren and Hemminger, 1982].

Comments

The adsorption energy of NO on metallic surfaces has been reported to be in the range of 20-30 kcal/mol or about 1 eV, and the NO-O bond energy is 3.1 eV. In the gas phase the chemiluminescent reaction rate of NO with O increases strongly with decreasing (high) temperature [Golomb and Brown, 1975]; this indicates that there is no activation barrier that needs to be lowered by a surface interaction, and that the rate for 5-eV oxygen atoms will be very low. The relevance of the kinetic energy of the air particles impacting spacecraft surfaces is discussed in the accompanying Kofsky and Barrett presentation [these Proceedings].

At reasonably low temperatures, 300-400 K, NO desorbs from some metal surfaces; and NO adsorbs dissociatively at 300 K on silicon (111). From these results on clean model substrates we may infer that for a given material there may be only a narrow range of temperatures--if any--under which NO combines with O to produce desorbed (excited) NO_2 . Different mean adsorption energies of the reaction participants on real surfaces would imply different spectrum distributions in the pseudo-continuum from NO_2 . The failure of N and O to recombine to NO^* on teflon at room temperature [Caubet et al., 1984] and the low recombination rate of N on teflon [Evenson and Burch, 1966] are reflected in the minimal glow off polyethylene in shuttle experiments [Mende et al., 1985], in that it suggests that these saturated polymers lack sites at which reactants can adsorb to form complexes whose fragments desorb with internal excitation (if in molecular form at all); further, these observations support the interpretation that spacecraft glow results (principally) from surface-catalyzed recombination of air species.

References

- Banks, P. M., P. R. Williamson, and W. J. Raitt, Space shuttle glow observations, Geophys. Res. Lett., **10**, 118-121, 1983.
- Caubet, P., S. J. Dearden, and G. Dorthe, The specific production of NO ($B^2\Pi$) from the recombination of NO on a nickel surface, Chem. Phys. Lett., **108**, 217-221, 1984. [7 in Table 1]
- Cheshnovsky, O., and A. Amirav, Lifetimes of electronically excited NO₂ in a collision free, differentially pumped supersonic molecular beam, Chem. Phys. Lett., **109**, 368-373, 1984.
- Clough, P. N., and B. A. Thrush, Mechanism of chemiluminescent reaction between nitric oxide and ozone, Trans. Faraday Soc., **63**, 915-925, 1967. [6a]
- Dahlgren, D. A., and J. C. Hemminger, Decomposition of NO₂ to NO and O on Pt (111), Surface Sci., **123**, L739-L742, 1982. [3]
- Donnelly, V. M., and F. Kaufman, Fluorescence lifetime studies of NO₂ I. Excitation of the perturbed 2B_2 state near 600 nm, J. Chem. Phys., **66**, 4100-4110, 1977.
- Engebretson, M. J., and K. Mauersberger, The impact of gas-surface reactions on mass spectrometric measurements of atomic nitrogen, J. Geophys. Res., **84**, 829-844, 1979. [5]
- Evenson, K. M., and D. S. Burch, Atomic nitrogen recombination, J. Chem. Phys., **45**, 2450-2460, 1966.
- Fontijn, A., C. B. Meyer, and H. I. Schiff, Absolute quantum yield measurements of the NO-O reaction and its use as a standard for chemiluminescent reactions, J. Chem. Phys., **40**, 64-72, 1964. [6b]
- Golomb, D., and J. H. Brown, The temperature dependence of the NO-O chemiluminous recombination. The RMC mechanism, J. Chem. Phys., **63**, 5246-5251, 1975. [6c]
- Jackels, C. F., and E. R. Davidson, The two lowest energy 2A_1 states of NO₂, J. Chem. Phys., **64**, 2908-2917, 1976.
- Kenner, R. D., and E. A. Ogryzlo, Orange chemiluminescence from NO₂, J. Chem. Phys., **80**, 1-6, 1984. [4]
- Mende, S. B., G. R. Swenson, K. S. Clifton, R. Gause, L. Leger, and O. K. Garriott, J. Spacecraft and Rockets, in press, 1985.
- Nishijima, M., H. Kobayashi, K. Edamoto, and M. Onchi, Reactions of NO with the Si (111) (7 x 7) surface: EELS, LEED, and AES studies, Surf. Sci., **137**, 473-490, 1984. [1]
- Papadopoulos, K., On the shuttle glow (the plasma alternative), Radio Sci., **19**, 571-577, 1984.
- Paulsen, D. E., W. F. Sheridan, and R. E. Huffman, Thermal recombination emission of NO₂, J. Chem. Phys., **53**, 647-657, 1970. [6d]
- Reeves, R. R., G. Mannella, and P. Harteck, Formation of excited NO and N₂ by wall catalysis, J. Chem. Phys., **36**, 946-947, 1960. [8]
- Schmick, H., and H. Wassmuth, Adsorption, desorption, and reaction kinetics of nitric oxide on a stepped Pd (111) surface, Surface Sci., **123**, 471-490, 1982. [2]
- Stair, A. T. Jr., and J. P. Kennealy, Infrared chemiluminescence and vibrational luminescence in the NO-O-NO₂ reaction system, J. Chem. Phys., **64**, 124-128, 1967. [6e]
- Swenson, G. R., S. B. Mende, and K. S. Clifton, Ram vehicle glow spectrum: Implication of NO₂ recombination continuum, Geophys. Res. Lett., **12**, 97-100, 1985.

TABLE 1. NO - NO₂ ON-SURFACE EXPERIMENTS

<u>Ref.</u> [†]	<u>Conditions</u>	<u>Surface/Temp.</u>	<u>Gas Flow</u>	<u>Measurements</u>
1*	High vacuum	Si 111 (7 x 7)/ 300-1300 K	Adsorption of NO	EELS, LEED, Auger. NO is adsorbed dissociatively.
2	High vacuum	Stepped Pd 111/ 160-600 K	Adsorption of NO (O ₂)	TPD, LEED, Auger, mass spectroscopy. N ₂ , NO, N ₂ O, but no NO ₂ desorbs; O ₂ saturates adsorp- tion-specific sites.
3	High vacuum coadsorption, isotope exchange	Pt 111/ 120-1000 K	Adsorption of NO ₂ , NO, ¹⁶ O ₂ , ¹⁸ O ₂	TPD, LEED, Auger, mass spectroscopy. ONO intermediate on surface but doesn't desorb.
4	Flow tube, microwave discharge source	Nickel mesh/300 K	O onto mesh, NO (or NO ₂) downstream or upstream	Spectrometry, photometry. O ₂ * precursor of O ₃ [†] forms on surface, but not NO ₂ *.
5	Inside Nier neutral mass spectrometer on spinning spacecraft	Gold, Nichrome 300-400 K; ionization by 25, 75 eV electrons	Ram atmosphere at 300 to 800 km altitude	Mass spectrometry. NO ₂ ⁺ , NO ⁺ , O ⁺ (N ⁺ , N ₂ ⁺ , O ₂ ⁺)
6a-e	NO + O recombination, ~5 laboratories	Principally glass/300 K	NO, O (O ₂ , O ₂ *)	Spectrometry of product NO ₂ from gas phase.
7	Flow tube, microwave discharge source	Nickel/ 300 K (No glow off teflon)	N, O onto surface	Optical spectroscopy. γ, β, δ bands of NO in gas; only β bands from surface, non-statistical T _v .
8	Flow tube, as [7]	Ni, Co, Ag/ 300 K	N, O onto surface	Optical spectroscopy. N ₂ 1P, NO β bands.

[†]Identified in brackets in the list of references.

*Also references other papers on surface kinetics of NO (only).

A MODEL FOR EXPLAINING SOME FEATURES OF SHUTTLE GLOW

Palmer N. Peters

Space Science Laboratory, Marshall Space Flight Center

Abstract. A solid state model is proposed which hopefully removes some of the objections to excited atoms being sources for light emanating from surfaces. Glow features are discussed in terms of excited oxygen atoms impinged on the surface, although other species could be treated similarly. Band formation, excited lifetime shortening and glow color are discussed in terms of this model. The model's inability to explain glow emanating above surfaces indicates a necessity for other mechanisms to satisfy this requirement. Several ways of testing the model are described.

Introduction

The predominant species striking forward facing shuttle surfaces in low-Earth orbits is atomic oxygen. The glow is reddish in color and excited oxygen has transitions that provide red emission. The glow is ram and altitude dependent and so is the flux of atomic oxygen to the surfaces. However, the emission from free excited oxygen atoms is observed in the form of sharply defined line spectra and the lifetimes of the excited states can be shown to be very long. Thus, it seems improbable that excited atoms, especially oxygen atoms, contribute to the observed glow, which produces a continuous band spectrum. Also, reflected oxygen atoms would de-excite at far greater distances from the surfaces than is observed, and if atoms were adsorbed they should be nonradiatively de-excited on the surface very quickly. This view of emission spectra from excited atoms is what should be expected, since atoms in a solid that are excited sufficiently to provide atomic spectra by means of an arc, or other sources, are already vaporized and the spectra originate from sharply defined energy levels associated with free atoms.

In the case of orbiting surfaces a unique situation exists which is not common to our experiences. Oxygen atoms and other species are incident to forward facing surfaces with sufficient energies to potentially excite such atomic states and enable the atoms to become part of a solid state at the same time. Solid state theories rely upon the fact that discrete energy levels of free atoms spread into energy bands upon assembly into solids.

The model to be described relies upon spreading of the energy levels of the atomic orbitals to provide the broadband emission and other features.

The Model

The relative velocity, in excess of 7 km/s, between forward facing orbiting surfaces and ambient particles provides a collisional interaction energy of 5 eV for oxygen atoms. This energy is considerably in excess of the 1.9 eV difference between the 1D and 3P states which leads to red emission lines at 6300 Å and 6364 Å (Figure 1). If losses during the collision were sufficiently low, then the 4.2 eV difference between the 3P normal state and the 1S state might be provided which leads to emissions in the green at 5577 Å and ultraviolet at 2972 Å. States requiring excitation energies greater than 5 eV are neglected for simplicity.

Also shown (Figure 1) is an approximation of the spreading that might be expected as discrete energy levels of a free atom are converted into energy bands of a solid. No attempt has been made to calculate densities of states for the poorly characterized case of an atom striking typical orbital surfaces, but the general trend can be noted by observing what occurs as progressively larger numbers of atoms are involved. Results for band calculations starting with six hydrogen atoms in a line show splitting of levels into six lines forming bands dependent upon lattice constant [Kittel, 1965]. Kittel also gives results for noble metals as a function of internuclear separation.

If specular reflection is assumed for an oxygen atom striking a surface with a speed of 8 km/s, it is easily determined that the atom would spend approximately 5×10^{-14} s within an atomic diameter on the surface. This is sufficient time for the atom to communicate at the speed of light with a large number of lattice atoms (within a hemisphere of radius 10^{-4} cm), which satisfies at least one requirement for producing many states within the bands. If it is necessary for the atom to become part of the lattice, it can be seen by comparison to self-diffusion coefficients that 5 eV minus 2 eV would leave sufficient energy to exceed most barriers to incorporation of the atom into a lattice (activation energies for self-diffusion are typically less than the 60 kcal/(g-atom) available from a kinetic energy of 3 eV [Askill, 1971]).

A broadband spectrum can be produced, assuming that the energy band structure is reasonably represented (Figure 1). Also, the peak intensity should be in the general vicinity of the discrete lines, though shifted, and have an asymmetrical distribution. A spectrum from STS 41-D [Mende et al., 1985] exhibits characteristics of this nature, with the peak shifted toward a longer wavelength and with a bandwidth in excess of 1.5 eV.

Model Testing

To test the model it seems appropriate that spectra of some type dependent upon solid state band structure should be compared to glow spectra. Soft x-ray emission spectra provide information on some band structures [Kittel, 1965] which arise when inner K and L levels are ionized by electron impact and outer electrons make transitions to the

inner vacancies. Since inner levels are relatively sharp because of shielding by the outer electrons, the bandwidths observed in the emission spectra are mostly due to the occupied width of the band from which the outer electrons made their transitions. The K emission band of lithium was found to have a full width of approximately 3 eV [Skinner, 1940], which should represent a good measure of the filled portion of the conduction band. Bandwidths of other materials are generally of the order 1 eV to 10 eV. Optical absorption coefficients versus wavelengths should also provide information about transitions between bands [Kittel, 1965]. Major absorption peaks for Cu and Au are 2000 Å to 3000 Å wide and peaked in the visible. Thus, the bandwidth for the glow is of the correct order compared to other spectra dependent upon solid state bandwidths (toward lower limit).

To provide a higher probability for glow from the surface the lifetime of the excited oxygen state should be less than the time spent traveling one atomic diameter during reflection ($<10^{-14}$ s, as mentioned earlier) or less than a period of lattice vibration ($\sim 10^{-13}$ s), if the atom is adsorbed. The exclusion principle $\Delta E * \Delta t \sim h$ provides a means of comparing linewidths to mean lifetimes [White, 1934]. Taking 0.7 eV for the half width of the spectral peak from STS 41-D data [Mende et al., 1985], and assuming the same uncertainty applies when $\Delta E = 0.7$ eV and Δt is the mean lifetime of the excited state, we obtain

$$\Delta t \sim \frac{h}{0.7 \text{ eV}} \approx 6 \times 10^{-15} \text{ s} . \quad (1)$$

In the derivation of pressure broadening of atomic spectra the collision damping contribution, which broadens the lines, has a correction added due to alteration of the energy levels due to the close approach of the second atom [White, 1934]. The initial and final states of the excited atom are not modified equally by collision since an excited, or outer, state is affected more than an inner tightly bound state. The effect is a shift toward lower frequencies for atoms emitting while spaced less than 10 Å. Asymmetry and redshifting of the spectral lines occur. This does not conflict in general with the appearance of the STS 41-D spectrum and the fact that a solid would produce greatly modified states.

Ground-based studies of airglow [Young, 1966] found a number of gases acted as quenching agents, reducing radiative de-excitations by collision losses. Carbon dioxide was particularly noted for this effect. If carbon dioxide or other contaminants have a high coverage on the surface, one might speculate quenching of the excitation or de-excitation of the incident atoms; this would provide for differences in glow intensities for different materials. Those materials producing a minimum of gaseous products, but exposing a cleaner, lattice-type structure might be expected to glow with more intensity (the opposite of what might be expected for chemical reactions providing the glow). The data from STS 41-D may show such a trend [Mende et al., 1985]. This could be further tested by using a high glow intensity surface coated with a thin plastic film. When the film is burned away, the glow should intensify. Using a half coated disk rotated behind an aperture and also phase-sensitive

detection would provide a low-noise measurement. Dosing of gases onto surfaces could also be used if limited so effects in the gaseous state above the surface did not dominate. If successful, such techniques (with acceptable gases or materials) might be useful for controlling shuttle glow. The distribution of oxygen atoms reflected from an orbiting surface (measurements by J.C. Gregory and P.N. Peters, to be published) may indicate a higher accommodation than would be predicted by hard sphere collision models. Mechanisms such as excitation/radiation which would deplete a large fraction of the particle's incident energy could help explain excessive accommodation coefficients where measured values exceed theoretical predictions. It should also be possible to measure incident energy thresholds for enhanced adsorption and glow if variable energy neutral oxygen atom sources are developed. If accommodation is found to be an adjustable parameter, numerous applications of this parameter to studies for understanding and controlling drag and torques in low-Earth orbits are possible.

As a solid state model, no mechanism is provided to explain glow emanating above surfaces.

Conclusions

A hypothetical solid state model appears to explain a number of features for glow emanating from a surface in low-Earth orbit. A specific case of oxygen atoms impacting the surface with 5 eV energy may provide the atom excitation, energy level broadening, and shortened lifetimes necessary to produce an appropriate spectrum. The model does not provide a mechanism for glow emanating above surfaces.

References

- Askill, J., Tracer diffusion in metals, in Handbook of Chemistry and Physics, edited by R. C. Weast, 52nd ed., pp. F-48-F-51, The Chemical Rubber Company, Cleveland, Ohio, 1971.
- Kittel, C., Introduction to Solid State Physics, 2nd ed., pp. 275-268, 318, 310, and 319, Wiley & Sons, New York, 1965.
- Mende, S. B., et al., Shuttle glow measurements on STS 41-D, Final Report to Space Telescope Program Office, MSFC, Alabama, 1985.
- Skinner, H.W.B., Trans. Roy. Soc., A239, 95, 1940.
- White, H. E., Introduction to Atomic Spectra, pp. 423-432, McGraw-Hill, New York, 1934.
- Young, R. A., The airglow, Scientific American, 214, 102-110, 1966.

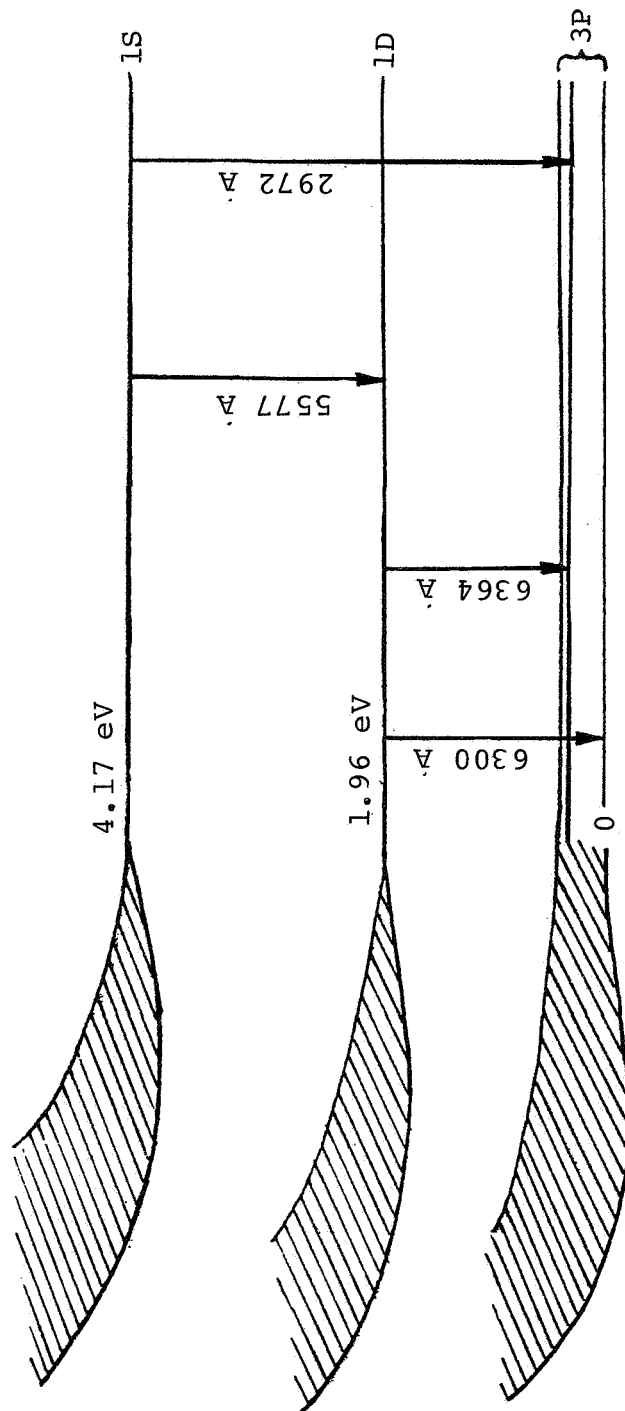


Fig. 1. A hypothetical representation of oxygen atom energy levels being spread on impacting surface.

THE PRODUCTION OF GLOW PRECURSORS BY OXIDATIVE
EROSION OF SPACECRAFT SURFACES

John C. Gregory

The University of Alabama in Huntsville

Palmer N. Peters

NASA, Marsall Space Flight Center

Abstract. Erosion rates of organic materials were measured during a recent flight of the shuttle (STS-8). Several forms of carbon and a variety of thermosetting and thermoplastic polymers were exposed to the ram beam of atomic oxygen. Arrhenius energies of about 1000-2000 cal mole⁻¹ were measured from the rate dependencies on temperature. If some simple assumptions are made about the chemical nature of the desorbed species, the data can be used to estimate production rates at surfaces in orbit under different conditions of temperature, oxygen atom flux and material surface conditions.

Introduction

Erosion of carbon and organic polymer surfaces by "active" or atomic oxygen has been known for decades [e.g., Blackwood and McTaggart, 1959; Hansen et al., 1965]. Gregory and Peters [1975] pointed out that the atmosphere in orbit at a few hundred km altitude would be at least as reactive and proposed the use of the returnable Long Duration Exposure Facility (LDEF) for a study of the effects. Although, at the time of writing, this spacecraft is still in orbit, a version of the atomic oxygen instrument was flown in 1983 on the STS-8 mission. The objectives of the experiment were to begin an investigation of the mechanisms of interaction of 5 eV oxygen atoms with solid surfaces by measuring the rate of reaction as a function of temperature and oxygen flux, and by examining the scattered distribution of atoms re-emitted from certain surfaces. In addition, a number of optical quality metal films were prepared and exposed to investigate the growth of their oxide films or any morphological changes induced by the oxygen atom beam. In this paper only the results on carbon and solid polymers is discussed.

In the context of glow, emission of reaction products from the surface may be relevant in two ways. Oxidation products may be desorbed in excited states which subsequently decay emitting radiation, or products may suffer reactive collision with another 5 eV oxygen atom producing new products in excited states. Evidence favoring the latter mechanism includes:

(a) New calculations [Rantanen, 1985; Brock, 1985] of mean-free-path of emitted species indicate large probability of collision with the ambient stream.

(b) Energetic collisions of organic molecules with oxygen atoms are

expected to have a significant probability for reaction producing excited products.

(c) Emission lines from C_2 species were observed [Torr and Torr, 1985] on Spacelab 1.

(d) An extended (tens of meters) glow around the orbiter in the unresolved infrared was observed [Witteborn, 1984] from the ground during a recent shuttle flight.

Experimental Approach

The experimental approach used was necessarily very simple as no electromechanical devices such as lids, shutters, etc. were available, and no intermediate measurements could be made; i.e., only a single integral effect could be measured for each sample. Samples were nominally 1-inch discs, with the hot-plate discs only being $\frac{1}{4}$ -inch diameter. For the case of the erodible materials discussed here, a bar-pattern of small rectangles of niobium was deposited on the surface using a photo-resist technique (Figure 1). The niobium was sputtered on as a uniform film $\sim 2000 \text{ \AA}$ thick. Although it oxidized heavily, it still served to protect the underlying carbonaceous material. The scanning electron microscope picture in Figure 2 shows both the eroded portion of a vitreous carbon disc and the part covered and protected by the niobium film. The height of the step on this sample was about $50,000 \text{ \AA}$ (5 \mu m). The bar-pattern allowed multiple measurements of the step-height to be made using a Dektak stylus profilometer. Amplitudes were checked using the SEM micrographs. Half of each sample was covered at all times before and during the flight, and served as a control.

Erodible surfaces studied included single crystal graphite (basal and prismatic planes), vitreous (or glassy) carbon from various manufacturers, polymethyl methacrylate (lucite), bisallyl diglycol carbonate (CR-39, a high quality optical plastic), and diamond.

The exposure obtained during the STS-8 mission was ideal from the point of view of the materials experiment in that about 95% of the atom fluence was accumulated while the vehicle attitude was held so that the ambient atom beam was within 1° of the normal to the material surfaces. The rest of the mission was spent at much higher altitudes or with the payload bay doors closed. Pertinent exposure data are shown in Table 1.

Table 1. STS-8 ATOMIC OXYGEN EXPOSURE DATA

Payload bay forward facing:	$t = 41.2 \text{ hrs.}$
Altitude:	120 nautical mi. (225 km)
Velocity:	7.8 km s^{-1}
Mean oxygen atom density (calculated):	$2.65 \times 10^9 \text{ cm}^{-3}$
Surface impact frequency:	$2.07 \times 10^{15} \text{ cm}^{-2} \text{ s}^{-1}$
Integral fluence:	$3.5 \times 10^{20} \text{ atoms cm}^{-2}$

Erosion observed by this experiment ranged from a thousand angstroms for diamond (which appears to be particularly resistant to oxidation under these conditions), to about 200,000 Å for the polycarbonate resin, CR-39, which was the most heavily eroded sample reported on any space flight exposure.

The temperature dependence of the oxidative effects was measured by conducting the erosion measurements at three temperatures spanning about 120°C. The Arrhenius activation energy, ΔE , was estimated, assuming:

$$r = A e^{-\Delta E/RT}$$

where r is the rate of the reaction and A is a constant assumed independent of temperature T . These studies were performed for six materials, vitreous carbon, two graphites, CR-39, silver, and osmium. All activation energies were small and positive.

Results

The conclusions from the measurements on various forms of carbon exposed in the STS-8 mission appear applicable to organic solids in general. They may be summarized as follows:

1. Measured erosion was linear with total fluence.
2. No induction time observed before onset of erosion.
3. Erosion rate linear with oxygen flux (i.e., reaction probability independent of flux) measured over a small range 1.5 to 2.5×10^{15} atoms $\text{cm}^{-2} \text{s}^{-1}$.

These results show that erosion and production of gas molecules at the surface can proceed indefinitely at such surfaces as long as oxidizable material remains exposed, in contrast with outgassing behavior which generally shows exponential decay of evolution rate with time. It should be emphasized, however, that our experiment used very pure materials and real or engineering materials may be contaminated either on the surface or by inclusions in the bulk. Such contamination, if less oxidizable than the matrix itself, may then serve to protect the rest of the matrix material from erosion. As erosion proceeds the density of these screening particles or films on the surface grows and the erosion rate may drop from its prior value.

4. Arrhenius activation energies for the reactions were measured as follows:

Vitreous Carbon	1200 (cal mole ⁻¹)
Graphite (basal plane)	1400
CR-39	1050

5. Reaction probabilities depend on temperature as shown in (4) above. Reaction probabilities for carbons exposed at $\sim 300^\circ\text{K}$ ranged from 0.1 to 0.15 where reaction probability equals the number of carbon atoms lost divided by the number of incident oxygen atoms.

6. Reaction probabilities for more complex organic materials have been expressed in $\text{cm}^3 \times 10^{-24}$ of material lost per incident O atom. For present purposes we use two examples at approximately 300°K :

CR-39 ($\text{C}_{12}\text{H}_{18}\text{O}_7$)_n (this work): $\sim 6 \times 10^{-24} \text{ cm}^3 \text{ atom}^{-1}$

Kapton [Leger et al., 1984]: $3 \times 10^{-24} \text{ cm}^3 \text{ atom}^{-1}$

Rates of Production of Volatile Species

Our assumption is that the erosion of carbonaceous materials in orbit was caused by the interaction of 5 eV oxygen atoms with a surface of the material, forming volatile products which evaporated into space. We have performed no experiments to measure the nature or composition of the volatile species, and must, therefore, make intelligent guesses. In the case of the pure carbons the range of choice is limited. From the published literature (at higher temperature) the main product is expected to be CO rather than CO₂. The mechanism for this production is not discussed here. In the cases of polymeric films, paints and other solid organic surfaces, the chemistry is likely to be much more complex and quite undefined by experiment. A survey of the experimental data for reactions with commonly used polymers has been given [Leger et al., 1984]. Using the data from 5 and 6 above we may then calculate the emission rates of product molecules from the eroding surfaces in the idealized case. The emitted flux of CO from carbon is given simply by the product of the reaction probability, P, times the flux of oxygen. Calculation of the molecular loss rate from polymers, on the otherhand, requires some assumption of mean molecular weight of the desorbed species.

For the polymers we assumed a mean molecular weight of 28 amu of solid-derived component (i.e., not including the atmospheric component). Since the product mixture may well be complex, and different components will differ radically in their capacity for reactive collision excitation to a glow condition, this level of understanding is clearly inadequate.

For the STS-8 mission, with an oxygen atom flux of $2 \times 10^{15} \text{ cm}^{-2} \text{ s}^{-1}$, we have:

Substrate	Emitted Species	Rate of Emission (molecules $\text{s}^{-1} \text{ cm}^{-2}$)
Carbon	CO	3×10^{14}
Kapton	(28+) amu	1.9×10^{14}
CR-39	"	3.0×10^{14}

Before these rates are used in any modeling of the gas cloud surrounding the shuttle it should be emphasized that they apply only to unprotected and rather pure organic surfaces. The extent to which impurities reduce the rate of mass loss requires further definition, and it is already quite clear that simple procedures of overcoating with oxidation-resistant materials can reduce mass loss by orders of magnitude. Model calculations of the dynamics of scattering of surface-desorbed species with ambient atmospheric species have suggested that the probability of collision with a streaming oxygen atom is quite high. Under these conditions a large fraction of all organic molecules leaving this shuttle surface may emit one or more photons, contributing to an extended ball of glowing gas around the vehicle, with the upper limit (for 1 mol \equiv 1 photon) for the integral number of photons emitted per second equaling the total number of glow precursors leaving the entire surface per second.

References

- Blackwood, J. D., and F. K. McTaggart, Austral. J. Chem., 12, 114, 1959.
- Brook, F. S., these proceedings, 1985.
- Gregory, J. C., and P. N. Peters, The Interaction of Atomic Oxygen with Solid Surfaces at Orbital Altitudes, experiment proposal to NASA, Langley Research Center, June 1975; see also, The Long Duration Exposure Facility (LDEF) Mission One Experiments, NASA SP-473, p. 14, NASA Headquarters, 1984.
- Hansen, R. H., J. V. Pascale, T. Benedictis, and P. M. Renzepis, J. Polymer Sci:PtA, 3, 2205, 1965.
- Leger, L. J., J. T. Visentine, and J. F. Kuminecz, AIAA Paper No. 84-9548, January, 1984.
- Rantanen, R., these proceedings, 1985.
- Torr, M., and D. G. Torr, A preliminary spectroscopic assessment of the Spacelab 1/shuttle optical environment, J. Geophys. Res., 90, 1683, 1985.
- Witteborn, F., unpublished results presented at the First Workshop on Spacecraft Glow, NASA/MSFC, 1984.

Acknowledgements

We are grateful to the University of Alabama Research Institute for a grant to build the instrument hardware. Part of the analysis at the University of Alabama in Huntsville was supported by Contract NAS8-36189.

Fig. 1. One-inch-diameter vitreous carbon disc exposed to the atomic oxygen stream normal to its surface in a 225-km orbit. Rectangles are thin films of niobium. The lighter annulus round the edge of the sample is protected by its holder and remains highly specular, while the inner circle shows the light-absorbing nature of the eroded surface.

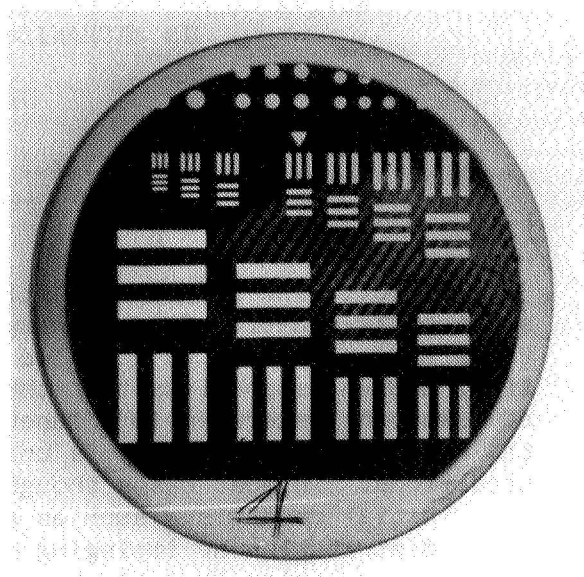
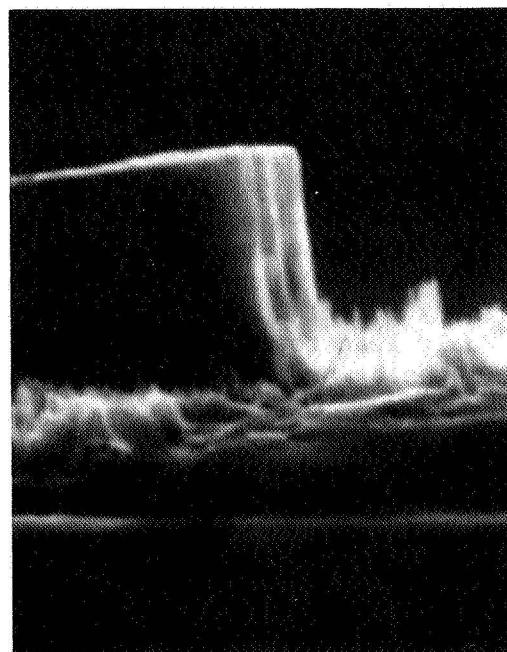


Fig. 2. Scanning electron micrograph of a sample similar to Figure 1 which has been cut through one of the niobium rectangles. Viewing direction is in the plane of the sample. The height of the step (a few μm) indicates the amount of carbon eroded.



ACTIVATED RECOMBINATIVE DESORPTION: A POTENTIAL COMPONENT
IN MECHANISMS OF SPACECRAFT GLOW

Jon B. Cross

Los Alamos National Laboratory
Los Alamos, New Mexico

Abstract. The concept of activated recombination of atomic species on surfaces is capable of explaining the production of vibrationally and translationally excited desorbed molecular species. Equilibrium statistical mechanics predicts that the molecular quantum state distributions of desorbing molecules is a function of only the surface temperature when the adsorption probability is unity and independent of initial collision conditions. In most cases though the adsorption probability is dependent upon initial conditions such as collision energy or internal quantum state distribution of impinging molecules. From detailed balance, such dynamical behavior is reflected in the internal quantum state distribution of the desorbing molecule. A number of surface-atom recombination systems demonstrate this "nonthermal" behavior: H_2 -Cu, N_2 -Fe, CO_2 -Pt, etc. It is proposed that this concept, activated recombinative desorption, may offer a common thread in proposed mechanisms of spacecraft glow. Ground-based experiments are proposed which will complement flight investigations probing the mechanism of the glow phenomenon. Using molecular beam techniques and equipment available at Los Alamos, which includes a high translational energy O-atom beam source, mass spectrometric detection of desorbed species, chemiluminescent/laser-induced fluorescence detection of electronic and rovibrationally excited reaction products, and Auger detection of surface-adsorbed reaction products, we propose a fundamental study of the gas-surface chemistry underlying the glow process. This would lead to the development of materials that could alter the spectral intensity and wavelength distribution of the glow.

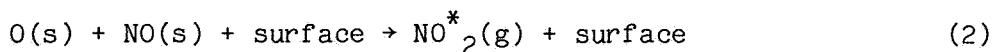
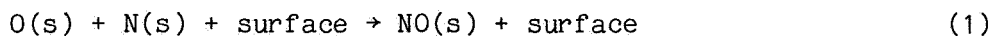
Introduction

Interaction of the low-Earth orbit (LEO) environment with ram-oriented spacecraft surfaces may involve both gas-surface and gas-phase components whose relative importance is poorly understood. From conservation of flux arguments the ram pressure can be 30 to 100 times the ambient LEO pressure depending upon the extent of gas-phase equilibration with the surface temperature. At low-altitude pressures as high as 10^{-5} torr may be present near ram surfaces, which could produce glow from the low rates of rotational and vibrational excitation produced by collisions with ram-directed O-atoms (5 eV) or N_2 (11 eV) as well as ion or electrons. An alternative mechanism to gas-phase excitation lies in desorption of vibrationally excited recombination or surface reaction products through activated recombination. Molecules not normally found in LEO can be formed by recombination of oxygen and nitrogen atoms on spacecraft surfaces as well as reactions of O-atoms with the surface substrate atoms forming species such as OH, CO, CO_2 , CN, NO, etc.; all of which may contribute to chemiluminescent glow through activated desorption.

Activated Recombinative Desorption

Figure 1 is a schematic potential energy representation of molecular and atomic particle interactions with a solid surface which illustrates the concept of activated recombinative desorption. Collisions of gas-phase molecules with a surface can result in physisorption of the molecule into a precursor van der Waals potential well or chemisorption into a dissociative atomic state by crossing from the molecular to the atomic state curve. In many cases a barrier must be surmounted to cross to the atomic state resulting in an activation energy for adsorption in molecule-surface collisions while adsorption of atomic species is rarely limited by barriers. The reverse process, molecular desorption, is accompanied by the release of molecules having a high translational energy; i.e., atomic recombination occurs with the molecule being born at an elevated potential and leaves the surface with this energy. A number of examples [Comsa and David, 1982; Kubiak et al., 1984; Robota et al., 1985] involving hydrogen can be found in the literature which show that H₂ desorbs with translational temperatures as high as 2000 K and with vibrational populations 50 times greater than expected from an equilibrium ensemble at the surface temperature of 300 K. Molecular nitrogen [Thorman and Bernasek, 1978] exhibits high vibrational excitation in the ground electronic state when desorbing from iron. Vibrational excitation of CO₂ produced by oxidation of CO on platinum [Brown and Bernasek, 1985] has been observed with the extent of excitation decreasing with increasing surface coverage of oxygen. In these cases the desorbing molecule loses memory of the initial conditions prevailing before desorption and is only influenced by its position at birth.

Even though there can be extensive etching of surfaces in LEO, oxygen or nitrogen atom reactions with spacecraft surfaces to produce excited products seem to be ruled out by the fact that most surfaces exposed to the ram direction glow with intensity variations of 2 to 3, i.e., that the glow is independent of surface composition. This suggests that surfaces simply act as a third body to catalyze recombination of existing atomic species found in LEO, most probably oxygen and nitrogen atoms. Since the altitude dependence of the glow intensity follows that of atomic and not molecular species, N₂ seems to be ruled out as a reaction partner with O-atoms, but it has been proposed [Swenson et al., 1985] that nitrogen atoms may be the reactant controlling the glow intensity. This suggests that the following reaction sequence may be one of the major components in the glow mechanism



where the surface acts as a third body to stabilize the newly formed molecules before desorption. Many investigations have been performed on the reaction



which have shown that NO₂ can be formed with substantial vibrational [Kahler et al., 1984] energy, and our work [van den Ende et al., 1982]

shown in Figure 2 shows both internal and translational excitation of the NO_2 product. Though it may be stretching the point a bit to consider (3) as a reaction of O-atoms on an oxide surface (O_2) with NO, nevertheless the results indicate that NO_2 formed from this reaction possesses the characteristics needed to fit the glow data, i.e., long life time (tens of microseconds) and strong spectral emission in the infrared (1-3 μ). Indeed it has been demonstrated [Brown and Bernasek, 1985] that vibrationally excited CO_2 is produced through oxidation of CO on platinum surfaces and chemiluminescence is observed in the gas phase. Satellite mass spectrometer measurements [Engebretson and Mauersberger, 1979] have shown formation of NO and NO_2 on surfaces in the ion source region, but no direct measurements of nitrogen oxide desorption from spacecraft surfaces have yet been made to confirm this hypothesis. High signal-to-noise mass spectrometric investigations of the spacecraft environment will be needed to identify the presence of NO_2 .

Gas-Phase Excitation

Even though activated recombinative desorption seems an attractive idea to explain spacecraft glow, there is no conclusive evidence from LEO experiments to support it and there may in fact be several mechanisms in operation which come into play as the concentration of species changes. NO_2 could indeed be formed at high surface coverages of oxygen and desorb in its ground state with subsequent excitation by gas-phase collisions with ion, electron, or neutral species. A combination of molecular beam scattering experiments and theory will be needed to determine cross sections for high energy O-atom excitation processes in order to realistically assess the contribution of gas-phase collisions to the glow phenomenon.

LEO Experiments

Extensive experimental data are needed from LEO in order to narrow down the possible mechanisms of spacecraft glow. Both high-resolution spectroscopic information and simultaneous mass spectrometer detection of surface-desorbed species will be necessary to distinguish between various proposed models. To study etching and glow mechanisms a mass spectrometer with high sensitivity and differential pumping and the ability to use modulation techniques will be needed in order to determine concentrations of reactants as well as surface reaction products. Existing mass spectrometers could be retrofitted with ion counting detectors, choppers for performing modulated molecular beam detection, and molecular shields for differential pumping. A strong emphasis should be placed on using state-of-the-art techniques in future LEO experiments.

Los Alamos LEO Simulation Facilities

A 5-eV O-atom source is being developed [Cross and Cremers, 1985] at Los Alamos that will be capable of delivering fluxes of 10^{15-17} O-atoms/ $\text{cm}^2\text{-s}$ to a sample surface for materials testing, ground-based calibration of flight hardware, and fundamental investigations of etching and

glow mechanisms. The source is based upon the use of CO₂-laser-sustained discharge techniques and using a 70-W laser has demonstrated translational temperatures of 9000 K in xenon. Calculations predict that similar discharges in helium will produce velocities in excess of 10 km/s but will require laser powers of 1 kW or greater. We have recently demonstrated operation of this concept at 400 W of laser power in argon and 30% oxygen for 2 hours using a boron nitride nozzle. We are presently integrating this laser (maximum power of 700 W) with the Los Alamos Molecular Beam Dynamics Apparatus 1 (LAMBDA 1) to obtain O-atom beam velocity distributions.

LAMBDA 1, [Cross, 1984] shown in Figure 3, is being configured to test and calibrate a mass spectrometer (provided by AFGL) which is to be flown on STS to detect surface-desorbed etching reaction products as well as reactants in the ambient atmosphere. Our objective will be to use the high-energy laser sustained O-atom source to 1) determine detection sensitivity for 5-eV O-atoms and etching reaction products, 2) demonstrate the advantage of modulated phase-sensitive detection techniques in LEO experiments, 3) determine the contribution to LEO observations from gas-surface reactions occurring in the ion source, and 4) calibrate the AFGL mass spectrometer against the LAMBDA 1 mass spectrometer detector in order to relate ground-based investigations to LEO observations. This effort will provide the unique ability to directly compare future studies of etching mechanisms with LEO experiments and to provide an O-atom testing facility for use in materials development programs. LAMBDA 1 has demonstrated [Pack et al., 1982] high sensitivity and resolution in measurements of gas-phase collision dynamics and could also be used to measure elastic, inelastic, and reactive high-energy O-atom collision cross sections that would be used in future glow modeling.

Though LAMBDA 1 can be configured to also detect chemiluminescence, LAMBDA 2, shown in Figure 4, is better suited for these types of experiments and provides the instrumentation to detect reaction products from beam-surface scattering by 1) mass spectrometry, 2) chemiluminescence, or 3) laser-induced fluorescence in a UHV environment as well as providing surface characterization using Auger or XPS/UPS spectroscopy. Beam sources developed for the LAMBDAs are interchangeable between the two instruments, thus allowing comparison of results. We propose using this machine to investigate surface-catalyzed, gas-phase chemiluminescence produced by the interaction of high-energy oxygen and nitrogen beams with spacecraft materials. Representative surfaces would be exposed to an N/O atom beam, and measurements of 1) translational energy using time of flight techniques and 2) internal energy using laser-induced fluorescence would be performed to determine the extent of excitation. Through the combined use of LAMBDA 1 and 2 a complete picture of etching and glow mechanisms can be obtained, which would lay the basis for design of materials and processes for use in low-Earth orbit.

Conclusion

To achieve a sustained presence in low-Earth orbit new and novel materials will need to be developed that can resist the effects of long-term O-atom exposure. Heat rejection systems will require high temperature surfaces that will not erode or alter their IR emissivity over long periods of time (20 years). High strength-to-weight ratio epoxy-fiber composite structural materials will need protective coatings for long-term,

maintenance-free operation while silver interconnects on solar cell panels will require coatings or be replaced with more inert material. Methods for controlling or eliminating ram surface glow need to be devised to provide optimum conditions for infrared astronomy and Earth viewing. Before new materials can be devised, a basic understanding of etching and glow mechanisms will be required after which optimum design parameters for materials can be decided upon. Activated recombinative desorption of reaction products from surfaces may be a common thread in mechanisms of spacecraft glow, but a great deal of basic research into gas-phase and gas-surface dynamics will be needed to fully explain this phenomenon.

Los Alamos is uniquely equipped with instrumentation and staff to collaborate with NASA in fundamental investigations of LEO material problems. A traditional strength of the Laboratory is materials chemistry and physics from which facilities have been developed for ion microprobe investigations of subsurface bulk diffusion processes [Thompson et al., 1983], surface chemistry and physics [Campbell and Paffett, 1984], and theory [Doll, 1985] of gas-surface processes. The combination of LAMBDA 1 used for mass spectrometric angular and translational energy particle detection, LAMBDA 2 used for internal state and fixed laboratory angle translational energy detection, and the high-energy O-atom source represents an additional unique resource that can be focused to provide solutions to the challenges of extended operation in low-Earth orbit.

References

- Brown, L. S., and S. L. Bernasek, J. Chem. Phys., 82, 2110, 1985.
Campbell, C. T., and M. T. Paffett, Surf. Sci., 139, 396, 1984; 143, 517, 1984.
Comsa, G., and R. David, Surf. Sci., 117, 77, 1982.
Cross, J. B., Thirteenth Space Simulation Conference, October 8-11, 1984, Orlando, Florida, NASA Conference Publication 2340.
Cross, J. B., and D. A. Cremers, AIAA 23rd Aerospace Sciences Meeting, January 14-17, 1985, Reno, Nevada, AIAA Paper #85-0473.
Doll, J. D., Monte Carlo Fourier Path Integral Methods in Chemical Dynamics, J. Chem. Phys., in press, 1985.
Engebretson, M. J., and K. Mauersberger, J. Geophys. Res., 84, 839, 1979.
Kahler, C. C., E. Ansell, C. M. Upshur, and W. H. Green, Jr., J. Chem. Phys., 80, 3644, 1984 (and references therein).
Kubiak, G. D., G. O. Sitz, and R. N. Zare, J. Chem. Phys., 81, 6397, 1984.
Pack, R. T., J. J. Valentini, and J. B. Cross, J. Chem. Phys., 77, 5486, 1982.
Robota, H. J., W. Vielhaber, M. C. Lin, J. Segner, and G. Ertl, Surf. Sci., in press, 1985.
Swenson, G. R., S. B. Mende, and K. S. Clifton, Geophys. Res. Lett., 12, 97, 1985.
Thompson, K. A., W. P. Ellis, T. N. Taylor, S. M. Valone, and C. J. Maggiore, Nucl. Instr. and Methods Phys. Res., 218, 475, 1983.
Thorman, R. P., and S. L. Bernasek, J. Chem. Phys., 74, 6498, 1978.
van den Ende, D., S. Stolte, J. B. Cross, G. H. Kwei, and J. J. Valentini, J. Chem. Phys., 77, 2206, 1982.

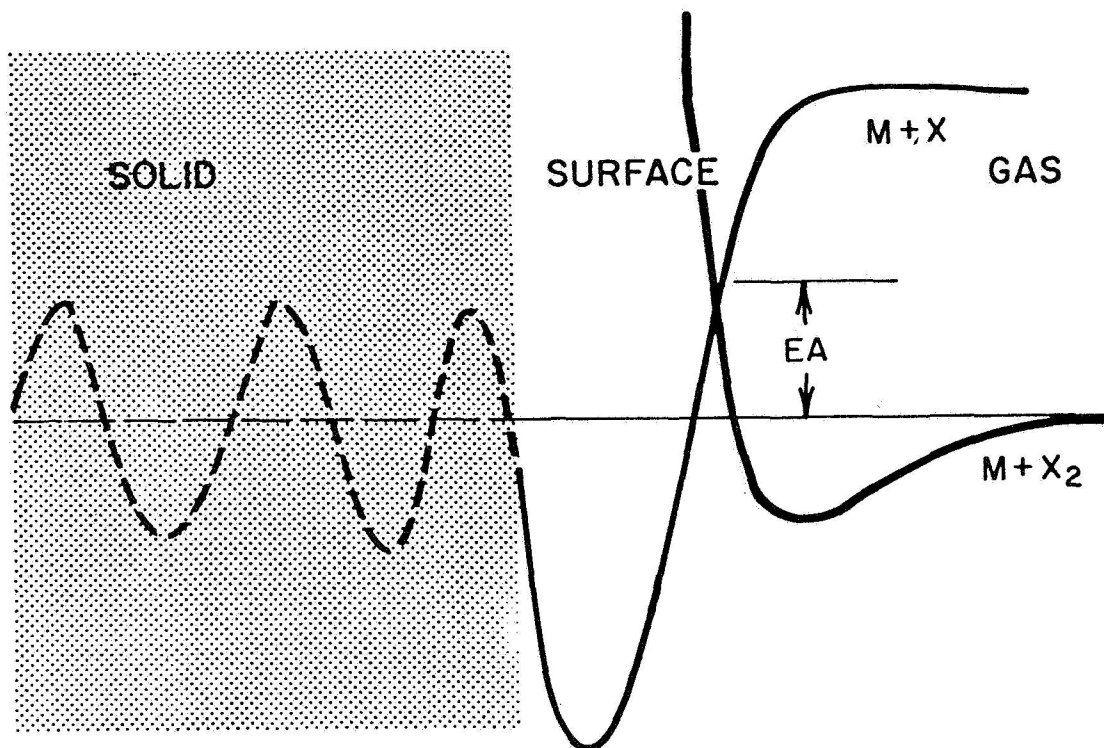


Fig. 1. Potential energy diagram representing activated desorption. Molecules colliding with a surface can be trapped in a molecular precursor well or with sufficient collision energy to surmount the barrier EA and cross to the dissociative atomic state curve and be chemically trapped. In most cases, desorption occurs with the expulsion of molecules X_2 rather than X , and the molecule exits the surface with energy EA . In some cases (see Comsa and David [1982]), the two-dimensional surface has holes in it and molecules can exit over the barrier and are not affected by surface temperature, while other molecules come from states without barriers and are accommodated to the surface conditions.

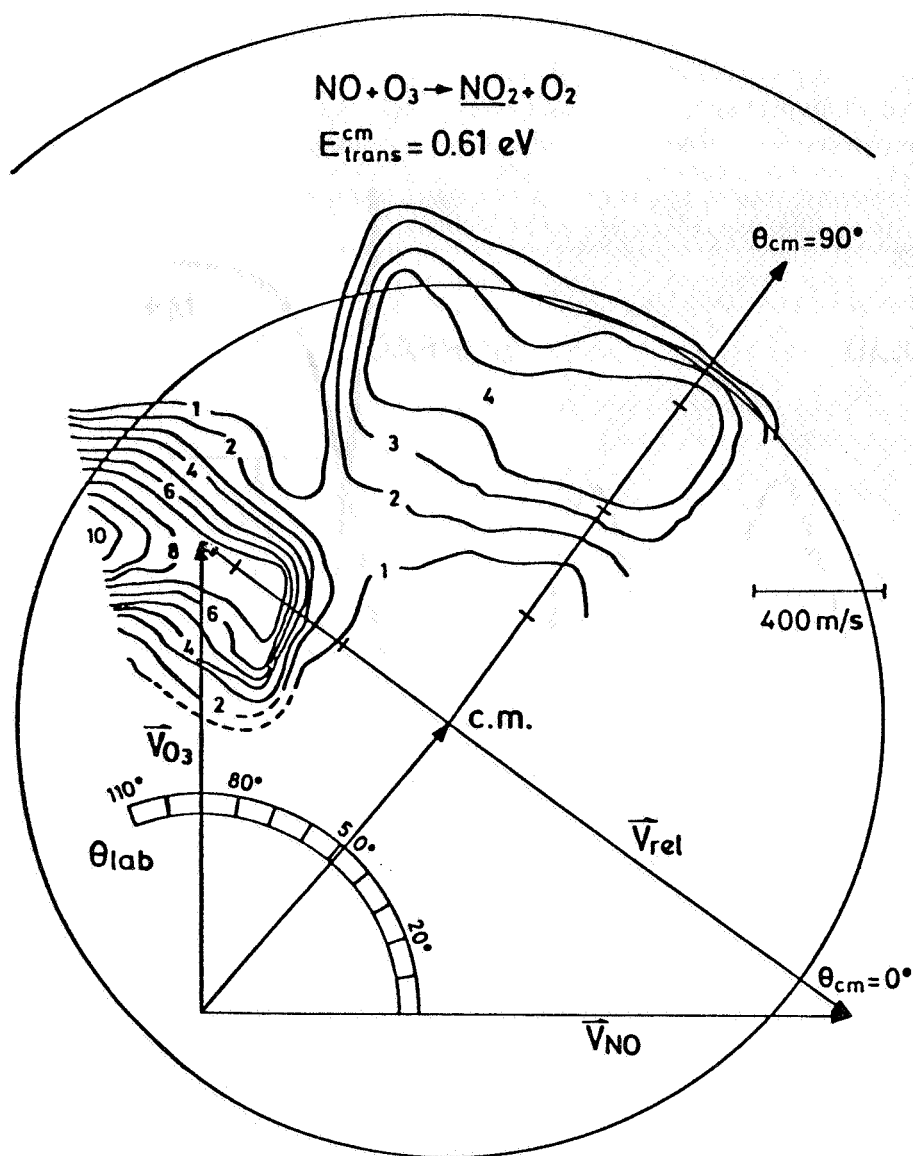


Fig. 2. Center-of-mass contour map of the NO_2 flux distribution obtained from laboratory angular and time-of-flight distribution measurements by performing a 1-Newton diagram transformation of the gas-phase data. There is a narrow backward NO_2 peak and a broad sideways peak which are clearly separated. The outer circle indicates the velocity of NO_2 when all available energy is put into translation while the inner one gives the maximum velocity at which chemiluminescence is possible. The majority of product has high internal excitation. NO_2 formed by recombination of $\text{NO} + \text{O}$ on oxide surfaces may exhibit similar dynamics.

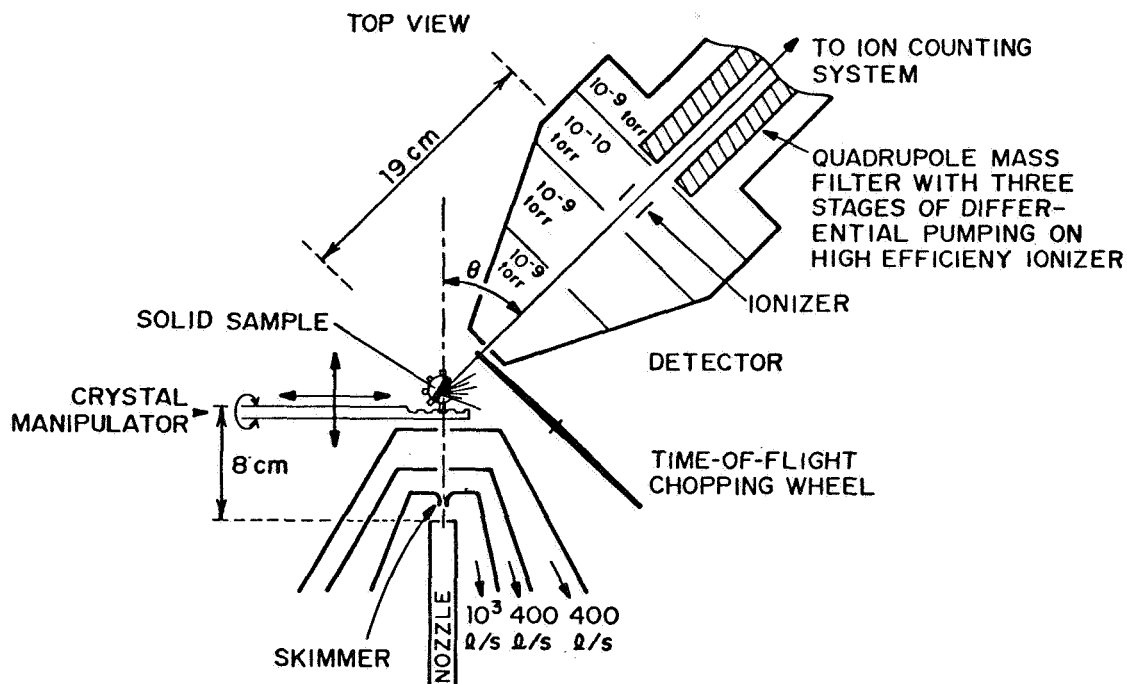


Fig. 3. Los Alamos Molecular Beam Dynamics Apparatus 1 (LAMBDA 1) showing the central portion of the instrument including the molecular beam source, sample manipulator-molecular beam intersection zone, and a portion of the movable detector. The detector is an electron bombardment ionizer-quadrupole mass spectrometer suspended from the rotatable lid of the main vacuum chamber for the measurement of angular distributions. Also shown is a time-of-flight chopping wheel, which allows for 50% transmission efficiency and time-of-flight measurement by cross correlating the data with the sequence. Pumping on the scattering chamber is accomplished with a liquid nitrogen cryoliner, turbomolecular pump, and a closed-cycle gaseous helium cryopump. Pressures of 10^{-8} to 10^{-9} torr are obtained in the scattering chamber.

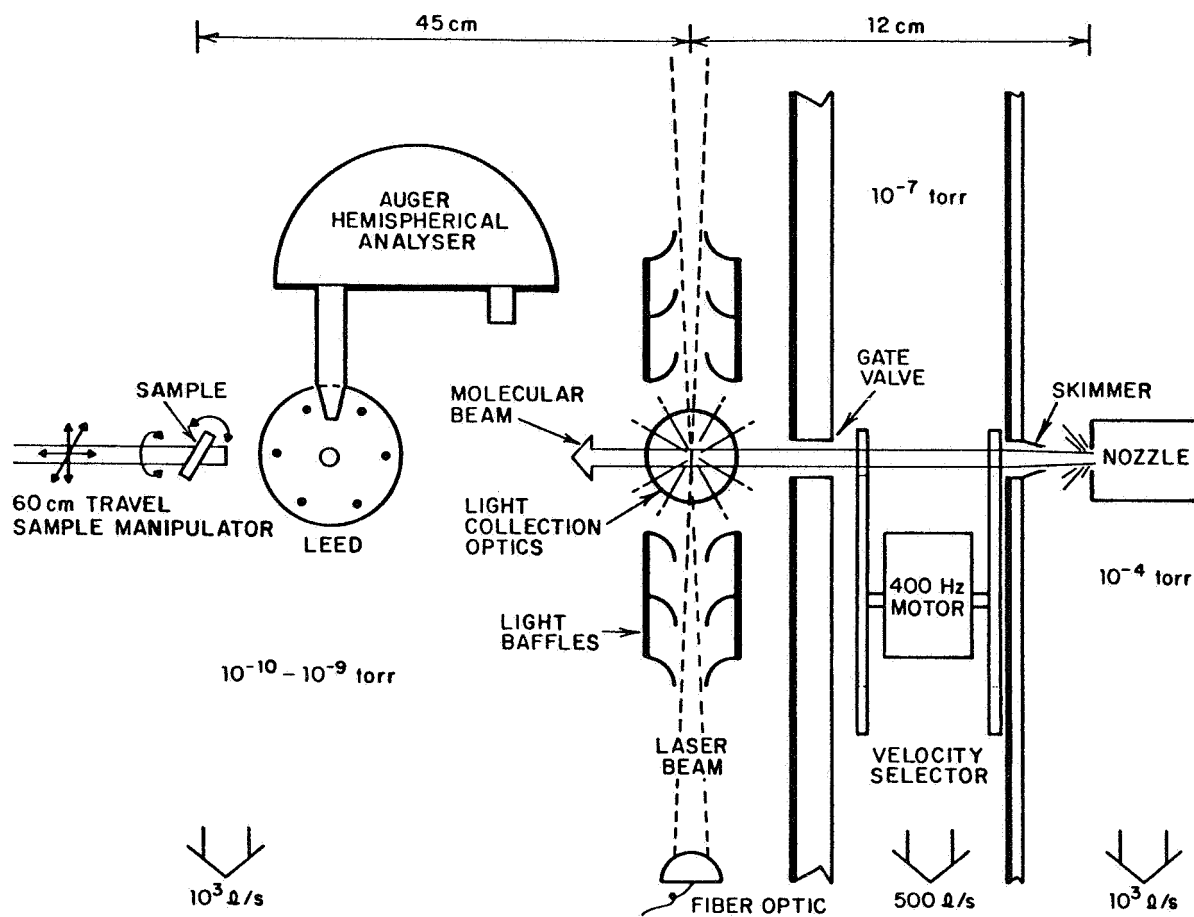


Fig. 4. LAMBDA 2. This figure shows a detailed view of the central portion of the apparatus that consists of a nozzle chamber, a differential pumping chamber containing flags, choppers, and a slotted disk velocity selector; and a UHV (10^{-10} torr) chamber containing a cyroshroud, sample manipulator, surface analysis equipment consisting of LEED and Auger units, provision for collecting fluorescence light and laser-induced fluorescence signals. A quadrupole mass spectrometer (not shown) with two stages of differential pumping and a cross correlation time-of-flight chopper is opposite the LEED unit and is limited to a fixed laboratory angle.

LABORATORY MEASUREMENTS

OPTICAL RADIATION FROM THE INTERACTION OF ENERGETIC ATOMS, IONS,
ELECTRONS, AND PHOTONS WITH SURFACES

N. H. Tolk, R. G. Albridge, R. F. Haglund, Jr., and M. H. Mendenhall

Department of Physics & Astronomy, Vanderbilt University

J. C. Tully

AT & T Bell Laboratories

Abstract. Heavy particle, electron, and UV photon bombardment of solid surfaces has been recently observed to result in the emission of infrared, visible, and ultraviolet radiation. This effect occurs over a wide range of incident projectile energies. Line radiation arising from transitions between discrete atomic or molecular levels may be attributed to the decay of excited particles which have been sputtered or electronically/chemically desorbed from the surface. Broadband continuum radiation, which is also observed, is believed to arise either from fluorescence of the near surface bulk or from the radiative decay of desorbed excited clusters. The spectral characteristics of the optical radiation as well as the efficiencies for producing it may vary substantially with the identity, form and cleanliness of the surface, and on the identity and energy of the bombarding particle. Spacecraft, in the ambient near-Earth environment, are subject to such bombardment. The dynamics of energetic particle and photon beam interactions with surfaces which lead to surface erosion and glow phenomena will be treated. In addition, projected experimental and theoretical studies of oxygen and nitrogen beam-surface interactions on materials characteristic of spacecraft surfaces will be discussed.

Introduction

Exterior surfaces of spacecraft in near-Earth orbit are bombarded by a formidable assortment of neutral and ionized atoms and molecules, in addition to electrons and ultraviolet photons. Heavy particle bombardment arises largely from the motion of the vehicle through the ambient environment. However, enhanced solar activity and artificial environments associated with disturbed nuclear atmospheres and directed energy beams may increase the energy and intensity of the bombarding particles.

Over a wide range of bombarding energies, particle and photon interactions with surfaces have been shown to result in the efficient desorption of surface atoms and molecules. Many of these are desorbed in excited states which subsequently emit characteristic infrared, visible, and ultraviolet radiation. We will review recent work on this topic and discuss future studies of ion-, electron-, and photon-induced erosion and glow phenomena.

Photon Emission from Ion and Neutral Particle Impact on Surfaces

In the experimental observations to be treated below, three distinct kinds of collision-induced optical radiation have been identified.

The first of these is line radiation due to sputtering with simultaneous excitation. The interaction of the impinging ion or neutral beam with the surface results in the sputtering of neutral atoms, neutral molecules, and ions from the surface. A significant portion of the sputtered particles leaves the surface in excited electronic states which then decays and gives rise to optical line radiation characteristic of surface constituents [Tolk et al., 1977].

The second kind of radiation observed has a similar nature but arises from backscattered excited beam particles which have escaped the surface after having experienced collisions in the bulk material [Leung et al., 1978]. To the extent that the momentum-changing collisions do not effect the final excited state configuration of the emerging particles, this class of phenomena is identical to the beam foil radiation phenomenon. Studies of backscatter radiation provide more complete information on final states than conventional charge state measurements and give important insights into the nature of the interaction of the emerging particle with the surface.

The final and perhaps least understood type of radiation is the broad continuum of radiation that is observed from many of the solid materials studied. In the case of metals, for a given beam projectile at a given energy, the shape of the continuum is observed not to change for a variety of metal surfaces [White et al., 1976]. For insulators, the shape of the continuum as a function of wavelength is entirely characteristic of the material and independent of the beam particle species. An important conclusion from these studies is that the collision participants, both the solid itself as well as the escaping atomic and molecular fragments, in general are in excited states following the collision interaction. The collision participants may then produce the observed photons by radiative decay or may undergo radiationless de-excitation processes such as Auger de-excitation.

Metallic Targets

The spectra of radiation observed when Ar^+ ions at 4000 eV impact on Ni and Cu targets are shown in Figure 1. Most of the prominent lines in these spectral scans have been identified as arising from low-lying energy levels of neutral Ni and Cu, sputtered off the surface in excited states by the incident ion beam. In addition to spectral lines from the surface target materials, radiation is also often observed which is characteristic of surface contaminants [Tolk et al., 1973]. The molecular radiation centered at 4300 Å and 3900 Å has been identified as arising from the $A^2\Delta \rightarrow X^2II$ and $B^2\Sigma - X^2II$ electronic transitions of the CH molecule. This radiation is believed to originate from collisional excitation of adsorbed hydrocarbon surface contamination. The prominent line which is often observed at approximately 5900 Å is the NaD line doublet which is assumed to arise from sodium contaminants deposited on the surface. The surface can be cleaned to such an extent that the contaminant radiation is negligible by prolonged exposure (approximately 20

minutes) to a 3-keV argon ion beam or by heating the target.

Our measurements show that for metallic targets, beams of neutrals and ions (of the same species) produce photons due to sputtering with equal efficiency. Low-velocity ions with sufficiently large ionization potential impacting on a metal surface are neutralized by non-radiative processes several angstroms in front of the surface, well before the sputtering interaction occurs. It is reasonable then to assume that the radiation which results from the sputtering interaction should be the same for beams of ions or neutrals at the same velocity. This assumption has been verified experimentally using a bolometer to independently measure the neutral "current." These results consequently suggest a means of directly measuring neutral beam flux in the low-energy region. It follows from the above discussion that the ratio of the intensity of the optical line radiation produced when a metallic target is bombarded with neutrals to that produced when the same target is bombarded with ions is equal to the ratio of the neutral to ion fluxes thus leading to a direct measurement of the neutral "current." In principle, this technique could also be extended to non-metallic surfaces using a more complicated calibration scheme.

Insulator Targets

The spectral distribution of radiation arising from excited sputtered particles due to the impact of nitrogen molecules (N_2^0) at a beam energy of 3.5 keV on aluminum oxide (Al_2O_3), lithium fluoride (LiF), and quartz (SiO_2) is shown in Figure 2. Optical scans taken using neutral beams of neon, argon, and other heavy particles give similar results. Neutral beams rather than ion beams are used for the bombardment of insulators in order to avoid ion beam energy decrease and defocusing due to charge buildup on the insulator surface. Ion beams may also be used, however, if the insulator surface is bathed in electrons emitted from a nearby heated filament. In Figure 2, the more intense lines are identified as arising from the decay of excited states of neutral aluminum, lithium, silicon, and hydrogen. Because the line widths are found in these experiments to be equal to the instrumental resolution (about 1 angstrom), we may assume that the radiation originates from individual atoms and molecules which have been sputtered off the surface in excited states which subsequently decay by photon emission. The Balmer lines of neutral hydrogen are believed to arise from the sputtering of surface contaminants.

For all cases studied--metals, semiconductors and insulators--optical radiation has been observed due to sputtering with simultaneous excitation. However, in the insulator case, the excitation efficiency is observed to be much larger than for metals. For the case of metals, typical prominent lines are estimated to have excitation efficiencies of the order of 10^{-5} (photons per incident ion) while in the insulator case, the excitation efficiencies are measured to be two or three orders of magnitude higher [Tolk et al., 1977].

Optical Radiation from Electronically Desorbed Particles

For the case of heavy-particle induced sputtering as discussed above, understanding the influence of surface parameters on the final state of sputtered particles is complicated by the fact that the ejection of atoms and molecules results from both electronic and momentum changing processes. Electron- and UV photon-stimulated desorption of atoms and molecules, on the other hand, involves only electronic interactions.

Even though it is known that the most abundant products of electronically induced desorption are neutral atoms and molecules, most studies have involved desorbed ions. This is due primarily to the ease of detection of ions. In only a few cases have neutrals desorbed by electron and photon impact been directly studied.

It is useful to describe the mechanisms of electron and photon-induced desorption as a three-stage process: (1) the initial deposition of electron energy by, for example, the creation of a hole, two holes, an exciton, or a defect; (2) a fast electronic rearrangement leaving a surface atom or group of atoms in a localized repulsive or energetic state; and (3) further particle-surface electronic interaction as the atom, or molecule, or cluster leaves the surface. Although not treated here, recent observations of strong elliptic polarization of optical radiation following grazing incidence of 9-keV protons on crystal surfaces contribute unique information on stage (3) electronic processes [Tully et al., 1981]. Studies of these phenomena promise to provide new insight into the electronic aspects of atomic collisions in solids [Tolk et al., 1981b]. In this paper we discuss recent measurements of electronically desorbed neutrals obtained by observing optical radiation which arises from neutrals desorbed in excited states.

Electron Stimulated Desorption (ESD) of Excited Particles

Although it is now generally accepted that the most abundant products of desorption from surfaces induced by electronic transitions, stimulated by energetic electrons or UV/soft x-ray photons, are neutral atoms and molecules, only a very few results have been published about neutral desorption. These experiments confirm the leading role of neutrals in the desorption process.

Our approach to the detection of desorbed neutrals is based on analysis of the optical radiation emitted by decays after desorption [Tolk et al., 1981a]. The experimental equipment included an ultrahigh vacuum chamber, a primary excitation source, and an optical detection/analysis system with a monochromator and computer-controlled data processing. Initially, the excitation source was an electron beam. Figure 3 shows spectra of atomic and molecular radiation emitted by desorbed atoms and molecules from NaCl, NaF, and LiF surfaces, principally from excited alkalis, hydrogen, OH, and an unidentified molecular species.

In marked contrast to ion bombardment and gas discharges, the only sodium and lithium radiation detected in these experiments are first resonance lines. This indicates that for alkali halides there exists a strong nonstatistical state selection mechanism of an as-yet undetermined nature. Energy-dependent measurements show

onsets correlated to core hole formation relating to the initial energy deposition process. Electron-stimulated erosion of alkali halides is usually attributed to the creation of defects which results in the ejection of halogen atoms and leaves excess alkali atoms to desorb thermally from the surface. This does not appear to be adequate to explain the emission of excited neutrals. It is likely that this latter process involves the creation of a long-lived localized surface excitation, perhaps an exciton, which results in ejection of a surface atom and in addition supplies the excited electron.

Photon Stimulated Desorption (PSD) of Excited Particles

Desorption of excited particles was recently observed when UV photons from the University of Wisconsin synchrotron storage ring, with energies of 40-200 eV, were incident on alkali-halide surfaces [Tolk et al., 1982]. As shown in Figure 4 photon energy dependent measurements were taken of optical radiation arising from the decay of desorbed excited Li atoms. These data are compared with PSD measurements of positive ions from the same LiF sample. Both measurements showed pronounced energy-dependent structure similar (though not identical) to soft x-ray absorption coefficient measurements also presented in Figure 4. It should be noted that the yield of excited neutrals was measured to be at least 3 orders of magnitude greater than the corresponding yield of desorbed ions. Similar to the ESD case, only the first resonance level is observed. In light of these observations, a plausible three-step desorption scheme for excited neutrals may be hypothesized [Tolk et al., 1983, 1984]: (1) The incoming photon creates a core or valence excitation near the surface which provides electronic energy to the system. (2) One or a series of secondary electronic processes occur, resulting in a localized valence excitonic state, which leaves the surface alkali atom in a highly energetic or repulsive state. (3) As the alkali atom departs, the lowest excited state is preferentially populated because it is both at lower energy and more localized than the higher excited states.

Laboratory Studies of Spacecraft Glow

At Vanderbilt University, we have initiated studies of the dynamics of particle- and photon-beam interactions which lead to surface erosion and glow phenomena, emphasizing materials and surface conditions relevant to spacecraft in the near-Earth environment. This research uses facilities available at Vanderbilt and at the University of Wisconsin synchrotron storage ring for studying the interactions of directed beams of ions, neutrals, electrons, and UV photons with well-characterized surfaces under carefully controlled vacuum conditions.

Work is progressing toward the development of a high-flux beam of energetic neutral oxygen and nitrogen atoms using an existing ion source at Vanderbilt to compare ion bombardment with corresponding neutral bombardment on relevant surfaces. Desorption experiments are also in progress on metallic surfaces with controlled doses of relevant adsorbates (e.g., N_2 and O_2), to ascertain changes in surface electronic and bonding properties induced by contaminants. Finally, experiments on possible synergistic effects--as in simultaneous ion-electron and ion-photon bombardment--are now feasible and will

be carried out in the near future.

Conclusions

As discussed above, when particles impact on surfaces, many complex interrelated processes occur as the incident energy is transformed into electronic and sometimes thermal excitations. Previous studies of electronically-induced desorption have shown much of the incident energy may be channeled into bond-breaking and desorption processes leading to ejection of surface atoms and molecules from metal oxides and insulators. Thus, electronic, chemical, and thermal processes stimulated by energetic beams can play a major role in surface modification and damage, through erosion, changes in tribological properties, and migration of electronically-induced defects. The primary effort is to understand the fundamental mechanisms underlying these processes. These studies will generate an increasingly detailed microscopic view of the dominant modes through which incident energy is absorbed, localized, and redirected to desorption. This, in turn, leads to a comprehensive macroscopic picture of material ejection, erosion, and ablation from surfaces and of the associated optical emissions.

References

- Leung, S. Y., N. H. Tolk, W. Heiland, J. C. Tully, J. S. Kraus, and P. Hill, Optical radiation from low-energy hydrogen atomic and molecular ion-surface collisions, Phys. Rev., A18, 447, 1978.
- Tolk, N. H., D. L. Simms, E. B. Foley, and C. W. White, Photon emission from low-energy ion and neutral bombardment of solids, Radiation Effects, 18, 221-229, 1973.
- Tolk, N. H., I.S.T. Tsong, and C. W. White, In-situ spectrochemical analysis of solid surfaces by ion beam sputtering, Analytical Chemistry, 49, 16A, 1977.
- Tolk, N. H., L. C. Feldman, J. S. Kraus, M. M. Traum, and J. C. Tully, Optical radiation from electron stimulated desorption of excited particles, Phys. Rev. Lett., 46, 134, 1981a.
- Tolk, N. H., L. C. Feldman, J. S. Kraus, J. C. Tully, M. Hass, Y. Niv, and G. M. Temmer, The role of surface interactions in beam foil excited state formation, Phys. Rev. Lett., 47, 487, 1981b.
- Tolk, N. H., M. M. Traum, J. S. Kraus, T. R. Pian, W. E. Collins, N. G. Stoffel, and G. Margaritondo, Optical radiation from photon-stimulated desorption of excited atoms, Phys. Rev. Lett., 49, 812, 1982.
- Tolk, N. H., W. E. Collins, R. J. Morris, T. R. Pian, J. S. Kraus, M. M. Traum, N. G. Stoffel, and G. Margaritondo, The electronic desorption of excited alkali atoms from alkali halide surfaces, chapter in Desorption Induced by Electronic Transition, edited by N. H. Tolk, M. M. Traum, J. C. Tully, and T. E. Madey, Springer-Verlag, Heidelberg, 1983.
- Tolk, N. H., P. Bucksbaum, N. Gershenfeld, J. S. Kraus, R. J. Morris, D. E. Murnick, J. C. Tully, R. R. Daniels, G. Margaritondo, and N. G. Stoffel, Desorption induced by electronic transitions, Nucl. Instr. and Meth. in Physics Research, B2, 457, 1984.

Tully, J. C., N. H. Tolk, J. S. Kraus, C. Ran, and R. Morris, Polarization on surfaces, chapter in Springer Tracts in Chemical Physics, edited by W. Heiland and E. Taglauer, p. 196, Springer-Verlag, Heidelberg, 1981.

White, C. W., N. H. Tolk, J. S. Kraus, and W. F. van der Weg, Continuum optical radiation produced by low-energy heavy particle bombardment of metal targets, Nucl. Instr. and Meth., 132, 419, 1976.

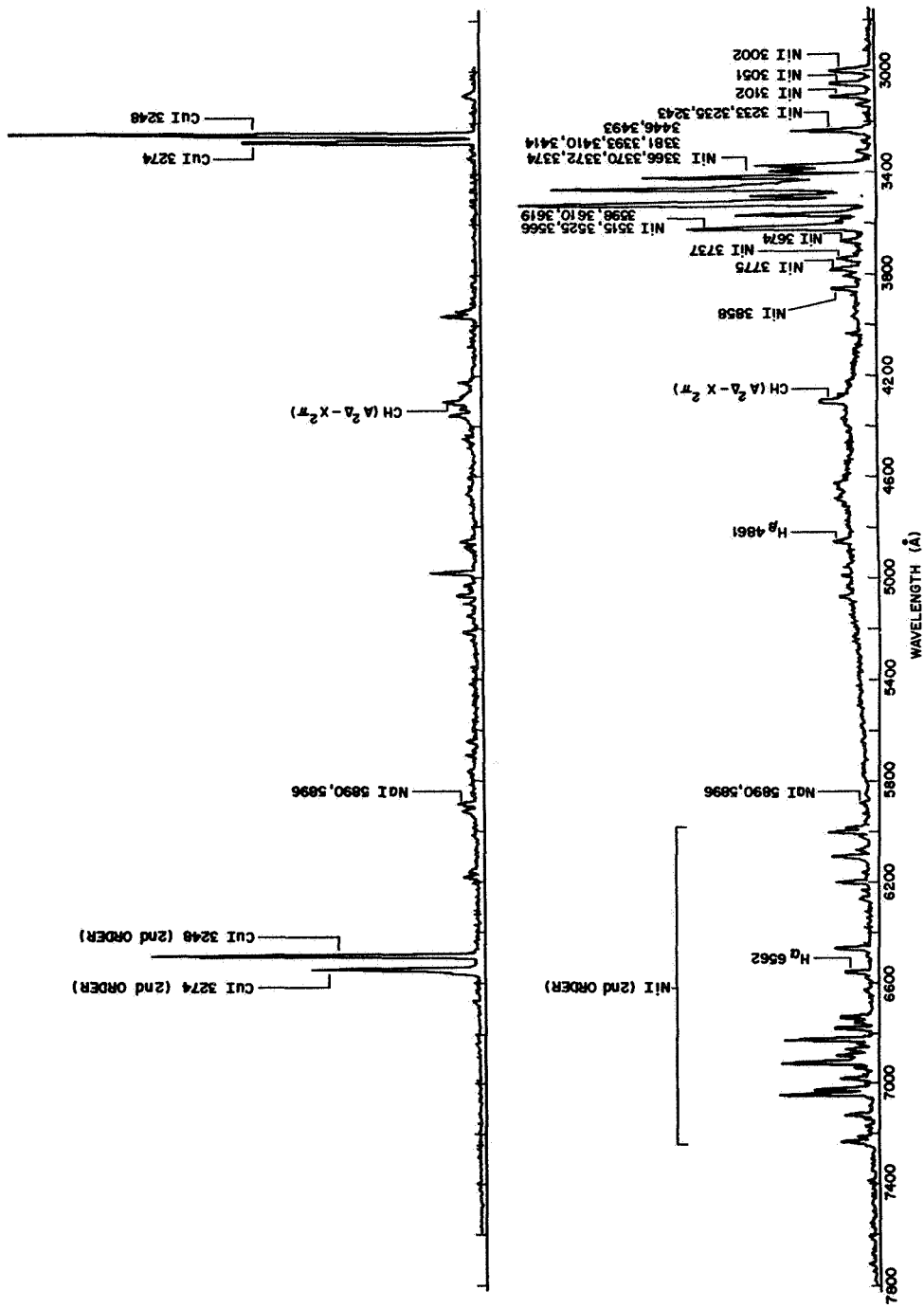


Fig. 1. Spectra of radiation produced by the impact of Ar^+ (at 4 keV) on copper (top) and nickel (bottom). Lines arising from excited states of sputtered copper, nickel, and various contaminants are observed in this wavelength interval.

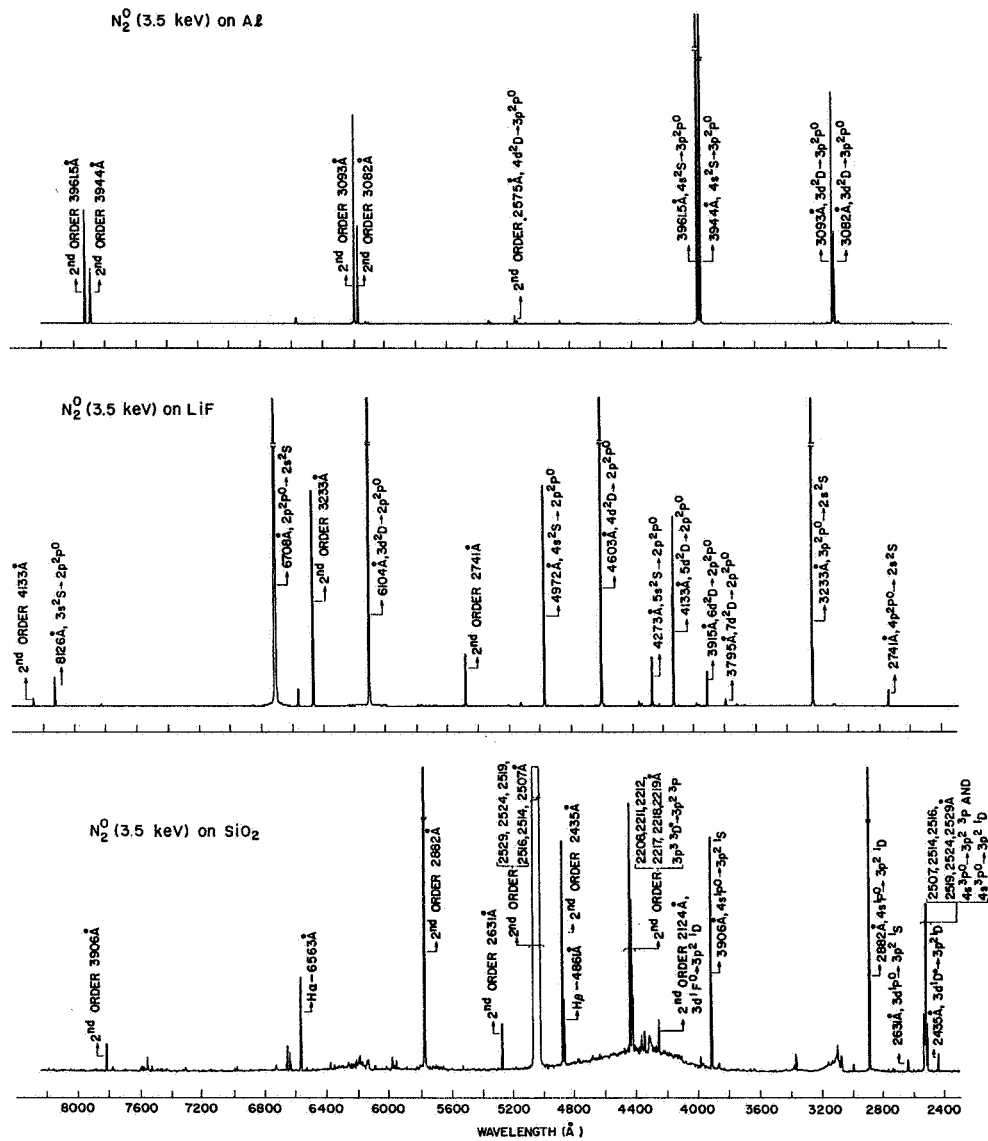


Fig. 2. Spectrum of radiation produced by the impact of N_2O (3.5 kiloelectron volts) on Al_2O_3 , LiF, and SiO_2 . Lines arising from excited states of neutral aluminum, lithium, and silicon are observed in this wavelength interval. The wavelength and electronic transition are indicated beside each line. Two Balmer lines of neutral hydrogen, H_α and H_β , are observed on the SiO_2 scan.

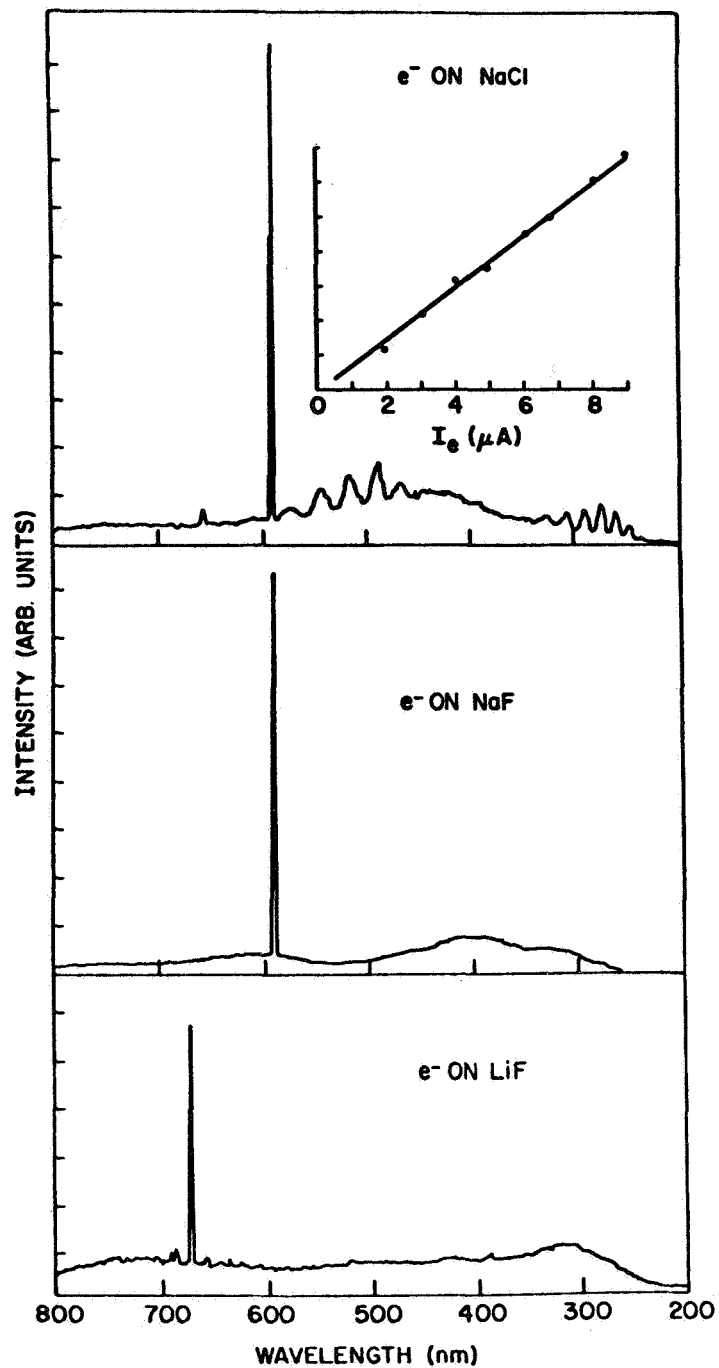


Fig. 3. Spectra of radiation produced by 1-keV e⁻ impact of NaCl, NaF, and LiF, obtained at approximately 90° to the surface normal. The inset shows the linear behavior of the intensity of the NaD line as a function of incident e⁻ current. A straight line has been drawn through the data points.

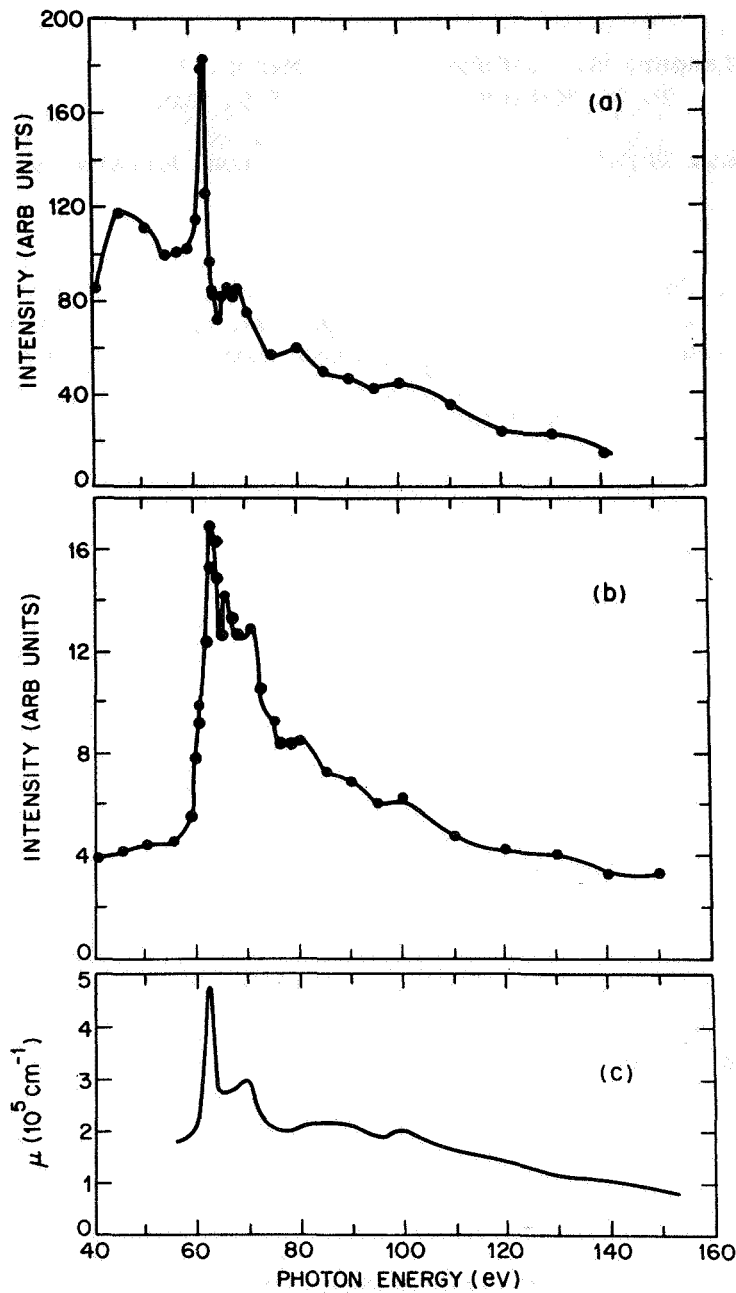


Fig. 4. (a) Li^* (670.7 nm) optical emission dependence on soft x-ray energy using a (100) single-crystal LiF sample at room temperature. (b) Positive-ion yields as a function of incident photon energy using the same sample at about 250 °C. (c) Photon absorption coefficient measurements.

A GROUND-BASED EXPERIMENTAL TEST PROGRAM TO
DUPLICATE AND STUDY THE SPACECRAFT GLOW PHENOMENON

W. D. Langer, S. A. Cohen, D. M. Manos, D. H. McNeill
R. W. Motley, M. Ono, and S. Paul

Plasma Physics Laboratory, Princeton University

Abstract. We discuss the use of a plasma device, the Advanced Concepts Torus-I, for producing atoms and molecules to study spacecraft glow mechanisms. A biased metal plate, located in the plasma edge, will be used to accelerate and neutralize plasma ions, thus generating a neutral beam with a flux $\gtrsim 5 \times 10^{14}/\text{cm}^2/\text{sec}$ at the end of a drift tube. Our initial experiments will be to produce a 10 eV molecular and atomic nitrogen beam directed onto material targets. Photon emission in the spectral range 2000 to 9000 Å from excited species formed on the target surface will be investigated.

Introduction

The Advanced Concepts Torus-I (ACT-I) will be used at the Princeton Plasma Physics Laboratory to produce a source of neutral atoms and molecules to study spacecraft glow. In this paper, we list the characteristics of the machine and describe the experimental arrangement and research program. We estimate that this plasma device can be used to produce the flux of neutrals on a sample located in a test chamber outside ACT-I greater than $5 \times 10^{14}/\text{cm}^2/\text{sec}$, similar to that encountered in the environment of the Atmosphere Explorer satellite and the space shuttle. We made spectroscopic studies of a nitrogen plasma in ACT-I and detected emission from N_2 and N_2^+ . Preliminary experiments have been conducted using a small biased limiter to generate neutrals, and the measured currents are consistent with our predictions that ACT-I has the properties to produce the desired neutral flux.

The ACT-I Device

ACT-I is a steady-state toroidal machine (Figure 1 and Table 1) built primarily to study radio frequency heating and current generation in plasmas [Wong et al., 1981]. The characteristics of the plasma formed in ACT-I are such that it can be converted into a copious source of neutrals with energies of 3 to 100 eV. The plasma characteristics for both steady-state and pulsed operation are given in Table 1. The machine consists of 26 sets of toroidal field coils which produce up to a 5.5 kg steady-state magnetic field. The vacuum chamber has 26 toroidal segments with large ports (10 cm

x 40 cm). A 600 kW motor-generator set provides steady-state power to the coils which are cooled by pressurized de-ionized water. ACT-I has been operated with a variety of gases, including H, He, Ne, Ar, N₂, and air.

A Neutral Source

Ions formed in ACT-I are confined for about 1 msec and most of them are lost by drifting radially outward across field lines onto the outer wall. A fraction of these ions (~0.3) can be intercepted on a metallic plate, a so-called limiter, where they are neutralized and reflected. A calculation of reflectivity of neutrals formed in this manner using the TRIM code [Biersack and Haggmark, 1980] predicts that a high percentage of the incoming particles is reflected with nearly their full energy if the mass of the atoms making up the target (limiter) is much greater than that of the incoming particles. Furthermore, the code predicts that by positioning and orienting the limiter appropriately a high percentage of the neutrals will be directed out of the machine where they can enter a drift tube (Figure 2). A target will be mounted in a test chamber at the end of this tube and the glow resulting from the neutral-surface interaction will be observed in this chamber. The limiter may be biased to accelerate the ions and produce neutrals with an adjustable range of energies.

Estimate of Neutral Flux

What makes this device an effective plasma source for the glow problem is that it can sustain a dense plasma with a warm bulk ion temperature ($T_i > 1$ eV), with sufficient volume, to produce a large steady-state source of plasma with $T_e = 1$ to 15 eV. The plasma source can readily be converted into a large flux of energetic neutrals as described above. The ion source from the entire plasma, S_i , can be estimated as

$$S_i = \frac{nV_p}{\tau_c} = 1 \times 10^{20}/\text{sec} , \quad (1)$$

[see Table 1 for the symbols and values used in Eq. (1)]. The neutral source, S_n , depends on the fraction of ions that intersect the biased limiter as they drift outward. Ions from the center of the plasma travel roughly half way around the torus in the time they drift radially outward. By inserting the biased limiter a few centimeters into the plasma about a third of the particles can be intercepted. In practice, the port opening to the drift tube restricts the fraction that can be used to about a quarter of the ion source. The energy will depend on the bias voltage applied to the limiter. The flux onto the sample depends on the fraction of neutrals reflected into a solid angle at the end of the drift tube, Ω_s . The reflected particles are forward-peaked giving $\Omega_s \approx \pi d^2$ where d is the distance from the limiter to the sample. Though the TRIM code predicts about eighty percent reflection, we assume only fifty

percent to make a conservative estimate of the neutral flux. Therefore, $S_n \approx S_i/8$, and the flux on a target located 1 meter away is

$$\Gamma_n = \frac{S_n}{\pi d^2} \sim 5 \times 10^{14} / \text{cm}^2 / \text{sec} . \quad (2)$$

Diagnostics and Spectroscopy

We will install diagnostics to look at the plasma source, the energetic neutrals in the drift tube, and the molecular emission in the test chamber. The plasma temperature and density are measured with a triple Langmuir probe and microwave interferometer; the spectroscopic signature of the plasma is also monitored. This information is needed to optimize the plasma for production of neutrals and identification of any contribution of the plasma light to the background in the test chamber.

Screening of Background Light and Velocity Selection

In the test chamber, it is crucial to screen out the background plasma light. An effective technique for screening is to use a rapidly rotating slotted chopper disk on the port end of the drift tube (Figure 2) [Voss and Cohen, 1982]. The flight time for 5 to 10 eV neutrals down a 1-meter tube is about 100 microseconds, and the rotor speed must be about 10,000 rpm for the configuration used here. The chopper can be used as a velocity selector if two slotted disks are mounted with a phase shift between the slots in the blades. Such devices have been built at PPPL and used for experiments with hydrogen neutrals produced by charge exchange within the Princeton Large Torus. The following techniques will also be employed to reduce the background light: (1) the position of the biased limiter over the port will obscure the line-of-sight to the bulk of the plasma (Figure 2), and (2) baffles in the drift tube to block light reflections. The sample will be mounted perpendicular to the drift tube and the line-of-sight will graze the target and pass into a light dump so that only photons from the glow should be detected. Prior to the installation of a rapidly rotating chopper a slow chopper containing open and glass slots can be used to subtract any remaining background light.

Spectroscopy

We estimate a photon source in the visible of $5 \times 10^{10} / \text{sec}$ produced on a sample with an area of 10^2 cm^2 , assuming an efficiency of photon production in the visible of 10^{-6} due to the interaction of the neutrals with the surface. Because most of the glow will appear within 10 cm of the target surface, the photon production rate coefficient within the emitting volume (10^3 cm^3) is $\phi = 5 \times 10^7 / \text{cm}^3 / \text{sec}$. We shall use

calibrated interference and/or color filters with photomultipliers for initial, sensitive broadband detection of glow effects. The sample will be viewed at different angles from 2000 to 9000 Å using two or more calibrated Czerny-Turner spectrometers. The spectra from a 1 cm wide slice of the volume will then be measured with 25 Å resolution using a f/4.8, 0.32 m monochromator with a 1200/mm grating. With this configuration the counting rate in the visible should be 4×10^2 pulses/band/sec assuming a detector quantum efficiency of 0.1 and a light source spread uniformly over a hundred bands from 3500 to 6000 Å. A larger counting rate is expected in the infrared regime, 6000-9000 Å, because the increased photon production due to the neutral-surface interaction will more than offset the decrease in detector sensitivity. Once any glow has been detected, we will observe the spectra with higher resolution and extend the observations into the infrared to 2 microns.

Characterization of the neutral beam is important and an in-line quadrupole mass spectrometer will be employed at the end of the drift tube to determine the relative concentration of atoms and molecules. Initially, the beam intensity will be estimated by the rise in gas pressure at the end of the drift tube. Later we will install a direct low-energy beam monitor, such as a pyroelectric detector.

Experimental Results

Our spacecraft glow experiment began in mid-April and, presently, we are studying the operation and characteristics of a nitrogen plasma. The spectrum of an ACT-I nitrogen plasma over 5000-9000 Å with 8 Å resolution is shown in Figure 3. Structure of bands from the first positive system of N_2 can be seen clearly between 5500 and 8000 Å. The spectrum shown here rolls off above 9000 Å because the GaAs photomultiplier loses sensitivity and below 5000 Å because a long pass filter with a 5000 Å cutoff was used to eliminate higher order signals in the spectrum. The figure includes a relative sensitivity curve, which must be multiplied by the spectrum intensity to give the relative intensity of the plasma light as a function of wavelength. Higher resolution spectra at 3500-4200 Å (Figure 4) show the first negative spectrum of N_2^+ and the second positive spectrum of N_2 . We also see in this figure features which may tentatively be identified as belonging to CN and trace amounts of other carbon containing species. The temperature and density of the bulk plasma in these discharges were $\sim 3 \times 10^{12} \text{ cm}^{-3}$ and $T_e \sim 5 \text{ eV}$, and the N_2 filling pressure was $\sim 1.6 \times 10^{-4}$ Torr. The plasma was operated in a pulsed mode with 10 ms pulses and a duty cycle of one-half driven by a 5 A electron beam produced by a filament biased to $\geq 200 \text{ V}$. Viewing the plasma by eye shows that the beam is responsible for a large fraction of the optical excitation observed in our data.

A test version of the biased limiter, 2 cm \times 4 cm, was mounted near one of the ports during this startup phase. The current was measured on the limiter to determine the rate at which ions were neutralized. We measured about 1.2 amps of current on the limiter at 20 eV (this voltage should produce 10 eV neutrals), corresponding to a collection rate of $7.5 \times 10^{18} \text{ ions s}^{-1}$, or 7.5 percent of the plasma ion source, S_1

[Equation (1)]. We estimate that the maximum plasma volume that this limiter could intercept corresponds to a collection efficiency of 15 percent, and, in practice, should be less. We conclude that the biased limiter is functioning as intended and that when we install a larger limiter a quarter of the ions will be collected in front of the opening to the drift tube.

The drift tube and sample chamber are under construction and will be installed in a few months along with spectroscopic diagnostics. Initially, measurements will be made to characterize the neutral source's composition, flux, density, and velocity, and for the presence of excited states. Various sample materials of the kind tested on spacecraft for glow will be mounted in the test chamber and exposed to the neutral flux. We will search for glow produced by the interaction of nitrogen on the surface and measure its intensity and spectral composition. The effect of impact energy on the glow will be studied by changing the biasing voltage on the limiter.

Acknowledgments. This work was supported by the National Aeronautics and Space Administration Grant No. NAG8-521 and the U.S. Department of Energy Contract No. DE-AC-2-76-CHO-3073.

References

- Biersack, J. P., and Haggmark, L.G., A Monte Carlo computer program for the transport of energetic ions in amorphous targets, Nucl. Instrum. Methods, 174, 257, 1980.
- Voss, D. E., and Cohen, S. A., Low-Energy Neutral Atom Spectrometer, Rev. Sci. Instrum., 53, 1696, 1982.
- Wong, K. L., Ono, M., and Wurden, G. A., ACT-I: A steady-state torus for basic plasma physics research, Princeton Plasma Physics Laboratory Report, No. TM-354, 1981.

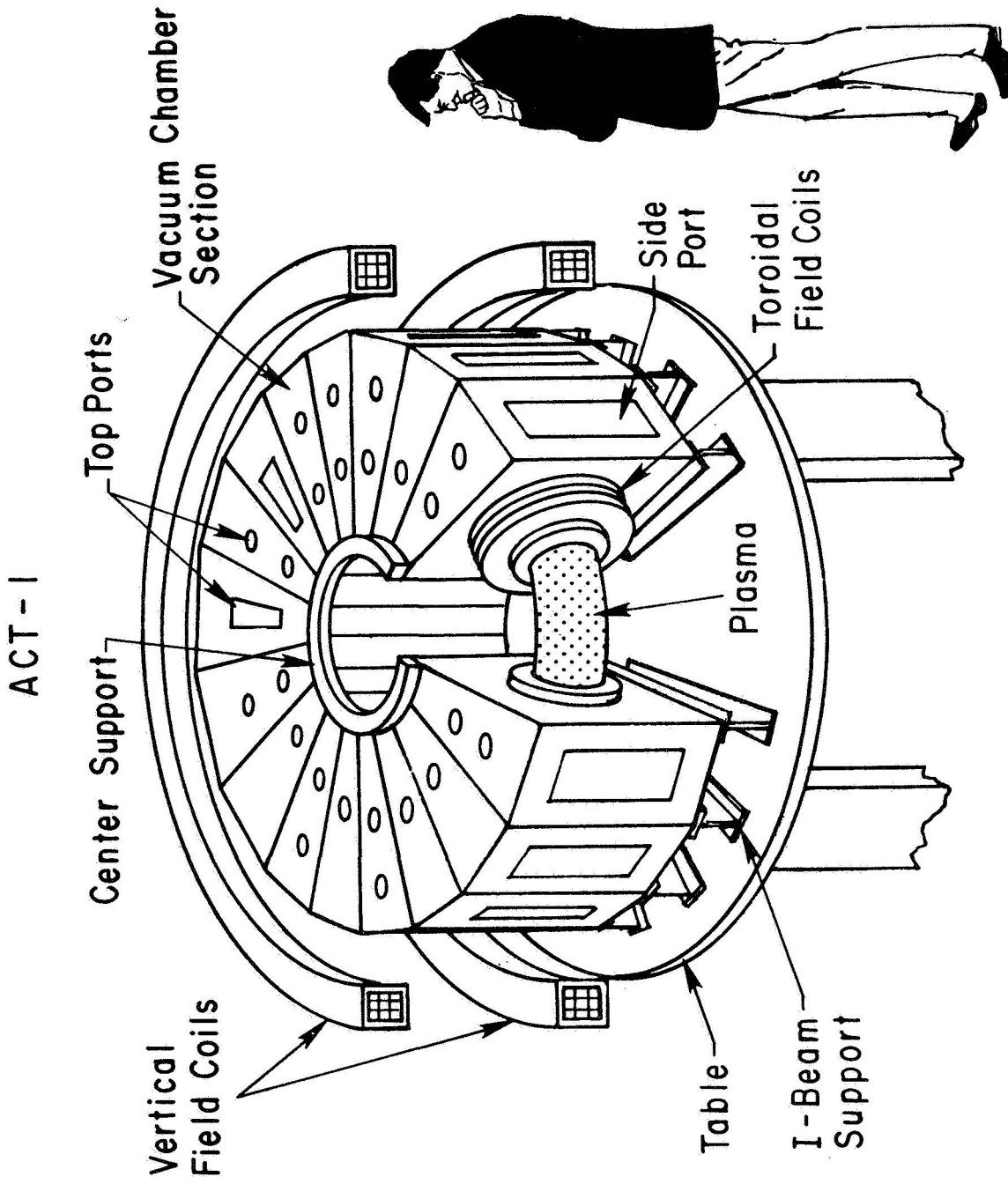


Fig. 1. Schematic of the ACT-I device.

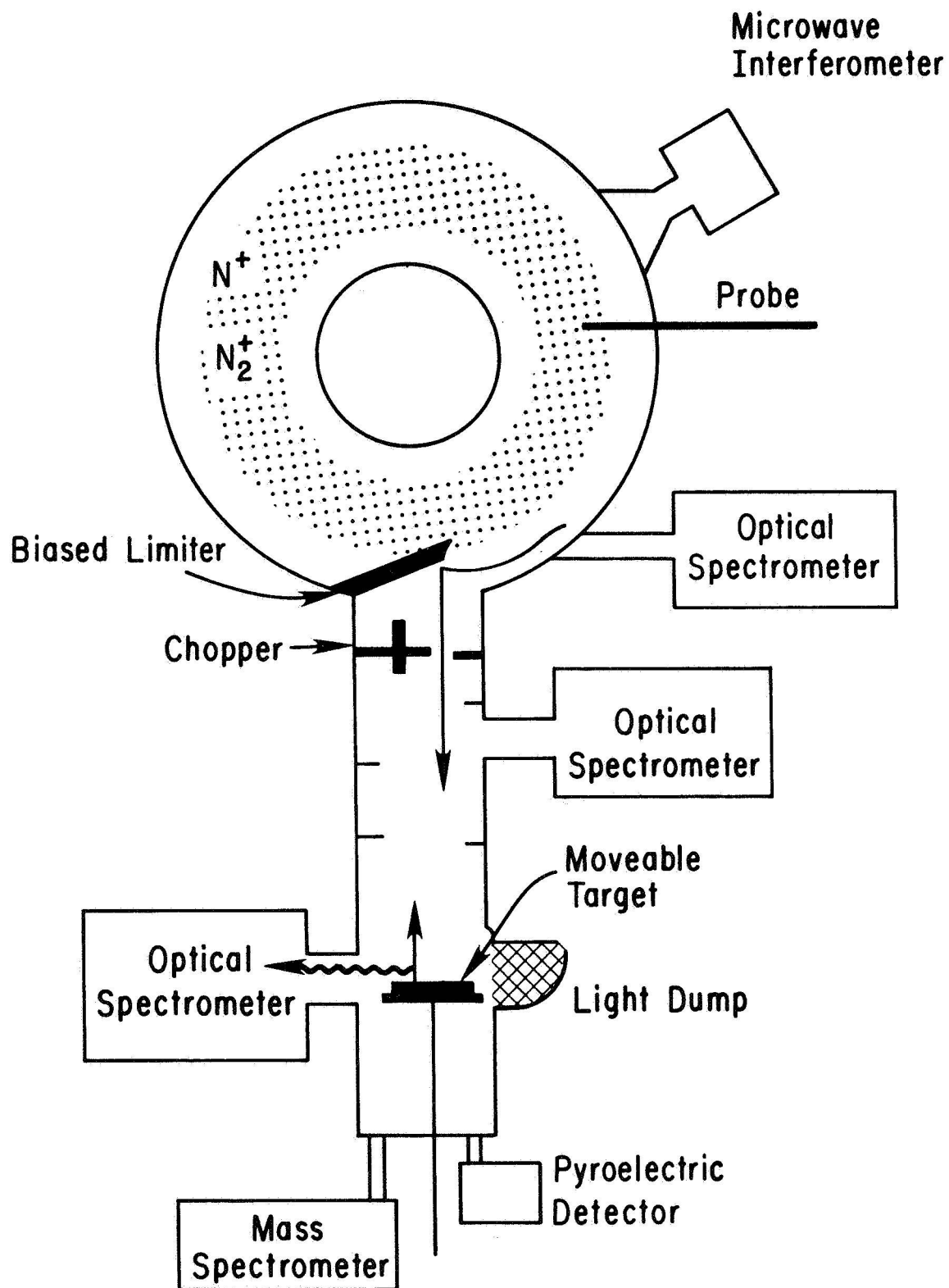


Fig. 2. Schematic of the experiment showing the drift tube, test chamber (not to scale), and diagnostics. The probe and interferometer measure the plasma density and temperature. Baffles (indicated by short lines on the sides) block reflected light.

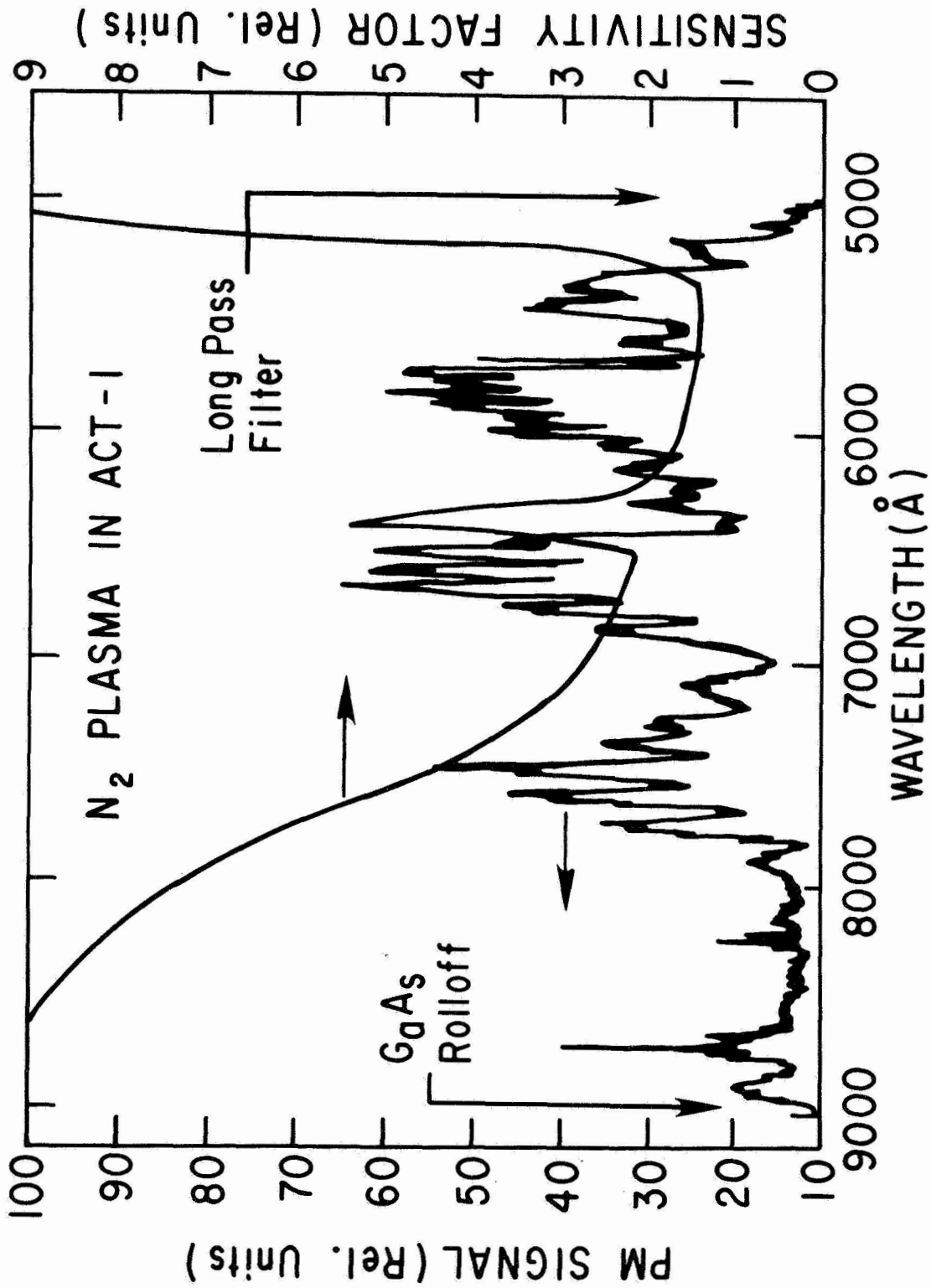


Fig. 3. The spectrum of a nitrogen discharge in ACT-I taken using a double monochromator with a FWHM bandpass of 8 Å. The multiplicative sensitivity factor can be used to scale the observed spectral intensity.

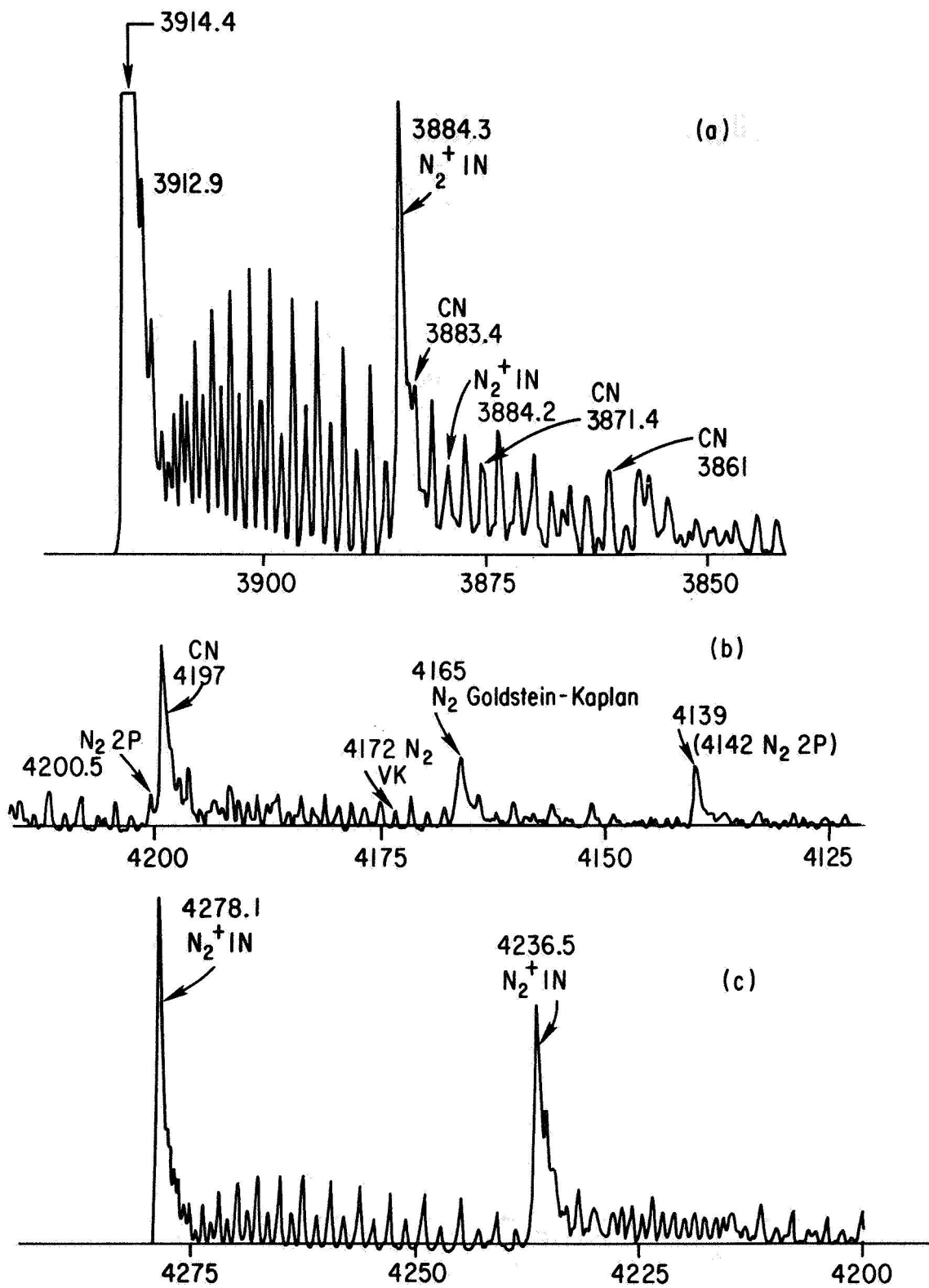


Fig. 4. Spectra, not corrected for instrumental response, of N_2 plasmas in ACT-I using a 0.66 m monochromator with a FWHM bandpass of 0.5 Å. The N_2^+ first negative (indicated by 1N) system dominates the spectrum. The shoulders on the 1N(1,1) band may come from CN emission.

TABLE 1. PHYSICAL AND PLASMA CHARACTERISTICS OF ACT-I

			<u>Comments</u>
r	Minor radius:	10 cm	
R	Major radius:	59 cm	
V	Volume:	$1.2 \times 10^5 \text{ cm}^3$	
r_p	Plasma radius:	7 cm	
V_p	Plasma volume:	$6 \times 10^4 \text{ cm}^3$	
n_e	Electron density:	10^{12} cm^{-3} 10^{13} cm^{-3}	continuous operation pulsed (20 μsec) with 20% duty cycle
T_e	Electron temperature:	$\leq 15 \text{ eV}$	up to 50 eV in the high energy tail
T_i	Ion temperature:	1-5 eV	without rf heating (in H_2)
τ_c	Confinement time:	1 msec	

APPLICATION OF AN ATOMIC OXYGEN BEAM FACILITY
TO THE INVESTIGATION OF SHUTTLE GLOW CHEMISTRY

Graham S. Arnold and Daniel R. Peplinski

Chemistry and Physics Laboratory
The Aerospace Corporation
El Segundo, California

Abstract. A facility for the investigation of the interactions of energetic atomic oxygen with solids is described. The facility is comprised of a four-chambered, differentially pumped molecular beam apparatus which can be equipped with one of a variety of sources of atomic oxygen. The primary source is a DC arc-heated supersonic nozzle source which produces a flux of atomic oxygen in excess of $10^{15} \text{ cm}^{-2} \text{ sec}^{-1}$ at the target, at a velocity of 3.5 km sec^{-1} . Results of applications of this facility to the study of the reactions of atomic oxygen with carbon and polyimide films are briefly reviewed and compared to data obtained on various flights of the space shuttle. A brief discussion of possible application of this facility to investigation of chemical reactions which might contribute to atmosphere-induced vehicle glow is presented.

Introduction

A spacecraft in the altitude range of 200-700 km experiences bombardment by an atmosphere whose primary constituent is neutral atomic oxygen [Hedin et al., 1977]. Although the ambient gas temperature is only on the order of 1000 K, the 8 km sec^{-1} velocity of the spacecraft causes the oxygen atoms to strike satellite surfaces at a relative kinetic energy of 500 kJ mole^{-1} (5 eV). At shuttle altitudes, the atomic oxygen density is on the order of 10^9 cm^{-3} , which corresponds to a flux of about $10^{15} \text{ cm}^{-2} \text{ sec}^{-1}$. These conditions present a regime of gas-surface chemistry which has been the subject of very little experimental investigation because of the difficulties inherent in reproducing them in the laboratory. A variety of effects observed on NASA and USAF spacecraft have been ascribed to the action of the ambient atmosphere. These include material erosion [Leger et al., 1983, 1984], optics degradation [Arnold et al., 1982], and luminescence [Banks et al., 1983; Yee and Abreu, 1983].

This paper describes a facility assembled specifically for the investigation of the interactions of energetic atomic oxygen with solid surfaces. The major elements of this facility, which are described below, are the four-chambered, differentially pumped molecular beam apparatus, the provisions for mounting and interrogating solid samples, and the DC arc-heated supersonic atomic beam source. Results of experimental work using this facility which demonstrate its utility in

performing its appointed task are briefly presented along with a brief assessment of the potential for application of this facility to investigation of chemistry which may contribute to vehicle glow.

Facility Description

Vacuum System

Figure 1 shows a schematic representation of the molecular beam apparatus. The vacuum system is comprised of four differentially pumped stainless steel chambers. The first three chambers are 0.46 m³ boxes equipped with Viton or Buna-N "O-ring" seals. Each is pumped by an oil diffusion pump. The pumps on the second and third chambers are equipped with gate valves and liquid nitrogen cooled baffles.

The fourth chamber is a cylindrical clean chamber utilizing crushed metal seals. It is recessed into chamber 3 to reduce the total length of the facility (as measured from the source). This chamber is equipped with a high vacuum gate valve (Huntington model GVAP-600) and a 570 l-sec⁻¹ turbomolecular pump (Balzers model TPU 510). The turbomolecular pump is used in preference to more conventional UHV pumping technology because of the large helium load which this chamber must bear.

Sample and Analysis Systems

The facility is equipped with a quadrupole mass spectrometer (Extranuclear Laboratories, Inc.) comprised of a crossed-beam electron-impact ionizer, a quadrupole mass filter with 17 mm diameter rods, and a Johnston MM-1 particle multiplier. The mass spectrometer has been used so far only for beam source characterization.

When solid samples are to be bombarded, they may be mounted either in chamber 2, when it is desirable to maximize the available beam flux on target, or in chamber 4 when sample cleanliness is the paramount concern. A liquid nitrogen cooled shroud surrounds samples in chamber 2 to inhibit contamination. The beam is typically collimated to subtend a circular spot of approximately 7 mm in diameter when samples are mounted in this shroud, however, spots as large as 17 mm are possible. A three-axis-plus-rotation precision manipulator is provided for mounting solid samples. Active temperature control on the range of 300-450 K is typical.

The only in situ diagnostics currently available in this facility are optical. Transmission measurements of samples mounted in either location are possible. Figure 2 shows a schematic representation of the optical path for transmission measurements in chamber 4. Ultraviolet transmission has been used to measure the rate of oxidation of carbon by high velocity atomic oxygen [Arnold and Peplinski, 1984a] and infrared transmission has been used to measure the effect of atomic oxygen on clean and contaminated infrared optics [Arnold et al., 1982].

Atomic Oxygen Sources

The primary beam source used in this facility is a DC arc-heated supersonic nozzle source which relies on a modified, commercially available plasma torch. The beam source has been described in detail elsewhere [Silver et al., 1982; Arnold and Peplinski, 1984b]. Typical beam source operating conditions and performance specifications are summarized in Table 1.

Two other beam sources for producing atomic oxygen are available for use in this facility: a microwave discharge source [Arnold et al., 1982] and a resistively-heated thermal dissociation source [Henderson et al., 1969] for which iridium or rhenium source tubes with a variety of orifice diameters are available. Both sources are capable of producing substantial fluxes of atomic oxygen, but with velocities on the order of 1 km sec^{-1} . These lower velocity sources are needed to gain a more complete understanding of the kinetics of the reactions of atomic oxygen with solids.

All three of the sources produce light as well as atomic beams. This light presents a potential interference to experiments aimed at measuring luminescence. In the case of the microwave discharge source, this problem can be circumvented by introducing a bend in the source between the discharge region and the nozzle. For the other two sources this is not possible.

Since the beam from either the DC arc source or the thermal dissociation source is comprised of neutral atoms and molecules, separation of the beam from the light can only be readily effected by a mechanical chopper. A two-segment slotted-disk velocity selector of 40% nominal transparency has been designed for this facility [Fluendy and Lawley, 1973]. The role of this device is not to prepare a beam of narrow velocity distribution, but merely to block species, such as photons, traveling at velocities in excess of the selected velocity. Since the selector has only two disks, it naturally has an infinite number of low-velocity side bands. This device has not heretofore been used for experiments performed in this facility.

Facility Applications

Reaction of Atomic Oxygen with Solids

This facility has been used to investigate the rate of reaction of atomic oxygen with two types of carbon [Arnold and Peplinski, 1984a, 1985a] and with Kapton film, a polyimide material manufactured by E.I. du Pont de Nemours & Co., Inc. [Arnold and Peplinski, 1985b] The results of these investigations are summarized very briefly below.

Carbon. Figure 3 shows an Arrhenius plot (in carbon surface temperature) of the probability of reaction of atomic oxygen with carbon including data from ground-based measurements and flight experiments and other observations from various flights of the space shuttle. The reaction probability plotted is defined as the probability that an oxygen atom impact will remove a carbon atom from the surface,

regardless of its final state of aggregation. (For a detailed discussion of these data the reader should consult [Arnold and Peplinski, 1984a] and works cited therein.)

The open circles and open triangle represent the results of measurements performed in this facility. The dashed line labeled "Park" is a fit to several laboratory measurements of the rate of reaction of atomic oxygen with various forms of carbon, under more or less thermal conditions [Park, 1976]. The other data include limits on the reaction probability inferred [Arnold and Peplinski, 1984a] from removal of carbon surfaces on the STS-3 Plasma Diagnostics Package (G.B. Murphy, University of Iowa, Department of Physics and Astronomy, Iowa City, IA, private communication, 1982) and on the STS-4 Marshall Space Flight Center's Induced Environment Contamination Monitor Passive Sample Array [Peters et al., 1983], a probability calculated from the observed thickness loss of vitreous carbon included on the STS-5 Evaluation of Oxygen Interaction with Materials (EOIM) passive sample array [Arnold and Peplinski, 1985a], and the reaction probability calculated from the observed rate of mass loss from and amorphous carbon-coated temperature-controlled quartz crystal microbalance on the Goddard Space Flight Center's Contamination Monitor Package flown as a "Get-Away Special" on STS-8 (J.J. Triolo, NASA/Goddard Space Flight Center, Greenbelt, MD, private communication, 1984).

These data lead one to the conclusion that the rate of reaction of atomic oxygen with carbon, at collision energies of up to 100 kJ mole^{-1} (1 eV), does not depend strongly on the translational energy of impact. Indeed when one compares laboratory and flight data for similar samples of carbon, the evidence that rates occurring on-orbit are significantly different from the thermal rate of reaction of O atoms with carbon is not strong. However, the results of Gregory and Peters (not shown on Figure 4), who infer probabilities in excess of 0.1 from STS-8 EOIM results, militate against drawing an unambiguous conclusion in this matter (J. C. Gregory, Chemistry Department, the University of Alabama at Huntsville, private communication, 1985).

Kapton. Table 2 shows a comparison between the average probabilities for the reaction of atomic oxygen with Kapton measured in this facility [Arnold and Peplinski, 1985b] and inferred from the STS-5 and STS-8 EOIM experiments [Leger et al., 1983, 1984]. In this case, the reaction probability is conventionally defined as the thickness of material removed divided by the fluence of atomic oxygen incident on the sample.

The agreement between the laboratory and flight data is quite good in comparison to the uncertainties in the various data. This relatively good agreement suggests that there is not a great dependence on O atom impact energy of the average efficiency of the reaction of atomic oxygen with Kapton over a range of impact energy from 1 to 5 eV.

Luminescent Reactions

Several possible contributing mechanisms have been proposed to explain the vehicle glow phenomenon. These include surface catalyzed recombination of atmospheric radicals [Torr et al., 1977; Reeves, 1982],

production of excited products from oxygen reactions with materials [Slanger, 1983], recombination collisionally dissociated of nitrogen [Green, 1984], and vehicle plasma interactions [Papadopoulos, 1984].

Considering the complexity of the problem and the scarcity of unambiguous data, one cannot yet make any definitive assessment of the relative importance of these various processes in creating the observed glows. However, one can proceed reasonably to investigate these processes experimentally, with both flight and laboratory experiments. It is a valid and important point that there appears to be no way to simulate the "shuttle glow" in the laboratory. The shuttle environment is too complex and uncertain. However, simulation is not necessarily the proper function of laboratory investigations of spacecraft environmental phenomena. Rather, their role is to elucidate mechanistic details which are difficult to address in flight experiments on account of operational constraints, background interferences, scarcity of opportunities, or expense.

Visible luminescence from surface catalyzed excitation. In the earliest published reference to atmosphere-induced vehicle glow [Torr et al., 1977], it was hypothesized that recombination of adsorbed atmospheric O and NO to produce excited NO₂ in the gas phase was responsible for the observed visible emission. This explanation has subsequently been proposed repeatedly. [Reeves, 1982; Mende and Swensen, 1985].

The production of excited products by surface catalyzed radical recombination is a well-documented phenomenon [Mannella and Harteck, 1961]. However, both Mende and Swenson and Torr et al. have suggested that for the O + NO recombination luminescence to account for the majority of the observed glows, the spectrum of the NO₂ product must be shifted compared to the spectrum obtained from 3-body gas-phase recombination [Golde et al., 1973]. There is not sufficient information from experiments in which the spectrum of the product NO₂ is not perturbed by subsequent gas-phase collisions to answer whether this mechanism is important in the creation of the observed shuttle glow.

Clearly one wishes to investigate the luminescence from surface-catalyzed NO₂ production under "single collision" conditions so that one measures the spectrum of the nascent products. This suggests that molecular beam techniques be used. A schematic representation of such an experiment is shown in Figure 4.

One may estimate the signal from such an experiment as follows. The number density of NO₂^{*} product near a surface on which O and NO are recombining may be formally expressed as

$$[\text{NO}_2^*] \cong k_1 F_O [\text{NO}_{\text{ads}}] / v_1 + k_2 F_{\text{NO}} [\text{O}_{\text{ads}}] / v_2 + k_3 [\text{O}_{\text{ads}}] [\text{NO}_{\text{ads}}] / v_3 \quad (1)$$

where three different processes are considered to be operational:

1. Reaction of an incident O atom with an adsorbed NO molecule;

2. Reaction of and incident NO molecule with an adsorbed O atom;
3. Reaction of an adsorbed O atom with an adsorbed NO molecule.

In equation (1) the rate coefficients k_1 and k_2 have units of area (reaction cross-section) and k_3 has units of area/time (like a diffusion coefficient). The quantities v_i are the average velocities with which the product is ejected as a result of each of the three formation processes.

In practice, to make a rough estimate of the photon emission rate from such an experiment, one approximates equation (1) by assuming that the NO_2 production rate will be limited by one or the other of the reagent fluxes. Therefore one obtains

$$[\text{NO}_2^*] \approx pF_1 / \langle v \rangle \quad (2)$$

where F_1 is the limiting flux, p is some effective probability, and $\langle v \rangle$ is an average velocity of the product.

If one approximates the volume emission rate as $[\text{NO}_2^*]$ divided by the average radiative lifetime, τ_{rad} , and assumes collection with $f/1$ optics from an 0.5 cm^3 volume, then the rate at which photons fall on the detector per unit wavelength, S , is given by

$$S \approx \frac{pF_1}{10 \langle v \rangle \tau_{\text{rad}} \Delta \lambda} \quad (3)$$

If one presumes that it is the O atom flux that limits the reaction rate, then one needs to invoke a value of about 10^{-7} for p to rationalize the orbital observations. In this facility O atom fluxes on the range of 10^{14} - $10^{15} \text{ cm}^{-2} \text{ sec}^{-1}$ are easily realized. The product $\langle v \rangle \tau_{\text{rad}}$ can be expected to range from 3-20 cm. The bandwidth, $\Delta \lambda$, is expected to be approximately 3000 Å. Thus total photon arrival rates range from 10-1000 photons/Å/sec. Using cooled, a red-sensitive photomultiplier tube, with photon counting detection, measurement of a moderately well resolved spectrum at these signal levels should be possible.

Infrared Luminescence

The observation of moderately intense luminescence in the visible near spacecraft surfaces naturally raises the question of whether there is also a significant infrared component associated with the glow. At least one of the proposed mechanisms for glow production suggests such to be the case [Slanger, 1983]. Observation of the shuttle from the ground suggests that there may be more near infrared emission from the shuttle than can be explained by thermal emission or scattering from other sources (F. Witteborn, NASA/Ames Research Center, private communication, 1985).

The long lifetimes associated with infrared emission render the laboratory investigation of infrared luminescence under "single collision conditions" difficult. Excited molecules tend to leave the

detector field-of-view or to strike chamber walls in times much less than their radiative lifetimes. However, the technology for direct, laser-induced fluorescence (LIF) measurement of internal state distributions of reaction products, from which one may readily calculate net emission spectra, is well established [Kinsey, 1977]. Recently this technology has begun to find application in gas-surface scattering research [Cardillo, 1985].

Because of the wide use of carbon, carbon-filled, and carbon-containing materials on spacecraft surfaces, the internal state distribution of the CO product of the $O + C_s$ reaction is of interest. Since LIF is a number density detector, one again needs to estimate the number density or "effective pressure" of products to ascertain whether a measurement is feasible. This number density is given by

$$[CO] \cong pF_O/v_{CO} \quad (4)$$

where p is the reaction probability, F_O is the flux of atomic oxygen, and v_{CO} is the product velocity. For a reaction probability of 0.01, a flux of $4 \times 10^{14} \text{ cm}^{-2} \text{ sec}^{-1}$, and a thermal product velocity, one estimates the CO number density to be approximately $8 \times 10^7 \text{ cm}^{-3}$, which is roughly equivalent to a pressure at room temperature of 3×10^{-9} Torr.

Detection of CO internal state distributions by LIF can be accomplished by excitation of the A-X transition at approximately 148 nm. Hepburn has reviewed the technology for coherent VUV generation for this application [Hepburn, 1984]. He estimates the detection limit for CO (at 300 K) to be 10^{-10} Torr. Thus, by the application of established technology, a useful experiment to assess the potential for non-thermal infrared luminescence from vehicles in LEO is feasible.

Summary

A facility which has proven to be useful in the investigation of oxygen atom interaction with materials has been described. Order-of-magnitude estimates of signal strengths suggest that this facility will be useful in the investigation of surface-catalyzed excitation reactions and of energy disposal in gas-solid reactions which produce volatile products. Both of these processes have been suggested as contributors to the "shuttle glow."

Acknowledgments. This work was supported by the Aerospace Sponsored Research program.

References

- Arnold, G.S., and Peplinski, D.R., Reactions of high velocity atomic oxygen with carbon, AIAA 22nd Aerospace Sciences Meeting, Reno, NV, AIAA Paper #84-0549, 1984a.

- Arnold, G.S., and Pelinski, D.R., A facility for Investigating interactions of energetic atomic oxygen with solids, 13th Space Simulation Conference, NASA Conference Publication 2340, pp. 150-168, 1984b.
- Arnold, G.S., Peplinski, D.R., and Herm, R.R., Atmospheric effects in low Earth orbit and the DMSP ESA offset anomaly, SD-TR-82-81, The Aerospace Corporation, El Segundo, CA, 1982.
- Arnold, G.S., and Peplinski, D.R., Reaction of atomic oxygen with vitreous carbon laboratory and STS-5 data comparisons, AIAA Journal, in press, 1985a.
- Arnold, G.S., and Peplinski, D.R., Reaction of atomic oxygen with polyimide films, AIAA Journal, accepted for publication, 1985b.
- Banks, P. M. Williamson, P. R., and Raitt, W. J., Space shuttle glow observations, Geophys. Res. Lett., 10(2), 118-121, 1983.
- Cardillo, M. J., Concepts in gas-surface dynamics, Langmuir, 1(1), 10-23, 1985.
- Fluendy, M.A.D., and Lawley, K.P., Chemical Applications of Molecular Beam Scattering, Chapman and Hall, London, pp. 97-104, 1973.
- Golde, M.F., Roche, A.E., and Kaufman, F., Absolute rate constant for the $O + NO$ chemiluminescence in the near infrared, SRCC Report #187, University of Pittsburgh, Pittsburgh, PA, 1973 (and references cited therein).
- Green, B.D., Atomic recombination into excited molecular states-A possible mechanism for Shuttle glow, Geophys. Res. Lett., 11, 576-579, 1984.
- Hedin, A.E., Reber, C.A., Newton, G.P., Spencer, N.W., Brinton, H.C., Mayr, H.G., and Potter, W.E., A global thermospheric model based on mass spectrometer and incoherent scatter data MSIS 2, composition, J. Geophys. Res., 82, 2148-2156, 1977.
- Henderson, W.R., Fite, W.L., and Brackmann, R.T., Dissociative attachment of electrons to hot oxygen, Phys. Rev., 183, 157-166, 1969.
- Hepburn, J.W., Coherent vacuum ultraviolet in chemical physics, CP-244 (Beams 83-7), University of Waterloo Chemical Physics Research Report, Waterloo, Ontario, Canada, 1984.
- Kinsey, J.L., Laser induced fluorescence, Annual Rev. Phys. Chem., 28, 349, 1977.

- Leger, L.J., Spiker, I.K., Kuminecz, J.F., Ballentine, T.J., and Visentine, J.T., STS flight 5 LEO effects experiment, background description and thin film results, AIAA Shuttle Environment and Operations Meeting, Washington, D.C., AIAA Paper #83-2631-CP, 1983.
- Leger, L.J., Visentine, J.T., and Kuminecz, J.F., Low Earth orbit atomic oxygen effects on surfaces, AIAA 22nd Aerospace Sciences Meeting, Reno, NV, AIAA Paper #84-0548, 1984.
- Mannella, G., and Harteck, P., Surface-catalyzed excitations in the oxygen systems, J. Chem. Phys., 34(6), 2177-2180, 1961 (and references cited therein).
- Mende, S.B., and Swensen, G.R., Measurements of vehicle glow characteristics during STS 41-D, AIAA Paper #85-0475, AIAA 23rd Aerospace Sciences Meeting, Reno, NV, 1985.
- Papadopoulos, K., Shuttle glow (the plasma alternative), Radio Sci., 19, 576-579, 1984.
- Park, C., Effect of atomic oxygen on graphite ablation, AIAA Journal, 14, 1640-1642, 1976.
- Peters, P.N. Linton, R.C., and Miller, E. R., Results of apparent atomic oxygen reactions on Ag, C, and Os exposed during the Shuttle STS-4 orbits, Geophys. Res. Lett., 10, 569-571, 1983.
- Reeves, R.R., Surface catalyzed excitation-Laboratory observations of solid catalyst induced molecular light emission in atomic oxygen and/or atomic nitrogen environment, NASA Induced Shuttle Luminosity Meeting, McLean, VA, 1982.
- Silver, J.A., Freedman, A., Kolb, C.E., Rahbee, A., and Dolan, C.P., Supersonic nozzle beam source of atomic oxygen produced by electric discharge heating, Rev. sci. Instrum., 53(11), 1714-1718, 1982.
- Slanger, T.G., Conjectures on the origin of the surface glow and space vehicles, Geophys. Res. Lett., 10, 130-132, 1983.
- Torr, M.R., Hays, P.B., Kennedy, B.C., and Walker, J.C.G., Intercalibration of airglow observatories with the Atmosphere Explorer Satellite, Planet. Space Sci., 25, 173-184, 1977.
- Yee, J.H., and Abreu, V.J., Visible glow induced by spacecraft-environment interaction, Geophys. Res. Lett., 10, 118-121, 1983.

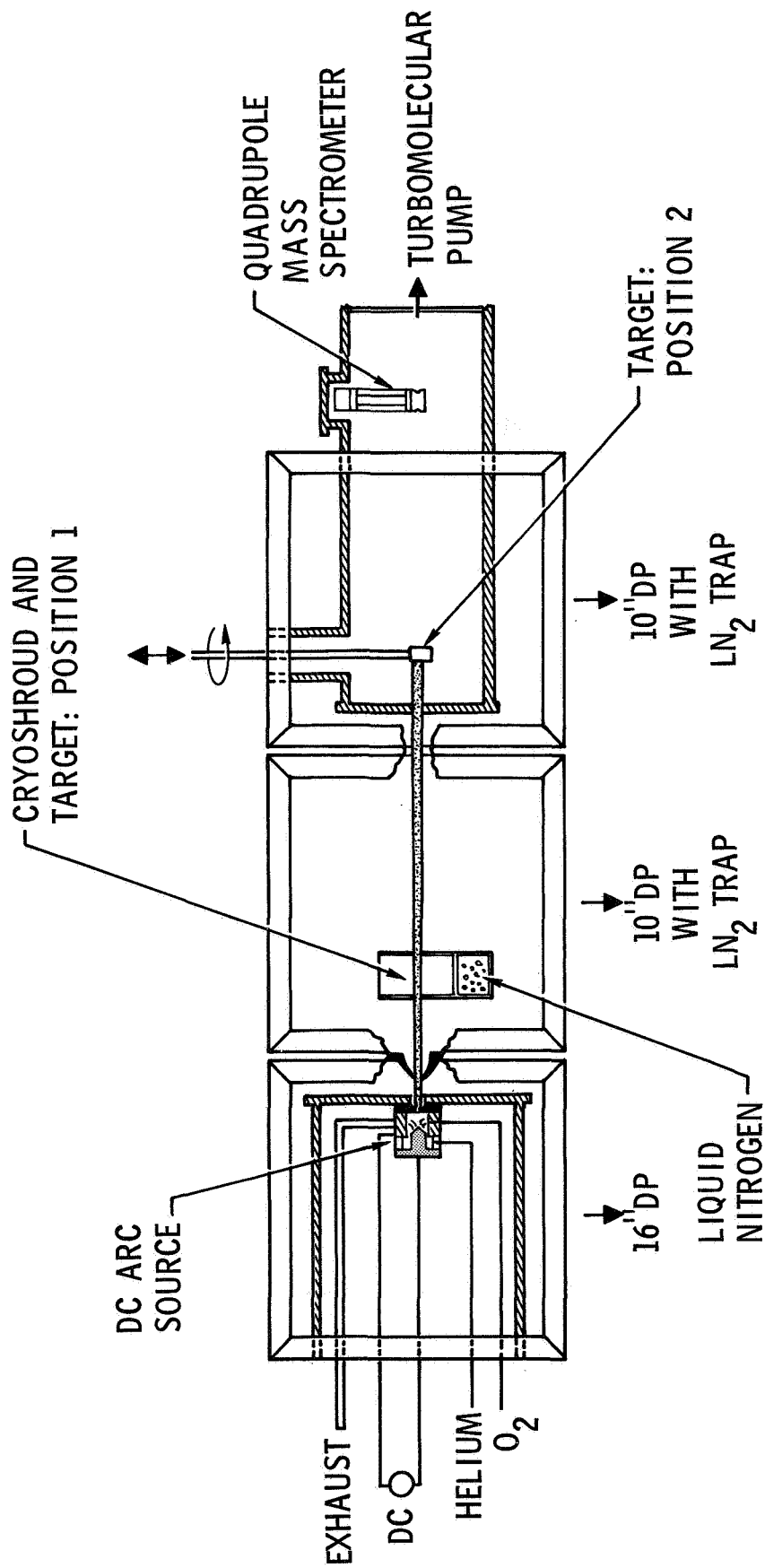


Fig. 1. Schematic representation of the atomic oxygen beam facility.

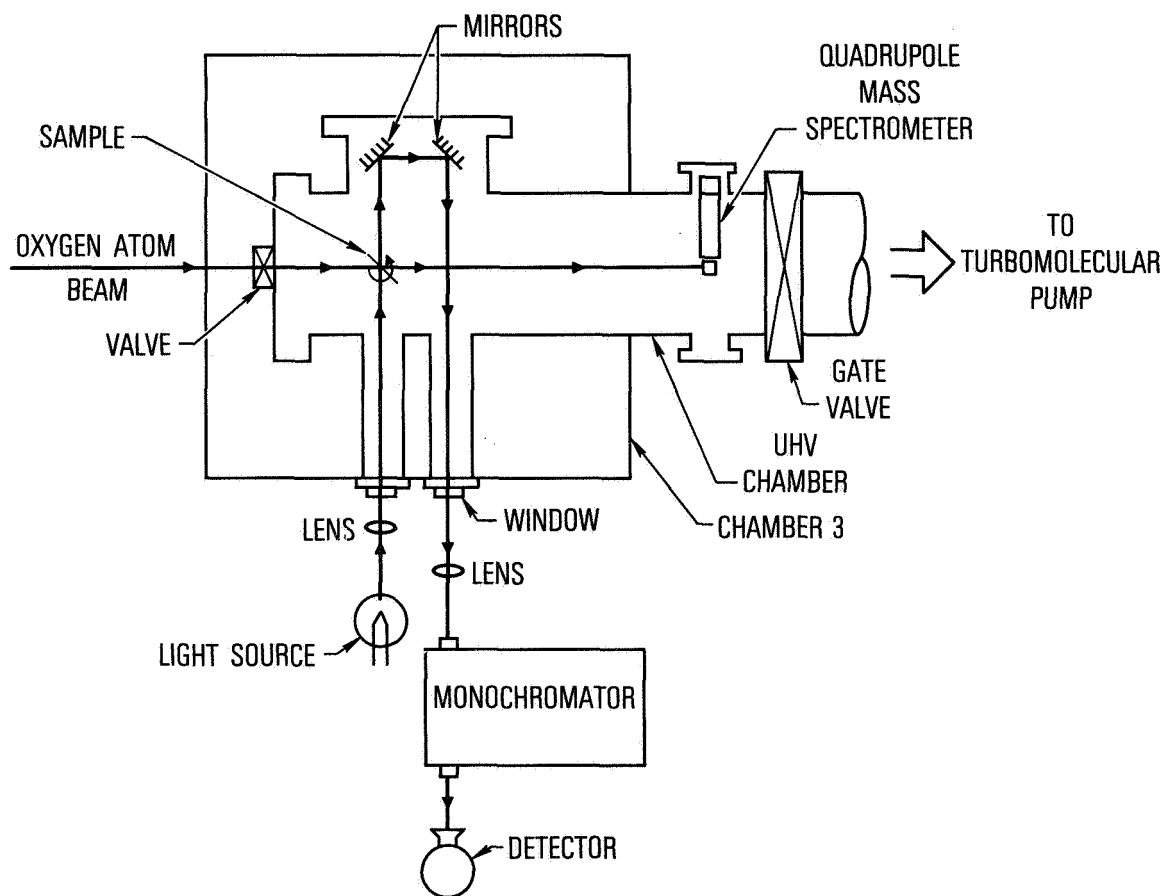


Fig. 2. Schematic representation of the fourth (clean) chamber showing path for in situ optical transmission measurements.

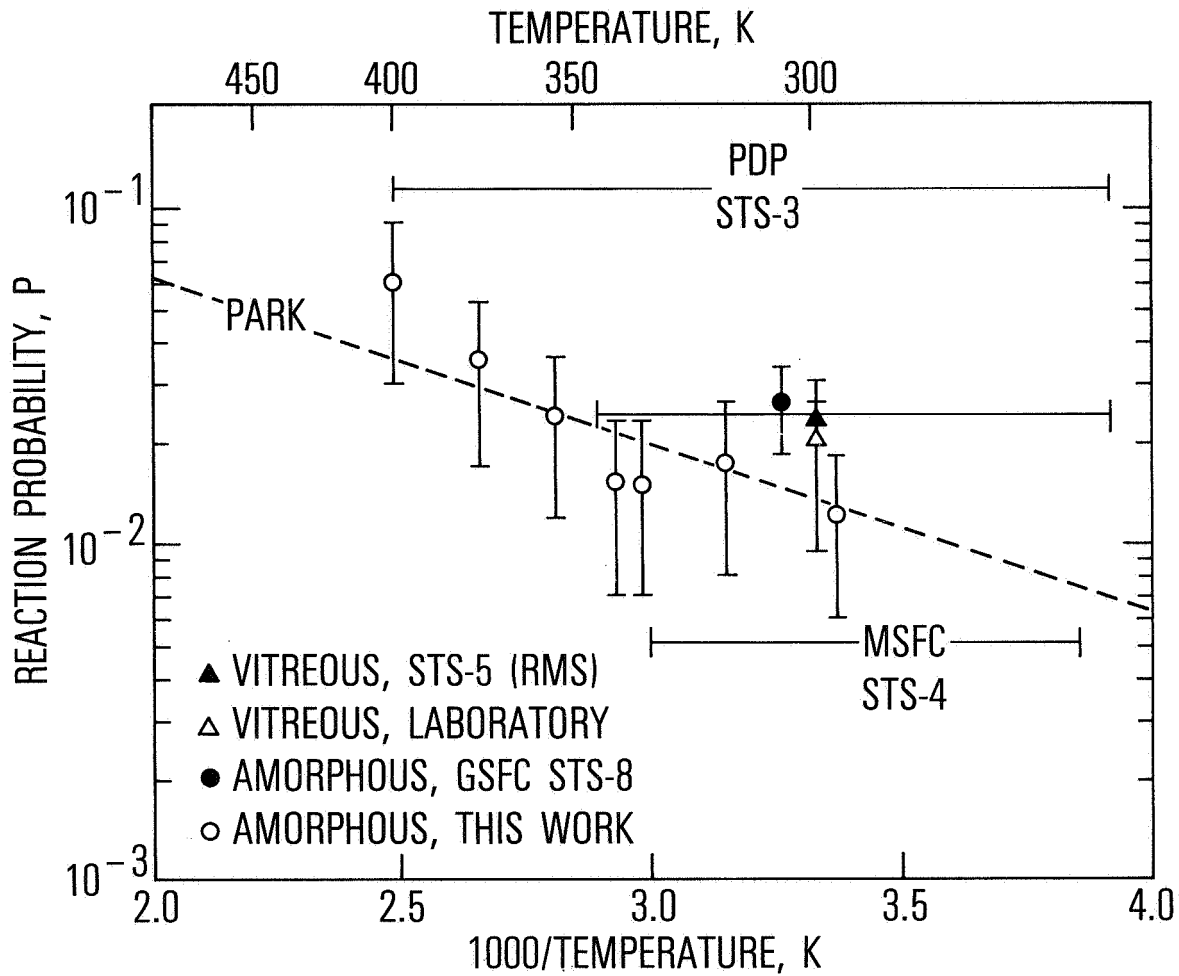


Fig. 3 Arrhenius plot (in carbon surface temperature) of the probability of the reaction of atomic oxygen with carbon. Various laboratory and flight data are shown. (See text.)

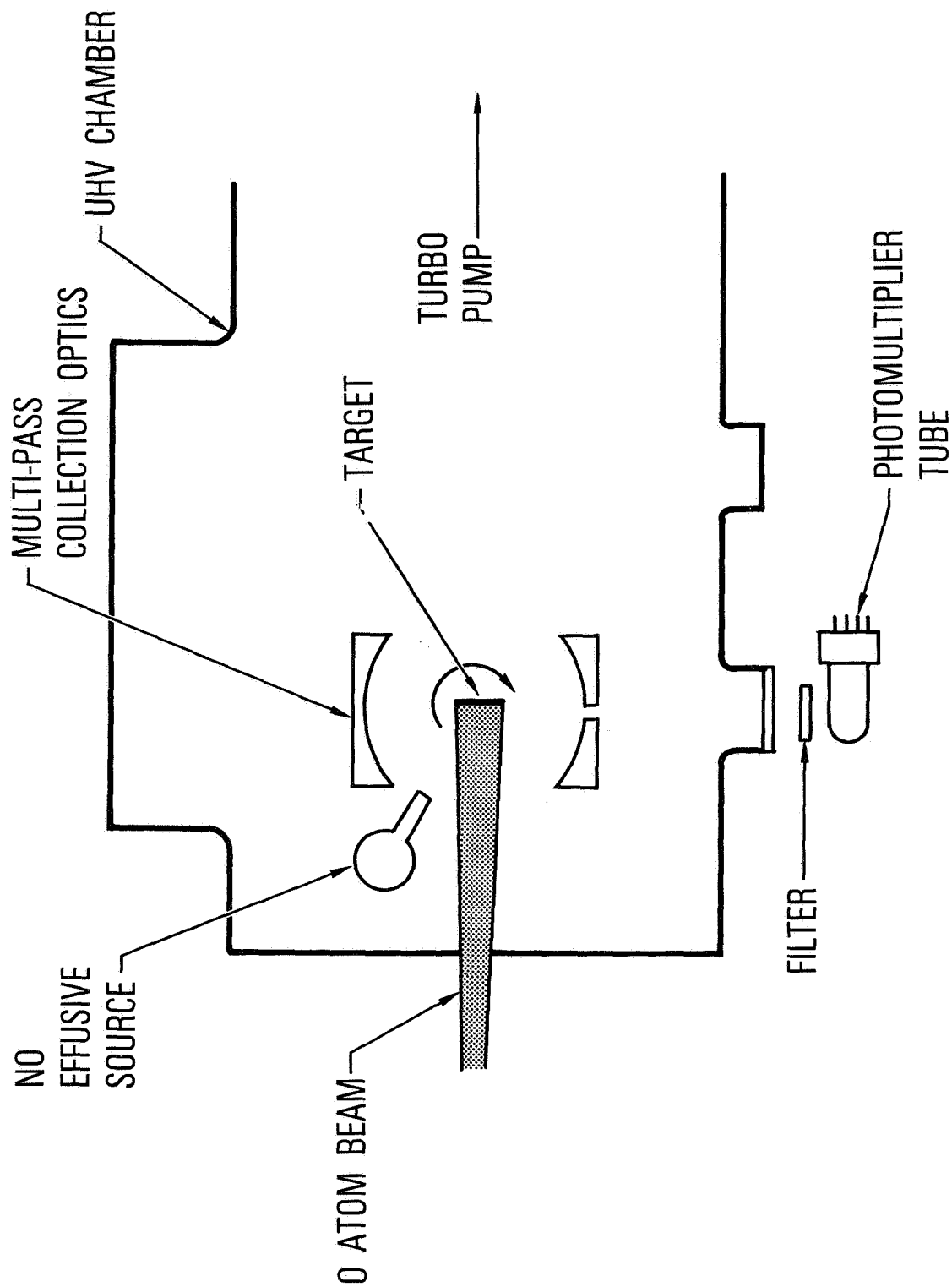


Fig. 4. Schematic representation of a molecular beam surface catalyzed excitation experiment.

TABLE 1. TYPICAL BEAM SOURCE CHARACTERISTICS

Feed Gas	He:O ₂ /98:2
Flow Rate	265 SCFH (2 l-atm sec ⁻¹)
Power Dissipated	16 kW
O Flux on Target ^a	5.0x10 ¹⁵ cm ⁻² sec ⁻¹
O ₂ Flux on Target ^a	7.5x10 ¹⁵ cm ⁻² sec ⁻¹
Beam Velocity (oxygen atoms)	3.5 km sec ⁻¹

^aTarget mounted in chamber 2; see Figure 1.

TABLE 2. COMPARISON OF LABORATORY AND FLIGHT MEASUREMENTS OF THE AVERAGE PROBABILITIES FOR THE REACTION OF ATOMIC OXYGEN WITH KAPTON

Kapton Temperature (kelvin)	Laboratory ^a	Reaction Probability 10 ⁻²⁴ cm ³ /O atom	
		STS-5 ^b	STS-8 ^c
300	2.1+1.1 1.7+0.9	2.3+0.9	---
338	1.4+0.9	2.0+0.8	3.0+1.2
393	1.5+0.9	2.1+0.9	2.9+1.2

^aArnold and Peplinski [1985b].

^bSee Table 3 of Leger et al. [1983]; Nominal uncertainty is +40%.

^cSee Table 5 of Leger et al. [1984]; Nominal uncertainty is ±40%.

FUTURE EXPERIMENTS

AN ASSESSMENT OF THE IMPACT OF SPACECRAFT GLOW
ON THE HUBBLE SPACE TELESCOPE

John T. Clarke
Space Telescope Project
NASA Marshall Space Flight Center

Summary of Existing Observations and Theory

Visible spacecraft glow was first observed on the Atmospheric Explorer spacecraft by Torr [1983] and studied in some detail with the Visible Airglow Experiment (VAE) on the AE-E spacecraft by Yee and Abreu [1983]. The AE-E was a spin-stabilized spacecraft without thrusters at an altitude of 140-280 km. The VAE contained six visible-wavelength photometers that measured a glow spectrum which: a. rose steeply in the red, b. decreased with a $\cos \phi$ dependence from pointing into the ram direction of the spacecraft orbital motion, and c. decreased in intensity with increasing altitude with the same dependence as the measured atomic oxygen number atmospheric density [O] and not with the measured molecular nitrogen density [N₂]. Yee and Abreu [1983] proposed that the glow is produced by chemical reactions on the spacecraft surface as it sweeps through the atmospheric O, with roughly 5-8 eV per O atom available for excitation from the orbital motion of the spacecraft. This glow may in principal be produced by any of a number of species, including molecular band emission from OH, NO, and NO₂ (see Figure 1). The physical picture for the estimation of the surface brightness of the glow emanating above a surface is therefore:

$$\text{column photon production} = [\text{O}] \times (\text{orbital speed}) \times (\text{efficiency})$$

where: $[\text{O}]$ at 590 km = $4 \times 10^5 \text{ cm}^{-3}$ (solar min average)
 $[\text{O}]$ at 590 km = $3 \times 10^7 \text{ cm}^{-3}$ (solar max average)

and the efficiency for optical photon production (4000-8000Å) is 10^{-5} to 10^{-6} (measured on STS-3 and AE-E).

It has been proposed by Slanger [1983] and by Langhoff et al. [1983] that the observed glow on AE-E is from the excitation of the OH Meinel band system, which may be capable of producing all of the observed glow above 160 km altitude. This identification is supported by the detection of two spectral lines of the OH system with the Fabry-Perot spectrometer on the Dynamics Explorer [Abreu et al., 1983]. The existence of OH band emission would imply that there exists a much brighter near-IR glow than observed to date in the visible (see Figure 2), and thus poses a risk for the development of second-generation IR SI's for Space Telescope.

Observations on the shuttle indicate that there are several different "glows" operating, and the functional dependencies governing the brightness of these different glows are not well understood. The situation is complicated by the existence of thruster firings on the shuttle, as well as the generally larger size of the spacecraft and resulting greater residual atmosphere and induced plasma and spacecraft charging. The early pictures of the shuttle tail and aft bulkhead taken on STS-3,-4,-5, and -9 revealed a glow which varied in brightness with the surface material, varied with

the timing with respect to the thruster firings, showed a $\cos^{1/2}\phi$ dependence in brightness with pointing away from the orbital ram direction, and exhibited a spectrum similar to that observed on AE-E. Ground-based imaging of STS-9 at wavelengths of 1.6 and 2 microns detected the shuttle (as a whole) only at 2 microns, as would be expected from OH band emission, but the intensity of the emission was uncertain due to tracking difficulties [Witteborn et al., 1985]. A hand-held movie camera operated by Owen Garriott revealed a dramatic brightening of the shuttle tail and aft bulkheads following the firings of the vernier thrusters. This emission appeared a few seconds after the thrusters fired and decayed a few seconds later. However, the surface glow has been observed on the shuttle even when the thrusters were not firing (STS-3). Two far-UV cameras flown on Spacelab 1 (FAUST and WFC) both showed considerable fogging of their film, which may have been due to any of a combination of atmospheric twilight emissions, tropical arc OI 1304 and 1356 Å emissions, or an additional far-UV glow on the Shuttle.

Moderate resolution (3-6 Å) spectroscopy was performed on the STS-9 mission with the Imaging Spectrometric Observatory (ISO) from 1150-8000 Å [Torr and Torr, 1985]. Specific observations for glow were performed in a dedicated pointing into the ram direction and tangent to the Earth at an altitude of 250 km, although the instrument did not view any direct surfaces. The ISO spectrometers were capable of detecting line and/or band emission but not continuum glow due to uncertain detector background caused by rapid temperature changes. The detected UV and visible spectra are shown in Figures 3 and 4. The emissions shown in these spectra are a combination of atmospheric and potential glow emissions: more detailed analysis of these data will be required to identify which of the observed features may be due to glow. The visible band emission observed from 4000-8000 Å has a spectral slope consistent with that observed on AE-E, but the brightness of the visible glow reported at 250 km is similar to that observed by AE-E at 140-145 km. These band spectra suggest a contribution from the N₂ first positive system, and at different times the brightness of the emission at all wavelengths was observed to vary by at least an order of magnitude.

Theoretical studies of the glow have been performed to study the physical processes responsible for the glow. Yee and Dalgarno [1983] have determined the lifetime(s) of the glowing species (0.3 ms) from the spatial decay of the emission above the shuttle surface [Banks et al., 1983]. They conclude that OH band emission is unlikely to explain all of the observed shuttle glow, but may still radiate strongly in the IR. Swenson et al. [1985] propose NO₂ recombination continuum as the dominant source of radiation based on energetic arguments and the apparent lack of band structure in the glow at 30 Å resolution from 4000-8000 Å. There are no near-IR observations available to test either of these hypotheses. Torr and Torr [1985] identify N₂ first positive band emission from their STS-9 spectra. There is additionally a plasma theory for the glow, in which a surface plasma layer heated by non-linear plasma-wave interactions provides the glow excitation. The required plasma density is known to exist near the shuttle, but only under sunlit conditions, and the AE-E glow data showed no dependence on daytime/nighttime electron density variations [Yee et al., 1985]. The plasma theory also predicts blue/UV enhanced glow emission, which has never been observed.

Scaling Observed Glows to Space Telescope

Accurately scaling the observed glows to Space Telescope requires much better information about the physical processes producing the glow and the functional dependencies of the glow brightness than is currently available. Many different species have been proposed as glow emitters (OH, NO₂, NO, N₂), making the spectral character of the glow uncertain. The glow brightness is believed to depend on atmospheric density, which varies quite strongly with solar activity at a given altitude (see Figure 5). Other functional dependencies to be determined are:

- the quantitative effect of thruster firings (not an issue for ST other than to interpret shuttle glow observations)
- changes in the glow spectrum during thruster firings
- dependence of glow on spacecraft size
- dependence of glow on spacecraft materials and cleanliness
- dependence of glow on angle to the orbital ram direction
- existence of extended glow above spacecraft surfaces

It must be concluded that the extrapolation to ST will be very uncertain until these factors are better understood. For example, the difference in scaling the observed glow brightnesses from AE-E and the ISO to ST altitudes by [O] is shown in Figure 6.

The actual contamination by glow in the focal plane of the Space Telescope depends not only on the surface brightness of the glow above a particular surface but also on the extent of the glow above each surface and how well the emission is baffled and thus prevented from reaching the focal plane. As long as the glow is confined to 10-20 cm above any given surface, the ST is a very well-baffled telescope and relatively little of that flux will penetrate to the focal plane. If any glow extends into the OTA field-of-view of the sky, however, the presumably isotropically emitting glow will be competing directly with the sky background to contaminate ST data. Perkin-Elmer has performed an analysis of the contribution to the total focal plane flux made by surface-localized glow using the following assumptions:

- [O] = $3 \times 10^7 \text{ cm}^{-3}$ (average solar max conditions)
- photon production efficiency $1-3 \times 10^{-5}$
- glow extends 20 cm above the surface

These efficiencies were roughly measured for the ST materials (Chemglaze Z306 and anodized aluminum) on previous shuttle flights, but no information is available on the glow of Al+MgF₂. The predicted focal plane fluxes are plotted in Figure 7 as a function of angle to the ram direction. The case within 15° of upwind is uncertain since we do not know how the primary mirror will glow under direct exposure to the ambient atmospheric ram, but this will hopefully never be put to the test in flight. At all other angles the focal plane glow flux is predicted to be safely below the average sky background level of roughly 23 mag/arc sec².

The tolerable levels of extended glow emission (where "tolerable" is defined as less than or equal to the sky background) are plotted in Figure 8 as a function of wavelength in the astronomer's units of Rayleighs/Å. Comparison with Figure 6 shows that even direct viewing glow emission should not be a problem due to the decreased [O] at 590 km. If the glow is somewhat extended and brightens in the near-IR (neither of which would be a particular surprise), however, the glow may be the limiting factor on ST sensitivity in the near-IR spectral range. An additional illustration of

the relation between glow brightness and ST detection limits is shown in Figure 9 as a plot of the sky brightness equivalent to the flux in one planetary camera (PC) pixel that would be received from the representative blue spectrum of a hot star or QSO of $m_v = 30$, which is in turn equal to the sky background per PC pixel at 5500 \AA .

Work Needed to Address Immediate Concerns for Space Telescope

The information required for Space Telescope can be divided into the near-IR, visible, and UV spectral ranges. Although a better understanding of the glow phenomenon is unlikely to influence any ST hardware at this stage of the program, the existence and characteristics of any unacceptably bright glow emissions will affect both ST operations and the planning for second-generation SI's. The ST project recommendations are therefore aimed at addressing the following problems before ST launch:

1. The existence and brightness of any near-IR glow.

The indication from the existing visible spectra is that the maximum glow brightness will be observed in the near-IR spectral range. The region from 8000 \AA to 5 microns is of great interest in planning for second-generation SI's and has never been observed for glow! Spectroscopy at these wavelengths is also crucial to identifying the emitting species and excitation conditions, including knowing the lifetimes of the excited states which in turn determines the extent of the glow above a surface. It should also be noted that the different theories for molecular glow predict vastly different brightnesses in the near-IR.

2. Validate the brightness and altitude dependence of the visible glow.

Although the rough spectrum of the glow from $4000\text{-}8000 \text{ \AA}$ is known, the brightness of the glow above any given surface is uncertain by 1-2 orders of magnitude due to our lack of knowledge of the excitation processes. Other factors to be studied are listed in the conclusion of this section.

3. Does there exist a UV glow?

The visible spectra suggest that the brightness of the continuum glow is decreasing into the UV, and upper limits to any UV glow derived from earlier spaceborne airglow spectrometers indicate that there is no bright UV continuum glow. None of the earlier instruments looked at surfaces exposed to the ram, however, and it is conceivable that known atmospheric UV line and band emissions may be enhanced by the passage of spacecraft through the atmosphere. Candidate atmospheric emissions are OI 1304 \AA and 1356 \AA (which are known to be particularly bright in the tropical arcs at $+15^\circ$ magnetic latitude), NO gamma and delta bands ($1900\text{-}2400 \text{ \AA}$), N_2 Lyman-Birge-Hopfield bands (roughly $1000\text{-}2000 \text{ \AA}$), and various lines of NI and N_2 .

For all spectral regions the functional dependencies need to be determined between glow brightness and:

- atmospheric density and species
- angle of pointing to the ram vector (including possible wake glow)
- surface material and composition
- spacecraft charging and outgassing
- distance above the surface (lifetimes of excited states)
- relation to thruster firings

References

- Abreu, V. J., W. R. Skinner, P. B. Hays, and J. H. Yee, in Proceedings of the AIAA Shuttle Environment and Operations Meeting, p. 178, Paper #83-2657, AIAA, New York, 1983.
- Banks, P. M., P. R. Williamson, and W. J. Raitt, Geophys. Res. Lett., 10, L118, 1983.
- Dube, R. R., W. C. Wickes, and D. T. Wilkinson, Astrophys. J. Lett., 215, L51, 1977.
- Langhoff, S. R., R. L. Jaffee, J. H. Yee, and A. Dalgarno, Geophys. Res. Lett., 10, L896, 1983.
- Mende, S. B., O. K. Garriott, and P. M. Banks, Geophys. Res. Lett., 10, L122, 1983.
- Slanger, T. G., Geophys. Res. Lett., 10, L114, 1983.
- Swenson, G. R., S. B. Mende, and K. S. Clifton, Geophys. Res. Lett., 12, L97, 1985.
- Torr, M. R., Geophys. Res. Lett., 10, L114, 1983.
- Torr, M. R., and D. G. Torr, J. Geophys. Res., 90, 1683, 1985.
- Witteborn, F. C., K. O'Brien, and L. Caroff, J. Geophys. Res., submitted, 1985.
- Yee, J. H., and V. J. Abreu, Geophys. Res. Lett., 10, L126, 1983.
- Yee, J. H., and A. Dalgarno, in Proceedings of the AIAA Shuttle Environment and Operations Meeting, Paper #83-2660, AIAA, New York, 1983.
- Yee, J. H., V. J. Abreu, and A. Dalgarno, J. Geophys. Res., in press, 1985.

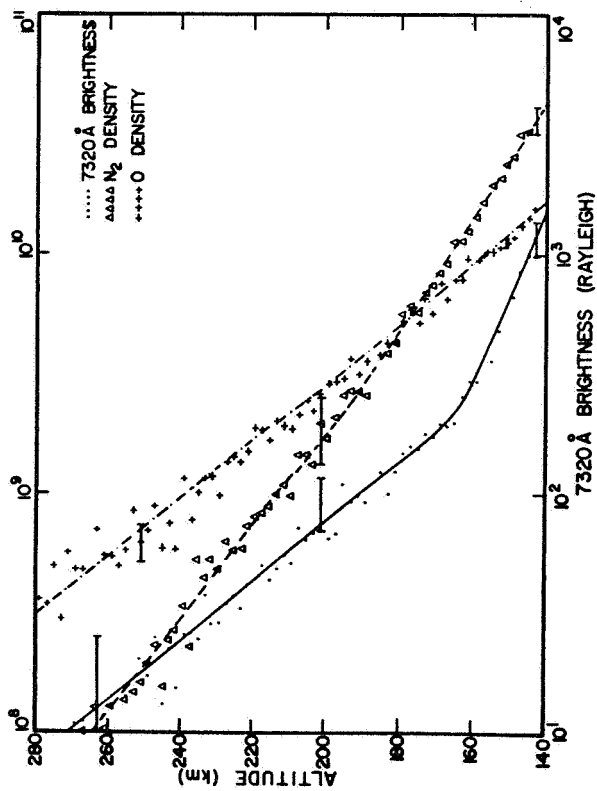


Fig. 1. The altitude variation of the glow emission at 7320 Å, along with the measured number densities of atomic oxygen and molecular nitrogen.

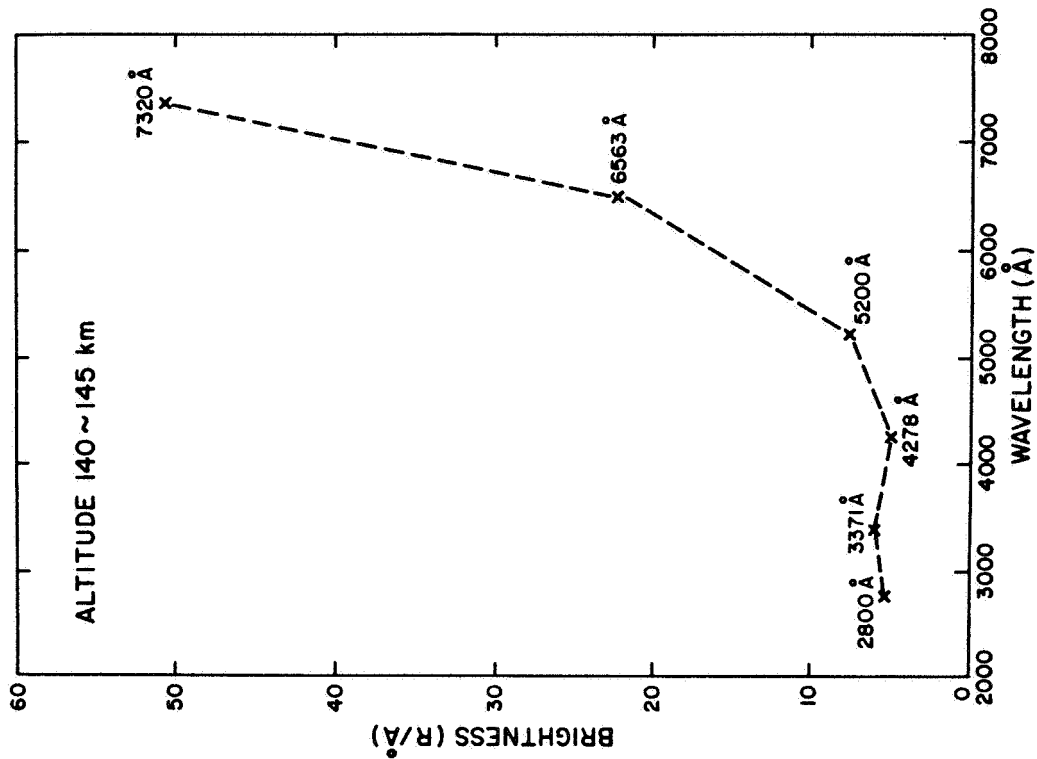


Fig. 3. The spectral variation of the glow emission at 140-145 km.

Fig. 1. Figures from Yee and Abreu [1983] showing AE glow properties.

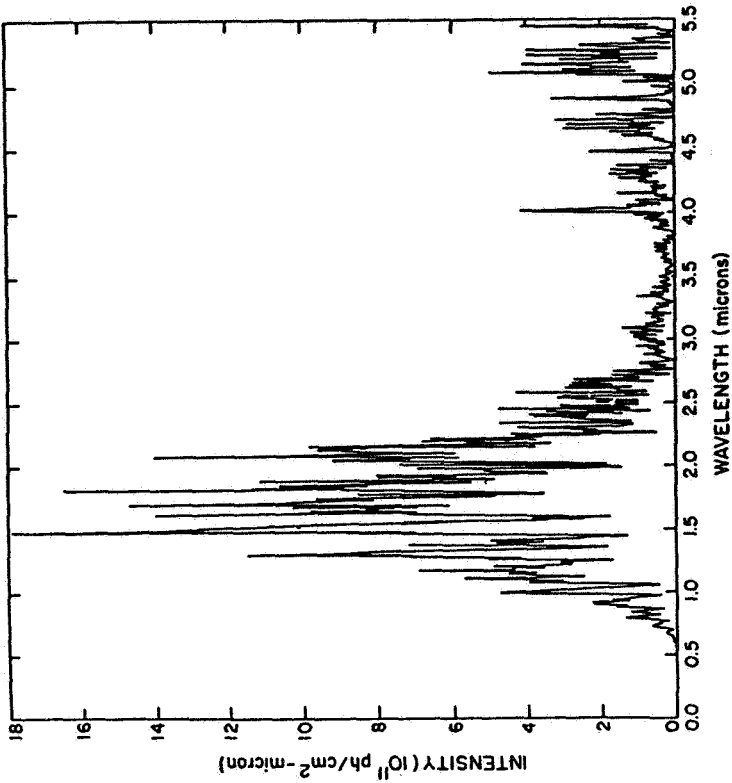


Fig. 1. The emission intensity of the OH Meinel system between 2000-7500 Å at 20 Å resolution. The spectrum is constructed for the case when all vibrational levels are equally populated and rotational distribution is thermal at 300 K. To give an absolute scale, we assume arbitrarily that there are 10^{10} particles cm^{-3} radiating in a layer 1 cm thick.

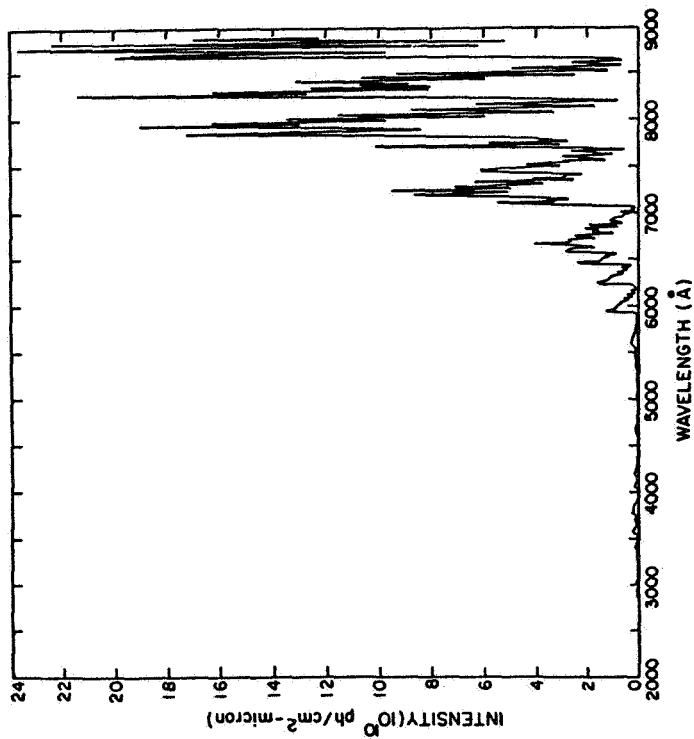


Fig. 2. Modeled OH band emission spectrum from Langhoff et al. [1983].

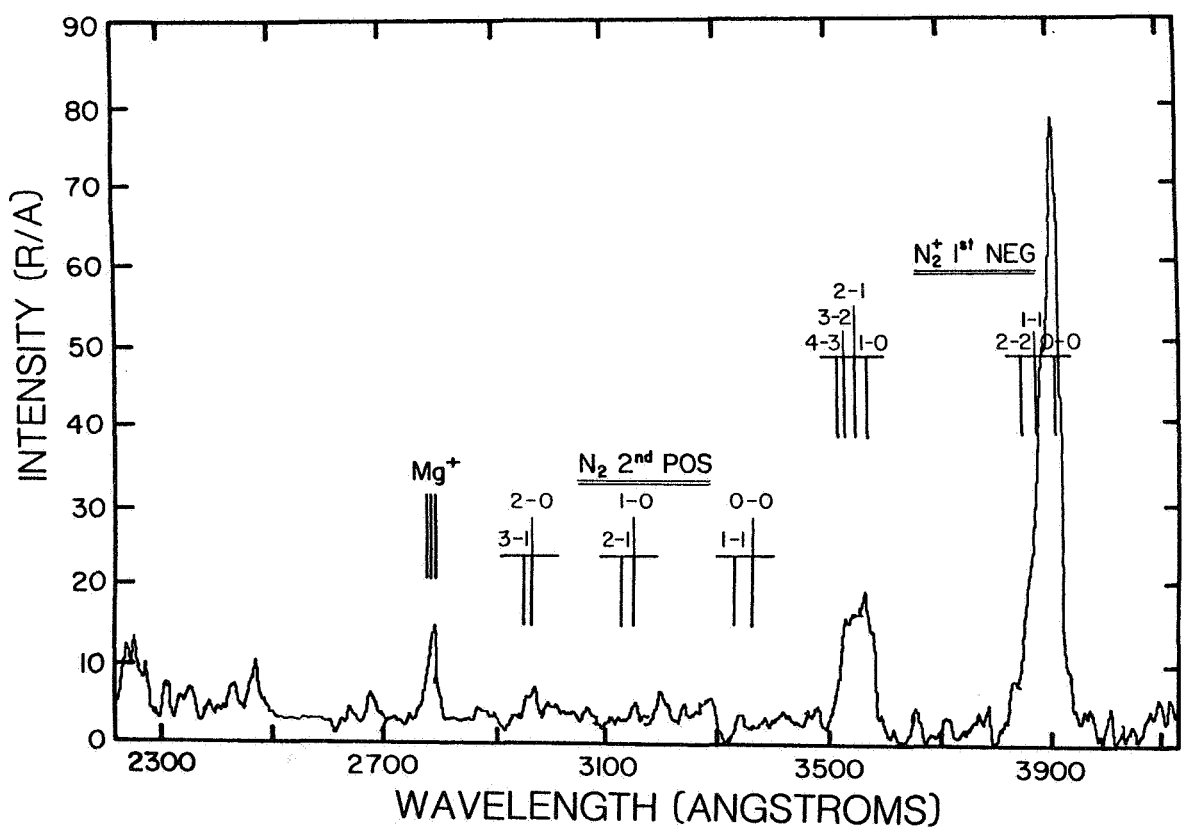
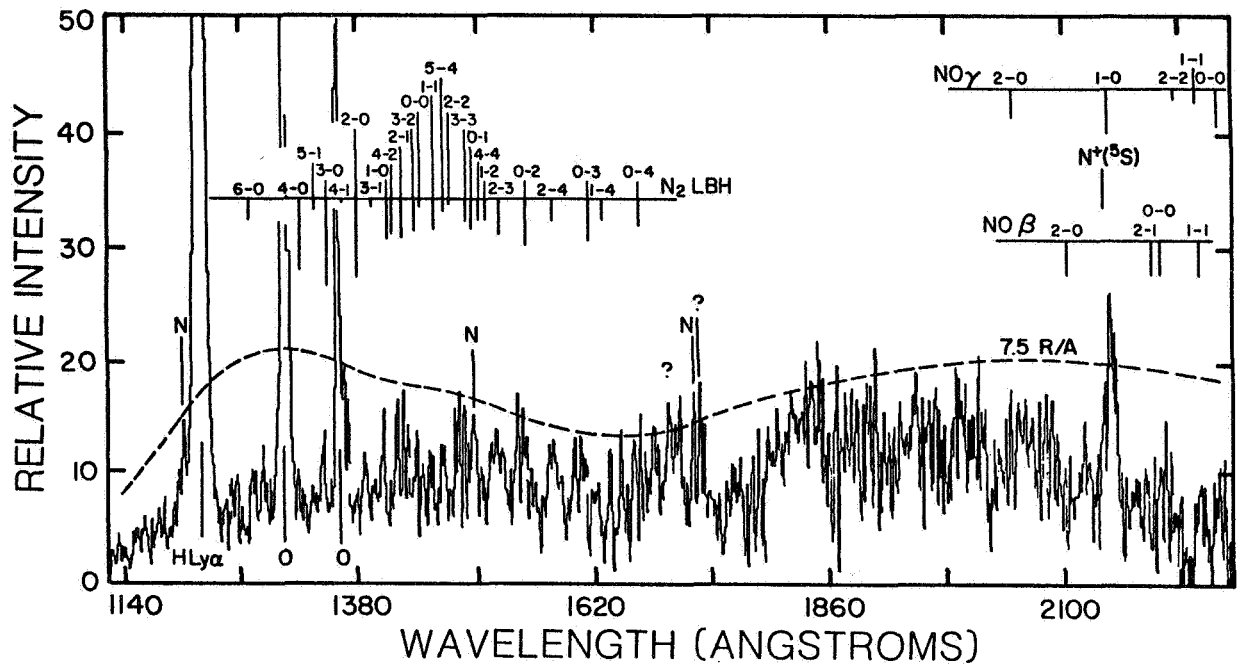


Fig. 3. Shuttle glow spectra from Spacelab 1 (from Torr and Torr [1985]).

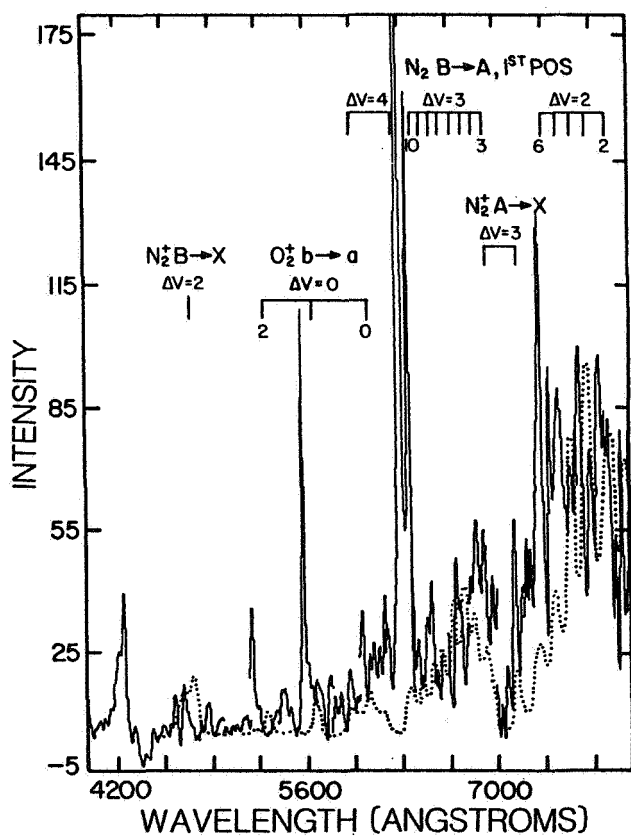
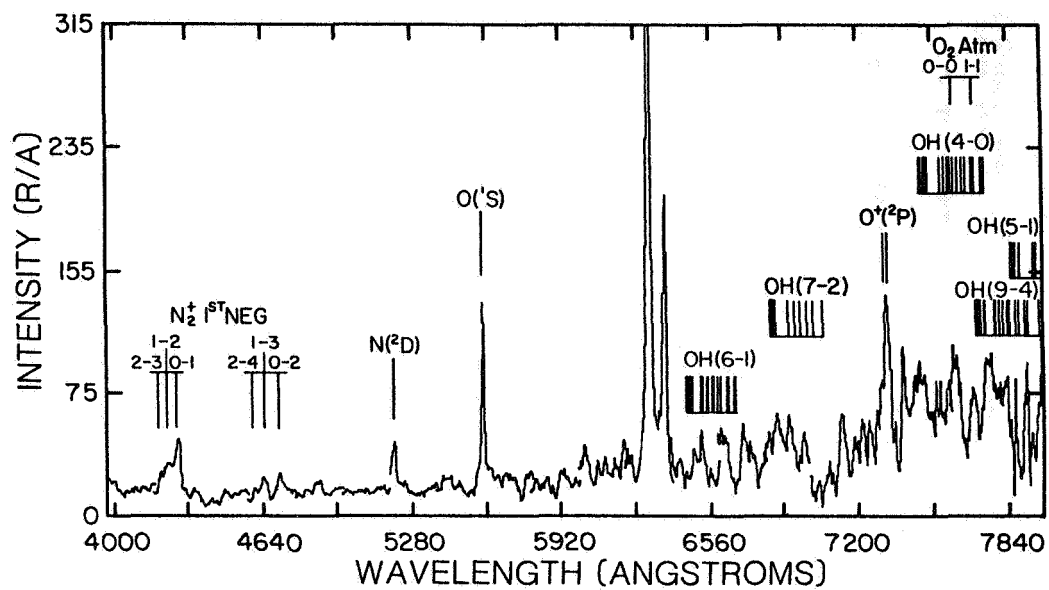


Fig. 4. Shuttle glow spectra from Spacelab 1 (from Torr and Torr [1985]).

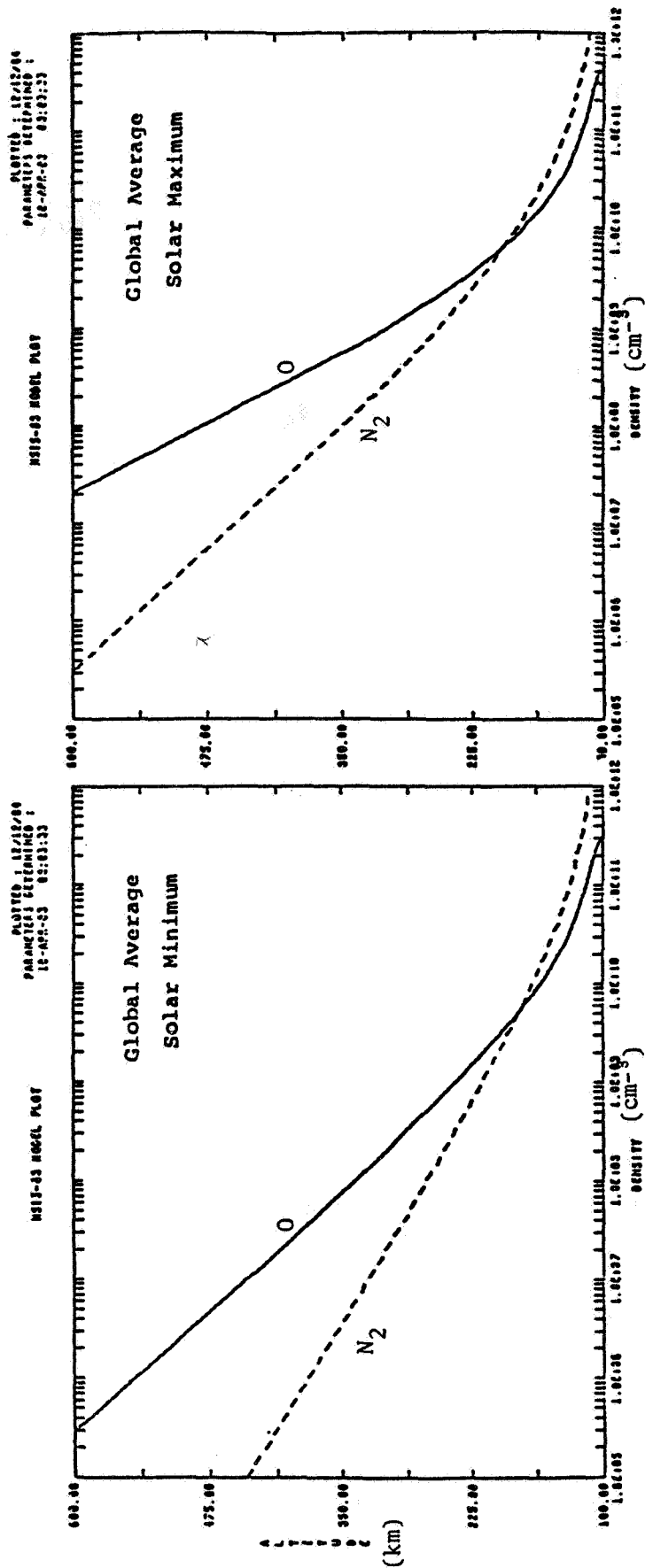


Fig. 5. MSIS model atmospheres from A. Hedin (GSFC).

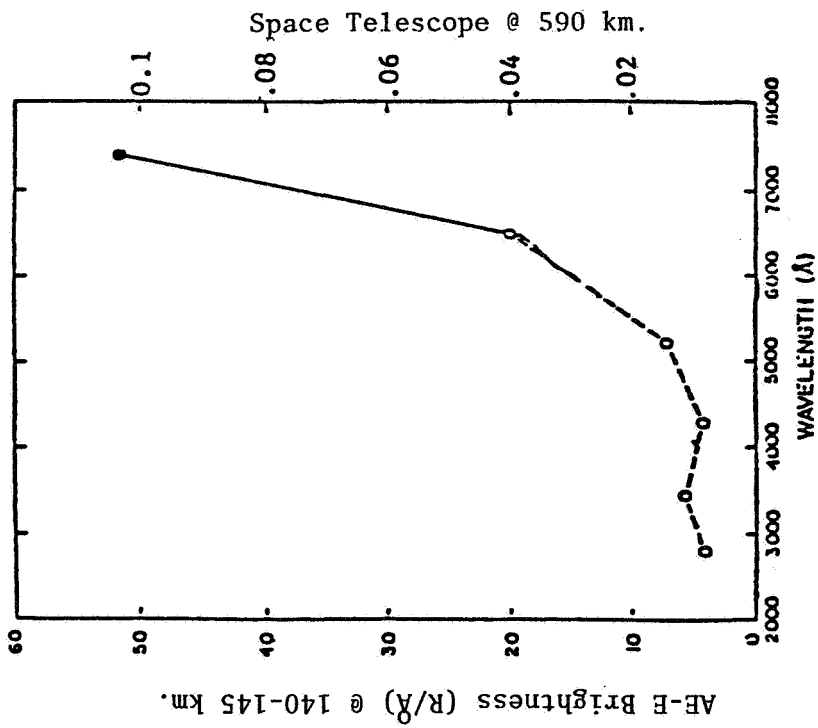
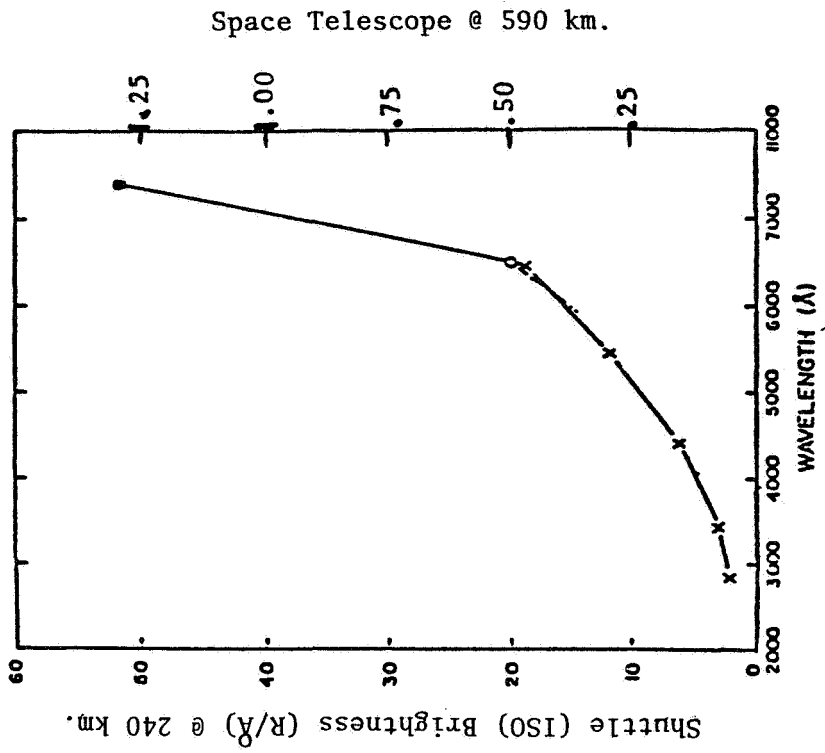


Fig. 6. Scaling observed glow brightnesses to ST altitudes (for solar max. [0] altitude profile).

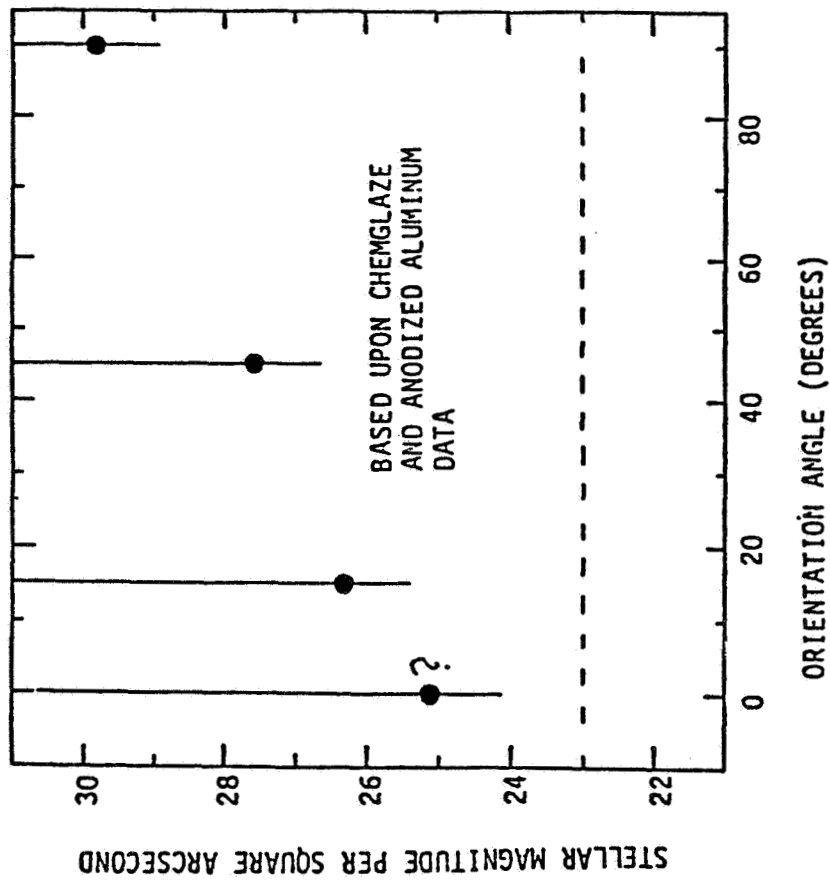


Fig. 7. Total glow induced focal plane straylight irradiance as a function of the angle between the telescope axis and incident oxygen vector. The zero degree case, being dominated by glow from the primary mirror, has the greatest uncertainty since glow from the MgF₂ coating has not yet been characterized.

1st Example: Plot the expected sky background due to zodiacal light in units of Rayleighs/ \AA

- Assume average zodiacal light brightness of 60 S10 units [Dube et al., 1977] at 5500 \AA : $60 \text{ S10} = 0.26 \text{ Rayleighs}/\text{\AA} = 23.3 \text{ m}_V/\text{arc sec}^2$.
- Scale to other wavelengths by solar spectrum (observed to be accurate from 1800 \AA to 3 microns)

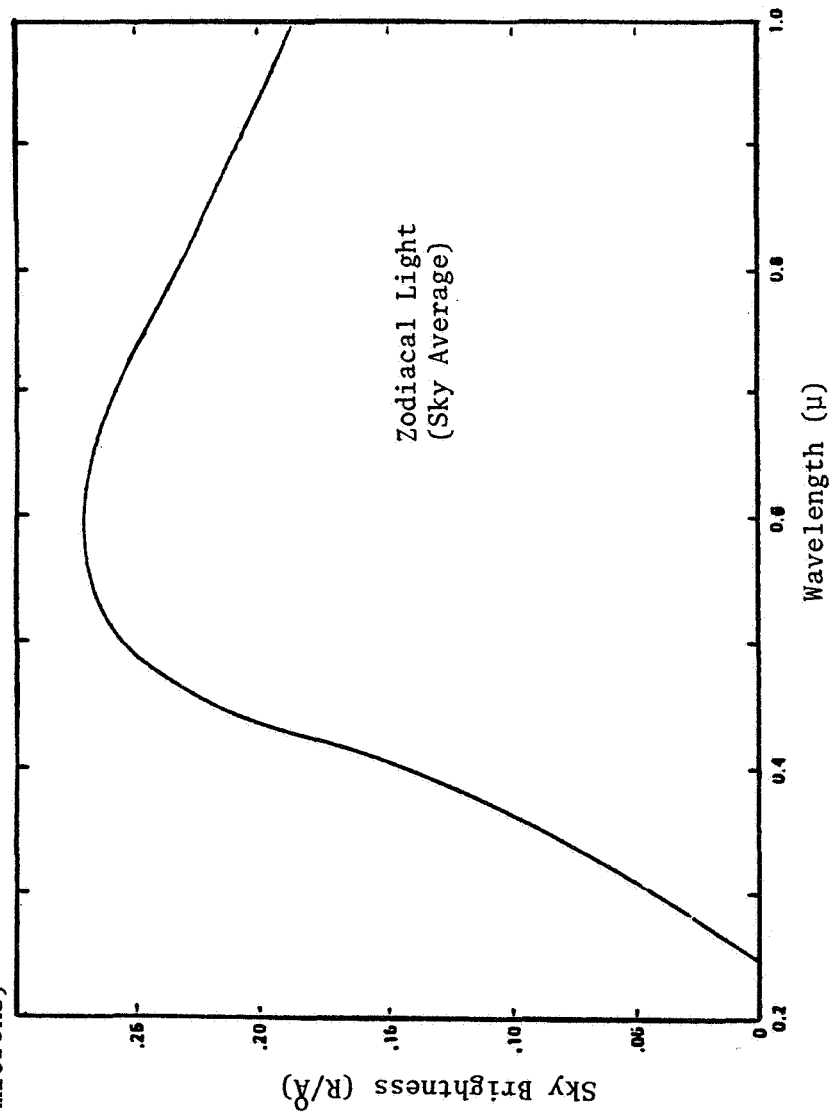


Fig. 8. Comparison of glow brightness with ST detection limits.

2nd Example: What sky brightness is equivalent to a point source with a flat spectrum (in F_{ν} units) filling one planetary camera pixel?

- Assume point source is equal to sky background of $23.3 \text{ mag/arc sec}^2$ scaled to 1 PC pixel of $0.048 \times 0.048 \text{ arc sec}^2$.
- Equivalent source (QSO or hot star) has $F_{\nu} = 4 \times 10^{-32} \text{ erg/cm}^2\text{-sec-Hz}$ or $m_{\nu} = 30$.

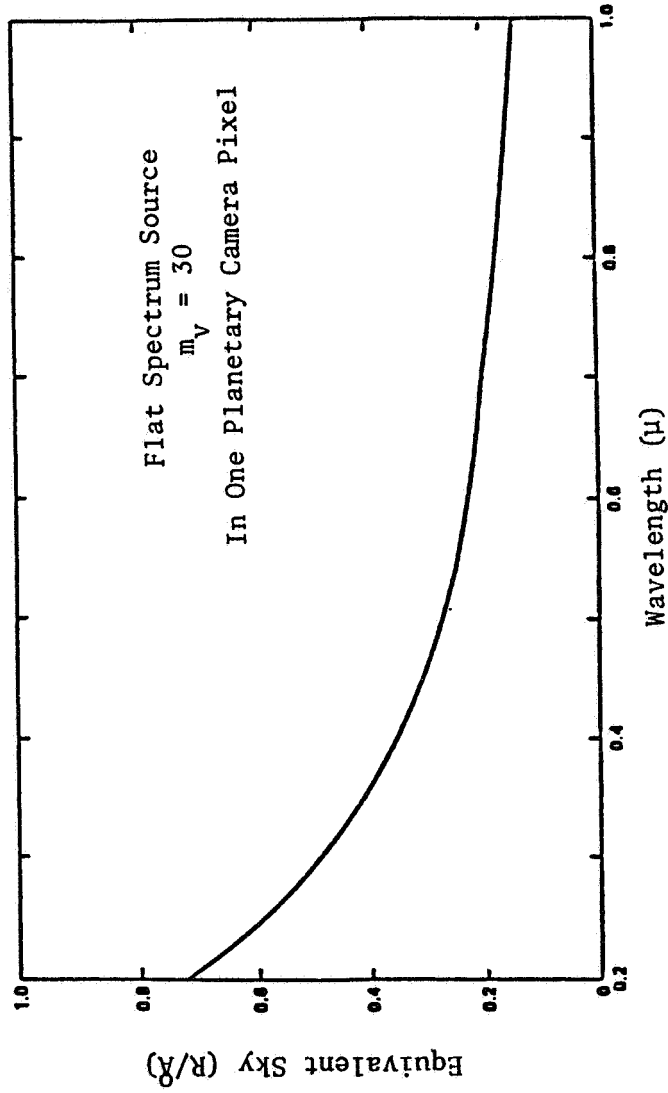


Fig. 9. Comparison of glow brightness with ST detection limits.

INFRARED MEASUREMENTS OF SPACECRAFT GLOW
PLANNED FOR SPACELAB 2

Giovanni G. Fazio and David G. Koch

Smithsonian Astrophysical Observatory

Abstract. A liquid helium cooled infrared telescope (IRT) will be flown in July 1985 on Spacelab 2. The instrument was designed to measure both diffuse and discrete infrared astronomical sources, including the zodiacal light, galactic, and extragalactic components, as well as to evaluate the induced Orbiter environment. The focal plane contains ten photoconductive detectors covering six broad bands from 2 to 120 microns. Each detector has a 0.6 by 1.0 deg. field-of-view optimized for detection of extended sources of IR radiation. Except for the 2-micron detector, the system noise is limited by the sky background noise.

This paper describes the measurements planned for the IRT using the 1-meter base of the Plasma Diagnostics Package (PDP), an already existing SL 2 experiment, as the glow generating surface. The measurements will be repeated changing the position of the PDP, the attitude of the Orbiter, and the ram direction in an effort to remove both the thermal component of the PDP emission and the cosmic background radiation.

Introduction

The primary intent of these observations is to obtain measurements of the glow phenomenon in the infrared produced by the base of the Plasma Diagnostics Package (PDP). The IRT is capable of obtaining data in six broad passbands: 2.0-3.0, 4.5-9.5, 6.1-7.1, 8.5-14.5, 18-30, and 70-120 microns. The two longest wavelength passbands, 18-30 and 70-120, include three detectors each. See Koch, et al. [1982] for a complete description of the instrument. Young, et al. [1981] contains a detailed description of the IR detector performance. Additional data that will be of use in interpreting the results will come from the in situ measurements by the PDP of the particles and fields associated with the ram gases. Specifically, data from the mass spectrometer will be used. Further data that will be of use are measurements available in the visible from the image-intensified camera [Mende et al., 1985]. The equatorial altitude for this mission will be 383 km and the inclination 49.5 deg.

Method of Observation

In an attempt to determine a dependence on material two observational methods will be used. One will be to see if there is any glow from the inside of the gold-coated mylar sunshade of the IRT. The other will be to look for the glow from the base of the PDP, which is covered with beta cloth and aluminum screen as the PDP is positioned near the beam of the IRT. The Orbiter Remote Manipulator System (RMS) will be used to position the PDP so that the flat base of the PDP will be in the Orbiter Y-Z plane. In both of the methods of observation described below the telescope will be fixed (stowed) and viewing along the Orbiter -Z axis (see Figure 1).

Observing Constraints

During the glow measurements, the field-of-view of the telescope must encompass regions of low infrared brightness. Such regions include the ecliptic pole or the galactic pole and must avoid regions near or crossing the galactic plane. (The preferred orbit would have the plane of the orbit pass near the ecliptic pole.) While the data are being taken the field-of-view, hence the Orbiter, must be held inertially on the sky. In addition, the data must be taken on the nighttime side of the orbit in order to observe with the lowest possible background and to permit optical photography of the glow. The velocity vector should be kept approximately normal to the base of the PDP. Data cannot be taken while near or passing through the South Atlantic Anomaly (SAA). Water dumps, operation of the flash evaporators, experiment purges, and other sources of effluent must be inhibited prior to and during data taking.

Since the thermal radiation from the PDP is substantial it will be important to have the thermal conditioning prior to and during the observing runs as nearly identical as possible.

Observing Sequence

Due to the uncertainties in both the absolute position of the PDP when manipulated by the RMS and the alignment of the telescope with respect to the Orbiter, it will be necessary to make the glow measurements by gradually cycling the PDP into and out of the field-of-view of the telescope. This will also provide a means of establishing the baseline intensity without the PDP. The intensity will be correlated with the RMS positional information. This cycling with the RMS will be repeated for each of four separate inertial positions on the sky during the 36 minutes of Earth shadow during two consecutive orbits. On the first orbit the PDP base will be pointed into the wake and on the second orbit the PDP base will be pointed into the ram, all other conditions remaining the same. During the first three inertial positions, the PDP will be moved in closer and closer to the telescope beam at about 15 cm above the sunshade aperture. During the fourth inertial position the PDP will be raised 5.7 meters above the aperture where the 1-meter PDP diameter will still fill the 15-cm telescope beam, but the thermal effects from the PDP will fill a much smaller portion of the telescope side

lobes. This alternate position is shown in Figure 2. Before each RMS cycle, the cold shutter at the focal plane will be actuated to provide an absolute flux level. On the second orbit when the PDP base is into the ram, the mass spectrometer on the PDP will be pointed into the ram to provide in situ measurements of the plasma.

Data Deconvolution

To be able to distinguish the thermal radiation of the PDP from the glow, as well as to measure the intensity scale height of the glow, the method of observation has to provide many differential experiments. These include moving the source (PDP) in and out of the telescope beam, repeating the cycles at different distances from the beam, and repeating at a different height above the aperture. Before and after each cycle the cold shutter is used to provide an absolute flux level. All of this is done first with the PDP base in the wake where there should not be any glow and only the infrared of the environment and sky is measured. Then the entire process is repeated on the next nighttime pass with the base into the ram where any difference in signal should be due to the glow. Any slight variations of the sky background due to variations in the inertial position can be corrected, since the prime objective of the IRT is to measure the large-scale structure of the sky. In addition to the many signal modulation and differentiation effects, the glow should be distinguishable spectrally from the zodiacal and the PDP thermal radiation, both of which are approximately 300 K blackbodies.

Finally, any glow off of the inner surface of the gold-coated mylar sunshade should be detectable and separable from other signals since during each cycle of the RMS, the telescope is held inertially on the sky, but during the 4 to 9 minutes of inertial hold, the orbital motion will result in the velocity vector varying from slightly into the sunshade aperture to slightly out of the sunshade. During normal IR mapping the telescope aperture will always be pitched slightly away from the velocity vector so that the inside of the sunshade is never exposed to the ram.

Expected Results

An estimate of the expected infrared flux can be made based on the following assumptions:

1. The glow is due to atomic oxygen impacting the surface at 7.7 km/sec.
2. The atomic oxygen flux at 400 km altitude is 1.5×10^{14} /cm²/sec.
3. The spectral shape of the emitted radiation will resemble that of highly excited OH.
4. The decay distance from the PDP base produced by oxygen impact is 1 meter or more.

In the paper by Banks et al. [1983] the volume density of the visible photon emission was estimated to be 2×10^7 photons/cm³/sec at the 280 km altitude for STS-3. This was observed in about a

0.1 micron band so that the spectral flux is 2×10^8 photons/cm³/sec/micron at about 0.65 microns. If the emitting species is OH we can use Langhoff's [1983] calculated spectrum to get volume densities of 10^{10} /cm³/sec/micron at 1.3 to 2.2 microns at 280 km and 10^9 /cm³/sec/micron at 4.5 to 6.5 microns beyond which it drops rapidly with increasing wavelength. The IRT will look through a 100-cm-thick volume of gas that is radiating into 4π sr. Therefore, the telescope should see a flux of 8×10^{10} photons/cm²/sec/sr/micron at 1.3 and 2.2 microns and $I_{280} = 16 \times 10^9$ photons/cm²/sec/sr from 4.5 to 6.5 microns. From ground-based measurements of STS-9 (240 km altitude) by Witteborn et al. [1985] a flux of 5×10^{11} photons/cm²/sec/sr/micron at 1.6 microns was observed and the observed flux at 2.3 microns was attributed entirely to the diffuse reflection of the Earth thermal emissions. This would imply a factor of about six times more emission at 1.6 microns than expected from using Langhoff's method.

The zodiacal emission in the 4.5-8.5 micron band is about 7×10^9 photons/cm²/sec/sr which is comparable to I_{280} . Since SL 2 will be at 400 km altitude, the oxygen incidence will be ten times lower, resulting in an equivalent decrease in the volume densities of photon emission. Consequently the irradiance at 400 km from "O-glow" would be $I_{400 \text{ km}} = 1.6 \times 10^9$ photons/cm²/sec/sr. This is only 20% of the zodiacal emission expected in the ecliptic, 90 deg. from the Sun. This irradiance would be about 60% of the zodiacal emission (away from ecliptic plane) over most of the hemisphere away from the Sun. Distinguishing the O-glow from the zodiacal emission should be easy, since the O-glow is not expected to contribute to the observed flux at wavelengths beyond 15 microns. Thus the O-glow should change the ratio of the radiation in the 4.5-9.5 micron band to that in the 18-30 micron band.

Conclusions

Although the plan to make the glow measurements have evolved only recently (after the final mission plan for SL 2 was formed), the opportunity to perform these IR measurements with existing hardware in so near a term has led us to dedicate two of the 18 revs. planned for IR celestial observations to making these measurements. It appears that in using the observing plan outlined above, the glow should be detectable in the near IR for the given geometry. Otherwise, the observations will put severe upper limits on the flux, limiting it to well below the zodiacal flux for the geometry described.

Acknowledgments. Funding for the IRT is provided by NASA Grant NAS8-32845. The calculations for the expected flux were performed by F. Witteborn, NASA/Ames Research Center.

References

- Banks, P. M., Williamson, P. R., and Raitt, W. J., Geophys. Res. Lett., 10, 118-121, 1983.
- Koch, D., G. G. Fazio, W. A. Traub, G. H. Rieke, T. N. Gautier, W. F. Hoffmann, F. J. Low, W. Poteet, E. T. Young, E. W. Urban, and L. Katz, Optical Engr., 21, 141-147, 1982.
- Langhoff, S. R., R. L. Jaffe, J. H. Yee, and A. Dalgarno, Geophys. Res. Lett., 10, 896-899, 1983.
- Mende, S. B., G. R. Swenson, K. S. Clifton, R. Gause, L. Leger, and O. K. Garriott, J. Spacecraft & Rockets, in press, 1985.
- Witteborn, F. C., K. O'Brien, and L. Caroff, NASA TM-85972, March 1985.
- Young, E. T., G. H. Rieke, T. N. Gautier, W. F. Hoffmann, F. J. Low, W. Poteet, G. G. Fazio, D. Koch, W. A. Traub, E. W. Urban, and L. Katz, in Infrared Astronomy--Scientific/Military Thrusts and Instrumentation, SPIE 280, pp. 12-19, 1981.

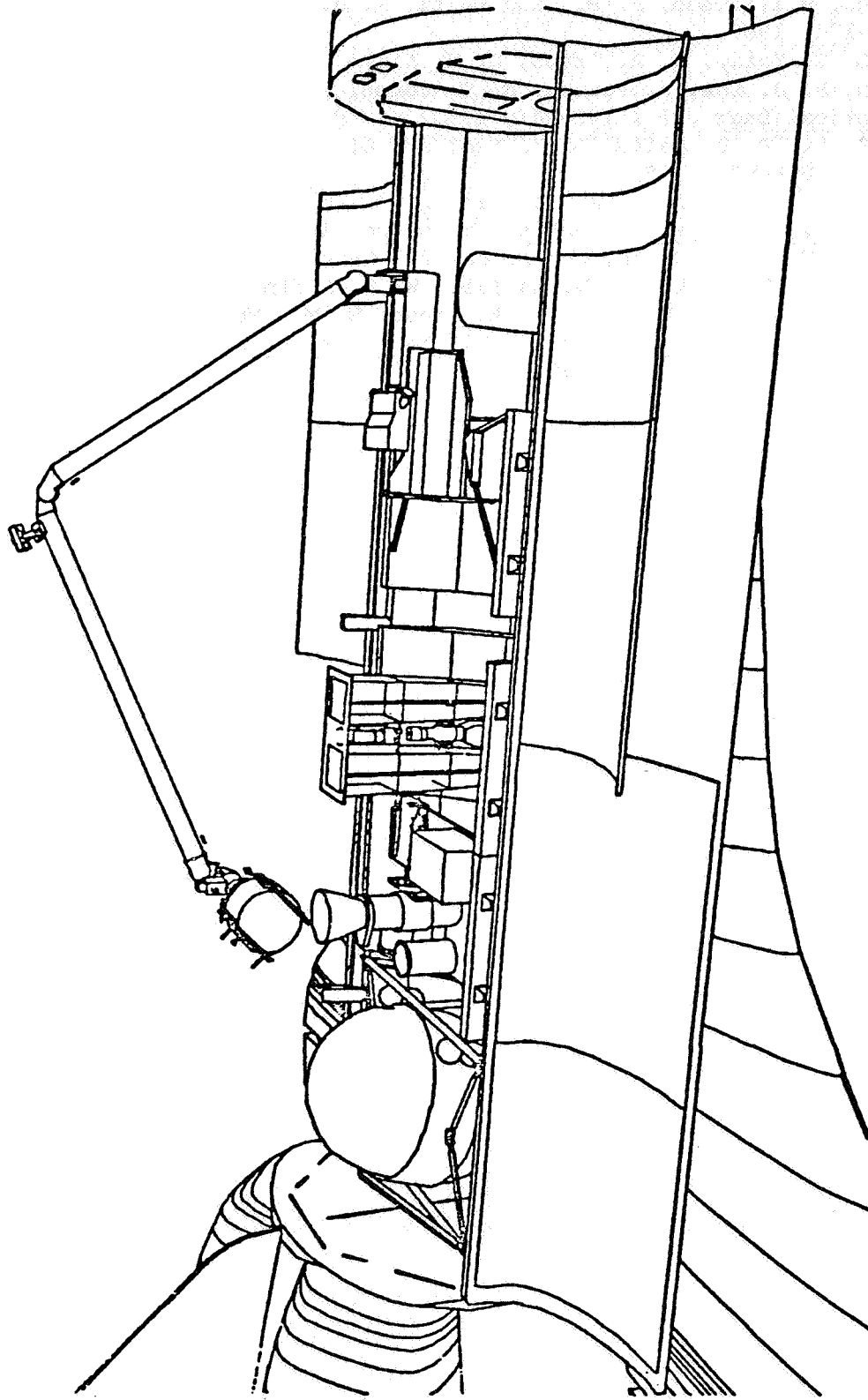


Fig. 1. View of the Spacelab 2 payload showing the Plasma Diagnostics Package being positioned above the Infrared Telescope by the Remote Manipulator System. The velocity vector is from wing-tip to wing-tip.

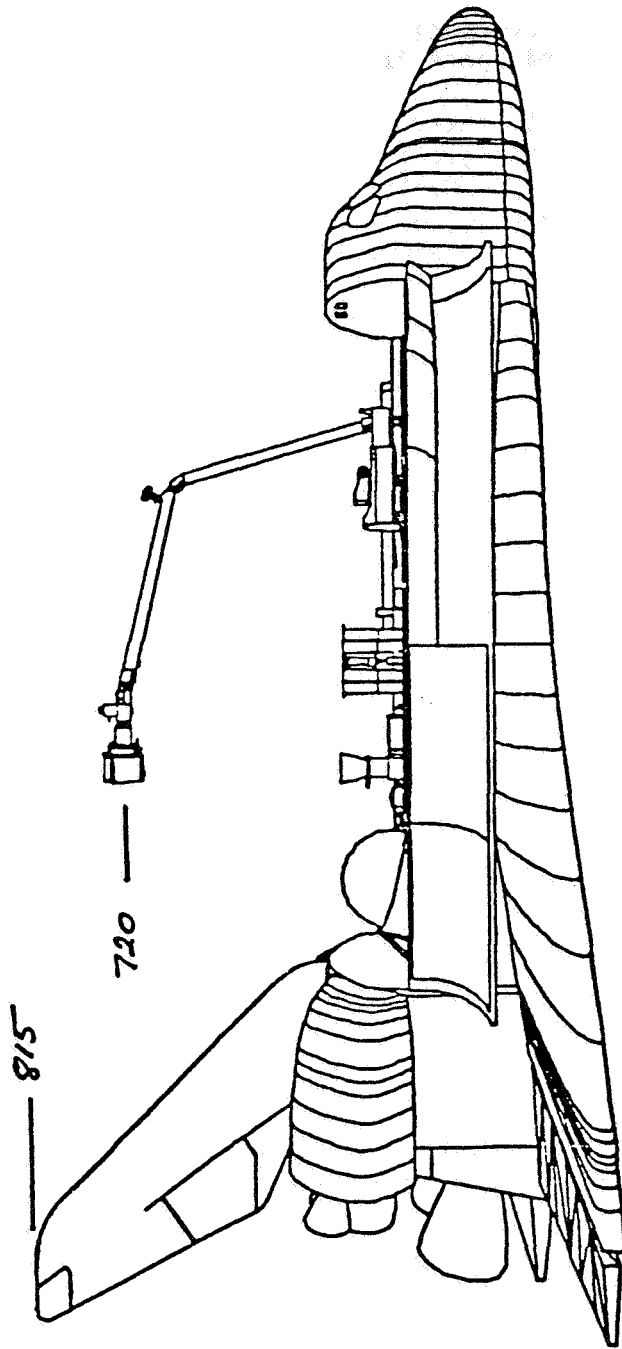


Fig. 2. View of the PDP position during the fourth inertial hold/RMS cycle.

PLANNED INVESTIGATION OF INFRARED EMISSIONS ASSOCIATED WITH
THE INDUCED SPACECRAFT GLOW:
A SHUTTLE INFRARED GLOW EXPERIMENT (SIRGE)

Michael J. Mumma and Donald E. Jennings

Planetary Systems Branch, Laboratory for Extraterrestrial Physics,
NASA/Goddard Space Flight Center

Abstract. We will investigate the characteristics of infrared molecular emissions induced by energetic collisions between ambient atmospheric species and surfaces in Earth orbit, using low-resolution infrared spectroscopy. The spectrometer will be a liquid-nitrogen-cooled filter wheel photometer covering the wavelength range 0.9-5.5 microns with a resolving power ($\lambda/\Delta\lambda$) of approximately 100. This resolving power will be sufficient for identification of the molecular or atomic fluorescent species causing the glow.

Introduction

The instrument to be used for the Shuttle Infrared Glow Experiment (SIRGE) will be a liquid nitrogen cooled spectrometer flown in a GAS canister in the Hitchhiker-G program. With it, we will study the infrared (0.9-5.5 micron) component of the induced shuttle glow [Abreu et al., 1983; Banks et al., 1983; Langhoff et al., 1983; Mende et al., 1983; Slinger, 1983; Yee and Abreu, 1983]. The spectrometer uses a circular variable filter (CVF) to provide a spectral resolving power ($\lambda/\Delta\lambda$) of 100 and a sensitivity (single scan NESR) of less than 2×10^{-14} watts/cm² sr cm⁻¹. This is necessary to reach the zodiacal light limit, which is considered the limiting flux source for astronomy in the near infrared. The infrared glow study has been requested by the Hubble Space Telescope (HST) project office because of concern expressed by the astronomical community regarding the impact which a glow from HST might have on the feasibility of infrared observations, and on the choice and design of infrared instruments for HST. It has also been proposed (C. R. O'Dell, private communication) that the infrared glow spectrometer be flown on the HST deployment mission, to determine the magnitude and character of the glow surrounding the telescope after ejection from the shuttle. The glow near the shuttle itself will be studied on this and subsequent missions to help characterize and model the emission so that predictions can be made for various spacecraft and various altitudes. The high sensitivity and moderate resolution specified for this instrument are necessary for a complete characterization of the glow.

Instrument Specifications

Figure 1 shows a conceptual drawing of the SIRGE instrument. Table 1 lists the basic specifications. The spectrometer will be mounted in a liquid nitrogen dewar, and housed in a Getaway Special (GAS) can. The instrument will be mated with the Hitchhiker-G avionics, and mounted on a single GAS beam for ease of manifesting on the space shuttle (Figure 2).

The inner liquid nitrogen container will be supported within the GAS can with a thermally isolated structure, and will be radiatively shielded with multiple-layer-insulation. Fill and vent ports will be provided, along with a pumping port for the dewar vacuum jacket, and these will be accessible from the top of the GAS can. The effluent gas will be routed away from the vicinity of the optical aperture to avoid potential modification of the local glow effects on orbit. A sealed aperture door will open in orbit to expose the instrument to the glow. This door will also provide a radiation (heat) shield for the aperture during the ground hold time. A sun sensor will close the door automatically. The dewar will have a minimum hold time of 15 days, including 5 days pre-launch hold time. The dewar will be filled with a carbonized rayon porous material to prevent phase separation in zero gravity. The dewar will be vented through a pressure regulator, maintaining the temperature of the liquid nitrogen at 65 kelvin (or lower, TBD).

The spectrometer will use entirely reflective optics (except for the CVF) to reduce scattered light and improve throughput (Figure 3). Reflective optics provide several additional advantages, principally related to the absence of dispersion. Thus, all wavelengths are focussed simultaneously at the same point, and the wavelength response can be extended in future by replacing only the detectors and the wavelength-selecting filters. Alignment can be carried out at visual wavelengths, and the parabolic mirrors can be diamond-machined under numerical control, which greatly assists assembly and alignment.

The input aperture will be baffled to minimize scattered light, e.g. from the Sun, Earth, and Moon. Rejection of off-axis stray light will be further enhanced with a Lyot stop in the fore-optics (Figure 3). The field-of-view of the spectrometer will be $4^\circ \times 4^\circ$ square and the collecting aperture will be 0.6 inch diameter. After passing the Lyot stop, the collected radiation is re-focussed onto a circular-variable-filter wheel (CVF) where wavelength selection occurs. The CVF will have three sections, variable in wavelength: 0.9-1.8, 1.5-3.0, and 2.7-5.5 microns. The spectral resolution of the CVF is 1% of the wavelength. All filter components are available commercially. The transmitted radiation is re-focussed onto an infrared detector (InSb), operated at 65 kelvin (or lower) to provide an NESR of less than 2×10^{-14} watts/cm² sr cm⁻¹ in a 5-second scan. The scan time will be as short as is possible ($\sqrt{5}$ seconds) without degrading sensitivity due to bandwidth limitations. The detector will use a trans-impedance amplifier with a load resistor of approximately 2×10^6 ohms. A stimulator (infrared source) will be located in the pre-optics area to provide an internal calibration source. The expected instrument sensitivity is compared with the zodiacal background, with various external calibration objects, and with possible glow intensities in Figure 4.

A second detector will be provided in the pre-optics area to be used in the broadband mode. It will be sampled at the same rate as the narrow-band detector in the focal plane, but will observe the full spectrum at once to monitor rapid changes in the glow flux level (during thruster firing, for instance) and to measure very weak fluxes. The flight electronics will oversample the focal plane detector signal by a

factor of 5-10 and provide a dynamic range of 10^5 . Additional channels will be provided for the broadband detector and several temperature sensors. The output of the electronics will be compatible with the Hitchhiker avionics. The power and instrument control lines, and the data lines, will be routed through the bottom of the GAS can (Figure 1). The power and instrument control will be supplied via the Hitchhiker avionics. Data will be recorded onboard and also downlinked to ground support equipment, providing direct control of the experiment and real-time data inspection during flight.

The entire assembly will be compatible with GAS/shuttle launch and orbit conditions, and will satisfy structural, thermal, and safety requirements for GAS payloads. The entire flight instrument will be contained in a single GAS can, so that the Hitchhiker avionics and instrument GAS canister can be flown on a single GAS beam (Figure 2).

Sensitivity

InSb detectors near 1 mm in diameter and having high sensitivity are commercially available, and will be used. The optical throughput (etendue) is then easily calculated from the f/1.83 detector focussing mirror to be

$$A_{\Omega} = 1.03 \times 10^{-2} \text{ cm}^2 \text{ sr} \quad (1)$$

This etendue is preserved throughout the optical system. The collecting mirror at the entrance aperture has an effective diameter of 3.14 cm and is operated at f/1.6. The field stop is 4 mm x 4 mm, corresponding to a square beam on the sky of $4.5^{\circ} \times 4.5^{\circ}$.

The Noise-Equivalent-Spectral-Radiance (NESR), for an extended source of uniform surface brightness which fills the field-of-view, is given by

$$\text{NESR} = \frac{\text{NEP}}{TA_{\Omega} \Delta\nu \sqrt{\tau}} \quad \text{watts/cm}^2 \text{ sr cm}^{-1} \quad (2)$$

where

- NEP = $(10^{-4} \nu) \text{NEP}_1$, the detector NEP at frequency ν (cm^{-1}),
- NEP₁ = $1.8 \times 10^{-15} \text{ W}/\sqrt{\text{Hz}}$, the NEP at $\lambda = 1 \mu\text{m}$ wavelength,
- T = 0.4, the total transmittance of the optical system,
- A_{Ω} = $1.03 \times 10^{-2} \text{ cm}^2 \text{ sr}$, the etendue,
- $\Delta\nu$ = ν/R , the spectral resolution element,
- R = 100, the spectral resolving power,
- t = τ_i/R , the integration time per spectral element,
- τ_i = 5 seconds, the integration time required for one complete scan,
- N = the number of complete scans, and
- τ = $N\tau_i$, the total integration time.

Then,

$$\text{NESR} = \frac{10^{-4} R^{3/2} \text{NEP1}}{\text{TA}_\Omega \sqrt{\tau}} \text{ watts/cm}^2 \text{ sr cm}^{-1} \quad (3)$$

or, using the values given above,

$$\text{NESR} = \frac{4.36 \times 10^{-14}}{\sqrt{\tau}} \text{ watts/cm}^2 \text{ sr cm}^{-1} \quad (4)$$

Note that the NESR expressed in equations (3) and (4) is independent of wavelength, if the resolving power is kept constant.

It is also useful to express the NESR in units of Rayleighs/Å (the Rayleigh is a unit of surface brightness equivalent to 10^6 photons $\text{cm}^{-2} \text{ sec}^{-1}$, radiated into 4π sr),

$$\text{NESR} = \frac{4\pi \cdot 10^{-18} \nu_c R^{3/2}}{hc \text{TA}_\Omega \sqrt{\tau}} \text{ Rayleighs/Å} \quad (5)$$

For the parameters given above, the NESR may be re-written

$$\text{NESR} = \frac{2.75}{\lambda \sqrt{\tau}} \text{ Rayleighs/Å} \quad (6)$$

where λ is given in μm . The expected NESR is shown in Figure 4 for $\tau=100$ seconds and a resolving power of 100, representing $\sqrt{20}$ co-added spectral scans.

For faint continuum emissions, the spectral resolving power can be degraded in software by $\sqrt{10}$ -fold (to $R = 10$), providing an NESR of $1.4 \times 10^{-16} \text{ W}/\sqrt{\text{Hz}}$ for $\tau = 100$ seconds. This is compared with the intensity of the zodiacal light towards the ecliptic pole in Figure 4, where it is seen that good signal-to-noise can be obtained on this important astronomical background source. The zodiacal light is typically 2-3 times brighter in the ecliptic plane, at 90° elongation. The apparent mean surface brightness of Mars, Jupiter, and Saturn, diluted to our beam size in August 1986, are also shown. Spectral structure has been omitted for representation purposes.

The strongest emissions of all may be those of the induced glow. For example, if the unresolved continuum level seen in the ISO spectra ($\sqrt{50} \text{ R/Å}$ at $0.6 \mu\text{m}$, Torr and Torr [1984]) were assumed to be due to OH Meinel band emission, then Langhoff's spectral model could be used to estimate the intensity expected at $1.5 \mu\text{m}$ [Langhoff et al., 1983]. According to this model, it would be $\sqrt{30}$ times brighter there. The ratio of signal-to-noise expected using the SIRGE spectrometer (single scan, $\tau = 5$ seconds) would then be $\sqrt{1800}$. However, this is probably an over-estimate for the OH intensity. In addition to potential OH emission, other bands may be present such as NO_2 ($\nu_1 + \nu_3$, and ν_3), H_2O (ν_1 and ν_3), NO (1-0, overtones, and hot bands), N_2O (ν_3), CO (fundamental, overtones, hot bands), and CO_2 (ν_3), to mention only those which have been suggested or which seem particularly likely.

The flux seen by the detector must be $< 2.5 \times 10^{-12}$ watts, for the NEP used, if amplifier saturation is to be avoided. Hence, the beam averaged surface brightness (at $1 \mu\text{m}$) cannot exceed

$$R_{\text{max}} = 2.5 \times 10^{-12} \text{ watts/cm}^2 \text{ sr cm}^{-1} \quad (7)$$

Thus, the maximum signal-to-noise ratio achievable in a single scan will be $\sqrt{125}$. If the induced glow were to be as bright as indicated in Figure 4, our amplifiers would be saturated, therefore a commandable ranging capability is included in the electronics design.

Test and Calibration

Careful optical calibration and testing will be conducted in the laboratory, with particular emphasis on measurements of the off-axis rejection of stray light, the absolute intensity calibration, the noise performance, and the measurement of linearity. Additional tests (vibration, thermal, EMI) will be carried out, as required.

Particular emphasis will be placed on intensity calibration. Ground calibration of the assembled system will be carried out in the laboratory, before and after flight. However, because of the long time (probably 1 year) between the calibrations, we plan to make in-flight calibration as well. An internal infrared source (stimulator, Figure 3) will provide relative intensity calibration, and external sources (Mars, Jupiter, Saturn, Figure 4) will provide absolute calibration. The external sources can be acquired by pointing the space shuttle, since our large beam size permits source acquisition with only modest pointing accuracy. Terrestrial limb scans will enable intensity, wavelength, and dynamic range calibration from the known OH Meinel airglow itself. Finally, when viewing deep space, the zodiacal emission provides an automatic signal for calibration of faint glow emissions.

References

- Abreu, V. J., W. R. Skinner, P. B. Hays, and J. H. Yee, Optical effects of spacecraft-environment interaction: Spectrometric observations by the DE-B satellite, AIAA-83-2657-CP, presented at Shuttle Environment and Operations Meeting, Washington, D.C., 1983.
- Banks, P. M., P. R. Williamson, and W. J. Raitt, Space Shuttle glow observations, Geophys. Res. Lett., 10, 118-121, 1983.
- Langhoff, S. R., R. L. Jaffe, J. H. Yee, and A. Dalgarno, The surface glow of the Atmospheric Explorer C and E satellites, Geophys. Res. Lett., 10, 896-899, 1983.
- Mende, S. B., O. K. Garriott, and P. M. Banks, Observations of optical emissions on STS-4, Geophys. Res. Lett., 10, 122-125, 1983.
- Slanger, T. G., Conjectures on the origin of the surface glow of space vehicles, Geophys. Res. Lett., 10, 130-132, 1983.
- Torr, M. R., and D. Torr, Preliminary results of the imaging spectrometric observatory on Spacelab 1, AIAA-84-0044, presented at AIAA 22nd Aerospace Sciences Meeting, Reno, 1984.
- Yee, J. H., and V. J. Abreu, Visible glow induced by spacecraft-environment interaction, Geophys. Res. Lett., 10, 126-129, 1983.

TABLE 1. SHUTTLE INFRARED GLOW EXPERIMENT: SPECIFICATIONS AND REQUIREMENTS

Wavelength Coverage	0.9-5.5 microns
Resolving Power	100
Detector	InSb
Sensitivity (single scan NESR)	$< 2 \times 10^{-14} \text{ W/cm}^2 \text{ sr cm}^{-1}$
Scan Time	$\lesssim 5$ seconds
Operating Temperature	$< 65 \text{ K}$
Dewar Hold Time (minimum)	5 days pre-flight 10 days in-flight
Field-of-View	$4^\circ \times 4^\circ$
Aperture Size	3.14 cm diameter

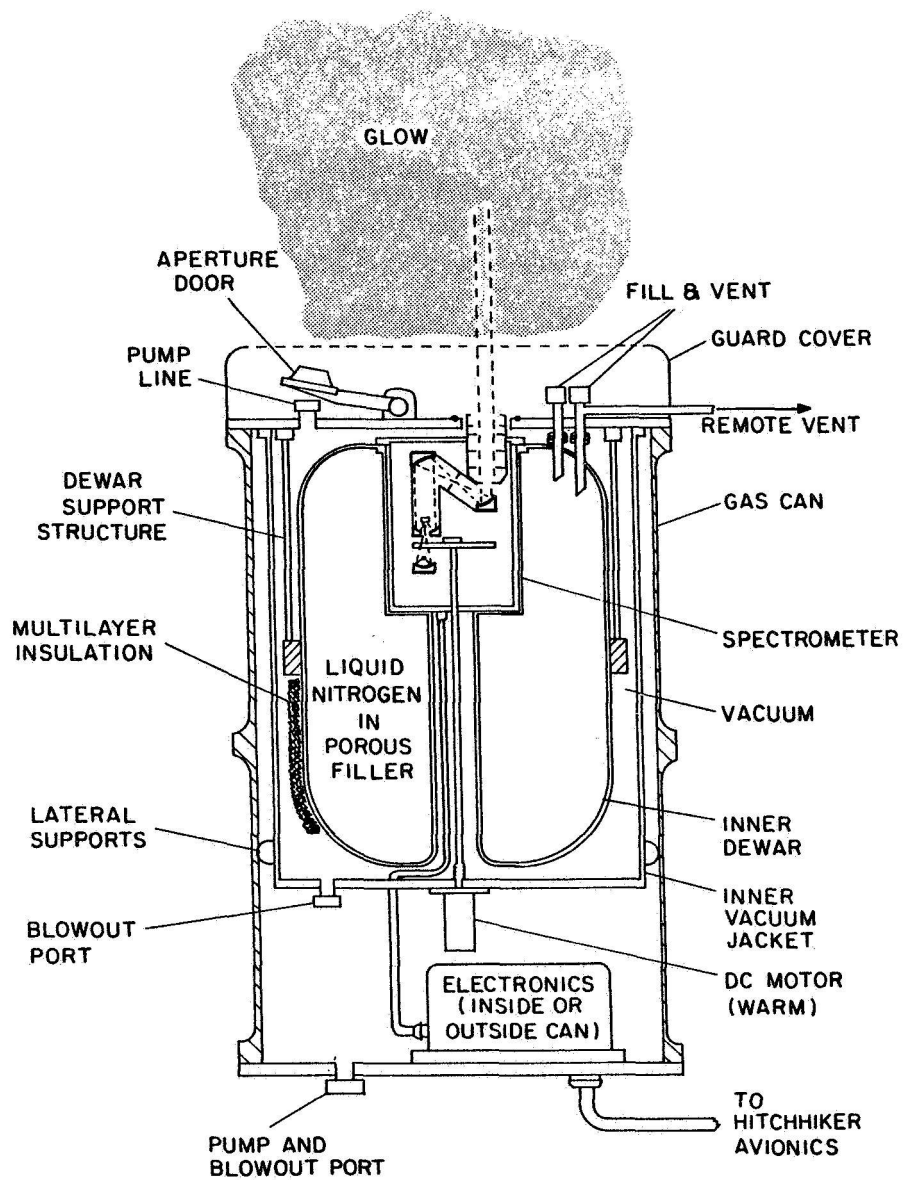


Fig. 1. Conceptual drawing of SIRGE instrument in GAS can.

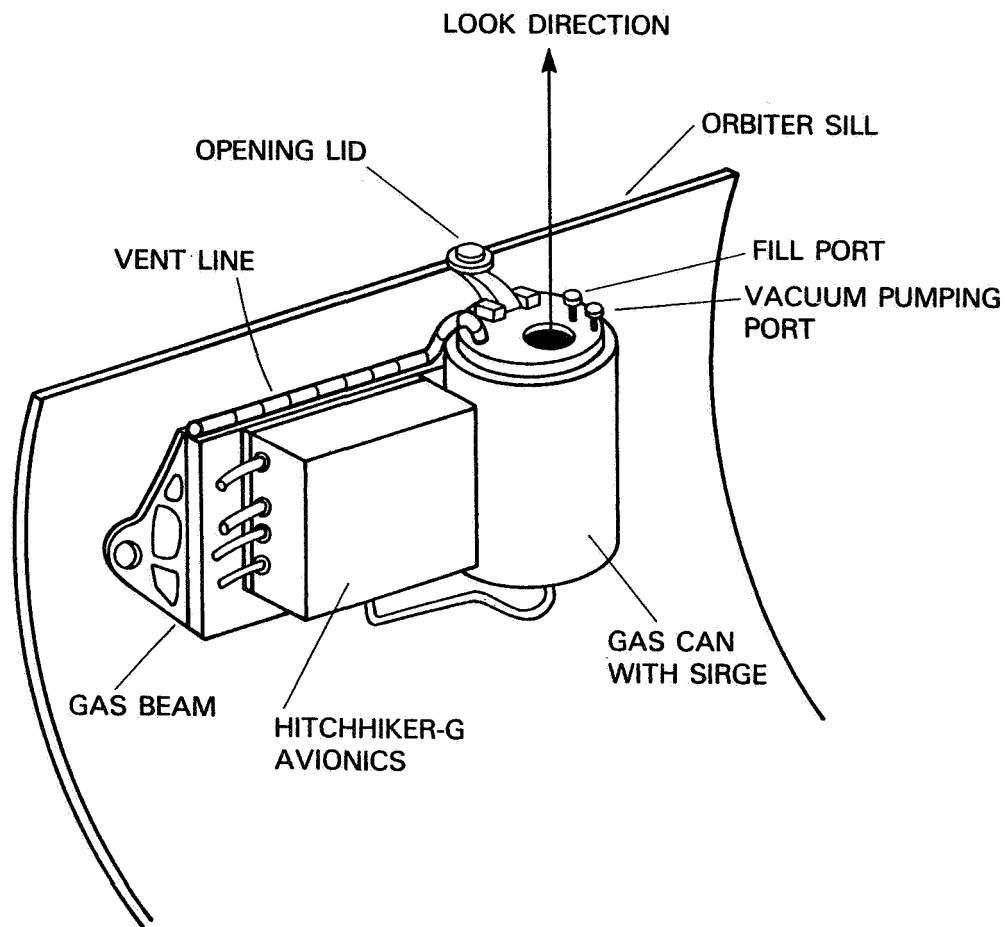


Fig. 2. SIRGE spectrometer Hitchhiker mounting Configuration.

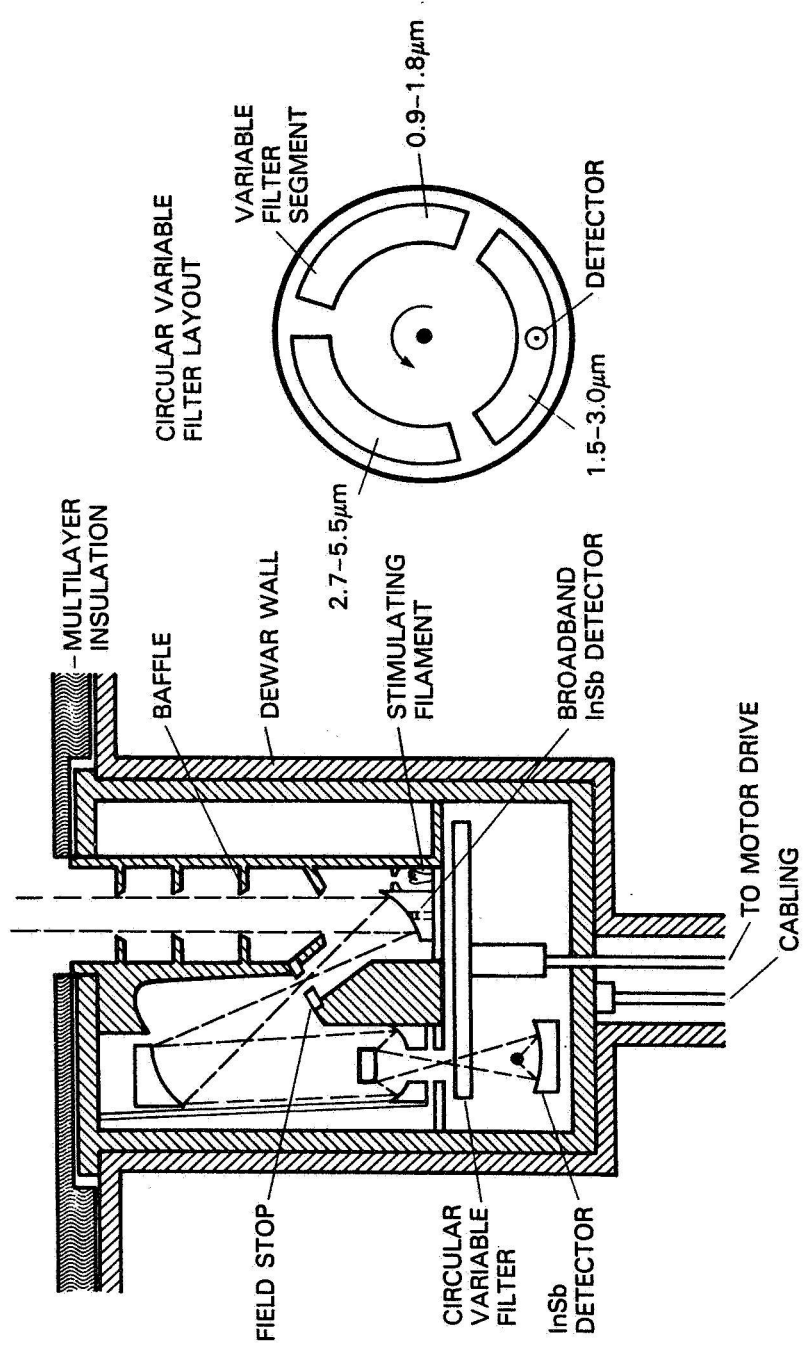


Fig. 3. SIRGE spectrometer optical layout.

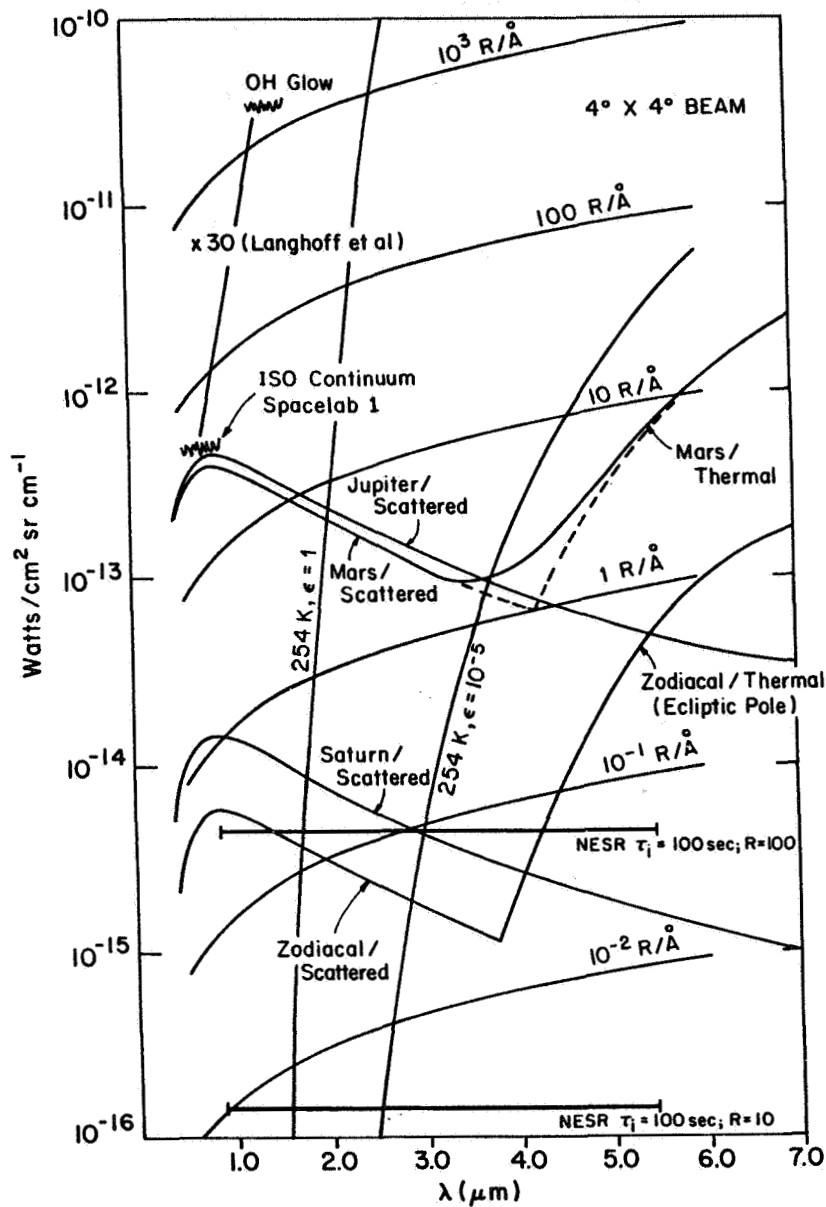


Fig. 4. SIRGE sensitivity limits, calibration sources, and possible glow intensities.

DATA REQUIREMENTS FOR VERIFICATION OF RAM GLOW CHEMISTRY

Gary Swenson and Steve Mende

Lockheed Palo Alto Research Laboratory

Abstract. A set of eleven questions has been posed regarding the surface chemistry producing the ram glow on the space shuttle. The questions surround verification of the chemical cycle involved in the physical processes leading to the glow. The questions, and a matrix of measurements required for most answers, are presented. The measurements include knowledge of the flux composition to and from a ram surface as well as spectroscopic signatures from the UV-visible-IR. A pallet set of experiments proposed to accomplish the measurements will be discussed. An interim experiment involving an available infrared instrument to be operated from the shuttle Orbiter cabin will also be discussed.

Introduction

Several papers in this report address the surface chemistry involved in production of the "red" ram glow associated with the space shuttle.

Questions to Address-Surface Ram Glow

The following is a set of questions that we have assembled which are aimed at further understanding and quantifying the glow processes. This set of questions is a general set that needs answers to further clarify and quantify the physical processes involved. First we address a set of questions for glow from a given material:

1. How does NO_2 material exit flux relate to the NO_2 continuum glow on the material?
2. How does NO material exit flux relate to NO beta, delta, and/or gamma band emission?
3. How does the NO_2 continuum glow extend into the infrared? Does it continue to drop as we observe between 7000 and 8000 Å?
4. Is the NO_2 "fine structure" superimposed on the continuum as it is in the laboratory spectrum?
5. Is there a component of N_2 LPG, and if so, how does it extend into the IR?
6. How does 1-5 vary with material temperature (between $\sim 250^\circ$ and 400° K)?
7. How does 1-5 vary with NI and OI flux from the atmosphere? (i.e., How can we expect the glow to vary with altitude?)
8. How does 1-5 vary with ram angle to the sample surface?
9. Does O_2 become a production factor at low altitude as implied by the AE-C data?
10. How do different material surfaces influence 1-9 above?
11. How does the chemistry become enhanced/quenched with controlled injection of NO and other gases?

This set of questions addresses process verification and quantification for temperature and materials. The experimental approach is outlined below as to how many of these questions can be addressed.

Technical Approach-Experimental Method

The all-up matrix approach with the pallet instruments yields the ultimate in answers to the questions regarding the physical processes, but there are some intermediate experiments that can be assembled quickly which can answer some very important questions.

A portable CVF (Circular Variable Filter) instrument has been fabricated and is available as a candidate instrument to observe the IR component of glow from the Orbiter cabin. The aft flight deck window has reasonable transmission between 1.2 and 2.4 microns (~40%-variable). Figure 1 shows a mechanical configuration of the instrument, and Table 1 is a summary of the optical characteristics.

We herein describe a set of experiments which would answer many of the questions addressed above. This constitutes operating a set of instruments in the space shuttle bay which would monitor the flux of molecules impinging on and emanating from a surface in ram. At the same time, observations of the glow on the surface would be monitored in the UV, visible, and IR wavelengths. A glow mission would require a few orbits of dedicated attitude to perform the glow studies, at low-Earth orbit (~250 km). The instruments would be preprogramed to perform the experiment sequences during the glow attitudes. We have structured a set of instruments which can provide significant information on the processes. Some of the questions posed would require a quality, high-resolution visible spectrometer, as well as a high-resolution cryogenic IR instrument. In the spirit of "a step at a time" and low cost, we have structured an essential set of pallet instruments which can provide many important answers to key processes. A high-resolution visible spectrometer (~1 Å resolution) and a cryogenic IR instrument are desirable for follow-up studies as we now understand the chemistry. A basic set of experiments without these refinements is described herein.

The instruments we envision include a sample surface plate (~1 meter x 1 meter) which would be positioned in the pallet in such a way that the ram atmosphere could be directed towards it. An optical sensing stand would view the plate from nearly edge-on to take advantage of the near surface brightness emanating from the plate surface. The plate would be tipped up, and a mass spectrometer would view the plate from near 45° to plate normal. This set of instruments would constitute the main glow package (see Figure 2).

The plate would be coated with one material and on subsequent mission opportunities, other materials would be studied. The plate would ideally have provision for heating electrically so the plate temperature could be elevated to near 400° K. It is possible to make a plate which could rotate to subject two-three different surfaces to ram during a mission, but our initial consideration is to have a single surface. The plate would contain a baffle on the down viewing side of the optical package, such that a black background would be provided to the glow viewing instruments.

The optical package will include three instruments which will document glow from the UV to the IR. The instruments are summarized in Table 2. Instrument 1 will be an automated version of the hand-held

instrument which has flown as a locker experiment in the Orbiter. This instrument will operate in an imaging mode, as well as a spectrometer mode, to clarify the glow in the 4000-8000 Å wavelength region. This instrument will document the spatial distributions of the glow and provide the bridge of measurement to the early data set. Instrument 2 will be the UV instrument to clarify NO band emission (as well as any presently unknown UV emissions). Filters for the known NO band emissions between 2000 and 4000 Å will be included. The instrument will consist of a UV imager bore-sighted with an f5, 1/8th meter spectrometer. The spectrometer would scan from 2000-4000 Å while the imager documents the spatial distributions of the UV glow. Instrument 3 will consist of a thermal, electrically cooled PbS detector to cover the IR wavelengths between 1 and 3+ microns. The IR shape of the NO₂ continuum and possibly other glowing candidates would be measured with this instrument.

A mass spectrometer of the type which is designed to examine the entrance and exit flux of NI, OI, NO, and NO₂ from the surface plate will be located separately from the optical instruments. This instrument is essential to document the constituent phenomena associated with the chemical processes. The instrument herein is one very different from the AE instrument in that the requirement is to make the measurement of ambient NO and NO₂ emanating from the plate. In order to accomplish this, the instrument must be of a type where the molecules are ionized external to an instrument orifice before any wall collisions have occurred. Next, this produced beam would be focused and mass-analyzed as in a conventional mass spectrometer. The instrument would be an orifice-pumped instrument with a mechanical flag in the orifice. The pumping is necessary to minimize orifice collisions in the high-density shuttle environment. The mechanical flag allows a degree of direction control of the sampling beam. The flag would alternately direct molecules from a surface sample plate and from the atmosphere to be sampled by the instrument.

The above surface plate, optical cannister, and mass spectrometer are all essential to a basic pallet payload. A matrix of problems versus instruments has been produced (see Table 3). For most of the questions at hand, several instruments are desired. Model atmospheres can be used with some reliability for the atmospheric flux to the spacecraft, but the measurement with the mass spectrometer is best. Only the mass spectrometer can resolve what is coming off the plate in the way of mass species.

We are also giving consideration to gas release cannisters which, when released, would be located such that the drift cloud would pass over the plate. It has been noted that the thruster effluent acts to enhance the stand-off ram glow significantly for several seconds when impinging on a ram Orbiter surface. The thruster gas consists of significant amounts of NO, which we believe adds to the surface monolayer of NO. This additional source of NO seems to deplete in less than 1 minute in ram. Gas cannisters with NO and other gases which in fact would act to quench the process would be considered. The gas cannisters could be relatively small in size and of the single release type.

We suggest that the "shuttle hitchhiker" concept be a candidate facility within which experiments could be structured. The "hitchhiker" offers a simple interface and minimal delivery time before mission execution. At the same time, it appears to offer command and data handling capabilities which are adequate for the required measurements.

Summary

There are a number of questions which need to be answered to further understand the physical and chemical processes involved in ram glow. The basic questions are scientifically important to understanding the interaction of the atmosphere with the fast moving spacecraft. The questions are well suited to be explored with well known, state-of-the-art instrumentation which can be implemented into a shuttle pallet payload for experiment implementation. The exciting results will be scientifically interesting in themselves since low-energy neutral beams of 5-10 eV are difficult to implement in the laboratory with significant flux levels. The experiments will also yield useful information regarding potential background contamination for planned and future experiments. Through understanding the physical processes, we can understand how to engineer our instrumentation and plan our operations of space optical instrumentation with minimal signal degradation.

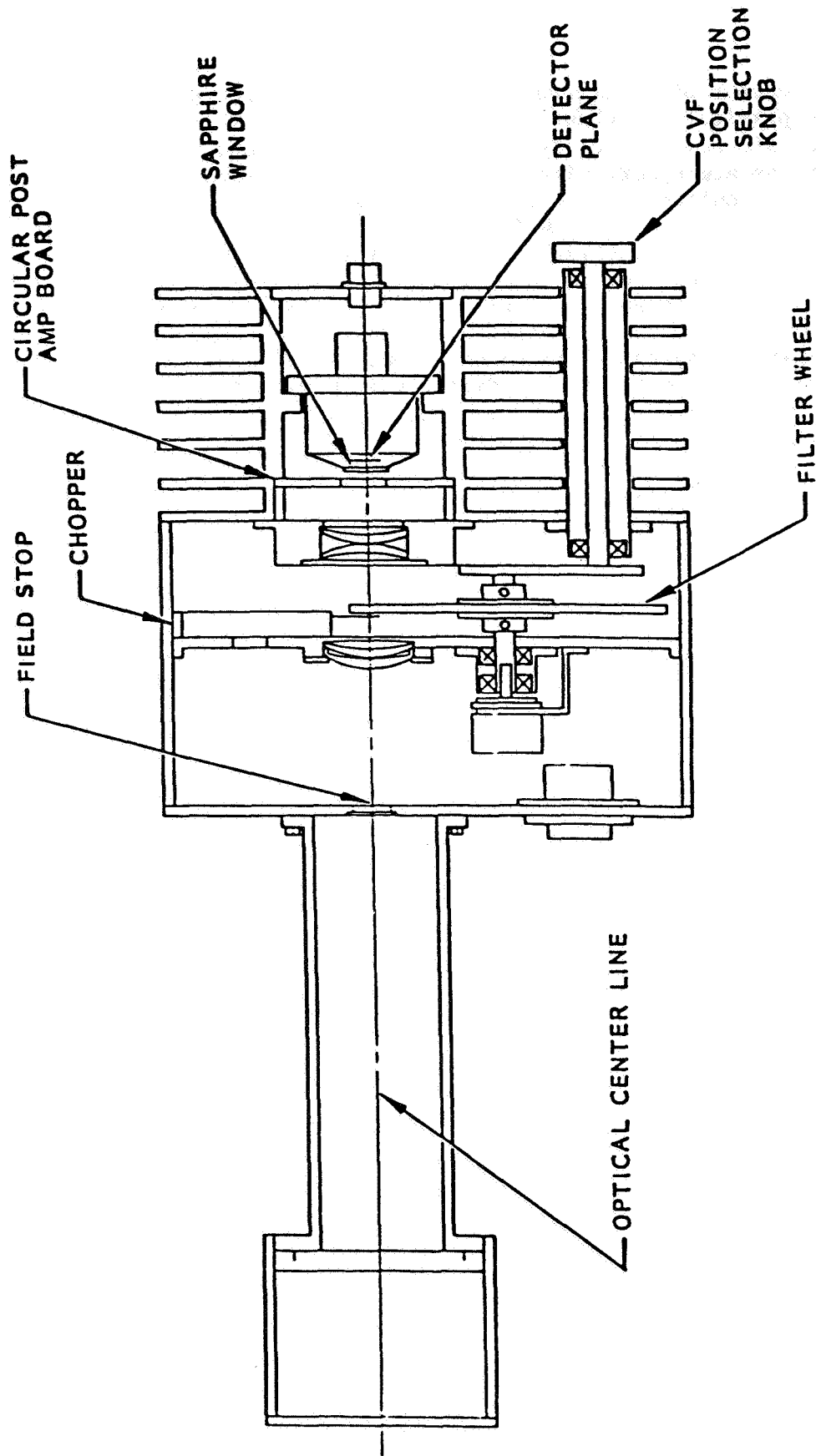


Fig. 1. A cross section of the Circular Variable Filter (CVF) instrument for infrared detection of the spacecraft glow. The instrument contains a five-element lens set defining a 2 degree FOV. The circular variable filter scans from 1.3 to 3.2 microns. The detector is a PbS material, 4 mm sq., thermal electrically cooled to 193° K. Detector and window temperatures are recorded as well as detector signal and wavelength position during instrument's operation.

PALLET GLOW INSTRUMENTS
(TOP VIEW)

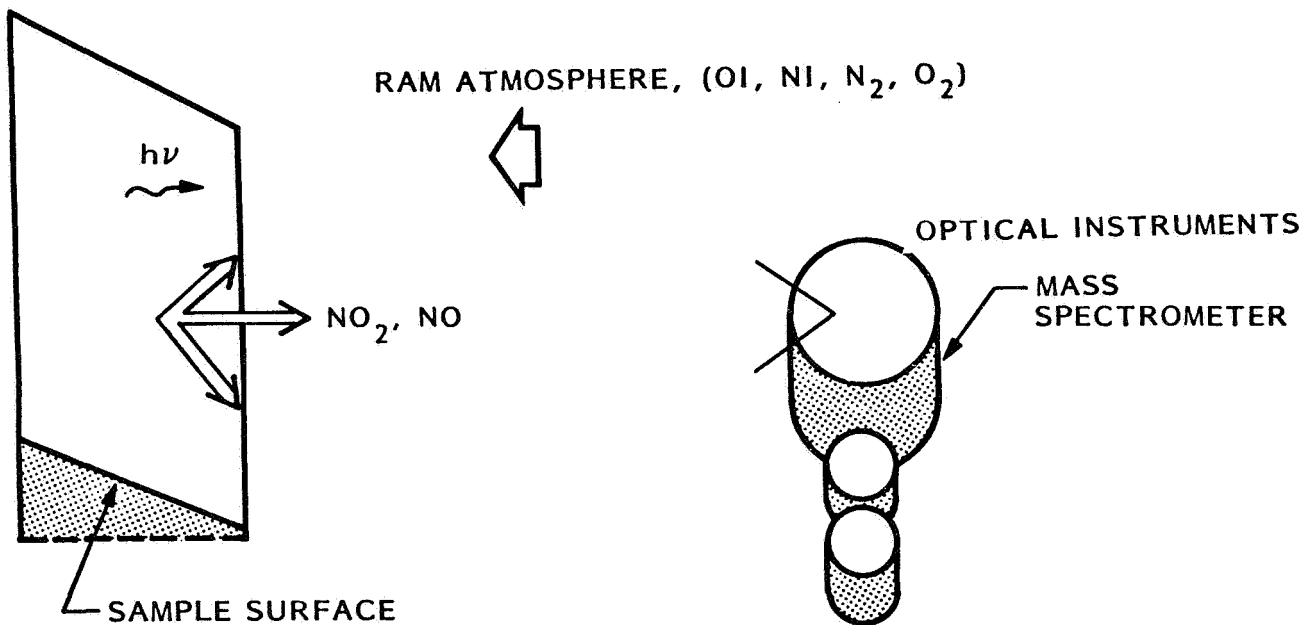


Fig. 2. A schematic representing the pallet-based instruments viewing molecules and glow emanating from a sample surface.

TABLE 1. OPTICAL CHARACTERISTICS OF THE CVF SPECTROPHOTOMETER

PORTABLE INFRARED SPECTROPHOTOMETER [CVF]

- * FIELD-OF-VIEW - 2 degrees (full)
- * WAVELENGTH RESOLUTION - Bandwidth <3% tuned wavelength
- * SPECTRAL RANGE - 1.3 to 3.2 microns per scan + shutter
[reasonable aft window transmission 1.2-2.4 microns]

- Broadband mode - use SC window as filter
- * SENSITIVITY - 80 Rayleighs/Angstrom for 1-second integration
[detector = 4 x 4 mm, PbS, TE cooled to <200 kelvin]
- * POWER - ~17 watts (measured)
- * VOLUME - Optical system: L = 35 cm, Width = 12.5 cm
Electronics: L = 20 cm, Width = 20 cm, Ht. = 20 cm
- * DATA AND CONTROL - TRS 80 + recorder

TABLE 2. A SUMMARY OF A CANDIDATE SET OF PALLET INSTRUMENTS SUITABLE FOR STUDY OF SPACECRAFT RAM GLOW

PALLET GLOW INSTRUMENTATION

- #1 RED BROADBAND IMAGING SPECTROPHOTOMETER
 - * 20 degree FOV
 - * 4000-8000 Angstroms
 - * Resolution 30 Angstroms
 - * Imaging or spectrometer mode

- #2 UV BROADBAND IMAGING SPECTROPHOTOMETER
 - * 20 degree FOV
 - * 2000-4000 Angstroms
 - * Resolution 30 Angstroms
 - * Imaging and spectrometer mode

- #3 IR CVF SPECTROPHOTOMETER
 - * 2 degrees FOV
 - * Spectral range 0.8-3.0 microns
 - * Resolution 3%

- #4 MASS SPECTROMETER (OPEN SOURCE)
 - * 2 degrees FOV
 - * Flag directed beam (10 degree deflection)
(monitor source flux and background)
 - * Pumped orifice

TABLE 3. A MATRIX OF QUESTIONS VERSUS INSTRUMENTS REQUIRED TO PROVIDE ANSWERS TO THE QUESTIONS
IN A GLOW EXPERIMENT SCENARIO

MATRIX OF CURRENT PROBLEMS VS. PROPOSED INSTRUMENT

Problem #	Instrument #	1 Im & Sp	2 Im & Sp	3 IR-CVF	4 Mass Spect.	5 (Future Release
1. NO ₂ flux versus NO ₂ glow?		X		*	X	
2. NO flux versus NO glow?			X		X	
3. NO ₂ extend to IR?		*		X		
4. NO ₂ fine structure?		*				
5. N ₂ LPG superimposed?		*		X		
6. 1-5 vary with temperature?		X	X	X	X	
7. 1-5 vary with NI and OI flux?		X	X	X	X	
8. 1-5 vary with ram angle?		X	X	X	X	
9. O ₂ at low altitude?		X	X	*	*	
10. Other materials response?		X	X	X	X	
11. Constituent enhance/quenching?		X	*	*	*	X

X - Major instrument

* - Contributing instrument

A POSSIBLE GLOW EXPERIMENT FOR THE EOM 1-2 MISSION

Marsha R. Torr

Department of Physics
Utah State University
Logan, Utah

Abstract

At this time, information on the surface glows and the spatial extent of these glows is very limited. Several fundamental aspects of the glow have yet to be measured, and this situation is not likely to change in the near future because of the limited flight opportunities for such studies. Thus, opportunities to gather the much needed data on this subject using investigations already planned are most valuable.

A possible opportunity for such a study exists during the EOM 1-2 mission scheduled for launch on September 3, 1986. An experiment during this mission could provide the VUV-VIS-NIR spectral characteristics of the glow at approximately 5 Å spectral resolution. However, the EOM 1-2 mission has a very full schedule that already places great demands on the mission planners and investigators. At this time it is not clear whether the natural concerns associated with inserting or substituting a new experiment, however nominal, can be satisfactorily overcome. Therefore, the concept outlined below is at present a concept only.

The EOM 1-2 payload includes spectroscopic and photometric instruments which operate in wavelength regions of great interest to the glow assessment activity. However, as in the case of many remote sensing instruments, these are located in the payload bay in such a way as to avoid viewing any shuttle or payload surfaces. If these instruments are to measure the spectral characteristics of surfaces, it is necessary for such surfaces to be positioned in the field of view of these instruments for the duration of the particular measurement sequence. It is possible that the shuttle on which the EOM 1-2 payload flies will have an RMS in place. An assessment has shown that it is indeed feasible to place a four-sided "cuff" around the end of the RMS. The four sides, each coated with a different material, can then be positioned in turn above the instruments, and in such a way that the surface is alternately pointed into the ram and into the wake.

The implementation of such a measurement sequence is still being evaluated at this time.

SPACE SHUTTLE MECHANISTIC STUDIES TO CHARACTERIZE
ATOMIC OXYGEN INTERACTIONS WITH SURFACES

Lubert J. Leger and James T. Visentine

NASA/Lyndon B. Johnson Space Center

Abstract. A materials interaction experiment has been approved to study atomic oxygen interaction mechanisms and develop coatings for Space Station elements requiring long-lived operation in the LEO environment. A brief summary of this experiment is presented and the required exposure conditions are reviewed.

Introduction

An understanding of the surface chemistry which gives rise to atom/surface interactions within the orbital environment is crucial to establishing a reliable materials interaction data base for Space Station and verifying the operational capability of ground-based neutral beam facilities which simulate the space environment. One of the more important effects of these interactions is oxidation of material surfaces by atomic oxygen, a major constituent of the low-Earth orbital environment. Material interaction studies conducted during flights STS-5 and STS-8 have provided most of the current information regarding the reactivity of spacecraft materials to atomic oxygen, and the results of these studies indicate many materials such as organic films, polymers, and many composites react readily with atomic oxygen and have reactivities in the range 2.5×10^{-24} to 3.0×10^{-24} cubic centimeters per atom.

The data base provided by these, as well as those to be obtained on LDEF, will be limited in its application, however, because no information will be available which adequately explains the basic mechanisms responsible for atom/surface interactions. Another more serious limitation to this data base is that the total integrated atomic oxygen flux (fluence), derived for these flights and used to determine material interaction rates, must be estimated using thermospheric models to predict atomic oxygen number densities within the orbital environment. Typically, errors of $\pm 25\%$ or greater can be expected for these density estimations, and since they are used to compute fluence, these errors also appear in the surface recession rates for Space Station materials.

Experiment Description

To resolve many of these uncertainties in the data base, a flight experiment has been proposed for the space shuttle that utilizes an ion-neutral mass spectrometer to obtain in situ ambient density measurements and identify reaction products from modeled polymers exposed to the atomic oxygen environment. Using the ambient density measurements from the mass spectrometer along with material recession measurements obtained during the same exposure, accurate reaction rate data will be provided for future spacecraft performance assessment and design.

The mass spectrometer which will be provided by the Air Force Geophysical Laboratory (AFGL) and a mounting arrangement used to expose surfaces to ambient impingement will be mounted in the payload bay on an appropriate structure as shown in Figure 1. For the required exposure

the Orbiter will be oriented with the -Z axis pointed into the velocity vector (payload bay in ram). This orientation will provide normal impingement on the exposed surfaces and, with the mass spectrometer entrance port aligned with the Z-axis, will provide for optimal ambient density measurements. A total exposure of 40 hours will be requested to provide significant recession and insure assessment of bulk material reactivity. Several ambient density measurements will be made during the 40-hour exposure.

In addition to the ambient density measurements, the mass spectrometer will also be used to measure products of reaction from atmospheric interaction with surfaces. For these measurements the mass spectrometer will rotate 90° relative to the Z-axis to sample gases evolved from several surfaces being exposed on a carrousel arrangement as shown in Figure 2. The carrousel will hold five surfaces which will be used to study the interaction mechanism and will be selected on the basis of information provided in that regard. One of the five surfaces may be a material which is known to produce glow such as Z-306 black paint.

To aid in providing the best ambient density and reaction product evolution measurements, the AFGL mass spectrometer will be calibrated using an atomic beam currently being developed at the Los Alamos National Laboratories. This beam generation concept is based on a laser heated plasma concept described in another paper of this meeting (see J. Cross, these proceedings) and should provide kinetic energies of up to 5 eV. Since the beam facility vacuum chamber is large, the flight mass spectrometer can be calibrated in situ and should allow a good understanding of transient processes inside the ion source. Furthermore, the beam facility will be used to characterize reaction products generated on the specific surfaces selected for inclusion on the flight experiment. This product distribution will be comparable with reaction products produced during flight to verify simulation fidelity and study reaction mechanisms.

This latter data should be of interest in glow mechanism studies, in that major constituents produced by ambient impingement will be identified and thereby provide a base of chemical species to consider for light production mechanisms.

Hardware development for the flight experiment is underway, and a late 1986 or early 1987 flight date will be requested from the STS. Funding for experiment development is being provided by Space Station and the Office of Aeronautics and Space Technology/NASA Headquarters.

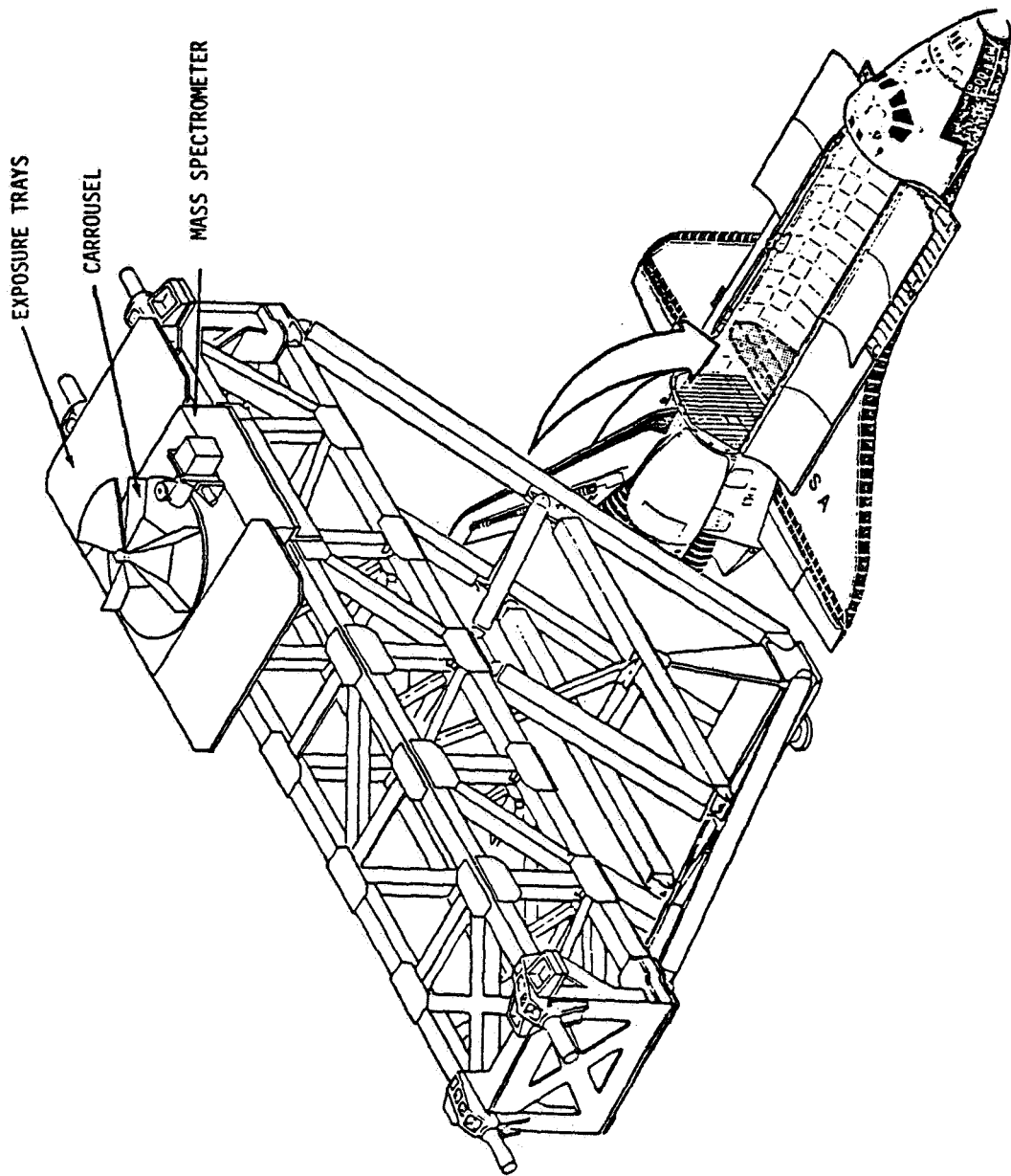


Fig. 1. Atomic oxygen experiment mounted on MPSS structure.

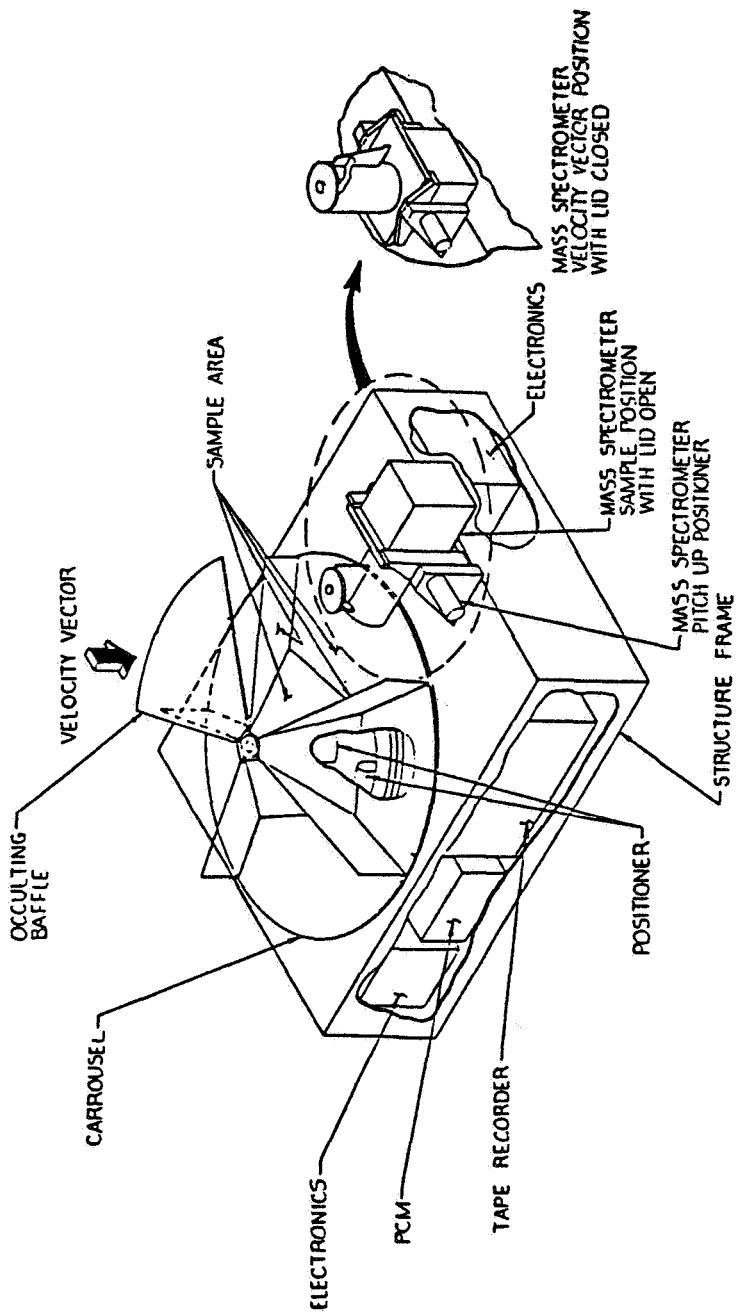


Fig. 2. Details of mass spectrometer carousel arrangement.

THE SHUTTLE GLOW:
A PROGRAM TO STUDY THE RAM-INDUCED PHENOMENA

Hugh R. Anderson

Science Applications International Corporation
Bellevue, Washington

The ram-induced phenomena almost surely involve a number of different physical interactions whose study historically is of interest to different disciplines. At a minimum, aeronomy (or aerochemistry), surface physics and chemistry, and plasma physics are important, and to this one should probably add rarefied gas dynamics. Each of these specialties was represented at the second conference, although aeronomy predominated. The significance of several different mechanisms was evident to some investigators much earlier than this second conference in May 1985. Papadopoulos published hypotheses relating glow and observed plasma effects in 1983; Kofsky discussed both aerochemical and surface chemistry in the same year.

In January 1984, SAIC submitted a proposal to NASA Headquarters entitled "The Shuttle Glow: A Program to Determine the Physics of the Ram Induced Phenomena." This proposal was prepared by Papadopoulos, Kofsky, and Anderson, and included the following elements in a shuttle-based experiment:

- The use of a special flat generating surface $>1 \times 3$ m on which the glow can be produced and observed. This surface will be maneuvered to vary the orientation of ram flow and of projected component of geomagnetic field.

- Remotely mounted optical instruments to view the glowing layer on the plate. By scanning, the variation of radiance as a function of wavelength and standoff distance from the plate will be observed looking parallel to the plate.

- The optical instruments include a visible light photographic camera that has already been flown on shuttle and a scanning grating spectrometer in the visible. These might be supplemented by the Orbiter video system.

- In situ plasma diagnostic sensors mounted on and just above the plate to measure effects in the glowing layer and in the medium adjacent to it.

- The plasma instruments include a neutral density gauge, a plasma density and temperature probe, an electric wave receiver, and an energetic electron detector to measure the flux striking the plate and moving in the volume just above it.

- Three near-infrared photometers were included in this set of sensors looking normally outward from the plate.

- The preferred location of the generating plate and in situ diagnostics is on the end of the Remote Manipulator System (RMS) arm. We suggested that a three- or four-sided structure be used, carrying a different surface material on each side; aluminum, kapton, tiles, and other organics were suggested. Only one side would carry the in situ diagnostic suite. Portions of this one side could be electrically biased to alter plasma flow. In this configuration, the optical instruments would be mounted rigidly in the shuttle bay with all motion being accomplished by the RMS.

- An alternative configuration was suggested to avoid dependence on the RMS. The generating plate is hinged at one end to fold up out of the bay so that either of the two sides can be exposed to the ram flow. In this case, the optical instruments will be mounted on a pan-tilt head.

Subsequent to submission of this proposal the desirability of using the MSFC Hitchhiker was pointed out to us by NASA. A preliminary instrument layout was prepared in which the generating plate covers much of the top of the Hitchhiker structure, with the diagnostic sensors above and behind the plate and the optical sensors at the edge. The plate does not hinge, and so the shuttle must be maneuvered to vary ram flow. Increasing knowledge of the phenomena led us to enlarge the set of sensors as follows:

- Four UV photometers were added to cover wavelengths down to 1200 Å, including the O resonance lines that could be excited by electron impact.

- A cryogenic CVF infrared photometer was substituted for the infrared photometers, covering the wavelength range from 0.8 to 14 microns. This instrument will be provided by Carl Rice of the Aerospace Corporation.

- Energetic ion energy spectrometers were added complementing the electron sensors.

- The use of controlled gas releases was suggested as a way of determining the effect of varying the density and constituency of the local gas phase.

- A large carousel was discussed to afford the capability of presenting four to six different samples to the ram flow.

Our objectives in carrying out this investigation are threefold:

- To observe the full range of ram-induced phenomena, bearing in mind those that are relevant to the Space Telescope and to other large systems. This includes not only photon emission, but the effects of bombarding dielectrics and other materials with energetic charged particles. Not only erosion, but charge implantation and microdischarges can result.

- To understand the full range of physical and chemical effects that result. It is likely that various mechanisms have different importance under different local conditions. For example, the plasma effects clearly occur. In some cases, they may dominate the production of glow. In other cases, they may be unimportant for glow but still significant for production of electrical noise, etc.

- To develop a predictive capability so that the magnitude of glow and the related effects can be calculated for any conditions. As a corollary, means to ameliorate the effects might be developed.

No formal response to our proposal has been received from NASA. Many of the experimental concepts that we suggested are now in general circulation. Their use is being planned in conjunction with existing NASA instrumentation. No dedicated instrument suite is being planned as yet. Now that NASA recognizes the interest and potential problem of the ram-induced phenomena, we look forward to participating in these investigations.

SURVEY OF ULTRAVIOLET SHUTTLE GLOW

Kerry A. Spear, Gregory J. Ucker, and Kent Tobiska

Laboratory for Atmospheric and Space Physics
University of Colorado

The University of Colorado Get Away Special (GAS) project (G-285) utilizes the efforts of over 100 students for the purpose of placing four experiments on the shuttle. The undergraduate and graduate students have designed and are constructing each experiment, as well as the engineering support subsystems.

The objective of one experiment, the shuttle glow study, is to conduct a general survey of emissions in the ultraviolet near vehicle surfaces. An approximate wavelength range of 1900-3000 Å will be scanned to observe predominant features. Special emphasis will be placed on studying the band structure of NO near 2000 Å and the Mg⁺ line at 2800 Å.

The spectrometer, of Ebert-Faste 1/8-meter design, will perform the experiment during spacecraft night. It will be oriented such that the optical axis points to the cargo bay zenith. In order to direct the field-of-view of the instrument onto the shuttle vertical stabilizer (tail), a mirror assembly is employed. The mirror system has been designed to rotate through 7.5 degrees of arc using 10 positions resulting in a spatial resolution of 30 x 3 cm, with the larger dimension corresponding to the horizontal direction. Such a configuration can be attained from the forwardmost position in the cargo bay. Each spatial position will be subjected to a full spectral scan with a resolution on the order of 10 Å.

Detection of shuttle glow in the ultraviolet is anticipated, particularly at lower flight altitudes. The intensity will likely remain below a few tens of rayleighs/angstrom at a distance up to 10 meters from the tail. Spatial scans up to 3 meters from the tail surface should exhibit an intensity which is dependent on the direction of the velocity vector. Results will be published by the University of Colorado students following post-flight data analysis.

AGENDA

SECOND WORKSHOP ON SPACECRAFT GLOW SPACE SCIENCE LABORATORY NASA MARSHALL SPACE FLIGHT CENTER HUNTSVILLE, ALABAMA

MAY 6-7, 1985

Monday - May 6, 1985

8:30 a.m. Welcome - E. A. Tandberg-Hanssen

8:35 a.m. Preconference Summary, Goals - M. R. Torr

<u>Time</u>	<u>Author(s)</u>	<u>Topic</u>
8:50 a.m.	J. Clarke	Space Telescope Implications
9:20 a.m.	S. Mende G. Swenson	Space Shuttle Glow: The Characteristics of the Glow
9:50 a.m.	M. Engebretson	AE and DE Mass Spectrometer Observations Relevant to the Shuttle Glow
10:20 a.m.	G. Swenson S. Mende K. Clifton	Space Shuttle Ram Glow: Implication of NO ₂ Recombination Continuum
10:50 a.m.	A. Dalgarno J. Yee M. LeCompte	The Atmosphere Explorer and the Shuttle Glow
11:30 a.m.	P. Peters	A Model for Explaining Some Features of Shuttle Glow
LUNCH		
1:00 p.m.	D. Kendall S. Mende E. Llewellyn	Orbital Glow Observations at High Spectral Resolution
1:30 p.m.	E. Llewellyn I. McDade	Conjectures on the Nature of the Shuttle Glow
2:00 p.m.	I. Kofsky J. Barrett	Surface-Catalyzed Recombination into Excited Electronic, Vibrational, Rotational, and Kinetic Energy States: A Review
2:30 p.m.	J. Barrett I. Kofsky	The NO-NO ₂ System at Laboratory Surfaces

Monday - May 6, 1985 (Concluded)

<u>Time</u>	<u>Author(s)</u>	<u>Topic</u>
3:00 p.m.	N. Tolk R. Albridge R. Haglund M. Mendenhall J. Tully	Neutral-Particle Erosion and Optical Radiation Processes Produced by Particle and Photon Beams on Surfaces
3:30 p.m.	L. Leger	Effects of Atomic Oxygen on Surfaces: A Flight Experiment
4:00 p.m.	J. Cross	Activated Recombination Desorption: A Potential Component in Mechanisms of Spacecraft Glow
4:30 p.m.	I. Kofsky	Infrared Emission from Desorbed NO_2^* and NO^*
5:00 p.m.	G. Carignan E. Miller	Mass Spectrometric Measurements of the Shuttle Environment
5:30 p.m.	W. Langer S. Cohen D. Manos D. McNeill R. Motley M. Ono S. Paul	A Ground-Based Facility for Studying the Mechanism of Spacecraft Glow
5:50 p.m.	G. Arnold D. Peplinski	A Facility for Investigating Interactions of Energetic Atomic Oxygen with Solids
DINNER		
8:00 p.m.	O. Garriot	The STS-9 Shuttle Glow Experience

Tuesday - May 7, 1985

8:30 a.m.	S. Chakrabarti	Investigation of Vehicle Glow in the Far Ultraviolet
8:55 a.m.	B. Green W. Marinelli W. Rawlins	Spectral Identification/Elimination of Molecular Species in Spacecraft Glow
9:20 a.m.	D. Torr A. Khojloo M. Torr	Enhanced N_2^+ Emissions in the Shuttle Environment
9:45 a.m.	R. Rantanen R. Swanson D. Torr	A Mechanism for the Local Concentration Enhancement of the Shuttle Atmosphere

Tuesday - May 7, 1985 (Concluded)

<u>Time</u>	<u>Author(s)</u>	<u>Topic</u>
10:15 a.m.	M. Torr	The UV-VIS Optical Environment of the Shuttle
10:40 a.m.	K. Papadopoulos R. Smith	Spacecraft-Induced Plasma Energization and Its Role on Glow Phenomena
11:10 a.m.	F. Brock	Shuttle Fin Flow Field
11:35 a.m.	G. Fazio D. Koch	Infrared Measurements of Spacecraft Glow Planned for Spacelab 2

LUNCH

1:00 p.m.	M. Torr	Glow Experiments Proposed for EOM-1/2
1:15 p.m.	G. Swenson S. Mende	Data Requirements for Verification of Ram Glow Chemistry

Discussion and Unscheduled Talks

1:30 p.m.	M. Mumma D. Jennings	Planned Investigation of Infrared Emissions Associated with the Induced Spacecraft Glow: A Shuttle Infrared Glow Experiment
1:45 p.m.	L. Bareiss	Materials Oxidation and Glow Phenomenon Overview
2:00 p.m.	K. Spear G. Ucker K. Tobiska	Survey of Shuttle Glow in the UV
2:15 p.m.	H. Anderson	Proposed Investigation of Glow and Induced Plasma Effects

SUMMARY - M. Torr

ADJOURN

LIST OF ATTENDEES

SECOND WORKSHOP ON SPACECRAFT GLOW
SPACE SCIENCE LABORATORY
NASA MARSHALL SPACE FLIGHT CENTER
HUNTSVILLE, ALABAMA 35812
MAY 6-7, 1985

Hugh R. Anderson
Science Applications International
Corporation
13400B Northup Way, Suite 36
Bellevue, WA 98005
(206) 747-7152

Vappu S. Nuotio-Antar
UTSI-USRA
12021 Comanche Trail, SE.
Huntsville, AL 35803
(205) 883-1911

Graham S. Arnold
The Aerospace Corporation
M2/271
P.O. Box 92957
Los Angeles, CA 90009
(213) 647-1935

James D. Austin, Mail #T-2
Ball Aerospace Systems Division
P.O. Box 1062
Boulder, CO 80306
(303) 939-4435

Lyle Bareiss, M0487
Martin Marietta Aerospace
P.O. Box 179
Denver, CO 80201
(303) 977-8713

Pierre Y. Bely
The Johns Hopkins University
Space Telescope Science Institute
3800 San Martin Drive
Balitmore, MD 21218

Dave H. Bouska
BMD SCOM-HS
P.O. Box 1500
Huntsville, AL 35807

David E. Brinza
NASA Jet Propulsion Laboratory
Mail Code 67-201
4800 Oak Grove Drive
Pasadena, CA 91109
(818) 354-6836

Lyle Broadfoot
University of Arizona
Lunar and Planetary Laboratory
3625 East Ajo Way
Tucson, AZ 85713

Frank J. Brock
Old Dominion University
Research Foundation
17 Research Drive
Hampton, VA 23666

William H. Brune
Harvard University
ESL 40
Cambridge, MA 02138

Supriya Chakrabarti
University of California, Berkeley
Space Sciences Laboratory
Berkeley, CA 94720
(415) 642-3524

Joseph Chamberlain
Rice University
Space Physics Department
P.O. Box 1892
Houston, TX 77251
(713) 527-8101

John T. Clarke, Code TA02
Universities Space Research
Association
NASA Marshall Space Flight
Center, AL 35812
(205) 453-3206

LIST OF ATTENDEES (Continued)

K. S. Clifton, Code ES63
Space Science Laboratory
NASA Marshall Space Flight
Center, AL 35812

Jon B. Cross
Los Alamos National Laboratory
CHM-2, MS G738
Los Alamos, NM 87545
(505) 667-4646

Alex Dalgarno
Harvard-Smithsonian Center for
Astrophysics
60 Garden Street
Cambridge, MA 02138
(617) 495-4403

Ilmars Dalins, Code EH22
Materials and Processes Laboratory
NASA Marshall Space Flight
Center, AL 35812
(205) 453-4350

Rudolf Decher, Code ES61
Space Science Laboratory
NASA Marshall Space Flight
Center, AL 35812
(205) 453-5130

Ralph Earle, MS19
Teledyne Brown Engineering
Cummings Research Park
300 Sparkman Drive
Huntsville, AL 35807

Richard F. Ellis
LPF
University of Maryland
College Park, MD 20742
(301) 454-7093

Mark J. Engebretson
Augsburg College
Department of Physics
731 21st Avenue South
Minneapolis, MN 55454
(612) 330-1067

Giovanni G. Fazio
Smithsonian Astrophysical Observatory
60 Garden Street
Cambridge, MA 02138
(617) 495-7458

Paul D. Feldman
The Johns Hopkins University
Department of Physics and Astronomy
Baltimore, MD 21218
(301) 338-7339

Henry Garrett
NASA Jet Propulsion Laboratory
Mail Code 144-218
4800 Oak Grove Drive
Pasadena, CA 91109
(818) 354-2644

Owen K. Garriott, Code PA
NASA Johnson Space Center
Houston, TX 77058
(713) 483-6581

Tim Gordon
Science and Engineering
Associates, Inc.
6535 South Dayton Street
Englewood, CO 80111
(303) 790-1572

B. David Green
Atmospheric Sciences Group
Physical Sciences Inc.
Dascomb Research Park
P.O. Box 3100
Andover, MA 01810-7100
(617) 475-9030

John C. Gregory
University of Alabama-Huntsville
Physics Department
Huntsville, AL 35899
(205) 895-6028

LIST OF ATTENDEES (Continued)

Joseph E. Hueser
Old Dominion University
Research Foundation
17 Research Drive
Hampton, VA 23666

Donald E. Jennings, Code 693.1
NASA Goddard Space Flight Center
Planetary Systems Branch
Laboratory for Extraterrestrial
Physics
Greenbelt, MD 20771
(301) 344-7701

Jeff Jeter
MDT SCO
Mail Stop 33
P.O. Box 1181
Huntsville, AL 35807

Irving L. Kofsky
PhotoMetrics, Inc.
4 Arrow Drive
Woburn, MA 01801
(617) 938-0300

John L. Kulandu
Lockheed Missiles and Space Company
Department 51-07/Building 592
P.O. Box 3504
Sunnyvale, CA 94088-3504

William D. Langer
Princeton University
Plasma Physics Laboratory
P.O. Box 451
Princeton, NJ 08544
(609) 683-2262

John K. Larabee
Lockheed Missiles and Space Company
Department 51-07/Building 592
P.O. Box 3504
Sunnyvale, CA 94088-3504
(408) 742-7485

M. A. LeCompte
Harvard-Smithsonian Center for
Astrophysics
60 Garden Street
Cambridge, MA 02138
(617) 495-7239

Lubert J. Leger, Code ES53
NASA Johnson Space Center
Houston, TX 77058
(713) 483-2059

John Patrick Lestrade
Mississippi State University
Physics Department
Mississippi State, MS 39762
(601) 325-2323

Harold Liemohn
Boeing Aerospace Company
Mail Stop 87-68
P.O. Box 3999
Seattle, WA 98124
(206) 773-9954

Edward J. Llewellyn
University of Saskatchewan
Institute of Space and
Atmospheric Studies
Saskatoon, SK S7N 0W0
Canada
(306) 966-6401

Mike Loudiana
Boeing Aerospace Company
Mail Stop 87-68
P.O. Box 3999
Seattle, WA 98124
(206) 773-9954

Charles A. Lundquist
Director, Research Institute
University of Alabama-Huntsville
Huntsville, AL 35899
(205) 895-6100

LIST OF ATTENDEES (Continued)

Rita Mahon
University of Maryland
College Park, MD 20742
(301) 454-7076

Dennis M. Manos
Princeton University
Plasma Physics Laboratory
P.O. Box 451
Princeton, NJ 08544
(609) 683-2018

Stephen B. Mende
Lockheed Palo Alto Research
Laboratory
Department 91-20, Building 255
3251 Hanover Street
Palo Alto, CA 94304
(415) 858-4082

Edgar R. Miller, Code ES61
Space Science Laboratory
NASA Marshall Space Flight
Center, AL 35812
(205) 453-5130

M. V. Milnes, Mail Code DA-23
Rockwell International
Space Transportation and Systems
Division
12214 Lakewood Boulevard
Downey, CA 90241

Robert A. Motley
Princeton University
Plasma Physics Laboratory
P.O. Box 451
Princeton, NJ 08544
(609) 683-2564

Michael J. Mumma, Code 693
NASA Goddard Space Flight Center
Planetary Systems Branch
Laboratory for Extraterrestrial
Physics
Greenbelt, MD 20771
(301) 344-6994

Edmond Murad
Air Force Geophysics Laboratory
PHK/3176
Hanscom Air Force Base
Bedford, MA 01731
(617) 861-3046

Charles R. O'Dell
Rice University
Space Physics and Astronomy
Department
P.O. Box 1892
Houston, TX 77251
(713) 527-4939

Peter J. Palmadesso
Naval Research Laboratory
Code 4700.1P
Washington, DC 20375
(202) 767-6780

K. Papadopoulos
University of Maryland
Department of Physics and Astronomy
College Park, MD 20742
(301) 454-6810

Charles E. Patty, Jr.
Teledyne Brown Engineering
Cummings Research Park
300 Sparkman Drive
Huntsville, AL 35807

Douglas L. Patz
Nichols Research Corporation
4040 South Memorial Parkway
Huntsville, AL 35802
(205) 883-1140

Steven Paul
Princeton University
Plasma Physics Laboratory
P.O. Box 451
Princeton, NJ 08544
(608) 683-3781

Walter T. Pease
BMD ATC-D
P.O. Box 1500
Huntsville, AL 35807

LIST OF ATTENDEES (Continued)

Palmer N. Peters, Code ES63
Space Science Laboratory
NASA Marshall Space Flight
Center, AL 35812
(205) 453-5134

Charles Pike
Air Force Geophysics Laboratory
PHK
Hanscom Air Force Base
Bedford, MA 01731
(617) 861-3177

Harry C. Poehlmann, Jr., Mail #T-2
Ball Aerospace Systems Division
P.O. Box 1062
Boulder, CO 80306
(303) 939-4318

Wilson T. Rawlins
Atmospheric Sciences Group
Physical Sciences, Inc.
Dascomb Research Park
P.O. Box 3100
Andover, MA 01810
(617) 475-9030

Ray O. Rantanen
Science and Engineering
Associates, Inc.
6535 South Dayton Street
Englewood, CO 80111
(303) 790-1572

R. D. Rempt
Boeing Aerospace Company
Mail Stop 87-68
P.O. Box 3999
Seattle, WA 98124
(206) 773-9954

Carl J. Rice
The Aerospace Corporation
M2/266
P.O. Box 92957
Los Angeles, CA 90009
(213) 647-1749

David A. Roalstad, Mail #LT-1
Ball Aerospace Systems Division
P.O. Box 1062
Boulder, CO 80306
(303) 939-4789

Robert Ruggeri
Boeing Aerospace Company
Mail Stop 87-68
P.O. Box 3999
Seattle, WA 98124
(206) 773-9955

Bill R. Sandel
University of Arizona
3625 East Ajo Way
Tucson, AZ 85713
(602) 745-6767

John A. Schmidt
Princeton University
Plasma Physics Laboratory
P.O. Box 451
Princeton, NJ 08544
(609) 683-2564

Thomas G. Slinger
SRI International
Chemical Physics Laboratory
333 Ravenswood Avenue
Menlo Park, CA 94025
(415) 859-2764

Kerry A. Spear
University of Colorado
Laboratory for Atmospheric and
Space Physics, Code 392
5525 Central Avenue
Boulder, CO 80301
(303) 492-5393

Fred A. Speer, Code DS30
NASA Marshall Space Flight
Center, AL 35812
(205) 453-3033

LIST OF ATTENDEES (Continued)

Roy A. Swanson
Boeing Aerospace Company
Mail Stop 87-68
P.O. Box 3999
Seattle, WA 98124
(206) 773-9955

Gary R. Swenson
Lockheed Palo Alto Research
Laboratory
Department 91-20, Building 255
3251 Hanover St.
Palo Alto, CA 94304
(415) 858-4097

Bruce Tatarchuk
Auburn University
Department of Chemical Engineering
Auburn, AL 36849
(205) 826-4827

Peter D. Tennyson
The Johns Hopkins University
Department of Physics and Astronomy
3800 San Martin Drive
Baltimore, MD 21218
(301) 338-7365

Dieter L. Teuber
Teledyne Brown Engineering
Cummings Research Park
300 Sparkman Drive
Huntsville, AL 35807
(205) 532-1431

James R. Thompson, Jr.
Princeton University
Plasma Physics Laboratory
P.O. Box 451
Princeton, NJ 08544
(609) 683-2207

Kent Tobisha
University of Colorado
Laboratory for Atmospheric and
Space Physics
Boulder, CO 80301
(303) 492-5440

Norman H. Tolk
Vanderbilt University
Department of Physics and Astronomy
P.O. Box 1807-B
Nashville, TN 37235
(615) 322-2828

Douglas G. Torr
Center for Atmospheric Research
Utah State University
Department of Physics, UMC 41
Logan, UT 84322
(801) 750-2779

Marsha R. Torr
Center for Atmospheric Research
Utah State University
Department of Physics, UMC 41
Logan, UT 84322
(801) 750-2685

James Tsacoyeanes
Perkin-Elmer Corporation
Danbury, CT 06810

Gregory J. Ucker
University of Colorado
Laboratory for Atmospheric and
Space Physics
5525 Central Avenue
Boulder, CO 80301
(303) 492-5440

Richard R. Vondrak
Lockheed Palo Alto Research
Laboratory
Department 91-20, Building 255
3251 Hanover St.
Palo Alto, CA 94304
(415) 858-4050

Hunter Waite, Code ES53
Space Science Laboratory
NASA Marshall Space Flight
Center, AL 35812
(205) 453-3918

LIST OF ATTENDEES (Concluded)

Francis C. Wang
Lockheed Missiles and Space Company
P.O. Box 1103
Huntsville, AL 35807
(205) 837-1800

Ann F. Whitaker, Code EH11
Materials and Processes Laboratory
NASA Marshall Space Flight
Center, AL 35812
(205) 453-4877

J.-H. Yee
Harvard-Smithsonian Center for
Astrophysics
60 Garden Street
Cambridge, MA 02138
(617) 495-5873

1. REPORT NO. NASA CP-2391		2. GOVERNMENT ACCESSION NO.		3. RECIPIENT'S CATALOG NO.	
4. TITLE AND SUBTITLE Second Workshop on Spacecraft Glow				5. REPORT DATE September 1985	
				6. PERFORMING ORGANIZATION CODE	
7. AUTHOR(S) J. H. Waite, Jr., and T. W. Moorehead, Editors				8. PERFORMING ORGANIZATION REPORT # ES53/ES01	
9. PERFORMING ORGANIZATION NAME AND ADDRESS George C. Marshall Space Flight Center Marshall Space Flight Center, Alabama 35812				10. WORK UNIT NO. M-502	
				11. CONTRACT OR GRANT NO.	
12. SPONSORING AGENCY NAME AND ADDRESS National Aeronautics and Space Administration Washington, DC 20546				13. TYPE OF REPORT & PERIOD COVERED Conference Publication	
				14. SPONSORING AGENCY CODE	
15. SUPPLEMENTARY NOTES Sponsored, in part, by the Universities Space Research Association, Washington, DC					
16. ABSTRACT This report contains results of a workshop held on May 6-7, 1985, at the Space Science Laboratory of NASA/Marshall Space Flight Center, Huntsville, Alabama. The contents of this report are divided as follows: <ul style="list-style-type: none"> o In Situ Observations o Theoretical Calculations o Laboratory Measurements o Future Experiments 					
17. KEY WORDS Spacecraft Glow Shuttle Glow Atmospheric Science Aeronomy Atmosphere/Vehicle Interaction			18. DISTRIBUTION STATEMENT Unclassified — Unlimited Subject Category: 88		
19. SECURITY CLASSIF. (of this report) Unclassified		20. SECURITY CLASSIF. (of this page) Unclassified		21. NO. OF PAGES 304	22. PRICE A14

**National Aeronautics and
Space Administration
Code NIT-3**

**SPECIAL FOURTH CLASS MAIL
BOOK**

**Postage and Fees Paid
National Aeronautics and
Space Administration
NASA-451**



**Washington, D.C.
20546-0001**

**Official Business
Penalty for Private Use, \$300**

NASA

**POSTMASTER: If Undeliverable (Section 158
Postal Manual) Do Not Return**
